CHAPTER 1

INTRODUCTION

Cycling has been useful over the years for sports, recreation and rehabilitation (Cerone, *et al.* 2010). In developed countries such as United State of America (USA), Japan, Britain, South Korea and Australia, their citizens are encouraged to exercise their bodies and thereby shed excessive weight, which lead healthier and longer live resulting in the increase of life expectancy. In USA, a lot of companies, such as IBM, Scotts Miracle-Geo, etc are offering financial incentives, for their employees to exercise and shed excess weight (Stobbe, 2010). Shedding of excessive weight could be achieved either through walking or cycling. Some developed countries such as Denmark, Holland, USA, South Korea, Spain and Australia have dedicated bicycle lanes which can permit outdoor use of bicycles either for going to work or exercising the bodies in the morning or evening. There have been renewed calls for countries to cut back on their green house gases emissions. Consequently, UN is advocating the use of the bicycle as a means of transportation and as a way of cutting back on green house gases emissions so as to reduce global warming (Omi, 2007).

Cycling exercise could be useful in the following ways: for transportation, for rehabilitation therapy of accident patients, for competition in sports, for recreation, for fitness (exercise), and for electricity generation.

During cycling, injuries due to repetitive use of muscles, bones, joints and tendon do occur. Among these are neck pain, low back pain, knee injuries, groins/buttock etc. Many researchers have examined different pain areas and overuse sites but proper understanding of this subject matter can not be over emphasized. The injury site that

affects performance and cycling in general is the knee. Therefore, biomechanical analysis of the lower limb segments during variable speed cycling is very important. This study therefore presents better understanding of the effects of variable speed cycling on the lower limb segments.

Figure 1: Cycling for transportation

Figure 2: Cycling for competition

1.1 Background to the Study

In the rural areas of Nigeria and most of other developing nations, bicycles provide mobility for the young and old. This is because they are cheap to acquire and maintain, and they could be used even on footpaths, as well as on terrains that are adjudged difficult for vehicular movement. Bicycles are ridden to farm as well as social functions. They are therefore an essential and integral part of the rural dwellers' life. Fatigue does occur over a period of time at the lower limb joints of the riders leading to health concerns that in most cases are not even attributed to cycling. The biomechanical analysis of the lower limb segments during variable speed cycling will provide useful information for the cycling community in general and the health practitioners. Health practitioners can then advise patients with cycling related health issues, as well as

prescribe appropriate therapy for patients with mobility impairments arising from stroke, spinal cord injury etc, which could eventually minimize stress and fatigue on lower limb segments' joints.

1.2 Statement of Problem

Cycling has been in use for transportation, fitness and recreation for over a century. It has also been prescribed as an intervention for individuals with disability and mobility impairments (Johnston, 2007). Injuries do occur in cycling during recreation, competition, rehabilitation therapy and in everyday normal use (Wilber *et al.*, 1995). The available literatures in this field do not properly address the issue of overuse injuries or the effect of crank speed, saddle height and horizontal acceleration on the lower limb segments during variable speed cycling. There is no existing model that affords in-depth understanding of the lower limb segments during variable speed cycling sessions so as to mitigate any injury occurrences. There is nothing to serve as a guide for the cycling community, equipment manufacturers and health practitioners.

1.3 Aim and Objectives of the Research

The aim of this research is to minimize knee injury related to cycling during variable speed cycling session.

The objectives of this research are:

i. To develop a model that can be used for the biomechanical analysis of the lower limb segments during variable speed cycling.

ii. To evaluate the effects of the change in crank speed, saddle height and horizontal acceleration on the lower limb of a cyclist during variable speed cycling.

iii. To determine the biomechanical optimum value of crank speed, saddle height and horizontal acceleration during variable speed cycling.

1.4 Scope and Delimitation of the Study

This research covers the biomechanical analysis of lower limb segment during variable speed cycling, horizontal acceleration and variable saddle height. It does not cover the age, race, sex and population trait of the cyclist.

1.5 Significance of the Study

Different people, young and old, around the world ride bicycles for different reasons such as for recreation, sports, rehabilitation, and transportation. Reports of cyclist injury at the lower limb are rife (Hull and Jorge, 1985; Wilber *et al.*, 1995; Boyd *et al.*, 1996, 1997; Marsh, *et al.* 2000; Bini, *et al*. 2011). It is therefore important to know the effects of change in crank speed, saddle height and horizontal acceleration on the lower limb segments in order to avoid injuries to cyclists and thereby make cycling comfortable and worthwhile. This research seek to provide a guide to equipment manufacturers, rehabilitation therapists, and the cycling community, which will lead to better equipment design and manufacture, appropriate equipment selection by cyclists and prevention of injuries during cycling respectively. It will also afford the therapist better understanding of appropriate prescriptions and lead to improved performance by cyclists during competition without fear of injury. It will also guide health practitioners in dealing with health issues relating to cycling in general.

1.6 Definition of Terms

1. **Biomechanics** – application of principle of mechanics to biological systems.

2. Chain wheel – the wheel attached to the crank arm

3. Crank angle – the angle between the vertical axis and the crank arm measured clockwise

4. Crank speed – the number of revolutions of a crank in one minute

5. **Cycling** – riding of bicycle

6. Fitness – a state of health or well-being

7. Flexion – contracting of muscle or reducing joint angle

8. Extension – increasing joint angle

9. Gait – mode of walking

10. Gear ratio – ratio of the number of teeth in chain to the number of teeth in rear cog wheel

11. Kink – a bend or curve in something

12. **Lower limb segments** – leg section from the hip joint to the toe

13. **Overuse injury** – muscle fatigue resulting from repetitive on human body part

14. Rear cog wheel – the wheel that transmits power to the rear bicycle wheel

15. **Recreation** – activity of leisure

16. Recumbent – reclining position

17. **Rehabilitation** – restoration to normal life through therapy

18. **Saddle height** – the vertical distance between saddle surface and centerline of crank Spindle

19. Shank segment – the section between the knee and ankle joints

CHAPTER 2

LITERATURE REVIEW

2.1 Human Muscles

Muscles usually develop their maximum power when they are contracting quickly against resistance (Sargeant *et al.,* 1981). There had been satisfactory use of muscle power in such applications as treadmill for grinding grains, Leonardo da Vinci's human-powered drum or cage for armaments, treadmill-driven pumps and cycling (Wilson 2004). Slob (2000) reported human power output in various human activities. Jansen (2011) provided insight into the knowledge required to design human-powered energy systems in consumer products from a scientific perspective. Hull and Jorge (1985) modeled the lower limb segments and bicycle frame as a five bar linkage in order to study how each muscle in the leg functions to either to drive the leg linkage and or generate the pedal forces. Individual muscles activities were highlighted and the forces such activities generated during cycling. Brown and Jensen (2003) studied the developmental progression that characterizes the interaction of muscular and non-muscular forces in tasks constrained by contact with the environment. Their results showed a task-appropriate adaptation to lower segmental mass and inertia. Baum and Li (2003) investigated the effect of frequency and inertia on lower extremity muscle activities during cycling. Their results indicated that inertia properties influenced the lower extremity muscular activity in addition to the cadence effect. But they did not examine the relationship between inertia and overuse injuries.

2.2 Work and Power Output during Cycling

Yoshihuku and Herzog (1990) studied the design parameters for a bicycle-rider system which maximizes the power output from the muscles of the human lower limb. They modeled the lower limb as a planar system of five rigid bodies connected by four smooth joints and driven by seven functional muscle groups which were assumed to behave according to Hill's equation (Hill, 1938). The maximal average power obtained for one full pedal revolution was found to be approximately 1100W for both lower limbs at 155 rpm for a nominal crank length of 170mm. Fregly *et al.,* (1996) tested the hypothesis that under steady-state conditions, the net joint torques produced by muscles at the hip, knee and ankle are unaffected by crank inertia load. Too and Williams (2001) predicted the crank arm length that would maximize human peak power, mean power and minimum power output in a recumbent cycling position. Martin and Spirduso (2001) investigated the effect of cycle crank length on maximum cycling power, optimal pedaling rate and optimal pedal speed and also investigated the optimal crank length to lower limb segments length ratio for maximal power production. Crouch (2004) described an electronically controlled automatic transmission which was designed and built for use on a bicycle. It focused on the algorithm which determines the optimal gear to select at any time for maximized performance but did not examine the fatigues at lower limb. Bertucci *et al.,* (2005) analyzed the crank torque in road cycling on level and uphill using different pedaling cadences in the seated position. It was discovered that at maximal aerobic power, the crank torque profile varied substantially according to the pedaling cadence and with a minor effect according to terrain, but did not present any dynamic equation to validate their findings. Hasson *et*

al., (2006) described the changes in pedal and joint kinetics that took place over the learning process using electromyography. His study is limited to learning process. Hue *et al.,* (2007) assessed whether an eccentric chain ring that increases crank arm length at the down stroke and decreases it during the upstroke improves performance in a track event in the 1000 m trial. It was discovered that the eccentric chain ring did not increase average performance when compared with the round chain and health implication of using either eccentric or round chain rings was not mentioned. Rankin and Neptune (2010) used muscle-actuated forward dynamics simulations of pedaling to identify the overall optimal seat configuration that produces maximum crank power, and they systematically varied seat tube angle to assess how it influenced maximum crank power. Bini, *et al.,* (2010) compared joint mechanical work distribution and kinematics at different saddle heights, workloads, and pedaling cadences. Nine healthy male participants aged 22 to 36 years without competitive cycling experience participated. It was discovered that there was an increased contribution of the ankle joint to the total mechanical work with increasing saddle height.

2.3 Bicycle Efficiency

Hansen *et al.,* (2002) tested the hypotheses that during cycling, a considerable increase in crank inertial load would cause freely chosen pedal rate to increase and as a consequence, gross efficiency to decrease, and peak crank torque to increase if a constant pedal rate is maintained. Busko (2004) studied the pedaling rate in relation to the gross and net mechanical efficiency efforts with the same intensity. He found that

gross and net values obtained at 100 rpm were significantly different from averages reached by 40, 60, and 80 rpm.

2.4 Modeling and Simulation

Kautz and Neptune (2002) simulated how muscles perform external work both directly and indirectly during pedaling. Bei and Fregly (2004) proposed a computational methodology for combining multi body dynamic simulation methods with a deformable contact knee model. Attia (2005) presented a two-step formulation for the dynamic analysis of generalized planar linkages by replacing a rigid body by a dynamically equivalent constrained system of particles and Newton's second law of motion was used to study the motion of the particles without introducing any rotational coordinates. Chavdarov (2005) used four-space Jacobi matrix to analyze a five-link mechanism as a forward kinematics problem. McCane *et al.,* (2005) showed least squares derivation for calculating the angle of rotation and finite centre of rotation of a set of marker points undergoing rigid planar rotation and translation. The results included the calculation of a scaling factor between the two point sets – the calculation of which was obvious in previous approaches. Lieh (2006) developed a closed-form method to solve non-linear equations derived from force and power balance for cycling speed but did not examine any health issues arising from cycling. Chang (2007) developed a dynamic model of a four bar linkage with clearance between coupler and rocker and used Modified Gear Method, a numerical method, to solve the dynamic equations. Lin *et al.,* (2010) presented a surrogate contact modeling that can improve the computational speed of three-dimensional multi-body dynamic simulations. Nott *et al.,* (2010) presented

quantitative relationships between individual joint moments and trunk control with respect to balance during gait to show that the ankle, knee, and hip joint moments all affect the angular acceleration of the trunk.

2.5 Effect of Saddle Height and Overuse Injuries

Wilber *et al.,* (1995) sampled 294 male and 224 female cyclists and discovered that over 85% of them reported one or more overuse injuries amongst which knee injury was 41.7%. Boyd, *et al*., (1996) described a six-load component pedal dynamometer designed for the study of knee overuse injury in cycling. They followed an optimal design technique in choosing dimensions of the load measuring cross-sections. In comparison with previously built dynamometer, they found that their dynamometer was more accurate than previous ones. Boyd, *et al.,* (1997) tested two hypotheses as a basis for the design of bicycle pedals that possibly alleviates knee injuries. They discovered that there were significant reductions in the coupled non-driving moments at the pedal for the dual-rotation platform compared to each of the single-rotation cases. Fregly *et al.,* (2009) in their study used data collected from a patient with a force-measuring knee replacement to quantify how muscle and contact forces contribute to inverse dynamic knee loads during gait. Bini, *et al.,* (2011) did comprehensive review of injury risks during cycling. It was discovered that methods for determining optimal saddle height varied and was not well established in literature. Also, there is limited information on the effects of saddle height on lower limb injury risk. They concluded that since the occurrence of overuse knee injury is 50% in cyclist, then future studies should focus on how saddle height can be optimized to improve cycle performance and reduce knee

joint forces to reduce lower limb injury risks. Bini, *et al.*, (2012) assessed the effects of saddle height, on pedal forces, joint mechanical work and kinematics in 12 cyclists and 12 triathletes. They found that changes of up to 5% of preferred saddle height for cyclist and 7% for triathletes affected hip and knee angles but not joint mechanical work but did not relate their findings to injury risks in the lower limb segments.

2.6 Crank Speed Dynamics

Fregly (1993) studied the significance of crank load dynamics to steady state pedaling. Marsh *et al.*, (2000) tested some hypotheses to show that there is a modest association between the net joint moment-based cost function cadence and the preferred cadence regardless of fitness or cycling experience. The cadence which minimized the cost function was found to increase with power output. They concluded that minimizing net joint moments is a major factor associated with preferred cadence selection. Vercruyssen and Brisswalter (2010), in their reviews of factors that determine freely chosen cadence during cycling, based their review on a multi-factorial analysis considering the cycling constraint, and the physiological and biomechanical factors of cadence selection so as to establish interrelationships between the factors. They noted that, although, metabolic cost is affected at high cadence, the improvement of cycling performance was systematically observed at this cadence range whatever competitive level of the rider but did not consider fatigue at this cadence.

2.7 Rehabilitation Cycling

Trumbower and Faghri (2005) evaluated the orthogonal pedal force generations of various muscles in the lower limb during different stimulation intensities at eight fixed

crank positions of an FES-LCE. They discovered that lowering the stimulation intensity during cycling and sequencing the activation of thigh and lower limb segments muscles within a closed-loop system may improve pedal effectiveness and reduce fatigue possibly due to over stimulation. Johnston (2007) noted in his review that individuals with physical disabilities can benefit from cycling interventions, which could address impairments while potentially minimizing stress on joints. These improvements in impairments may have an impact on mobility, activity and participation. Haapala *et al.*, (2008) investigated the biomechanics of the hip, knee and ankle during a progressive resistance cycling protocol in an effort to detect and measure the presence of muscle fatigue. They hypothesized that the knee power output can be used as an indicator of fatigue in order to assess the cycling performance of spinal cord injury subjects but did not develop any equation to validate their findings. Fregly (2009) presented how patient-specific multi-body dynamic models could be used to design new or improved treatments for clinical problems involving the human neuro-musculoskeletal system.

It is seen that the available literatures in this field do not properly address the issue of muscle fatigue that eventually leads to overuse injuries or the effects of crank speed, saddle height and horizontal acceleration on the lower limb segments during variable speed cycling. It is therefore important to develop an appropriate model and its analysis, in order to enhance understanding of the lower limb segments during variable speed cycling to mitigate any injury occurrence from it.

CHAPTER THREE

3.0 METHODOLOGY

3.1.0 Theoretical Framework

Knee overuse injuries among recreational and competitive cyclists has been established in the literature (Hull and Jorge, 1985; Wilber *et al.,* 1995; Boyd *et al.,* 1996, 1997; Marsh, *et al.*, 2000, Bini *et al.*, 2011). The subject has not been exhaustive; there is still need for more understanding of the subject. In other to enhance more understanding of the subject, the lower limb segments were modeled as a five-bar linkage mechanism, and the related kinematics and kinetic equations were developed using inverse dynamics. The rider is in a sitting position on the bicycle saddle, with his two feet resting on the bicycle pedals at angle that is convenient for him. The start off point of the crank arm is the top dead centre (TDC). The toe is on the pedal axis with the ankle joints are neither flexing nor extending. The following assumptions were made in the work:

(i) The movement of the lower limb segments is restricted to a plane,

(ii) The hip is stationary relative to the saddle,

(iii) All joints are pinned and revolute,

(iv) The bicycle does not have any mechanical defect,

(v) The centre of mass is the centre of the segments

(vi) Singularity is avoided

3.1.1 Horizontal Velocity and Acceleration

Figure 3.1 is the schematic of the propulsion system of the bicycle. In Figure 3.1, the crank arm of the bicycle makes an angle q_1 with the vertical axis, and a resultant force, F_R , is applied to the pedal by the foot segment. The horizontal and vertical components of the resultant pedaling force respectively are:

$$F_{fx} = F_R \cos q_1 \tag{3.1}$$

$$F_{fy} = F_R \sin q_1 \tag{3.2}$$

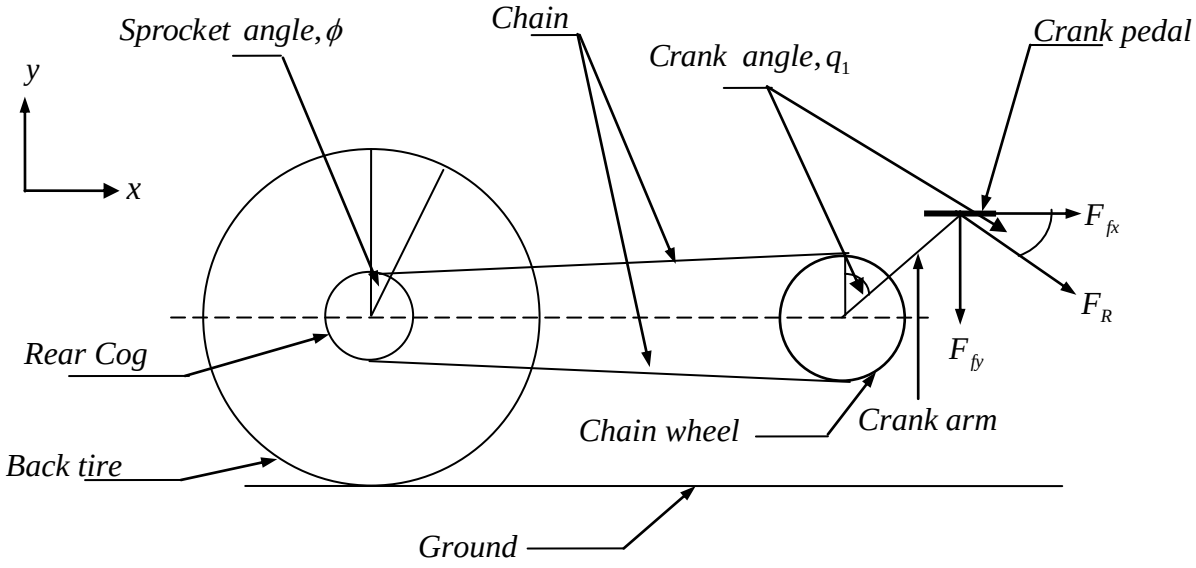

Figure 3.1: Schematic of bicycle pedaling

As the chain wheel with T_{wheel} number of gear teeth turns at $\dot{q}_1$ radians per second, the rear cog with T_{cog} number of teeth turns according to gear ratio *gr*, then, the bicycle wheel angular velocity, $\dot{\phi}$, is determined from gear ratio, *gr*, as follows:

$$g_r = \frac{T_{wheel}}{T_{cog}} = \frac{\dot{\phi}}{\dot{q}_1} \tag{3.3}$$

$$\dot{\phi} = \frac{\dot{q}_1 \times T_{wheel}}{T_{cog}} \tag{3.4}$$

If the rider tries changing or increasing its horizontal velocity by accelerating, changing the chain wheel angular acceleration at $\ddot{q}_1$ rad/s^2, then the bicycle wheel angular acceleration follows from Eq. 3.4 above

$$\ddot{\phi} = \frac{\ddot{q}_1 \times T_{wheel}}{T_{cog}} \tag{3.5}$$

If the bicycle is moving, the bicycle wheel will undergo rotational as well as translational motions. If the bicycle and the rider are moving in the *x*-*y* plane and their displacement vector, **s**, at any time, *t* is given by

$$\mathbf{s}(t) = x\ i + y\ \ j \tag{3.6}$$

The velocity and acceleration are therefore,

$$\mathbf{v}(t) = \dot{\mathbf{s}}(t) = \dot{x}\ i + \dot{y}\ \ j \tag{3.7}$$

$$\mathbf{a}(t) = \ddot{\mathbf{s}}(t) = \ddot{x}\ i + \ddot{y}\ \ j \tag{3.8}$$

If the bicycle riding plane is inclined to the horizontal at an angle ($\theta = 0$), the vertical component of the translational velocity and acceleration are zero. Therefore, from Eq. (3.4) and (3.7), the horizontal component of the velocity is

$$\dot{x} = r_{bw}\dot{\phi}$$

$$= \frac{r_{bw} \times \dot{q}_1 \times T_{wheel}}{T_{cog}} \tag{3.9}$$

Similarly, from Eq. 3.5 and Eq. 3.8, the horizontal acceleration of the bicycle in the positive *x* direction is

$$\ddot{x} = a(t) = r_{bw}\ddot{\phi}$$

$$= \frac{r_{bw} \times \ddot{q}_1 \times T_{wheel}}{T_{cog}} \tag{3.10}$$

$$\ddot{q}_1 = \frac{\ddot{x} \times T_{cog}}{r_{bw} \times T_{wheel}} \tag{3.11}$$

Figure 3.2 is the free body diagram of the bicycle tire. If we assume that the load on the bicycle is shared equally between the two tires, then, Figure 3.2 is assumed to depict the two tires.

$$W = N = M_{BR} g \tag{3.12}$$

When the bicycle starts moving, the velocity is greater than zero, and if we assume no slipping between the tires and the road, then,

$$F_F = -\mu N \quad (\text{when} \quad \dot{x} > 0) \tag{3.13}$$

$$F_R = M_{BR} \ddot{x} = -\mu N \quad (\text{where} \quad N = M_{BR} g) \tag{3.14}$$

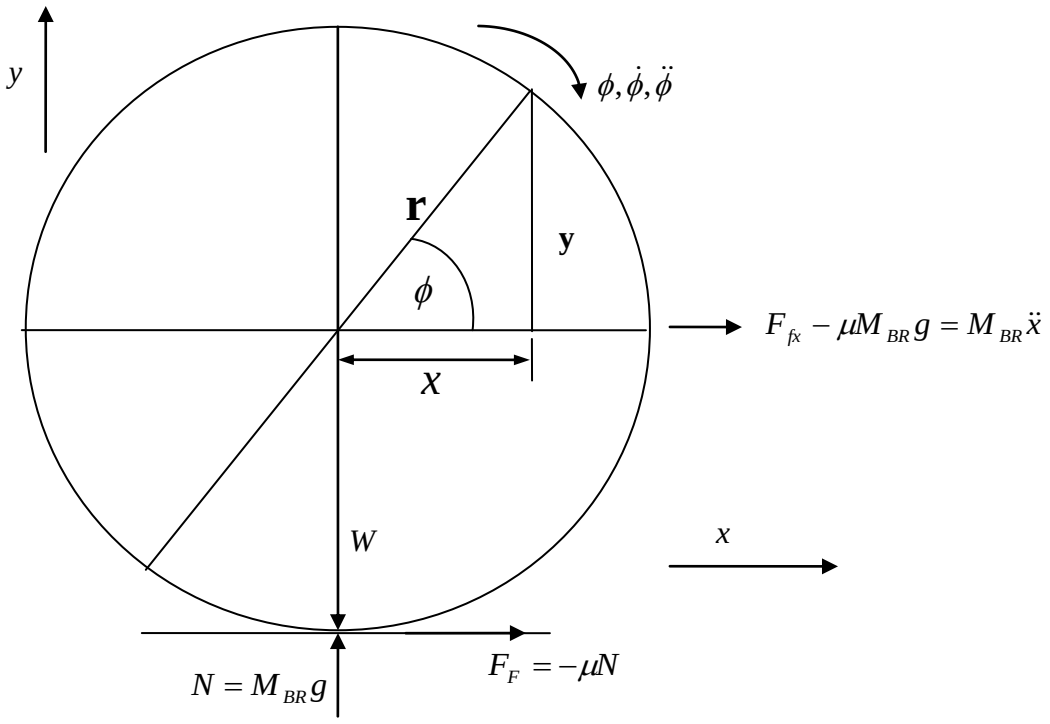

Figure 3.2: Free body diagram of the bicycle Tire

From Eq. 3.1 and Eq. 3.2,

$$F_{fx} = F_R \cos q_1 = M_{BR} \ddot{x} + \mu M_{BR} g \tag{3.15}$$

$$F_{fy} = F_R \sin q_1 \tag{3.16}$$

3.1.2 Kinematics of the Lower Limb Segments

A rider on a bicycle is shown in Figure 3.3. The rider's lower limb segments and the bicycle is modeled as a five – bar linkage as shown in Figure 3.4, with four numbers of active links, the thigh, shank, foot and crank arm and one inactive link described by vertical and horizontal distances of the hip from the crank axis. The thigh, the leg (shank), the foot segments and crank arm form the active links, while the line joining the centre of the seat and the centre of the crank spindle forms the inactive link. The model is assumed to be revolute rigid bodies in planar motion with frictionless pinned joints. The configuration of this model depends on two coordinates, the foot angle, q_2 and the angle between the crank arm, and the y axis, q_1. The lower limb rotates in *x*-*y* plane of the inertia frame.

Figure 3.3: A rider portraying the five bar linkage model

3.1.2.1 Position Analysis of Thigh and Shank Segments

Using inverse dynamics, the position loops equations in *x* and *y* directions are:

$$f_x\left(q_{1,}q_{2,}\theta_{1,}\theta_2\right) = l_c \sin q_1 + l_f \cos q_2 + l_s \cos\theta_1 + l_t \cos\theta_2 - l_x = 0 \qquad (3.17a)$$

$$f_y\left(q_{1,}q_{2,}\theta_{1,}\theta_2\right) = l_c \cos q_1 + l_f \sin q_2 + l_s \sin\theta_1 + l_t \sin\theta_2 - l_y = 0 \qquad (3.17b)$$

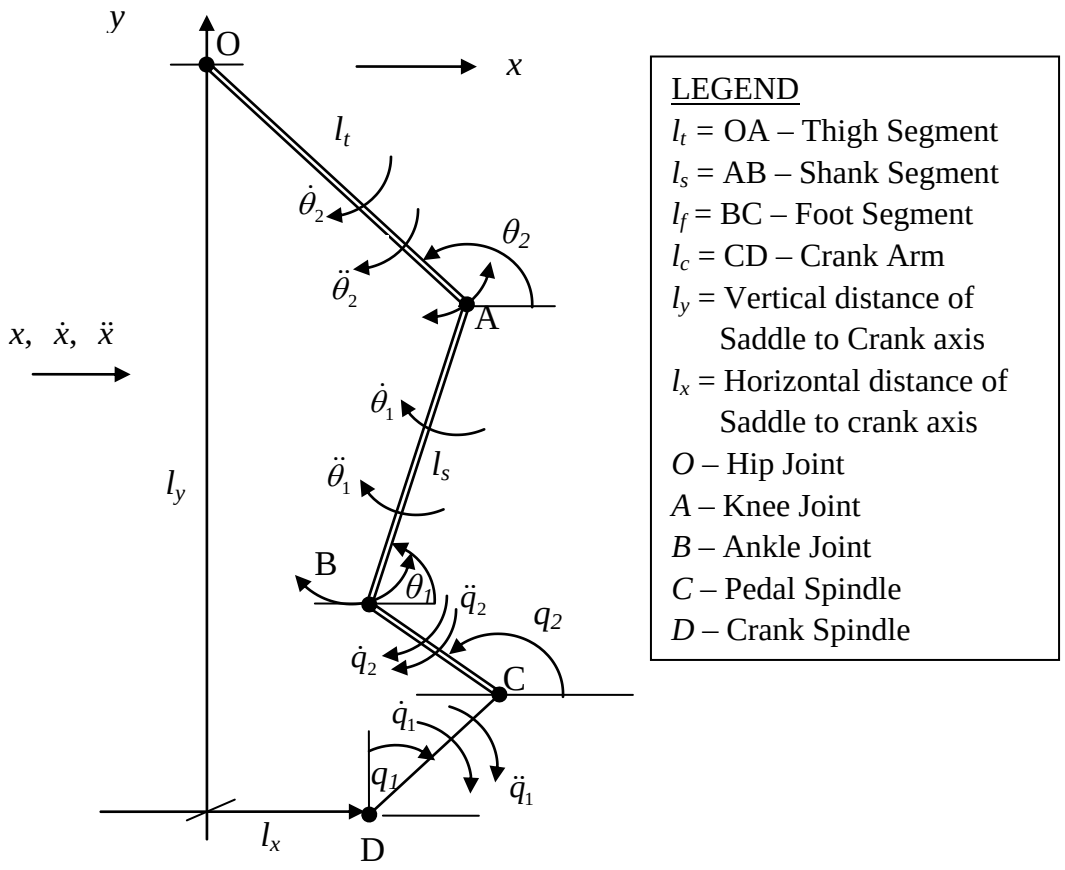

Figure 3.4: 5-bar linkage model (Hull and Jorge, 1985)

The unknown angles are θ_1 andθ_2, the shank and the thigh inclination angles to the horizontal

Figure 3.5 shows the resolutions of the lower limb segments in the x – and y – axes. From right angled triangle ABF in Figure 3.5, it is found that

$$\tan\theta_1 = \frac{l_y + l_c\cos q_1 - l_f\sin q_2 - l_t\sin\theta_2}{l_f\cos q_2 + l_t\cos\theta_2 - l_c\sin q_1 - l_x} \tag{3.18}$$

$$\theta_1 = \tan^{-1}\left[\frac{l_y + l_c\cos q_1 - l_f\sin q_2 - l_t\sin\theta_2}{l_f\cos q_2 + l_t\cos\theta_2 - l_c\sin q_1 - l_x}\right] \tag{3.19}$$

The expression for the thigh angle θ_2, is also obtained from triangle ABF in Figure 3.5 as follows:

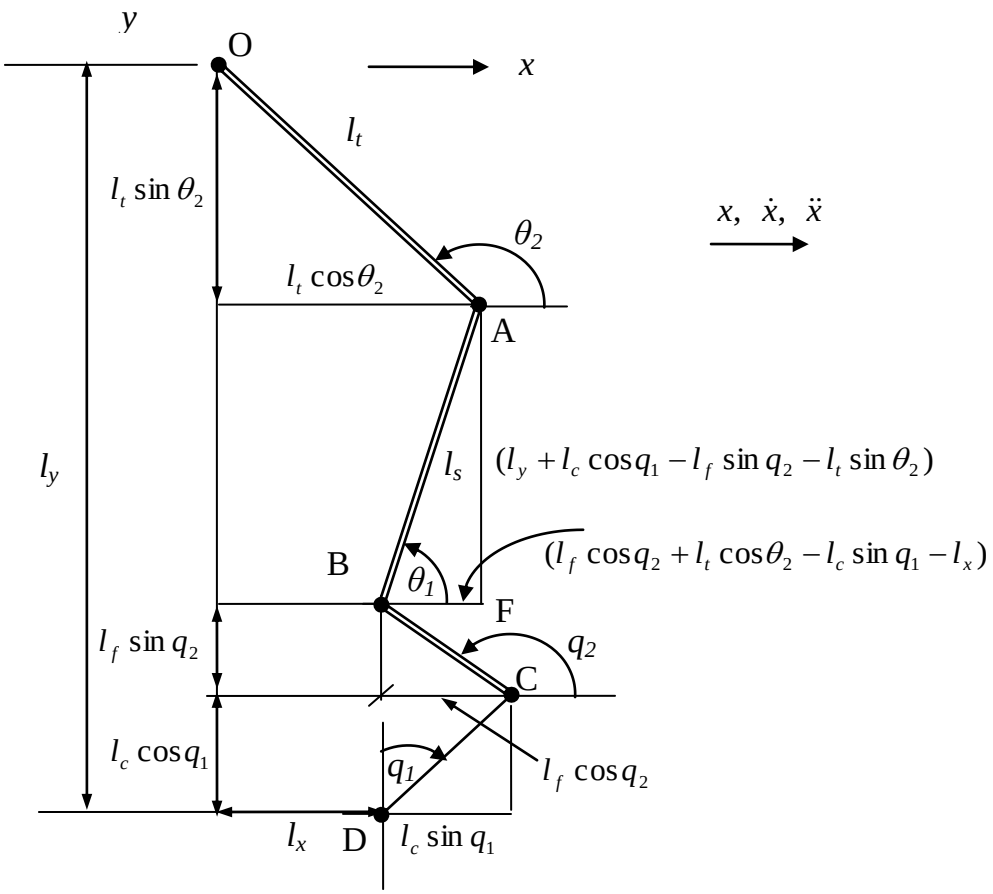

Figure 3.5: Space Analysis of shank and thigh angles

Using Pythagoras' theorem,

$$l_s^2 = \left[\left(l_y + l_c \cos q_1 - l_f \sin q_2\right) - l_t \sin\theta_2\right]^2 + \left[\left(l_f \cos q_2 - l_c \sin q_1 - l_x\right) + l_t \cos\theta_2\right]^2 \tag{3.20}$$

$$= \begin{Bmatrix} \left(l_y + l_c \cos q_1 - l_f \sin q_2\right)^2 - 2\left[\left(l_y + l_c \cos q_1 - l_f \sin q_2\right)(l_t \sin\theta_2)\right] + (l_t \sin\theta_2)^2 + \\ \left(l_x + l_c \sin q_1 - l_f \cos q_2\right)^2 - 2\left[\left(l_x + l_c \sin q_1 - l_f \cos q_2\right)(l_t \cos\theta_2)\right] + (l_t \cos\theta_2)^2 \end{Bmatrix} \tag{3.21}$$

$$= \begin{Bmatrix} \left(l_y + l_c \cos q_1 - l_f \sin q_2\right)^2 + \left(l_x + l_c \sin q_1 - l_f \cos q_2\right)^2 + l_t^2 Sin^2\theta_2 + l_t^2 Cos^2\theta_2 - \\ 2\left[\left(l_y + l_c \cos q_1 - l_f \sin q_2\right)(l_t \sin\theta_2)\right] - 2\left[\left(l_x + l_c \sin q_1 - l_f \cos q_2\right)(l_t \cos\theta_2)\right] \end{Bmatrix} \tag{3.22}$$

$$= \begin{Bmatrix} \left(l_y + l_c \cos q_1 - l_f \sin q_2\right)^2 + \left(l_x + l_c \sin q_1 - l_f \cos q_2\right)^2 + l_t^2\left(Sin^2\theta_2 + Cos^2\theta_2\right) - \\ 2\left[\left(l_y + l_c \cos q_1 - l_f \sin q_2\right)(l_t \sin\theta_2)\right] - 2\left[\left(l_x + l_c \sin q_1 - l_f \cos q_2\right)(l_t \cos\theta_2)\right] \end{Bmatrix} \tag{3.23}$$

$$= \begin{Bmatrix} \left(l_y + l_c \cos q_1 - l_f \sin q_2\right)^2 + \left(l_x + l_c \sin q_1 - l_f \cos q_2\right)^2 + l_t^2 - \\ 2\left[\left(l_y + l_c \cos q_1 - l_f \sin q_2\right)\left(l_t \sin \theta_2\right)\right] - 2\left[\left(l_x + l_c \sin q_1 - l_f \cos q_2\right)\left(l_t \cos \theta_2\right)\right] \end{Bmatrix} \quad (3.24)$$

$$\begin{Bmatrix} 2\left[\left(l_y + l_c \cos q_1 - l_f \sin q_2\right)\left(l_t \sin \theta_2\right)\right] + \\ 2\left[\left(l_x + l_c \sin q_1 - l_f \cos q_2\right)\left(l_t \cos \theta_2\right)\right] \end{Bmatrix} = \begin{Bmatrix} \left(l_y + l_c \cos q_1 - l_f \sin q_2\right)^2 + \\ \left(l_x + l_c \sin q_1 - l_f \cos q_2\right)^2 + l_t^2 - l_s^2 \end{Bmatrix} \quad (3.25)$$

If we let

$$A = \left(l_y + l_c \cos q_1 - l_f \sin q_2\right)^2 + \left(l_x + l_c \sin q_1 - l_f \cos q_2\right)^2 + l_t^2 - l_s^2 \quad (3.26)$$

$$B = 2\left(l_x + l_c \sin q_1 - l_f \cos q_2\right) l_t \quad (3.27)$$

$$C = 2\left(l_y + l_c \cos q_1 - l_f \sin q_2\right) l_t \quad (3.28)$$

Then, equation (3.25) becomes

$$C Sin\theta_2 + B Cos\theta_2 = A \quad (3.29)$$

Using trigonometry identity and let $\tan \frac{\theta_2}{2} = t$

From triangle ABC in Figure 3.6,

$$Sin\frac{\theta_2}{2} = \frac{t}{\sqrt{1+t^2}} \quad (3.30)$$

$$Cos\frac{\theta_2}{2} = \frac{1}{\sqrt{1+t^2}} \quad (3.31)$$

$$Sin\theta_2 = 2Sin\frac{\theta_2}{2} Cos\frac{\theta_2}{2} = 2 \cdot \frac{t}{\sqrt{1+t^2}} \cdot \frac{1}{\sqrt{1+t^2}} = \frac{2t}{1+t^2} \quad (3.32)$$

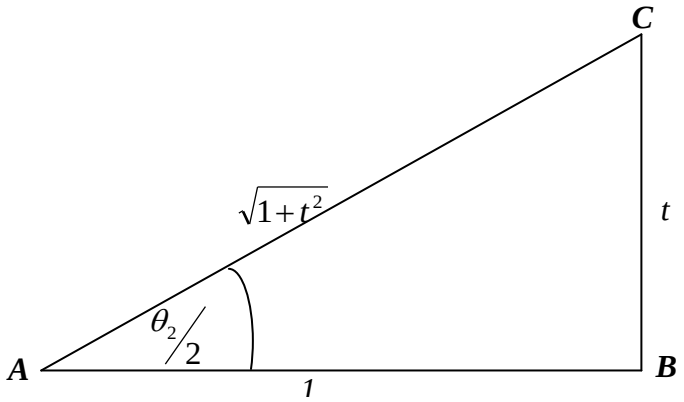

Figure 3.6: Trigonometry identity for the full angle, $\theta_2/2$

$$Cos\theta_2 = 2Cos^2\frac{\theta_2}{2} - 1 = 2\left[\frac{1}{\sqrt{1+t^2}}\right]^2 - 1 = \frac{2}{1+t^2} - 1 = \frac{2-1-t^2}{1+t^2} = \frac{1-t^2}{1+t^2} \quad (3.33)$$

$$\tan\theta_2 = \frac{Sin\theta_2}{Cos\theta_2} = \frac{\frac{2t}{1+t^2}}{\frac{1-t^2}{1+t^2}} = \frac{2t}{1+t^2} \times \frac{1+t^2}{1-t^2} = \frac{2t}{1-t^2} \quad (3.34)$$

Figure 3.7, is the representation for the angle θ, recall equation (3.29)

$$CSin\theta_2 + BCos\theta_2 = A \quad (3.29)$$

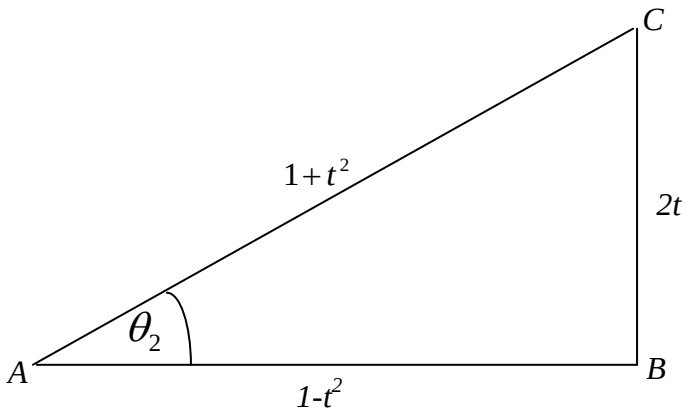

Figure 3.7: Trigonometry identity for the full angle, θ_2

Substituting equations (3.32) and (3.33) into equation (3.29), we have

$$C\left[\frac{2t}{1+t^2}\right] + B\left[\frac{1-t^2}{1+t^2}\right] = A \quad (3.35)$$

Multiplying through by $1+t^2$, we have

$$C(2t) + B(1-t^2) = A(1+t^2) \quad (3.36)$$

$$2Ct + B - Bt^2 = A + At^2 \quad (3.37)$$

$$A + At^2 - 2Ct - B + Bt^2 = 0 \quad (3.38)$$

$$(A+B)t^2 - 2Ct + (A-B) = 0 \quad (3.39)$$

Recall equations (3.26), (3.27) and (3.28)

$$A = \left(l_y + l_c\cos q_1 - l_f\sin q_2\right)^2 + \left(l_x + l_c\sin q_1 - l_f\cos q_2\right)^2 + l_t^2 - l_s^2 \quad (3.26)$$

$$B = 2\left(l_x + l_c\sin q_1 - l_f\cos q_2\right)\, l_t \quad (3.27)$$

$$C = 2\left(l_y + l_c\cos q_1 - l_f\sin q_2\right)\, l_t \quad (3.28)$$

Then equation (3.39) becomes

$$\left\{\begin{array}{l}\left\{\begin{array}{l}\left[\left(l_y+l_c\cos q_1-l_f\sin q_2\right)^2+\left(l_x+l_c\sin q_1-l_f\cos q_2\right)^2+l_t^2-l_s^2\right]+\\ \left[2\left(l_x+l_c\sin q_1-l_f\cos q_2\right)\,l_t\right]\end{array}\right\}t^2\\ -2\left[2\left(l_y+l_c\cos q_1-l_f\sin q_2\right)\,l_t\right]\,t\\ +\left\{\begin{array}{l}\left[\left(l_y+l_c\cos q_1-l_f\sin q_2\right)^2+\left(l_x+l_c\sin q_1-l_f\cos q_2\right)^2+l_t^2-l_s^2\right]-\\ \left[2\left(l_y+l_c\cos q_1-l_f\sin q_2\right)\,l_t\right]\end{array}\right\}\end{array}\right\}=0 \quad (3.40)$$

Equation (3.40) is a quadratic equation of the form $ax^2+bx+c=0$ where

$$a=\left\{\begin{array}{l}\left[\left(l_y+l_c\cos q_1-l_f\sin q_2\right)^2+\left(l_x+l_c\sin q_1-l_f\cos q_2\right)^2+l_t^2-l_s^2\right]+\\ \left[2\left(l_x+l_c\sin q_1-l_f\cos q_2\right)\,l_t\right]\end{array}\right\} \quad (3.41)$$

$$b=-2\left[2\left(l_y+l_c\cos q_1-l_f\sin q_2\right)\,l_t\right] \quad (3.42)$$

and

$$c=\left\{\begin{array}{l}\left[\left(l_y+l_c\cos q_1-l_f\sin q_2\right)^2+\left(l_x+l_c\sin q_1-l_f\cos q_2\right)^2+l_t^2-l_s^2\right]-\\ \left[2\left(l_y+l_c\cos q_1-l_f\sin q_2\right)\,l_t\right]\end{array}\right\} \quad (3.43)$$

The solution of equation (3.40) is then,

$$t=\left\{\begin{array}{l}\left(2\left[2\left(l_y+l_c\cos q_1-l_f\sin q_2\right)\,l_t\right]\right.\\ \pm\left\{\begin{array}{l}\left(2\left[2\left(l_y+l_c\cos q_1-l_f\sin q_2\right)\,l_t\right]\right)^2\\ -4\left\{\begin{array}{l}\left[\begin{array}{l}\left(l_y+l_c\cos q_1-l_f\sin q_2\right)^2+\\ \left(l_x+l_c\sin q_1-l_f\cos q_2\right)^2+l_t^2-l_s^2\end{array}\right]+\\ \left[2\left(l_x+l_c\sin q_1-l_f\cos q_2\right)\,l_t\right]\end{array}\right\}\times\\ \left\{\begin{array}{l}\left[\begin{array}{l}\left(l_y+l_c\cos q_1-l_f\sin q_2\right)^2+\\ \left(l_x+l_c\sin q_1-l_f\cos q_2\right)^2+l_t^2-l_s^2\end{array}\right]-\\ \left[2\left(l_y+l_c\cos q_1-l_f\sin q_2\right)\,l_t\right]\end{array}\right\}\end{array}\right\}^{0.5}\left.\right)\times\\ \left(2\left\{\begin{array}{l}\left[\left(l_y+l_c\cos q_1-l_f\sin q_2\right)^2+\left(l_x+l_c\sin q_1-l_f\cos q_2\right)^2+l_t^2-l_s^2\right]+\\ \left[2\left(l_x+l_c\sin q_1-l_f\cos q_2\right)\,l_t\right]\end{array}\right\}\right)^{-1}\end{array}\right\} \quad (3.44)$$

Recall $t=\tan\dfrac{\theta}{2}$

$$\tan\frac{\theta_2}{2}=\left\{\begin{array}{l}\left(2\left[2\left(l_y+l_c\cos q_1-l_f\sin q_2\right)\ l_t\right]\right.\\ \left.\pm\left\{\begin{array}{l}\left(2\left[2\left(l_y+l_c\cos q_1-l_f\sin q_2\right)\ l_t\right]\right)^2\\ -4\left\{\begin{bmatrix}\left(l_y+l_c\cos q_1-l_f\sin q_2\right)^2+\\ \left(l_x+l_c\sin q_1-l_f\cos q_2\right)^2+l_t^2-l_s^2\end{bmatrix}+\right\}\times\end{array}\right\}^{0.5}\right)\times\\ \left(2\left\{\begin{bmatrix}\left(l_y+l_c\cos q_1-l_f\sin q_2\right)^2+\\ \left(l_x+l_c\sin q_1-l_f\cos q_2\right)^2+l_t^2-l_s^2\end{bmatrix}-\right\}\right.\\ \left.\left\{\begin{bmatrix}\left(l_y+l_c\cos q_1-l_f\sin q_2\right)^2+\\ \left(l_x+l_c\sin q_1-l_f\cos q_2\right)^2+l_t^2-l_s^2\end{bmatrix}+\right\}\right)^{-1}\end{array}\right\}$$

(3.45)

$$\theta_2=2\tan^{-1}\left\{\begin{array}{l}\left(2\left[2\left(l_y+l_c\cos q_1-l_f\sin q_2\right)\ l_t\right]\right.\\ \left.\pm\left\{\begin{array}{l}\left(2\left[2\left(l_y+l_c\cos q_1-l_f\sin q_2\right)\ l_t\right]\right)^2\\ -4\left\{\begin{bmatrix}\left(l_y+l_c\cos q_1-l_f\sin q_2\right)^2+\\ \left(l_x+l_c\sin q_1-l_f\cos q_2\right)^2+l_t^2-l_s^2\end{bmatrix}+\right\}\times\end{array}\right\}^{0.5}\right)\times\\ \left(2\left\{\begin{bmatrix}\left(l_y+l_c\cos q_1-l_f\sin q_2\right)^2+\\ \left(l_x+l_c\sin q_1-l_f\cos q_2\right)^2+l_t^2-l_s^2\end{bmatrix}-\right\}\right.\\ \left.\left\{\begin{bmatrix}\left(l_y+l_c\cos q_1-l_f\sin q_2\right)^2+\\ \left(l_x+l_c\sin q_1-l_f\cos q_2\right)^2+l_t^2-l_s^2\end{bmatrix}+\right\}\right)^{-1}\end{array}\right\}$$

(3.46)

3.1.2.3 Velocity Analysis of Thigh and Shank Segments

The differentiation of the position loop equations Eq. 3.17a and Eq. 3.17b give the velocity loop equation. The resulting linear equations are:

$$\frac{\partial f_1}{\partial t} = l_c \dot{q}_1 \cos q_1 - l_f \dot{q}_2 \sin q_2 - l_s \dot{\theta}_1 \sin \theta_1 - l_t \dot{\theta}_2 \sin \theta_2 = 0 \qquad (3.47a)$$

$$\frac{\partial f_2}{\partial t} = -l_c \dot{q}_1 \sin q_1 + l_f \dot{q}_2 \cos q_2 + l_s \dot{\theta}_1 \cos \theta_1 + l_t \dot{\theta}_2 \cos \theta_2 = 0 \qquad (3.47b)$$

Which become

$$-l_s \dot{\theta}_1 \sin \theta_1 - l_t \dot{\theta}_2 \sin \theta_2 = -l_c \dot{q}_1 \cos q_1 + l_f \dot{q}_2 \sin q_2 \qquad (3.48a)$$

$$l_s \dot{\theta}_1 \cos \theta_1 + l_t \dot{\theta}_2 \cos \theta_2 = l_c \dot{q}_1 \sin q_1 - l_f \dot{q}_2 \cos q_2 \qquad (3.48b)$$

Which, when cast in matrix form becomes

$$\begin{bmatrix} -l_s \sin \theta_1 & -l_t \sin \theta_2 \\ l_s \cos \theta_1 & l_t \cos \theta_2 \end{bmatrix} \begin{Bmatrix} \dot{\theta}_1 \\ \dot{\theta}_2 \end{Bmatrix} = \dot{q}_1 \begin{Bmatrix} -l_c \cos q_1 \\ l_c \sin q_1 \end{Bmatrix} + \dot{q}_2 \begin{Bmatrix} l_f \sin q_2 \\ -l_f \cos q_2 \end{Bmatrix} \qquad (3.49)$$

Which become

$$J \begin{Bmatrix} \dot{\theta}_1 \\ \dot{\theta}_2 \end{Bmatrix} = \dot{q}_1 \begin{Bmatrix} -l_c \cos q_1 \\ l_c \sin q_1 \end{Bmatrix} + \dot{q}_2 \begin{Bmatrix} l_f \sin q_2 \\ -l_f \cos q_2 \end{Bmatrix} \qquad (3.50)$$

where

$J = \begin{bmatrix} -l_s \sin \theta_1 & -l_t \sin \theta_2 \\ l_s \cos \theta_1 & l_t \cos \theta_2 \end{bmatrix}$ is the system Jacobian matrix

The knee and thigh angular velocities are evaluated as:

$$\begin{Bmatrix} \dot{\theta}_1 \\ \dot{\theta}_2 \end{Bmatrix} = J^{-1} \dot{q}_1 \begin{Bmatrix} -l_c \cos q_1 \\ l_c \sin q_1 \end{Bmatrix} + J^{-1} \dot{q}_2 \begin{Bmatrix} l_f \sin q_2 \\ -l_f \cos q_2 \end{Bmatrix} \qquad (3.51)$$

Inverse of the System's Jacobian Matrix

The system Jacobian Matrix is

$$J = \begin{bmatrix} -l_s \sin \theta_1 & -l_t \sin \theta_2 \\ l_s \cos \theta_1 & l_t \cos \theta_2 \end{bmatrix} \qquad (3.52)$$

The determinant of Matrix J is

$$|J| = \begin{vmatrix} -l_s \sin\theta_1 & -l_t \sin\theta_2 \\ l_s \cos\theta_1 & l_t \cos\theta_2 \end{vmatrix} = (-l_s \sin\theta_1)(l_t \cos\theta_2) + (l_s \cos\theta_1)(l_t \sin\theta_2)$$

$$= l_s l_t \left(-(\sin\theta_1 \cos\theta_2) + (\cos\theta_1 \sin\theta_2)\right)$$

$$= l_s l_t \left((\cos\theta_1 \sin\theta_2) - (\sin\theta_1 \cos\theta_2)\right)$$

$$= l_s l_t \sin(\theta_2 - \theta_1) \tag{3.53}$$

The Cofactor, J^C , for Matrix *J*, is

$$J^C = \begin{bmatrix} l_t \cos\theta_2 & -l_s \cos\theta_1 \\ l_t \sin\theta_2 & -l_s \sin\theta_1 \end{bmatrix} \tag{3.54}$$

The adjoint of J^C is J^C Transpose (J^{CT}) which is

$$J^{CT} = \begin{bmatrix} l_t \cos\theta_2 & l_t \sin\theta_2 \\ -l_s \cos\theta_1 & -l_s \sin\theta_1 \end{bmatrix} \tag{3.55}$$

Inverse of Matrix J is

$$J^{-1} = \frac{AdjJ}{|J|} = \frac{1}{l_s l_t \sin(\theta_2 - \theta_1)} \begin{bmatrix} l_t \cos\theta_2 & l_t \sin\theta_2 \\ -l_s \cos\theta_1 & -l_s \sin\theta_1 \end{bmatrix} \tag{3.56}$$

Putting Eq. 3.56 into Eq. 3.51, Eq. 3.51 becomes

$$\begin{Bmatrix} \dot{\theta}_1 \\ \dot{\theta}_2 \end{Bmatrix} = \frac{1}{l_s l_t \sin(\theta_2 - \theta_1)} \begin{bmatrix} l_t \cos\theta_2 & l_t \sin\theta_2 \\ -l_s \cos\theta_1 & -l_s \sin\theta_1 \end{bmatrix} \left[\dot{q}_1 \begin{Bmatrix} -l_c \cos q_1 \\ l_c \sin q_1 \end{Bmatrix} + \dot{q}_2 \begin{Bmatrix} l_f \sin q_2 \\ -l_f \cos q_2 \end{Bmatrix} \right]$$

$$\begin{Bmatrix} \dot{\theta}_1 \\ \dot{\theta}_2 \end{Bmatrix} = \frac{1}{l_s l_t \sin(\theta_2 - \theta_1)} \begin{bmatrix} \dot{q}_1 \begin{bmatrix} l_t \cos\theta_2 & l_t \sin\theta_2 \\ -l_s \cos\theta_1 & -l_s \sin\theta_1 \end{bmatrix} \begin{Bmatrix} -l_c \cos q_1 \\ l_c \sin q_1 \end{Bmatrix} \\ + \dot{q}_2 \begin{bmatrix} l_t \cos\theta_2 & l_t \sin\theta_2 \\ -l_s \cos\theta_1 & -l_s \sin\theta_1 \end{bmatrix} \begin{Bmatrix} l_f \sin q_2 \\ -l_f \cos q_2 \end{Bmatrix} \end{bmatrix} \tag{3.57}$$

$$\begin{Bmatrix} \dot{\theta}_1 \\ \dot{\theta}_2 \end{Bmatrix} = \frac{1}{l_s l_t \sin(\theta_2 - \theta_1)} \begin{bmatrix} \dot{q}_1 \begin{Bmatrix} -l_t \cos\theta_2 l_c \cos q_1 + l_t \sin\theta_2 l_c \sin q_1 \\ l_s \cos\theta_1 l_c \cos q_1 - l_s \sin\theta_1 l_c \sin q_1 \end{Bmatrix} \\ + \dot{q}_2 \begin{Bmatrix} l_t \cos\theta_2 l_f \sin q_2 - l_t \sin\theta_2 l_f \cos q_2 \\ -l_s \cos\theta_1 l_f \sin q_2 + l_s \sin\theta_1 l_f \cos q_2 \end{Bmatrix} \end{bmatrix} \tag{3.58}$$

Shank angular velocity is

$$\dot{\theta}_1 = \frac{1}{l_s \sin(\theta_2 - \theta_1)} \begin{pmatrix} -\dot{q}_1 l_c (\cos\theta_2 \cos q_1 - \sin\theta_2 \sin q_1) + \\ \dot{q}_2 l_f (\cos\theta_2 \sin q_2 - \sin\theta_2 \cos q_2) \end{pmatrix}$$

$$\dot{\theta}_1 = \frac{\left(\dot{q}_2 l_f \sin(q_2 - \theta_2) - \dot{q}_1 l_c \cos(\theta_2 + q_1)\right)}{l_s \sin(\theta_2 - \theta_1)} \tag{3.59a}$$

Thigh angular velocity is

$$\dot{\theta}_2 = \frac{1}{l_t \sin(\theta_2 - \theta_1)} \begin{bmatrix} \dot{q}_1 l_c (\cos\theta_1 \cos q_1 - \sin\theta_1 \sin q_1) + \\ \dot{q}_2 l_f (-\cos\theta_1 \sin q_2 + \sin\theta_1 \cos q_2) \end{bmatrix}$$

$$= \frac{\left(\dot{q}_1 l_c \cos(\theta_1 + q_1) + \dot{q}_2 l_f \sin(\theta_1 - q_2)\right)}{l_t \sin(\theta_2 - \theta_1)} \tag{3.59b}$$

3.1.2.4 Acceleration Analysis of Thigh and Shank Segments

The acceleration loop equation is determined by differentiating velocity loop equations and the resulting system of linear equations is

$$\frac{\partial^2 f_1}{\partial t^2} = \begin{pmatrix} l_c(-\dot{q}_1^2 \sin q_1 + \ddot{q}_1 \cos q_1) - l_f(\dot{q}_2^2 \cos q_2 + \ddot{q}_2 \sin q_2) - \\ l_s(\dot{\theta}_1^2 \cos\theta_1 + \ddot{\theta}_1 \sin\theta_1) - l_t(\dot{\theta}_2^2 \cos\theta_2 + \ddot{\theta}_2 \sin\theta_2) \end{pmatrix} = 0 \tag{3.60a}$$

$$\frac{\partial^2 f_2}{\partial t^2} = \begin{pmatrix} -l_c(\dot{q}_1^2 \cos q_1 + \ddot{q}_1 \sin q_1) + l_f(-\dot{q}_2^2 \sin q_2 + \ddot{q}_2 \cos q_2) + \\ l_s(-\dot{\theta}_1^2 \sin\theta_1 + \ddot{\theta}_1 \cos\theta_1) + l_t(-\dot{\theta}_2^2 \sin\theta_2 + \ddot{\theta}_2 \cos\theta_2) \end{pmatrix} = 0 \tag{3.60b}$$

Equation 3.60 a and b become

$$-l_s \ddot{\theta}_1 \sin\theta_1 - l_t \ddot{\theta}_2 \sin\theta_2 = \begin{pmatrix} \dot{q}_1^2 l_c \sin q_1 - \ddot{q}_1 l_c \cos q_1 + l_f \dot{q}_2^2 \cos q_2 + \\ l_f \ddot{q}_2 \sin q_2 + l_s \dot{\theta}_1^2 \cos\theta_1 + l_t \dot{\theta}_2^2 \cos\theta_2 \end{pmatrix}$$

(3.61a)

$$l_s \ddot{\theta}_1 \cos\theta_1 + l_t \ddot{\theta}_2 \cos\theta_2 = \begin{pmatrix} l_c \dot{q}_1^2 \cos q_1 + l_c \ddot{q}_1 \sin q_1 + \dot{q}_2^2 l_f \sin q_2 - \\ \ddot{q}_2 l_f \cos q_2 - \dot{\theta}_1^2 l_s \sin\theta_1 + \dot{\theta}_2^2 l_t \sin\theta_2 \end{pmatrix} \tag{3.61b}$$

Cast in matrix form, Eq. 3.61 a and b becomes

$$\begin{bmatrix} -l_s \sin\theta_1 & -l_t \sin\theta_2 \\ l_s \cos\theta_1 & l_t \cos\theta_2 \end{bmatrix} \begin{Bmatrix} \ddot{\theta}_1 \\ \ddot{\theta}_2 \end{Bmatrix} = \begin{Bmatrix} \dot{q}_1^2 \begin{Bmatrix} l_c \sin q_1 \\ l_c \cos q_1 \end{Bmatrix} + \dot{q}_2^2 \begin{Bmatrix} l_f \cos q_2 \\ l_f \sin q_2 \end{Bmatrix} + \dot{\theta}_1^2 \begin{Bmatrix} l_s \cos\theta_1 \\ l_s \sin\theta_1 \end{Bmatrix} + \\ \dot{\theta}_2^2 \begin{Bmatrix} l_t \cos\theta_2 \\ l_t \sin\theta_2 \end{Bmatrix} - \ddot{q}_1 \begin{Bmatrix} l_c \cos q_1 \\ l_c \sin q_1 \end{Bmatrix} + \ddot{q}_2 \begin{Bmatrix} l_f \sin q_2 \\ -l_f \cos q_2 \end{Bmatrix} \end{Bmatrix} \tag{3.62}$$

Putting the system's Jacobian matrix, Eq. 3.62 becomes

$$J\begin{Bmatrix}\ddot{\theta}_1\\ \ddot{\theta}_2\end{Bmatrix}=\begin{pmatrix}\dot{q}_1^2\begin{Bmatrix}l_c\sin q_1\\ l_c\cos q_1\end{Bmatrix}+\dot{q}_2^2\begin{Bmatrix}l_f\cos q_2\\ l_f\sin q_2\end{Bmatrix}+\dot{\theta}_1^2\begin{Bmatrix}l_s\cos\theta_1\\ l_s\sin\theta_1\end{Bmatrix}+\\ \dot{\theta}_2^2\begin{Bmatrix}l_t\cos\theta_2\\ l_t\sin\theta_2\end{Bmatrix}-\ddot{q}_1\begin{Bmatrix}l_c\cos q_1\\ l_c\sin q_1\end{Bmatrix}+\ddot{q}_2\begin{Bmatrix}l_f\sin q_2\\ -l_f\cos q_2\end{Bmatrix}\end{pmatrix} \tag{3.63}$$

The solution for Eq. 3.63 is:

$$\begin{Bmatrix}\ddot{\theta}_1\\ \ddot{\theta}_2\end{Bmatrix}=\left(J^{-1}\left[\begin{matrix}\dot{q}_1^2\begin{Bmatrix}l_c\sin q_1\\ l_c\cos q_1\end{Bmatrix}+\dot{q}_2^2\begin{Bmatrix}l_f\cos q_2\\ l_f\sin q_2\end{Bmatrix}+\dot{\theta}_1^2\begin{Bmatrix}l_s\cos\theta_1\\ l_s\sin\theta_1\end{Bmatrix}+\\ \dot{\theta}_2^2\begin{Bmatrix}l_t\cos\theta_2\\ l_t\sin\theta_2\end{Bmatrix}-\ddot{q}_1\begin{Bmatrix}l_c\cos q_1\\ l_c\sin q_1\end{Bmatrix}+\ddot{q}_2\begin{Bmatrix}l_f\sin q_2\\ -l_f\cos q_2\end{Bmatrix}\end{matrix}\right]\right) \tag{3.64}$$

Putting Eq. 3.56 into Eq. 3.64 gives

$$\begin{Bmatrix}\ddot{\theta}_1\\ \ddot{\theta}_2\end{Bmatrix}=\frac{\begin{bmatrix}l_t\cos\theta_2 & l_t\sin\theta_2\\ -l_s\cos\theta_1 & -l_s\sin\theta_1\end{bmatrix}}{l_s l_t\sin(\theta_2-\theta_1)}\left(\left[\begin{matrix}\dot{q}_1^2\begin{Bmatrix}l_c\sin q_1\\ l_c\cos q_1\end{Bmatrix}+\dot{q}_2^2\begin{Bmatrix}l_f\cos q_2\\ l_f\sin q_2\end{Bmatrix}+\\ \dot{\theta}_1^2\begin{Bmatrix}l_s\cos\theta_1\\ l_s\sin\theta_1\end{Bmatrix}+\dot{\theta}_2^2\begin{Bmatrix}l_t\cos\theta_2\\ l_t\sin\theta_2\end{Bmatrix}+\\ \ddot{q}_1\begin{Bmatrix}l_c\cos q_1\\ l_c\sin q_1\end{Bmatrix}+\ddot{q}_2\begin{Bmatrix}l_f\sin q_2\\ -l_f\cos q_2\end{Bmatrix}\end{matrix}\right]\right) \tag{3.65}$$

$$\begin{Bmatrix}\ddot{\theta}_1\\ \ddot{\theta}_2\end{Bmatrix}=\frac{1}{l_s l_t\sin(\theta_2-\theta_1)}\left(\left[\begin{matrix}\dot{q}_1^2\begin{bmatrix}l_t\cos\theta_2 & l_t\sin\theta_2\\ -l_s\cos\theta_1 & -l_s\sin\theta_1\end{bmatrix}\begin{Bmatrix}l_c\sin q_1\\ l_c\cos q_1\end{Bmatrix}+\\ \dot{q}_2^2\begin{bmatrix}l_t\cos\theta_2 & l_t\sin\theta_2\\ -l_s\cos\theta_1 & -l_s\sin\theta_1\end{bmatrix}\begin{Bmatrix}l_f\cos q_2\\ l_f\sin q_2\end{Bmatrix}+\\ \dot{\theta}_1^2\begin{bmatrix}l_t\cos\theta_2 & l_t\sin\theta_2\\ -l_s\cos\theta_1 & -l_s\sin\theta_1\end{bmatrix}\begin{Bmatrix}l_s\cos\theta_1\\ l_s\sin\theta_1\end{Bmatrix}+\\ \dot{\theta}_2^2\begin{bmatrix}l_t\cos\theta_2 & l_t\sin\theta_2\\ -l_s\cos\theta_1 & -l_s\sin\theta_1\end{bmatrix}\begin{Bmatrix}l_t\cos\theta_2\\ l_t\sin\theta_2\end{Bmatrix}-\\ \ddot{q}_1\begin{bmatrix}l_t\cos\theta_2 & l_t\sin\theta_2\\ -l_s\cos\theta_1 & -l_s\sin\theta_1\end{bmatrix}\begin{Bmatrix}l_c\cos q_1\\ l_c\sin q_1\end{Bmatrix}+\\ \ddot{q}_2\begin{bmatrix}l_t\cos\theta_2 & l_t\sin\theta_2\\ -l_s\cos\theta_1 & -l_s\sin\theta_1\end{bmatrix}\begin{Bmatrix}l_f\sin q_2\\ -l_f\cos q_2\end{Bmatrix}\end{matrix}\right]\right) \tag{3.66}$$

$$\begin{Bmatrix}\ddot{\theta}_1\\ \ddot{\theta}_2\end{Bmatrix}=\frac{1}{l_s l_t \sin(\theta_2-\theta_1)}\left(\begin{bmatrix}\dot{q}_1^2\begin{Bmatrix} l_t\cos\theta_2(l_c\sin q_1)+l_t\sin\theta_2(l_c\cos q_1)\\ -(l_s\cos\theta_1(l_c\sin q_1)+l_s\sin\theta_1(l_c\cos q_1))\end{Bmatrix}+\\ \dot{q}_2^2\begin{Bmatrix}(l_t\cos\theta_2(l_f\cos q_2)+l_t\sin\theta_2(l_f\sin q_2))\\ -(l_s\cos\theta_1(l_f\cos q_2)+l_s\sin\theta_1(l_f\sin q_2))\end{Bmatrix}+\\ \dot{\theta}_1^2\begin{Bmatrix} l_t\cos\theta_2(l_s\cos\theta_1)+l_t\sin\theta_2(l_s\sin\theta_1)\\ -(l_s\cos\theta_1(l_s\cos\theta_1)+l_s\sin\theta_1(l_s\sin\theta_1))\end{Bmatrix}+\\ \dot{\theta}_2^2\begin{Bmatrix}(l_t\cos\theta_2(l_t\cos\theta_2)+l_t\sin\theta_2(l_t\sin\theta_2))\\ -(l_s\cos\theta_1(l_t\cos\theta_2)+l_s\sin\theta_1(l_t\sin\theta_2))\end{Bmatrix}-\\ \ddot{q}_1\begin{Bmatrix} l_t\cos\theta_2(l_c\cos q_1)+l_t\sin\theta_2(l_c\sin q_1)\\ -(l_s\cos\theta_1(l_c\cos q_1)+l_s\sin\theta_1(l_c\sin q_1))\end{Bmatrix}-\\ \ddot{q}_2\begin{Bmatrix} l_t\cos\theta_2(l_f\sin q_2)-l_t\sin\theta_2(l_f\cos q_2)\\ -l_s\cos\theta_1(l_f\sin q_2)+l_s\sin\theta_1(l_f\cos q_2)\end{Bmatrix}\end{bmatrix}\right) \quad (3.67)$$

Eq. 3.67 is evaluated as

$$\begin{Bmatrix}\ddot{\theta}_1\\ \ddot{\theta}_2\end{Bmatrix}=\frac{1}{l_s l_t \sin(\theta_2-\theta_1)}\left(\begin{bmatrix}\dot{q}_1^2\begin{Bmatrix} l_t l_c\sin(\theta_2+q_1)\\ -l_s l_c(\sin(\theta_1+q_1))\end{Bmatrix}+\dot{q}_2^2\begin{Bmatrix} l_t l_f(\cos(\theta_2-q_2))\\ -l_s l_f\cos(q_2-\theta_1)\end{Bmatrix}+\\ \dot{\theta}_1^2\begin{Bmatrix} l_t l_s\cos(\theta_2-\theta_1)\\ -l_s l_s\end{Bmatrix}+\dot{\theta}_2^2\begin{Bmatrix} -l_t l_t\\ l_s l_t\cos(\theta_2-\theta_1)\end{Bmatrix}-\\ \ddot{q}_1\begin{Bmatrix} l_t l_c\cos(\theta_2-q_1)\\ -(l_s l_c\cos(\theta_1-q_1))\end{Bmatrix}+\ddot{q}_2\begin{Bmatrix} l_t l_f\sin(q_2-\theta_2)\\ -(l_s l_f\sin(\theta_1-q_2))\end{Bmatrix}\end{bmatrix}\right) \quad (3.68)$$

From Eq. 3.68, the angular acceleration of the Shank is

$$\ddot{\theta}_1=\frac{1}{l_s\sin(\theta_2-\theta_1)}\left(\begin{bmatrix}\dot{q}_1^2 l_c\sin(\theta_2+q_1)+\dot{q}_2^2 l_f(\cos(\theta_2-q_2))+\\ \dot{\theta}_1^2 l_s\cos(\theta_2-\theta_1)-\dot{\theta}_2^2 l_t-\\ \ddot{q}_1 l_c\cos(\theta_2-q_1)+\ddot{q}_2 l_f\sin(q_2-\theta_2)\end{bmatrix}\right) \quad (3.69a)$$

and the angular acceleration of the thigh segment is

$$\ddot{\theta}_2=\frac{1}{l_t\sin(\theta_2-\theta_1)}\left(\begin{bmatrix}-\dot{q}_1^2 l_c(\sin(\theta_1+q_1))-\dot{q}_2^2 l_f\cos(q_2-\theta_1)-\\ \dot{\theta}_1^2 l_s+\dot{\theta}_2^2 l_t\cos(\theta_2-\theta_1)+\\ \ddot{q}_1(l_c\cos(\theta_1-q_1))+\ddot{q}_2(l_f\sin(\theta_1-q_2))\end{bmatrix}\right) \quad (3.69b)$$

3.1.2.5 Position, Angular Velocity and Angular Acceleration of the Foot Segment

In Figure 3.4 above, in order to obtain the expression for the foot angle q_2, the two links, the crank arm and the foot segment, are assumed to form two sides of triangle

BCD. This is shown in Figure 3.8 below. A horizontal line is drawn from point C to point E to form a perpendicular to line BD. If line CE is named *h*, then angle q_2 can be obtained from the figure as follows:

$$h = l_f \sin q_2 = l_c \sin q_1 \tag{3.70}$$

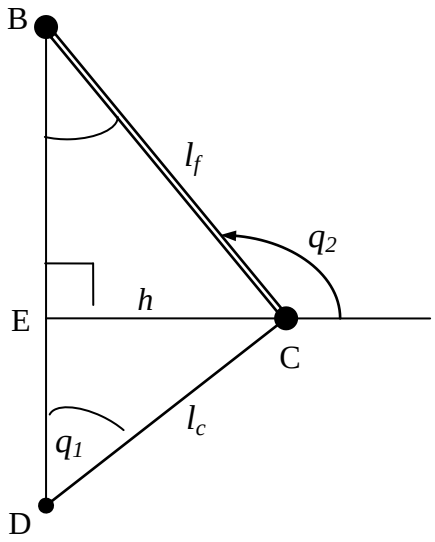

Figure 3.8: Space analysis of the crank arm and foot segment

$$l_f \sin q_2 = l_c \sin q_1 \tag{3.71}$$

$$q_2 = \sin^{-1}\left(\frac{l_c \sin q_1}{l_f}\right) \tag{3.72}$$

The velocity of the foot angle is obtained by taken the time derivatives of the foot angle:

$$\frac{d}{dt}(q_2) = \frac{d}{dt}\left\{\sin^{-1}\left(\frac{l_c \sin q_1}{l_f}\right)\right\} \tag{3.73}$$

$$\dot{q}_2 = \frac{-l_c \dot{q}_1 \cos q_1}{l_f \sqrt{\left(1 - \left(\frac{l_c}{l_f}\sin q_1\right)^2\right)}} \tag{3.74}$$

The acceleration of the foot is given by the take the time derivatives of the velocity expression above, assuming the differentiation of a quotient of two functions:

$$\frac{d}{dt}\left(\dot{q}_2\right)=\frac{d}{dt}\left(\frac{-l_c\dot{q}_1\cos q_1}{l_f\sqrt{\left(1-\left(\frac{l_c}{l_f}\sin q_1\right)^2\right)}}\right) \tag{3.75}$$

If $u=-l_c\dot{q}_1\cos q_1$, $\dot{u}=l_c\left(\dot{q}_1^2\sin q_1-\ddot{q}_1\cos q_1\right)$

and $v=l_f\sqrt{\left(1-\left(\frac{l_c}{l_f}\sin q_1\right)^2\right)}$, $\dot{v}=l_c\dot{q}_1\cos q_1\left[1-\left(\frac{l_c}{l_f}\sin q_1\right)^2\right]^{-1/2}$

$$\frac{d}{dt}\left(\dot{q}_2\right)=\ddot{q}_2=\frac{u}{v}=\frac{v\dot{u}-u\dot{v}}{v^2} \tag{3.76}$$

$$\ddot{q}_2=\frac{\left\{\begin{array}{l} l_f\sqrt{\left(1-\left(\frac{l_c}{l_f}\sin q_1\right)^2\right)}\left(l_c\left(\dot{q}_1^2\sin q_1-\ddot{q}_1\cos q_1\right)\right) \\ -\left(-l_c\dot{q}_1\cos q_1\right)\left(l_c\dot{q}_1\cos q_1\left[1-\left(\frac{l_c}{l_f}\sin q_1\right)^2\right]^{-1/2}\right)\end{array}\right\}}{l_f^2\left(1-\left(\frac{l_c}{l_f}\sin q_1\right)^2\right)} \tag{3.77}$$

$$\ddot{q}_2=\frac{\left\{\begin{array}{l} l_f\sqrt{\left(1-\left(\frac{l_c}{l_f}\sin q_1\right)^2\right)}\left(l_c\left(\dot{q}_1^2\sin q_1-\ddot{q}_1\cos q_1\right)\right)+ \\ \left(\left(l_c\dot{q}_1\cos q_1\right)^2\left[1-\left(\frac{l_c}{l_f}\sin q_1\right)^2\right]^{-1/2}\right)\end{array}\right\}}{l_f^2\left(1-\left(\frac{l_c}{l_f}\sin q_1\right)^2\right)} \tag{3.78}$$

3.1.3 Centre of Mass Position, Velocity and Acceleration Loop Equations

The position, velocity and acceleration loop equations for the centre of mass of the components are determined as follows:

3.1.3.1 The Crank Arm

The position of the centre of mass of the crank arm with respect to the horizontal and vertical axes is given by

$$X_{CCG} = \frac{1}{2} l_c \sin q_1 \tag{3.79a}$$

$$Y_{CCG} = \frac{1}{2} l_c \cos q_1 \tag{3.79b}$$

The velocity of the centre of mass of the crank arm with respect to the horizontal and vertical axes is given by

$$\dot{X}_{CCG} = \frac{1}{2} l_c \left[\dot{q}_1 \cos q_1\right] = \frac{\dot{q}_1}{2} l_c \cos q_1 \tag{3.80a}$$

$$\dot{Y}_{CCG} = \frac{1}{2} l_c \left[-\dot{q}_1 \sin q_1\right] = -\frac{\dot{q}_1}{2} l_c \sin q_1 \tag{3.80b}$$

The acceleration of the centre of mass of the crank arm with respect to the horizontal and vertical axes is given by:

$$\ddot{X}_{CCG} = \frac{1}{2} l_c \left(-\dot{q}_1^2 \sin q_1 + \ddot{q}_1 \cos q_1\right) = -\frac{1}{2} \dot{q}_1^2 l_c \sin q_1 + \frac{1}{2} \ddot{q}_1 l_c \cos q_1 \tag{3.81a}$$

$$\ddot{Y}_{CCG} = -\frac{1}{2} l_c \left(\dot{q}_1^2 \cos q_1 + \ddot{q}_1 \sin q_1\right) = -\frac{1}{2} \dot{q}_1^2 l_c \cos q_1 - \frac{1}{2} \ddot{q}_1 l_c \sin q_1 \tag{3.81b}$$

3.1.3.2 The Foot Segment

The position of the centre of mass of the foot segment with respect to the horizontal and vertical axes is given by:

$$X_{FCG} = l_c \sin q_1 + \frac{1}{2} l_f \cos q_2 \tag{3.82a}$$

$$Y_{FCG} = l_c \cos q_1 + \frac{1}{2} l_f \sin q_2 \tag{3.82b}$$

The velocity of the centre of mass of the foot with respect to the horizontal and vertical axes is given by:

$$\dot{X}_{FCG} = l_c \dot{q}_1 \cos q_1 - \frac{\dot{q}_2}{2} l_f \sin q_2 \tag{3.83a}$$

$$\dot{Y}_{FCG} = -l_c \dot{q}_1 \sin q_1 + \frac{\dot{q}_2}{2} l_f \cos q_2 \tag{3.83b}$$

The acceleration of the centre of mass of the foot segment with respect to the horizontal and vertical axes is given by:

$$\ddot{X}_{FCG} = l_c\left(-\dot{q}_1^2 \sin q_1 + \ddot{q}_1 \cos q_1\right) - \frac{1}{2} l_f \left(\dot{q}_2^2 \cos q_2 + \ddot{q}_2 \sin q_2\right) \tag{3.84a}$$

$$\ddot{Y}_{FCG} = -l_c\left(\dot{q}_1^2 \cos q_1 + \ddot{q}_1 \sin q_1\right) + \frac{1}{2} l_f \left(-\dot{q}_2^2 \sin q_2 + \ddot{q}_2 \cos q_2\right) \tag{3.84b}$$

3.1.3.3 The Shank Segment

The position of the centre of mass of the shank segment with respect to the horizontal and vertical axes is given by:

$$X_{SCG} = l_c \sin q_1 + l_f \cos q_2 + \frac{1}{2} l_s \cos\theta_1 \tag{3.85a}$$

$$Y_{SCG} = l_c \cos q_1 + l_f \sin q_2 + \frac{1}{2} l_s \sin\theta_1 \tag{3.85b}$$

The velocity of the centre of mass of the shank segment with respect to the horizontal and vertical axes is given by:

$$\dot{X}_{SCG} = l_c \dot{q}_1 \cos q_1 - l_f \dot{q}_2 \sin q_2 - \frac{1}{2} l_s \dot{\theta}_1 \sin\theta_1 \tag{3.86a}$$

$$\dot{Y}_{SCG} = -l_c \dot{q}_1 \sin q_1 + l_f \dot{q}_2 \cos q_2 + \frac{1}{2} l_s \dot{\theta}_1 \cos\theta_1 \tag{3.86b}$$

The acceleration of the centre of mass of the shank segment with respect to the horizontal and vertical axes is given by:

$$\ddot{X}_{SCG} = \begin{pmatrix} l_c\left(-\dot{q}_1^2 \sin q_1 + \ddot{q}_1 \cos q_1\right) - l_f \left(\dot{q}_2^2 \cos q_2 + \ddot{q}_2 \sin q_2\right) - \\ \frac{1}{2} l_s \left(\dot{\theta}_1^2 \cos\theta_1 + \ddot{\theta}_1 \sin\theta_1\right) \end{pmatrix} \tag{3.87a}$$

$$\ddot{Y}_{SCG} = \begin{pmatrix} -l_c\left(\dot{q}_1^2 \cos q_1 + \ddot{q}_1 \sin q_1\right) + l_f \left(-\dot{q}_2^2 \sin q_2 + \ddot{q}_2 \cos q_2\right) + \\ \frac{1}{2} l_s \left(-\dot{\theta}_1^2 \sin\theta_1 + \ddot{\theta}_1 \cos\theta_1\right) \end{pmatrix} \tag{3.87b}$$

3.1.3.4 The Thigh Segment

The position of the centre of mass of the thigh segment with respect to the horizontal and vertical axes is given by:

$$X_{TCG} = l_c \sin q_1 + l_f \cos q_2 + l_s \cos\theta_1 + \frac{1}{2} l_t \cos\theta_2 \tag{3.88a}$$

$$Y_{TCG} = l_c \cos q_1 + l_f \sin q_2 + l_s \sin\theta_1 + \frac{1}{2} l_t \sin\theta_2 \tag{3.88b}$$

The velocity of the centre of mass of the thigh segment with respect to the horizontal and vertical axes is given by:

$$\dot{X}_{TCG} = l_c \dot{q}_1 \cos q_1 - l_f \dot{q}_2 \sin q_2 - l_s \dot{\theta}_1 \sin\theta_1 - \frac{1}{2} l_t \dot{\theta}_2 \sin\theta_2 \tag{3.89a}$$

$$\dot{Y}_{TCG} = -l_c \dot{q}_1 \sin q_1 + l_f \dot{q}_2 \cos q_2 + l_s \dot{\theta}_1 \cos\theta_1 + \frac{1}{2} l_t \dot{\theta}_2 \cos\theta_2 \tag{3.89b}$$

The acceleration of the centre of mass of the thigh segment with respect to the horizontal and vertical axes is given by:

$$\ddot{X}_{TCG} = \begin{pmatrix} l_c\left(-\dot{q}_1^2 \sin q_1 + \ddot{q}_1 \cos q_1\right) - l_f\left(\dot{q}_2^2 \cos q_2 + \ddot{q}_2 \sin q_2\right) - \\ l_s\left(\dot{\theta}_1^2 \cos\theta_1 + \ddot{\theta}_1 \sin\theta_1\right) - \frac{1}{2} l_t\left(\dot{\theta}_2^2 \cos\theta_2 + \ddot{\theta}_2 \sin\theta_2\right) \end{pmatrix} \tag{3.90a}$$

$$\ddot{Y}_{TCG} = \begin{pmatrix} l_c\left(\dot{q}_1^2 \cos q_1 + \ddot{q}_1 \sin q_1\right) + l_f\left(-\dot{q}_2^2 \sin q_2 + \ddot{q}_2 \cos q_2\right) + \\ l_s\left(-\dot{\theta}_1^2 \sin\theta_1 + \ddot{\theta}_1 \cos\theta_1\right) + \frac{1}{2} l_t\left(-\dot{\theta}_2^2 \sin\theta_2 + \ddot{\theta}_2 \cos\theta_2\right) \end{pmatrix} \tag{3.90b}$$

3.1.4 Equations of Motion of Lower Limb Segments

Newton's Second Law of motion is applied to each of the lower limb segments schematized by Figure 3.9 to obtain the equations of motion for each segments.

The equation of motion of the foot segment is given by:

$$F_R \sin q_1 - F_{ay} - m_f g = m_f \ddot{Y}_{FCG} \tag{3.91a}$$

$$F_{ax} - M_{BR}(\ddot{x} + \mu g) + m_f \ddot{x} = m_f \ddot{X}_{FCG} \tag{3.91b}$$

$$-M_a - I_{FCG}\ddot{q}_2 + \frac{l_f}{2}\left(F_{ay}\sin q_2 - F_{ax}\cos q_2 - F_R \sin q_1 \sin q_2 + M_{BR}(\ddot{x}+\mu g)\cos q_2\right) = 0$$

$$-M_a - I_{FCG}\ddot{q}_2 + \frac{l_f}{2}\left(F_{ay}\sin q_2 - F_{ax}\cos q_2 - F_R \sin q_1 \sin q_2 + F_R \cos q_1 \cos q_2\right) = 0$$

$$-M_a - I_{FCG}\ddot{q}_2 + \frac{l_f}{2}\left(F_{ay}\sin q_2 - F_{ax}\cos q_2 + F_R \cos(q_1 + q_2)\right) = 0 \quad (3.91c)$$

The equation of motion of the shank segment is given by:

$$F_{ay} - F_{ky} - m_s g = m_s \ddot{Y}_{SCG} \quad (3.92a)$$

$$F_{kx} - F_{ax} + m_s \ddot{x} = m_s \ddot{X}_{SCG} \quad (3.92b)$$

$$-M_k - I_{SCG}\ddot{\theta}_1 + \frac{l_s}{2}\left(F_{ky}\sin\theta_1 - F_{kx}\cos\theta_1 + F_{ay}\sin\theta_1 - F_{ax}\cos\theta_1\right) + M_a = 0 \quad (3.92c)$$

The equation of motion of the thigh segment is given by:

$$F_{ky} - F_{hy} - m_t g = m_t \ddot{Y}_{TCG} \quad (3.93a)$$

$$F_{hx} - F_{kx} + m_t \ddot{x} = m_t \ddot{X}_{TCG} \quad (3.93b)$$

$$-M_t - I_{TCG}\ddot{\theta}_2 + \frac{l_t}{2}\left(F_{hy}\sin\theta_1 - F_{hx}\cos\theta_1 + F_{ky}\sin\theta_1 - F_{kx}\cos\theta_1\right) + M_K = 0 \quad (3.93c)$$

3.1.5 Reaction forces at the Joints

Figure 3.9 is the free body diagram of the lower limb segments. The joint reaction forces are obtained by resolving all forces in *x* and *y* directions

3.1.5.1 Reaction Forces at the foot Joints

The reaction forces of the foot can be obtained by analyzing the foot bone segment in Figure 3.9

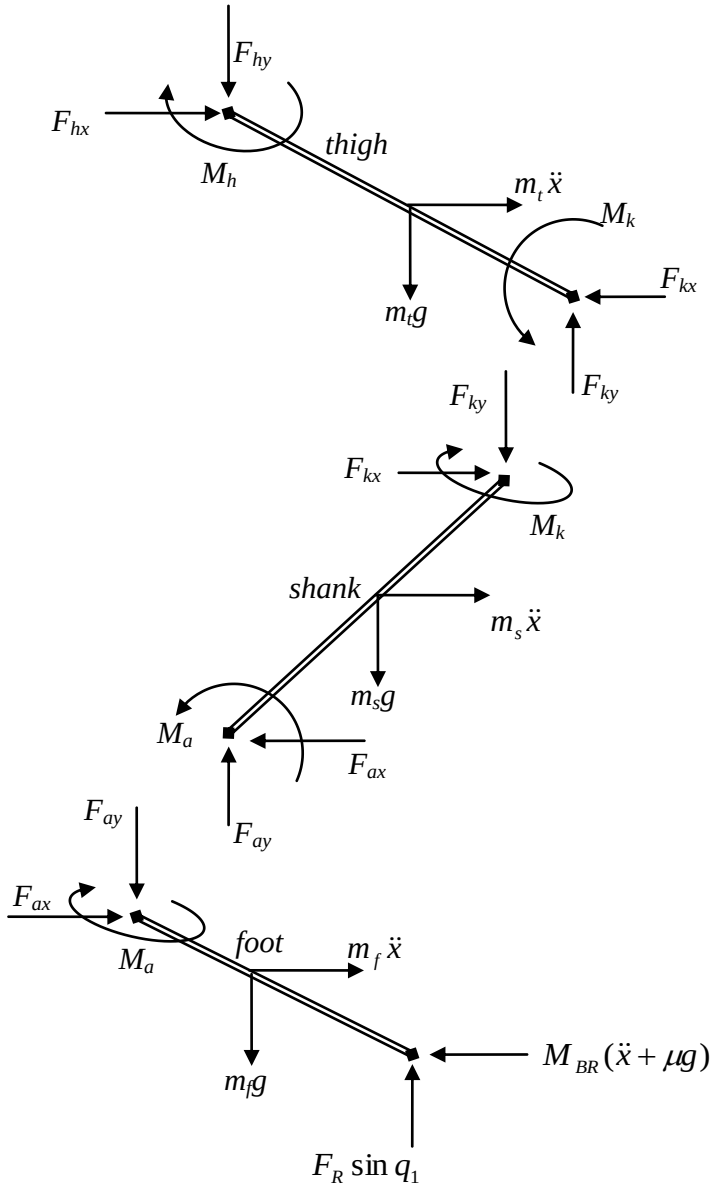

Figure 3.9: Free-body diagram of the lower limb segments

$$\sum F_y = 0 : \uparrow +ve$$

$$F_R \sin q_1 - F_{ay} - m_f g = m_f \ddot{Y}_{FCG}$$

$$F_{ay} = F_R \sin q_1 - m_f (g + \ddot{Y}_{FCG}) \tag{3.94}$$

$$\sum F_x = 0 : \rightarrow +ve$$

$$F_{ax} - M_{BR}(\ddot{x} + \mu g) + m_f \ddot{x} = m_f \ddot{X}_{FCG}$$

$$F_{ax} = M_{BR}(\ddot{x} + \mu g) + m_f (\ddot{X}_{FCG} - \ddot{x}) \tag{3.95}$$

But $\ddot{x} = a_x = \dfrac{r_{bw} \times \ddot{q}_1 \times T_{wheel}}{T_{cog}}$

Therefore, $F_{ax} = M_{BR}(\ddot{x} + \mu g) + m_f \left(\ddot{X}_{FCG} - \dfrac{r_{bw} \times \ddot{q}_1 \times T_{wheel}}{T_{cog}} \right)$ (3.96)

3.1.5.2 Reaction Forces at the Shank Joints

The reaction forces for the shank bone can be obtained by analyzing the shank segment in Figure 3.9,

$\sum F_y = 0 : \uparrow +ve$

$$F_{ay} - F_{ky} - m_s g = m_f \ddot{Y}_{SCG}$$

$$F_{ky} = F_{ay} - m_s(\ddot{Y}_{SCG} + g) \quad (3.97)$$

$\sum F_x = 0 : \rightarrow +ve$

$$F_{kx} - F_{ax} + m_s \ddot{x} = m_s \ddot{X}_{SCG}$$

$$F_{kx} = F_{ax} + m_s(\ddot{X}_{SCG} - \ddot{x})$$

But $\ddot{x} = a_x = \dfrac{r_{bw} \times \ddot{q}_1 \times T_{wheel}}{T_{cog}}$

$$F_{kx} = F_{ax} + m_s \left(\ddot{X}_{SCG} - \frac{r_{bw} \times \ddot{q}_1 \times T_{wheel}}{T_{cog}} \right) \quad (3.98)$$

3.1.5.3 Reaction Forces at the thigh Joints

The reaction forces for the thigh segment is obtained by analyzing the thigh segment shown in Figure 3.9,

$\sum F_y = 0 : \uparrow +ve$

$$F_{ky} - F_{hy} - m_t g = m_t \ddot{Y}_{TCG}$$

$$F_{hy} = F_{ky} - m_t(\ddot{Y}_{TCG} + g) \quad (3.99)$$

$\sum F_x = 0 : \rightarrow +ve$

$$F_{hx} - F_{kx} + m_t \ddot{x} = m_t \ddot{X}_{TCG}$$

$$F_{hx} = F_{kx} + m_t(\ddot{X}_{TCG} - \ddot{x}) \tag{3.100}$$

But $\ddot{x} = a_x = \dfrac{r_{bw} \times \ddot{q}_1 \times T_{wheel}}{T_{cog}}$

Therefore, $F_{hx} = F_{kx} + m_t\left(\ddot{X}_{TCG} - \dfrac{r_{bw} \times \ddot{q}_1 \times T_{wheel}}{T_{cog}}\right)$ (3.101)

3.1.6 Joint Moments

Joint moment equations are derived using the free body diagram of lower limb segments in Figure 3.9 and analyzing the segments individually.

3.1.6.1 The Foot Segment

Taking the moments about the centre of gravity of the foot segment in Figure 3.9, we have,

$$-M_a - I_{FCG}\ddot{q}_2 + \frac{l_f}{2}\left(F_{ay}\sin q_2 - F_{ax}\cos q_2 + F_R \sin q_1 \sin q_2 - M_{BR}(\ddot{x} + \mu g)\cos q_2\right) = 0$$

$$-M_a - I_{FCG}\ddot{q}_2 + \frac{l_f}{2}\left(F_{ay}\sin q_2 - F_{ax}\cos q_2 - (F_R \cos q_1 \cos q_2 - F_R \sin q_1 \sin q_2)\right) = 0$$

$$-M_a - I_{FCG}\ddot{q}_2 + \frac{l_f}{2}\left(F_{ay}\sin q_2 - F_{ax}\cos q_2 - F_R \cos(q_1 + q_2)\right) = 0 \tag{3.102}$$

The ankle joint moment is

$$M_a = -I_{FCG}\ddot{q}_2 + \frac{l_f}{2}\left(F_{ay}\sin q_2 - F_{ax}\cos q_2 - F_R \cos(q_1 + q_2)\right) \tag{3.103}$$

Putting the values of F_{ay} in Eq. 3.94 and F_{ax} in Eq. 3.96 into Eq. 3.103 gives

$$M_a = -I_{FCG}\ddot{q}_2 + \frac{l_f}{2}\left(\begin{array}{l}\left(2F_R \sin q_1 - m_f(g + \ddot{Y}_{FCG})\right)\sin q_2 - \\ \left(2F_R \cos q_1 + m_f\left(\ddot{X}_{FCG} - \dfrac{r_{bw} \times \ddot{q}_1 \times T_{wheel}}{T_{cog}}\right)\right)\cos q_2\end{array}\right) \tag{3.104}$$

3.1.6.2 The Shank Segment

Taking the moments about the centre of gravity of the shank segment in Figure 3.9, we have,

$$-M_k - I_{SCG}\ddot{\theta}_1 + \frac{l_s}{2}\left(F_{ky}\sin\theta_1 - F_{kx}\cos\theta_1 + F_{ay}\sin\theta_1 - F_{ax}\cos\theta_1\right) + M_a = 0 \quad (3.105)$$

the knee joint moment is

$$M_k = -I_{SCG}\ddot{\theta}_1 + \frac{l_s}{2}\left(F_{ky}\sin\theta_1 - F_{kx}\cos\theta_1 + F_{ay}\sin\theta_1 - F_{ax}\cos\theta_1\right) + M_a \quad (3.106)$$

$$= -I_{SCG}\ddot{\theta}_1 + \frac{l_s}{2}\left(\left(F_{ky} + F_{ay}\right)\sin\theta_1 - \left(F_{kx} + F_{ax}\right)\cos\theta_1\right) + M_a \quad (3.107)$$

Putting the values of F_{ay} in Eq. 3.97 and F_{ax} in Eq. 3.98 into Eq. 3.107 gives

$$M_k = -I_{SCG}\ddot{\theta}_1 + \frac{l_s}{2}\left(\begin{array}{l}\left(2F_{ay} - m_s(\ddot{Y}_{SCG} + g)\right)\sin\theta_1 \\ -\left(2F_{ax} + m_s\left(\ddot{X}_{SCG} - \dfrac{r_{bw}\times\ddot{q}_1\times T_{wheel}}{T_{cog}}\right)\right)\cos\theta_1\end{array}\right) + M_a \quad (3.108)$$

3.1.6.3 The Thigh Segment

Taking moment about the centre of gravity of the thigh segment in Figure 3.9,

$$-M_t - I_{TCG}\ddot{\theta}_2 + \frac{l_t}{2}\left(F_{hy}\sin\theta_2 - F_{hx}\cos\theta_2 + F_{ky}\sin\theta_2 - F_{kx}\cos\theta_2\right) + M_k = 0 \quad (3.109)$$

The thigh joint moment is

$$M_t = -I_{TCG}\ddot{\theta}_2 + \frac{l_t}{2}\left(F_{hy}\sin\theta_2 - F_{hx}\cos\theta_2 + F_{ky}\sin\theta_2 - F_{kx}\cos\theta_2\right) + M_k \quad (3.110)$$

$$= -I_{TCG}\ddot{\theta}_2 + \frac{l_t}{2}\left(\left(F_{hy} + F_{ky}\right)\sin\theta_2 - \left(F_{hx} + F_{kx}\right)\cos\theta_2\right) + M_k \quad (3.111)$$

Putting the values of F_{ky} in Eq. 3.99 and F_{kx} in Eq. 3.101 into Eq. 3.111 gives

$$M_h = -I_{TCG}\ddot{\theta}_2 + \frac{l_t}{2}\left(\begin{array}{l}\left(2F_{ky} - m_t(\ddot{Y}_{TCG} + g)\right)\sin\theta_2 \\ -\left(2F_{kx} + m_t\left(\ddot{X}_{TCG} - \dfrac{r_{bw}\times\ddot{q}_1\times T_{wheel}}{T_{cog}}\right)\right)\cos\theta_2\end{array}\right) + M_k \quad (3.112)$$

3.1.7 Saddle Height Prediction

One of the causes of lower limb segments' overuse injuries is the inappropriate saddle height. Saddle Height can be expressed as a proportion of the total length of the lower limb segments measured from the hip joint to the surface of the pedal in a straight line in such a way that the limb forms the hypotenuse of a right angle triangle and the vertical and the horizontal distances of the hip joint to crank axis forming the two remaining sides. The lower limb segments' length were obtained by using Drillis and Contini (1966) work in which approximate values of the segment lengths, moment of inertia, segment mass and joint centre locations were stated.

The,

estimated Thigh segment length = $0.245H$ (3.113)

estimated Shank segment length = $0.246H$ (3.114)

estimated foot segment length = $0.153H$ (3.115)

Total length of the lower limb segments = $0.644H$ (3.116)

where H is the total height of the cyclist.

The saddle height $= l_f + l_s + l_t$ (3.117)

The proportion of 100% is when the saddle height $= l_f + l_s + l_t$ (3.118)

3.2.0 Materials Preparation and Methods

The equipment used for the research are mentioned below.

3.2.1 Exercise Bike HC

The Exercise Bike (EB) Figure 3.10, below is a class HC apparatus EN 957 – 1, - 5. Its maximum load design is 100kg. Before the exercises began, all screws, nuts, bolts, the

saddle and pedals are tightened properly. The foot and hands were kept clear of the housing. Baggy clothes were avoided during the exercise in other to avoid being

Figure 3.10: Model HC Exercise Bike

entangled. The EB was placed on a solid flat surface. Exercise immediately before and after meal was avoided. The EB has a display monitor which display speed, distance, calorie and pulse. The blood pressure of each subject was taken immediately before and immediately after the exercise.

3.2.2 Subjects

Ten students were used for this workout at different speed for 5 minutes. Their experiences were reported and recorded. Figures 3.11 (a – d) are some of the pictures of the subjects exercising on model HC Exercise Bike.

(a)

(b)

(c)

(d)

Figure 3.11 (a – d): Some of the Subjects Exercising on Model HC Exercise Bike.

Figure 3.12: One of the Subjects measuring his BP after Exercising on Model HC Exercise Bike.

Table 3.1: Responses of Non-Athletic Participants at a saddle height of 95% of the total length of the lower limb segments at 64 rpm

Participants	Weight (Kg)	Height (m)	Responses		
			Ankle	Knee	Hip
A	78	1.94	2	3	3
B	71	1.78	1	2	2
C	79	1.72	2	2	3
D	80	1.76	3	3	4
E	60	1.70	1	2	2
G	56	1.70	1	2	2
H	65	1.78	1	2	3
*I	90	1.62	3	4	4
SD	72.375 ± 10.735	1.750 ± 0.087	1.75 ± 0.829	2.50 ± 0.707	2.88 ± 0.781

Table 3.2: Responses of Participants at a seat height of 75% of the total length of the lower limb segments at 64 rpm

Participants	Weight (Kg)	Height (m)	Responses		
			Ankle	Knee	Hip
A	78	1.94	1	1	1
B	71	1.78	1	1	1
C	79	1.72	1	1	1
D	80	1.76	1	1	2
E	60	1.70	1	1	1
G	56	1.70	1	1	1
H	65	1.78	1	1	1
*I	90	1.62	1	2	2
SD	72.375 ± 10.735	1.750 ± 0.087	1.0 ± 0.0	1.12 ± 0.331	1.25 ± 0.331

* = Female Participant

Table 3.3: Responses of Participants at a seat height of 40% of the total length of the lower limb segments

Participants	Weight (Kg)	Height (m)	Responses		
			Ankle	Knee	Hip
A	78	1.94	3	5	5
B	71	1.78	3	5	5
C	79	1.72	4	5	5
D	80	1.76	4	5	5
E	60	1.70	4	5	5
G	56	1.70	3	5	5
H	65	1.78	4	5	5
*I	90	1.62	4	5	5
SD	72.375 ± 10.735	1.750 ± 0.087	3.625 ± 0.484	5.0 ± 0.0	5.0 ± 0.0

* = Female Participant

Table 3.4: Responses of Athletic Participants at a seat height of 95% of the total length of the lower limb segments

Participants	Weight (Kg)	Height (m)	Responses		
			Ankle	Knee	Hip
F	98	1.75	2	3	3
J	80	1.78	1	2	3
SD	89.0 ± 9.0	1.765 ± 0.015	1.5 ± 0.5	2.5 ± 0.5	3.0 ± 0.0

Table 3.5: Responses of Athletic Participants at a seat height of 75% of the total length of the lower limb segments

Participants	Weight (Kg)	Height (m)	Responses		
			Ankle	Knee	Hip
F	98	1.75	1	1	1
J	80	1.78	1	1	1
SD	89.0 ± 9.0	1.765 ± 0.015	1.0 ± 0.0	1.0 ± 0.0	1.0 ± 0.0

Table 3.6: Responses of Athletic Participants at a seat height of 40% of the total length of the lower limb segments

Participants	Weight (Kg)	Height (m)	Responses		
			Ankle	Knee	Hip
F	98	1.75	3	3	3
J	80	1.78	1	2	2
SD	89.0 ± 9.0	1.765 ± 0.015	2.0 ± 1.00	2.5 ± 0.5	2.5 ± 0.5

CHAPTER 4

RESULTS AND DISCUSSIONS

In order to achieve the objectives of this research, and enable the understanding and interpretation of the equations developed in the previous chapter, the parametric studies of a physical model was carried out using values given in Table 4.1.

Table 4.1: Values used for the Parametric Studies.

S/N	DESCRIPTION	SYMBOL	VALUES USED
1	Height of the Rider	H	1.78m
2	Mass of the Rider	M_R	75.0kg
3	Crank arm length of the bicycle	l_c	0.170m
4	Rider's hip to the crank axis (horizontal)	l_x	0.212m
5	Rider's hip to the crank axis (vertical) – Saddle Height	l_y	72 – 100%
6	Bicycle horizontal accelerations	$\ddot{x}$	*0, 1, 2, 3, 4, 5 m/s^2*
7	Bicycle wheel radius	r_{bw}	*0.311 m*
8	Number of teeth in Chain wheel	T_{wheel}	*52*
9	Number of teeth in the rear cog	T_{cog}	*15*
10	Mass of Bicycle	M_B	*15kg*
11	Resultant Pedaling Force	F_R	*500N*
12	Crank speed	$\dot{q}_1$	*5 – 130 rpm*

4.1 Ankle Joint Moments

Figures 4.1a – 4.5a are the plots of the variation of ankle joint moments with crank angles over a complete revolution at various crank speeds of 10, 50, 80, 110 and 130 revolutions per minute (rpm) respectively while Figures 4.1b – 4.5b are the plots of variations of the components of ankle joint moments and the crank angles at 10, 50, 80, 110 and 130 rpm respectively. The moments generated by the horizontal forces as shown in Figures 4.1b – 4.5b are sinusoidal in shape but completing two cycles in one revolution while the vertical forces generated a cosine shaped moment that completed one cycle in one revolution. These two moments cross the x-axis two at the same points. The sum of these two moments gave the ankle moment its shape since the moment generated by the torque is virtually zero for all the crank speed considered aligning itself with the x axis. The ankle joint moments of the five considered crank speed are almost the same showing no significant difference in shape and value. The ankle joint moment started 0^0 increasing immediately until it picked at 30^0 and started to decrease to a minimum value at about 150^0, then started to rise again until it got to 360^0 crossing the x-axis at 90^0 and 270^0. The region of $0^0 – 180^0$ is the region of power stroke while the back stroke region is $180^0 – 360^0$.

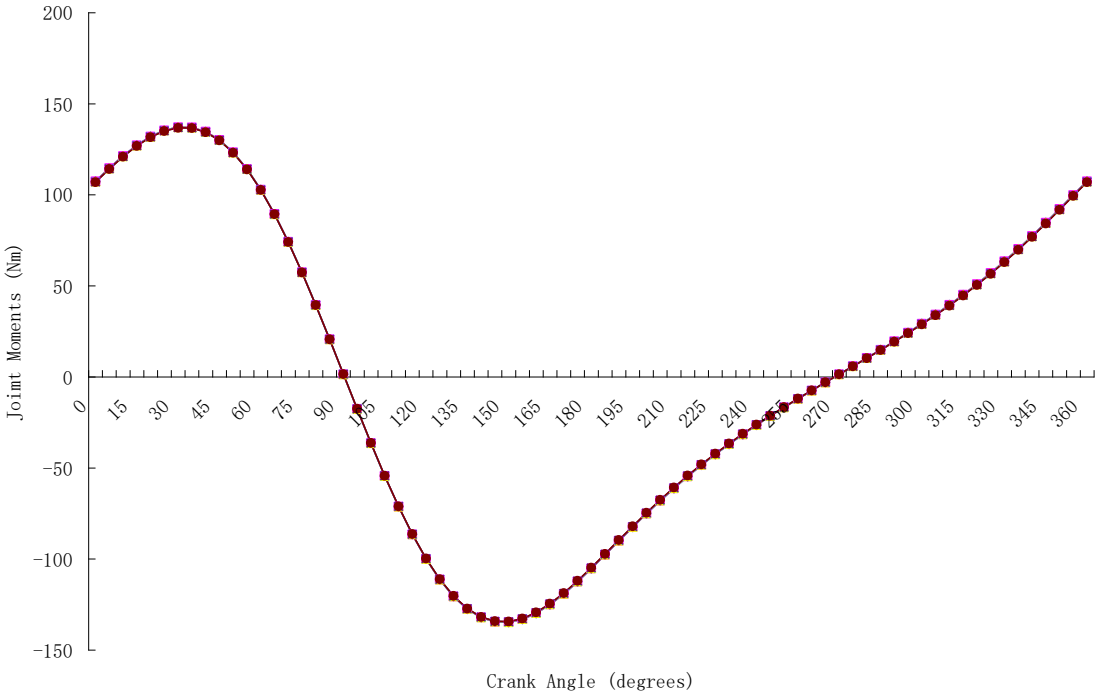

Figure 4.1a: Ankle Joint Moments vs crank angles at 10 rpm

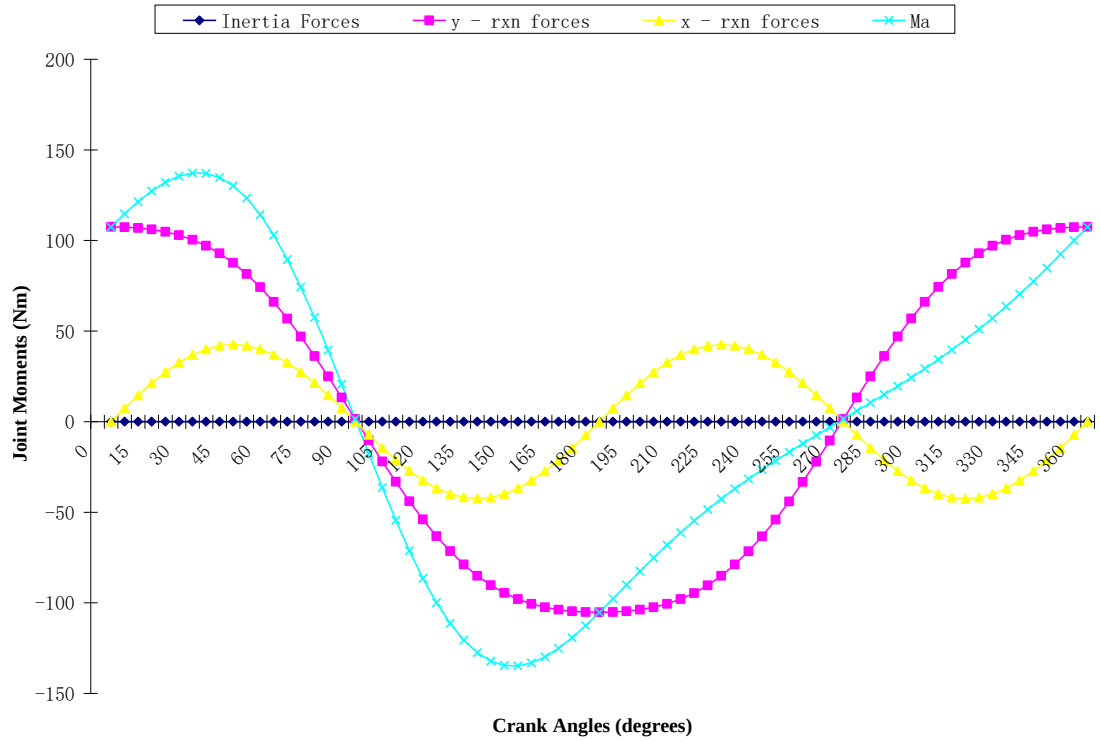

Figure 4.1b: Components of Ankle Joint Moments vs crank angles at 10 rpm

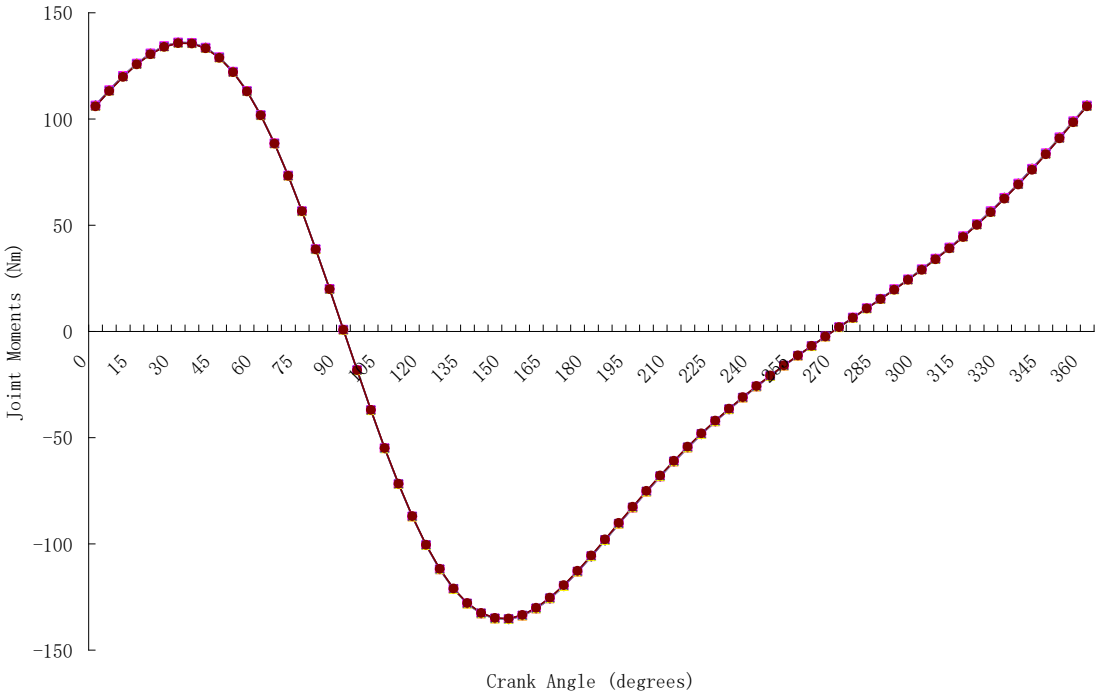

Figure 4.2a: Ankle Joint Moments vs crank angles at 50 rpm

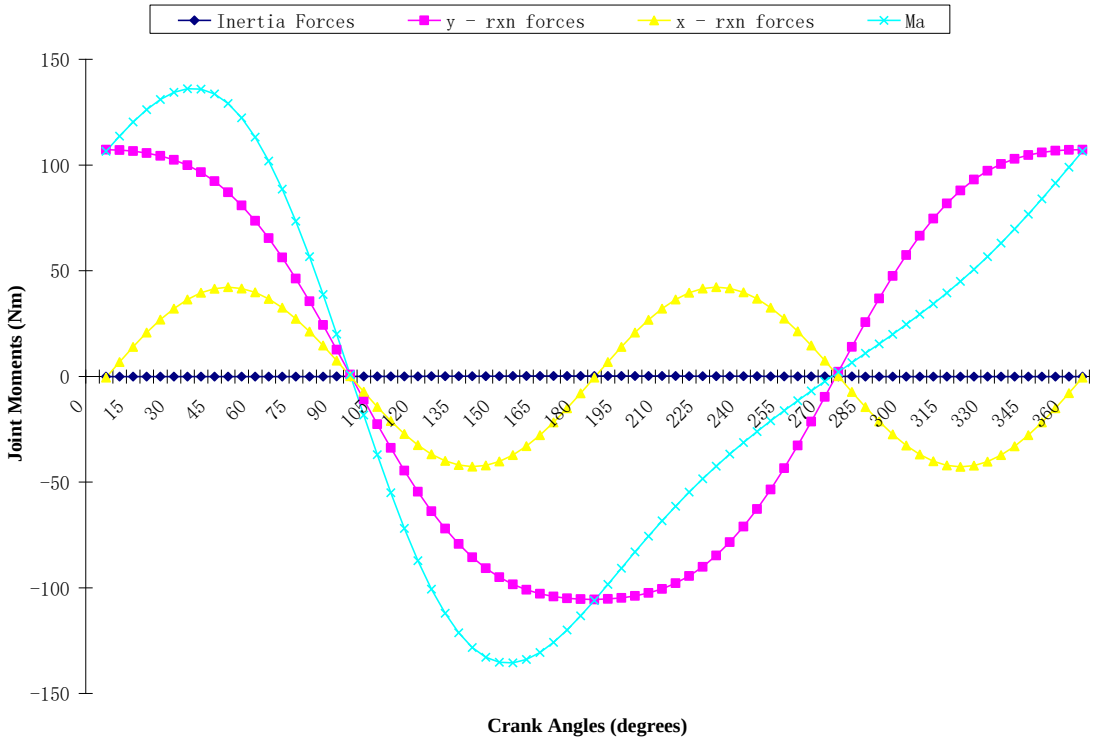

Figure 4.2b: Components of Ankle Joint Moments vs crank angles at 50 rpm

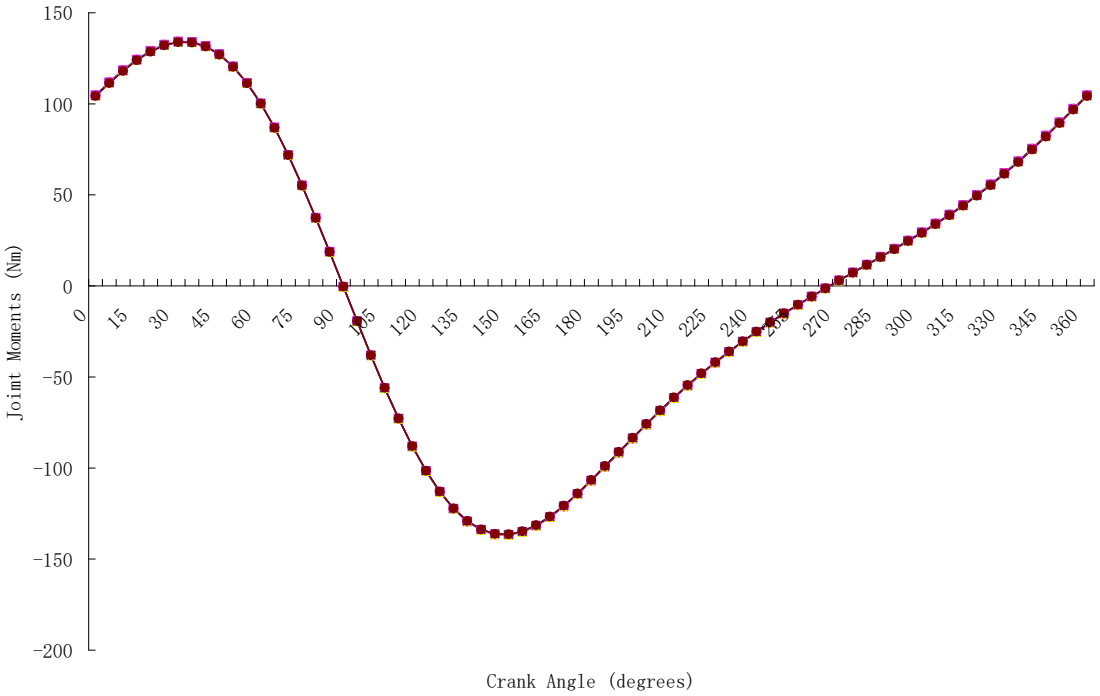

Figure 4.3a: Ankle Joint Moments vs crank angles at 80 rpm

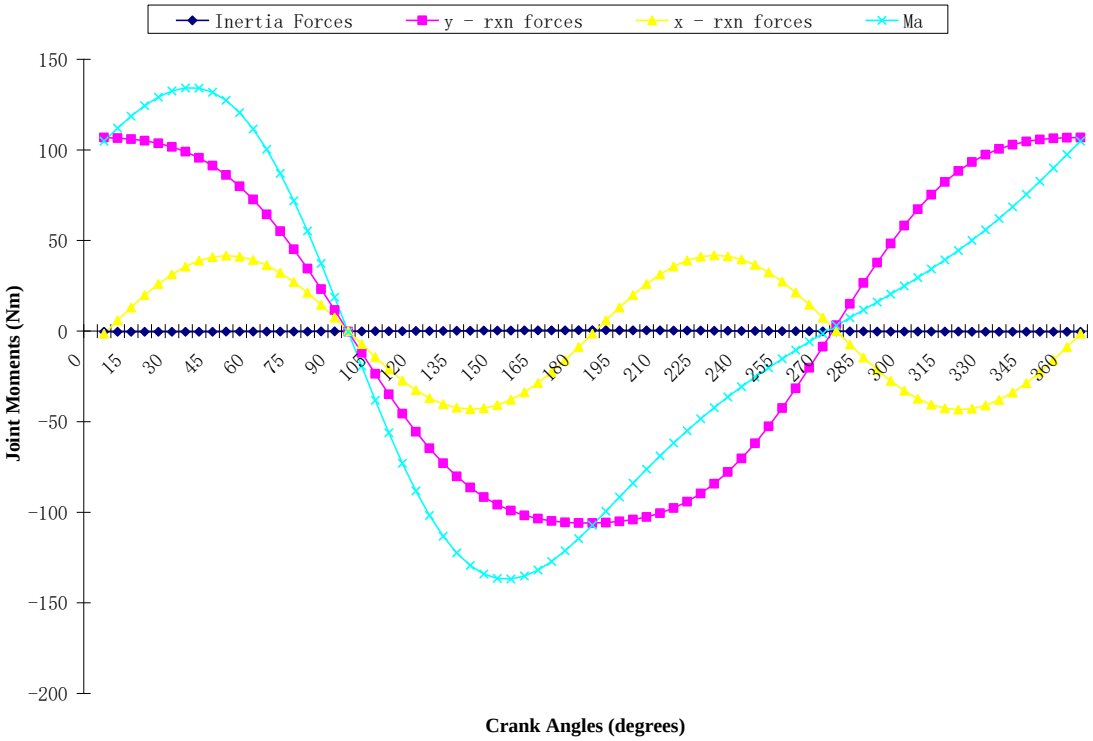

Figure 4.3b: Components of Ankle Joint Moments vs crank angles at 80 rpm

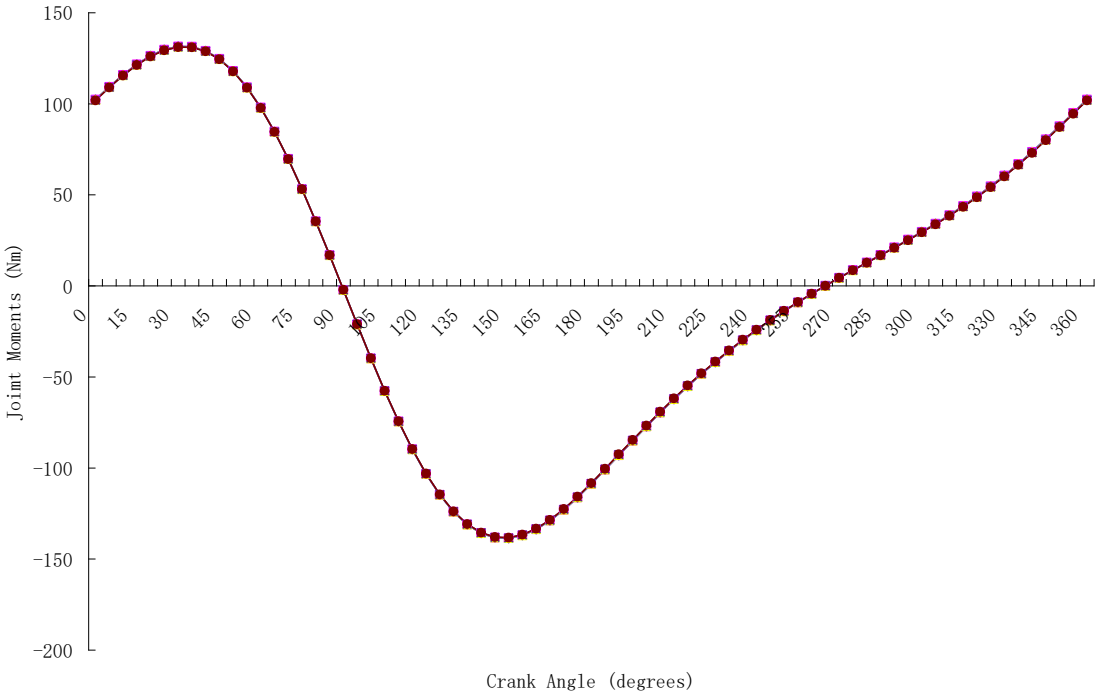

Figure 4.4a: Ankle Joint Moments vs crank angles at 110 rpm

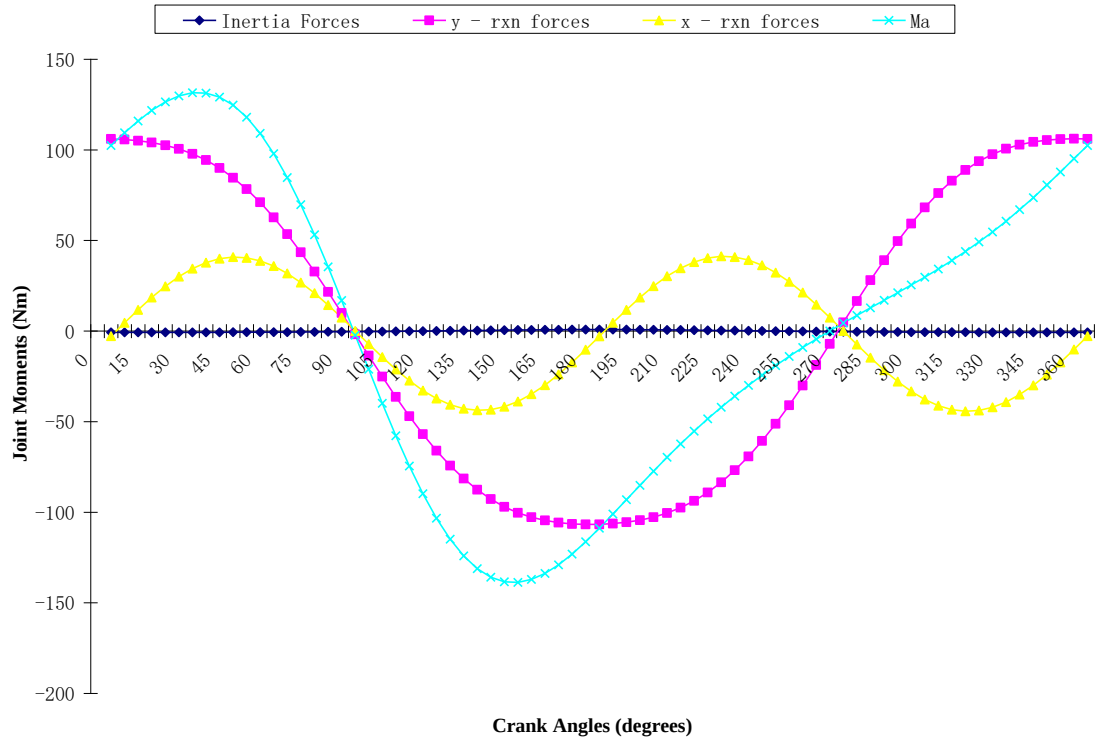

Figure 4.4b: Components of Ankle Joint Moments vs crank angles at 110 rpm

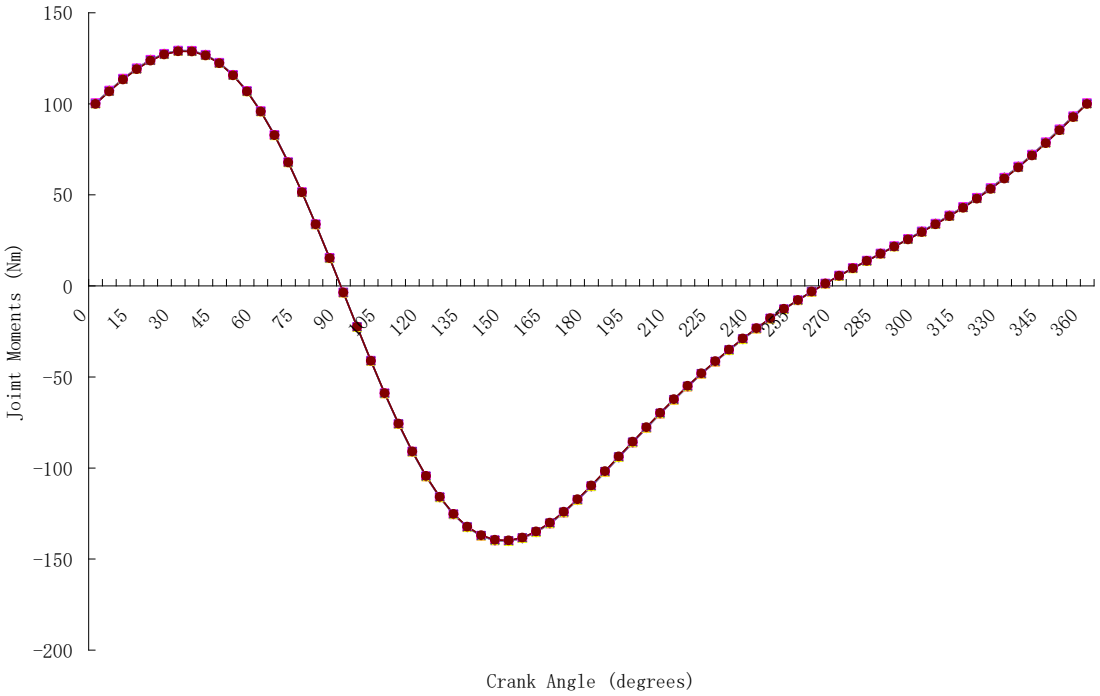

Figure 4.5a: Ankle Joint Moments vs crank angles at 130 rpm

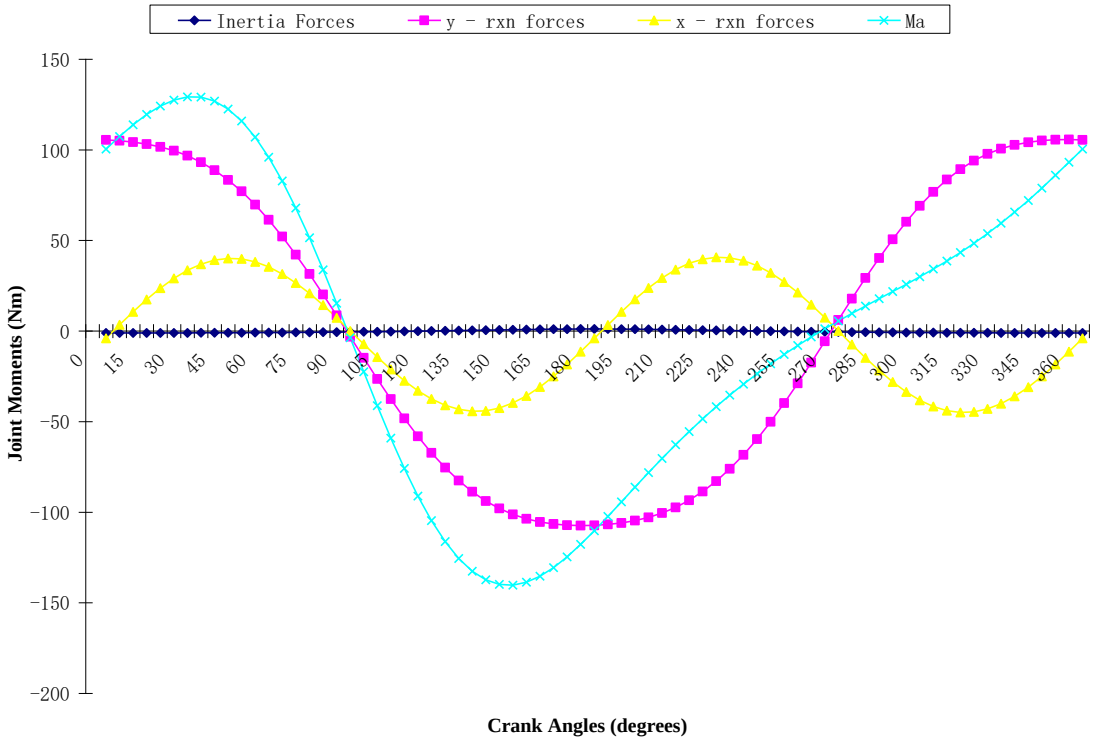

Figure 4.5b: Components of Ankle Joint Moments vs crank angles at 130 rpm

The average ankle joint moments for 10, 50, 80, 110, and 130 rpm are shown in Figures 4.6 – 4.10 respectively. These figures give the average ankle joint moments variation

with acceleration. These figures were obtained by summing up together the absolute values of the ankle joint moments over a complete revolution and divided by seventy two (the number of points considered in each revolution). The aim of this is to obtain a comparison of the joint moment at different horizontal acceleration. Although, they are straight lines graph with negative slope indicating that the ankle joint moment decreases linearly with the acceleration but the percentage decrease is so small (less than 0.2%) compared to the magnitude of the ankle joint moment that we can assume that this decrease to be negligible.

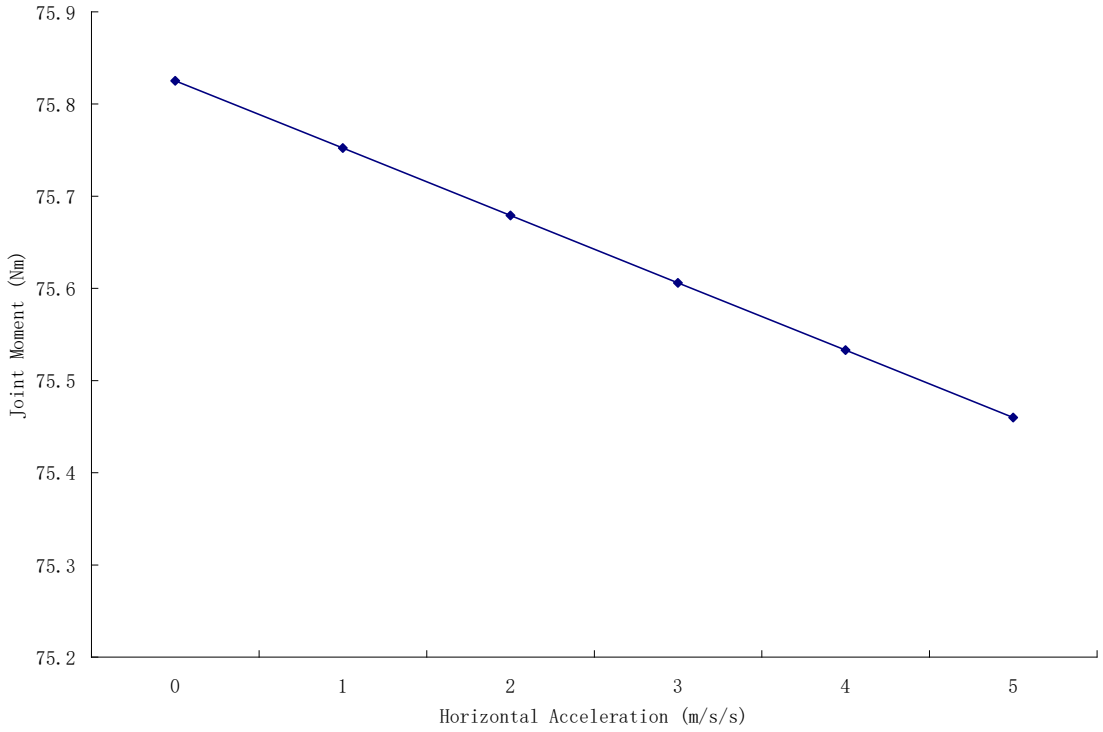

Figure 4.6: Average ankle joint moment vs horizontal accelerations at 10 rpm

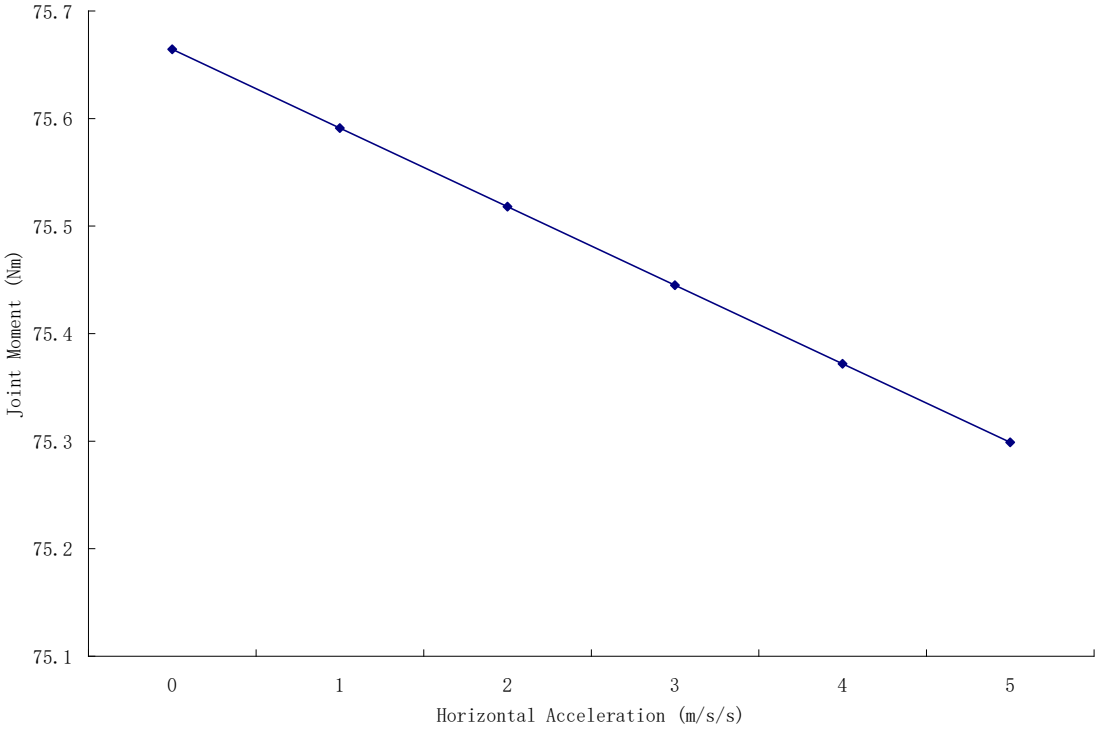

Figure 4.7: Average ankle joint moments vs horizontal accelerations at 50 rpm

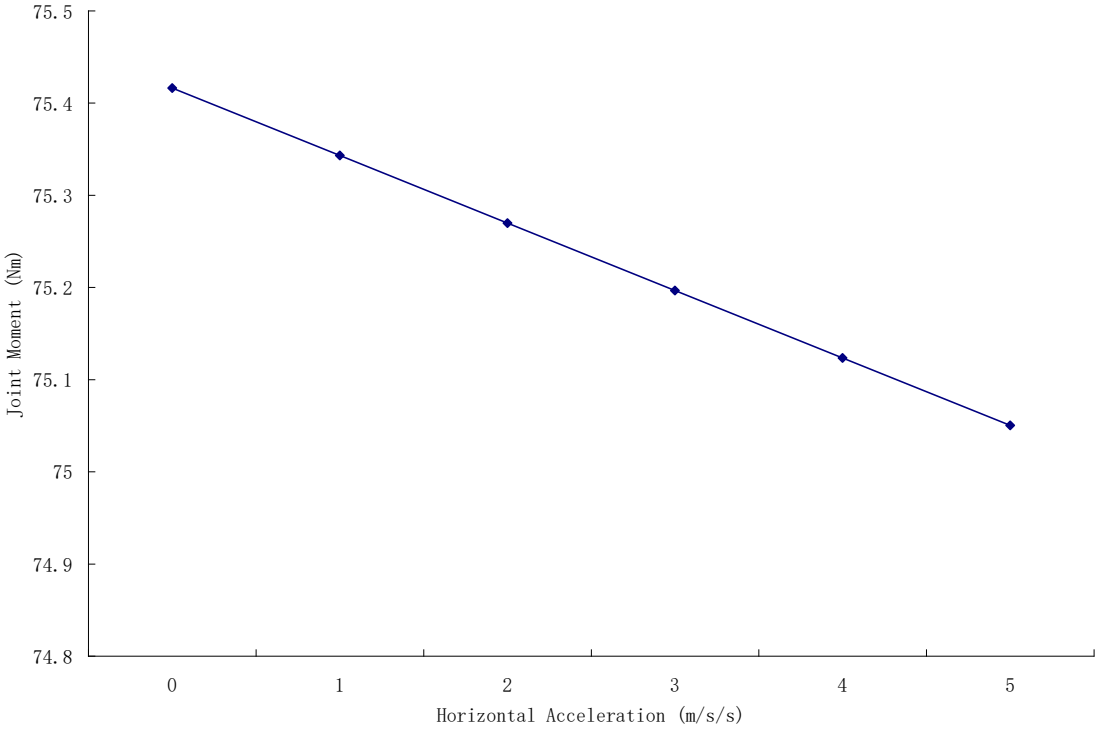

Figure 4.8: Average ankle joint moments vs horizontal accelerations at 80 rpm

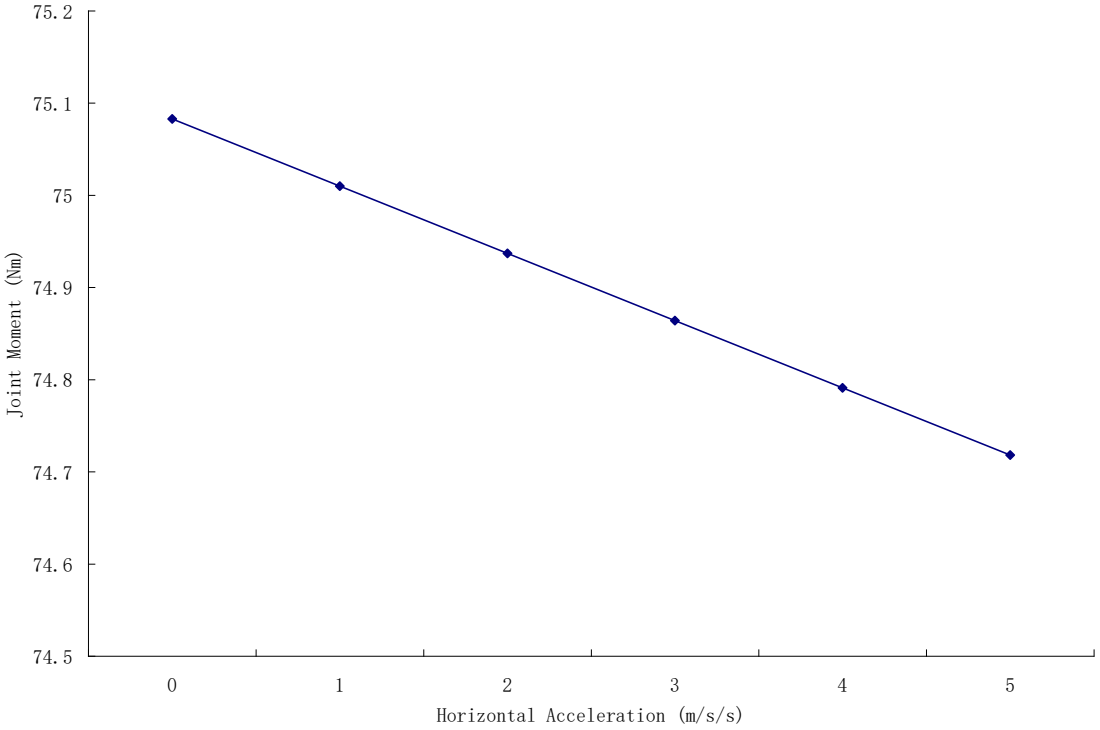

Figure 4.9: Average ankle joint moments vs horizontal accelerations at 110 rpm

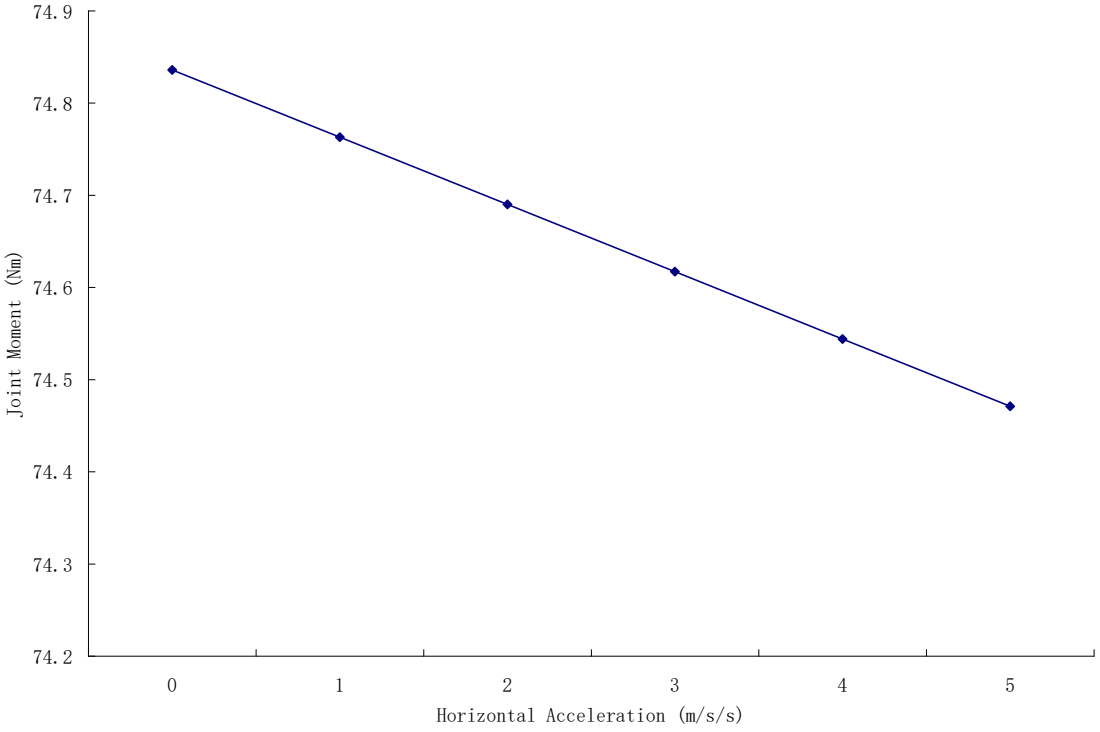

Figure 4.10: Average ankle joint moments vs horizontal accelerations at 130 rpm

4.2 Knee Joint Moments

Figures 4.11a – 4.15a are the variations of ankle joint moments with crank angles over a complete revolution at various crank speeds of 10, 50, 80, 110 and 130 rpm respectively while Figures 4.11b – 4.15b are the plots of variations components of ankle joint moments and the crank angles at 10, 50, 80, 110 and 130 rpm respectively. There are four components that are responsible for the knee joint moment and its pattern, namely the shank torque, the ankle joint moment, the horizontal and the vertical moments. The moment generated by the vertical force starts almost at the peak at 0^0 decreasing gradually to zero at 105^0 and crosses the x axis at this same point as the ankle joint moment. It continues to decrease until it gets to its minimum at 210^0 then increase back to zero at 285^0 then continue to increase gradually till the end of the cycle at 360^0, while the horizontal component starts at about 0^0 decreasing to the minimum at 75^0 then starts to increase, crossing x axis at 135^0 peaking first at 165^0 then starts to decrease to zero at 195^0 then increases to maximum at 285^0 then decreasing back to zero at 360^0. As the crank speed increase, the horizontal moment decreases in magnitude with phase shifts while the vertical moment remain almost the same in shape and magnitude except increase in magnitude of the crest that is between 150^0 and 210^0. The torque component is almost constant, remaining horizontal straight line along the x-axis except for a trough below the x-axis noticeable from the crank speed of 80 rpm but very prominent at 130 rpm. The sum of these four components gives the knee joint moment its magnitude and shape. The knee joint moment of the five crank speed are the same shape but not in magnitude. It starts at the peak at 0^0, decreasing gradually crossing the x-axis at about 80^0, then decreasing to the minimum at 195^0, with a crest around 135^0 to 195^0

which almost flattens out at 130 rpm, then rising to the peak at 285^0, there-from maintaining a dwell till 360^0.

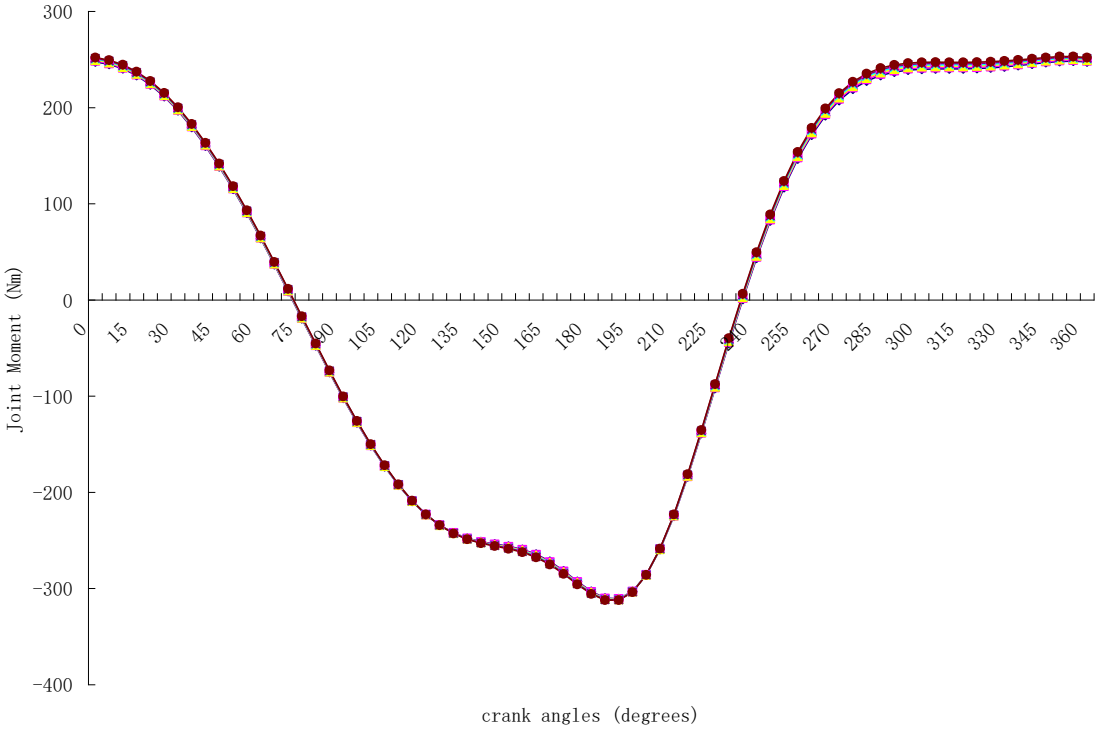

Figure 4.11a: Knee Joint Moments vs crank angles at 10 rpm

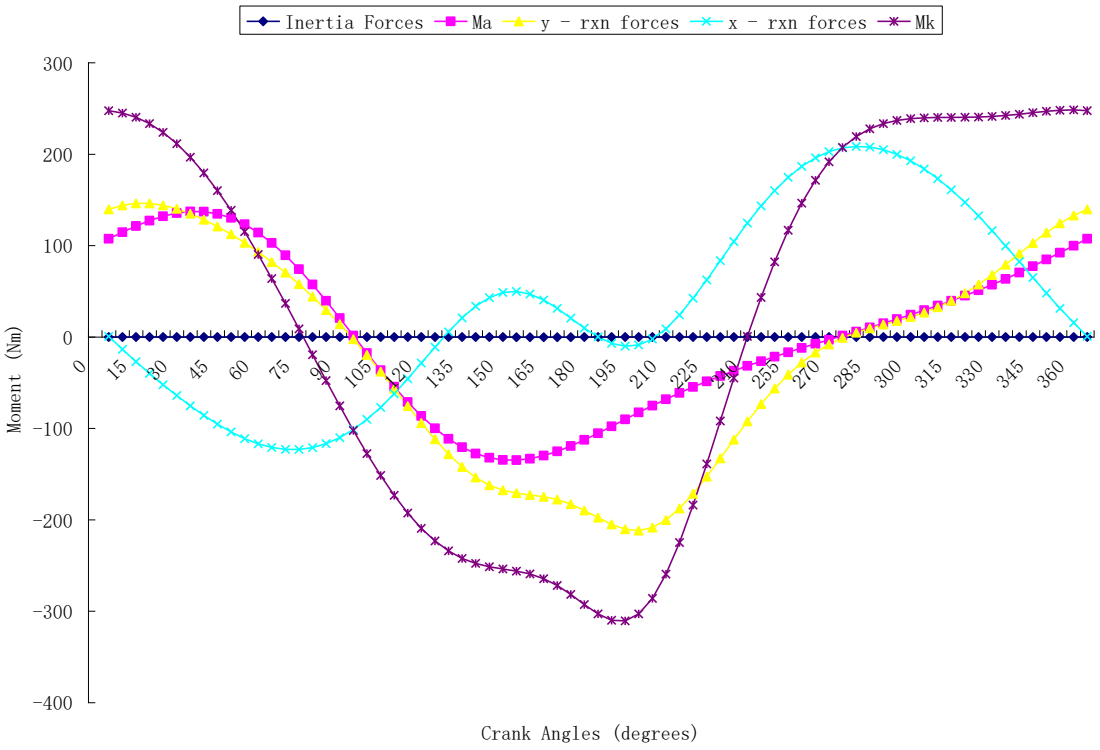

Figure 4.11b: Components of Knee Joint Moments vs crank angles at 10 rpm

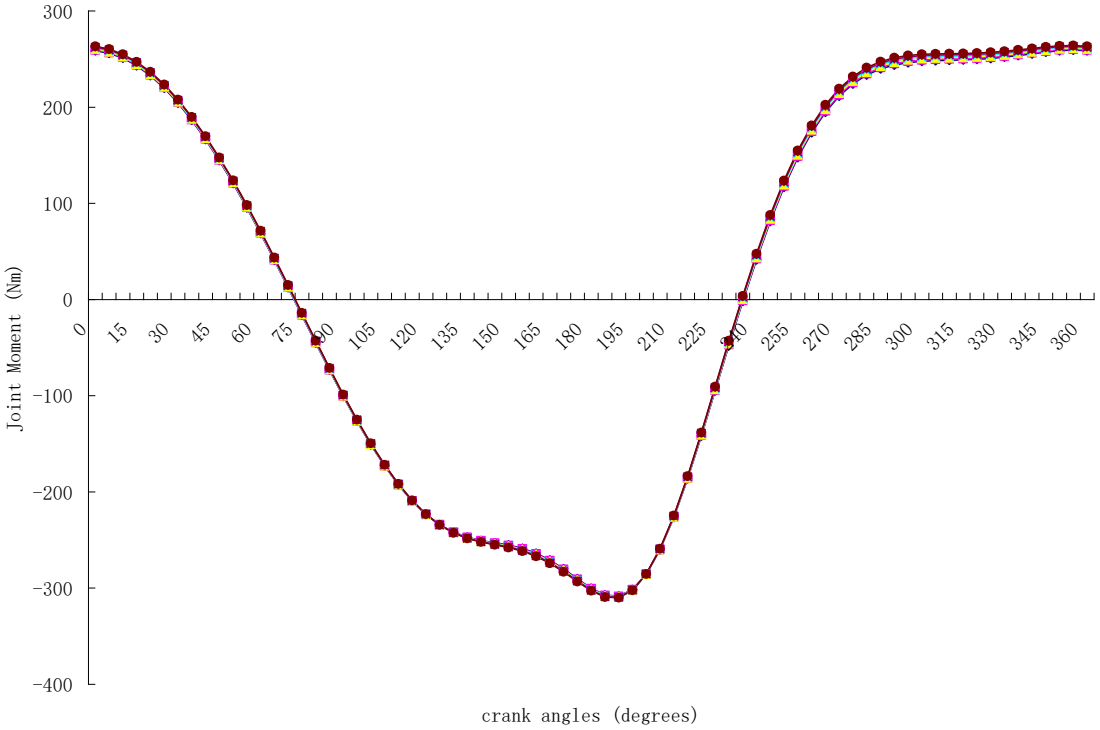

Figure 4.12a: Knee Joint Moments vs crank angles at 50 rpm

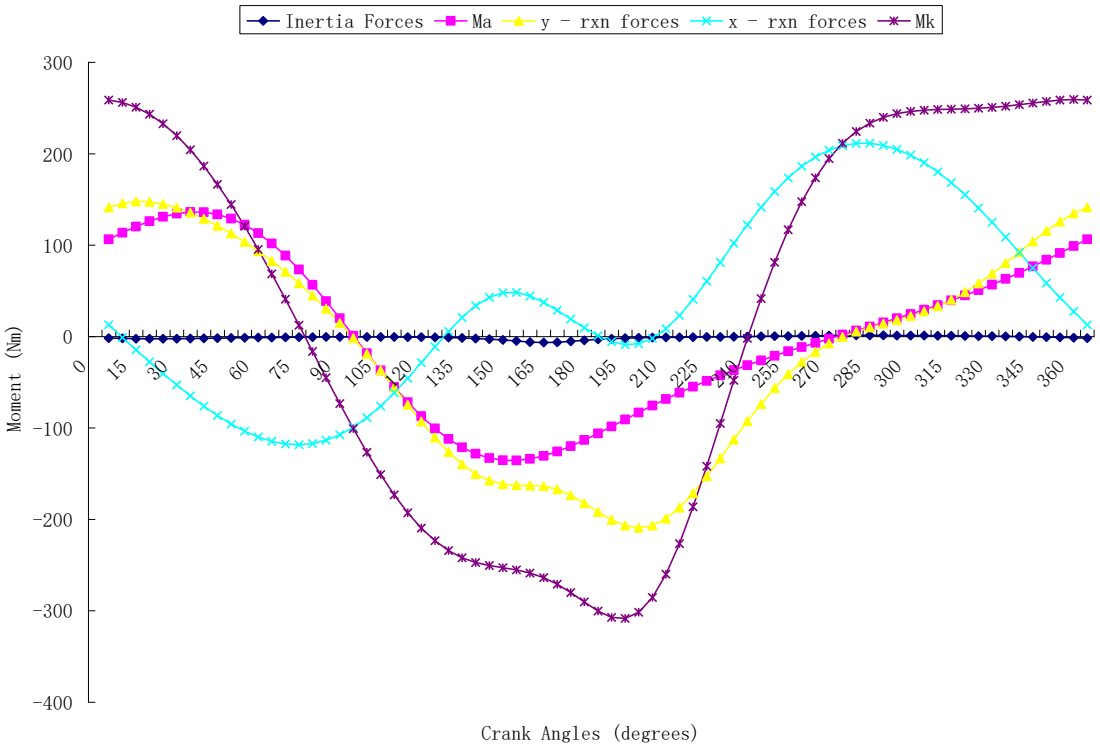

Figure 4.12b: Components of Knee Joint Moments vs crank angles at 50 rpm

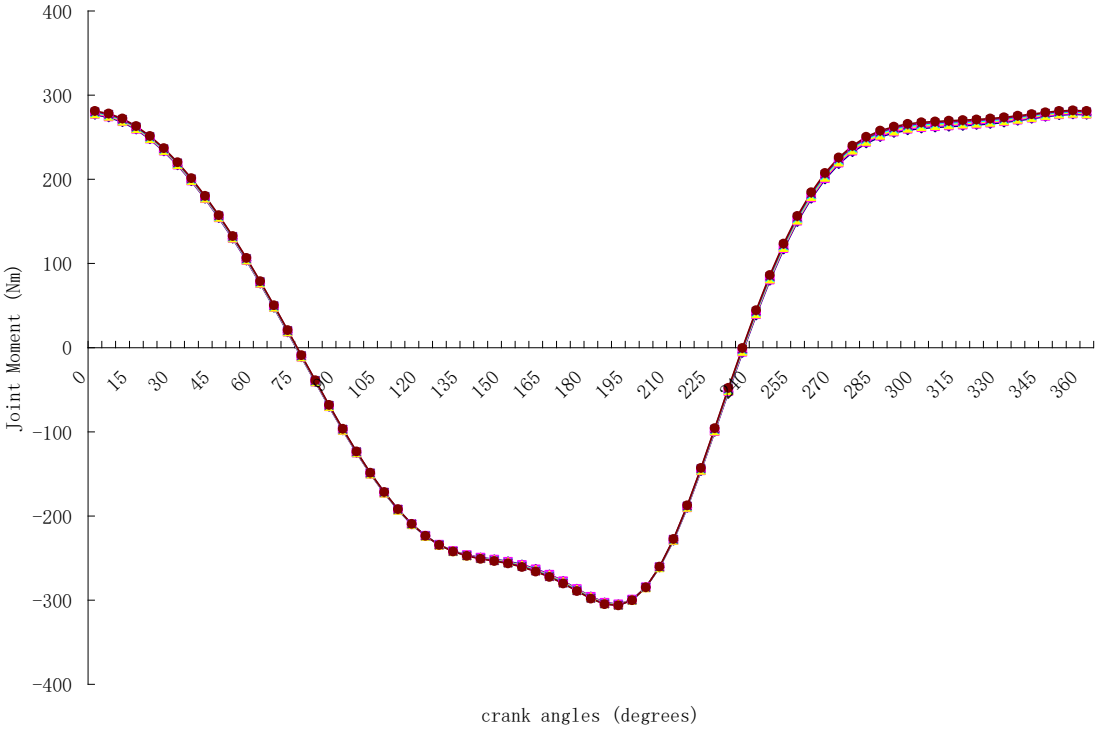

Figure 4.13a: Knee Joint Moments vs crank angles at 80 rpm

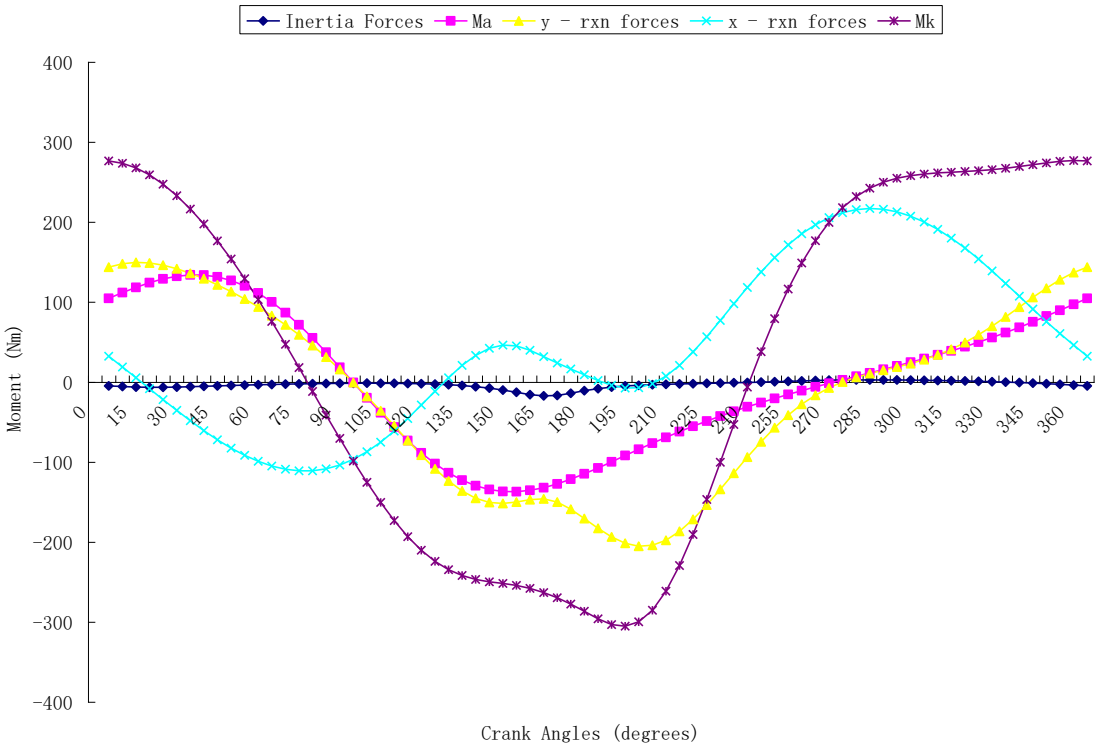

Figure 4.13b: Components of Knee Joint Moments vs crank angles at 80 rpm

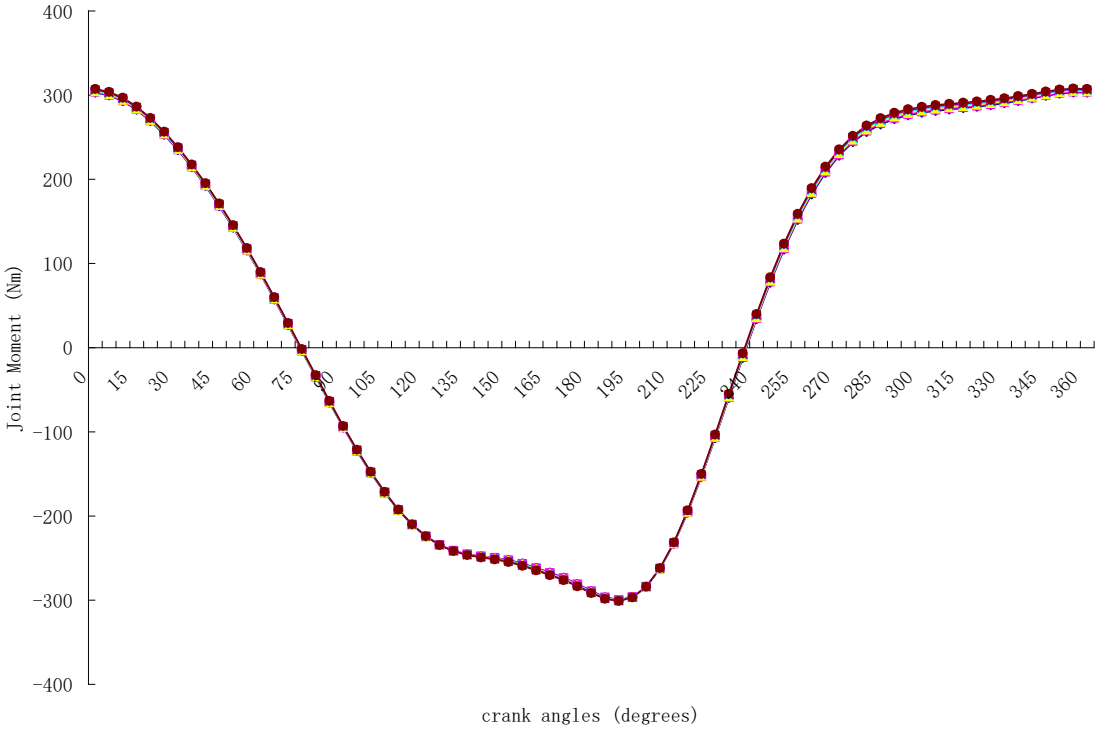

Figure 4.14a: Knee Joint Moments vs crank angles at 110 rpm

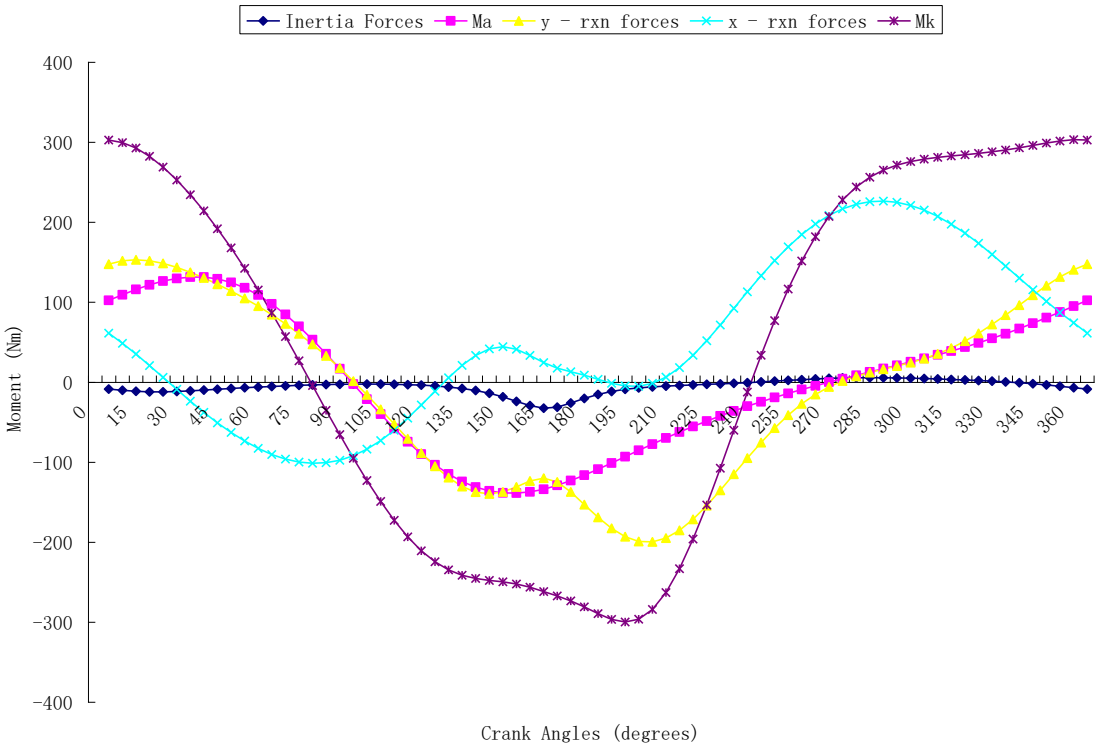

Figure 4.14b: Components of Knee Joint Moments vs crank angles at 110 rpm

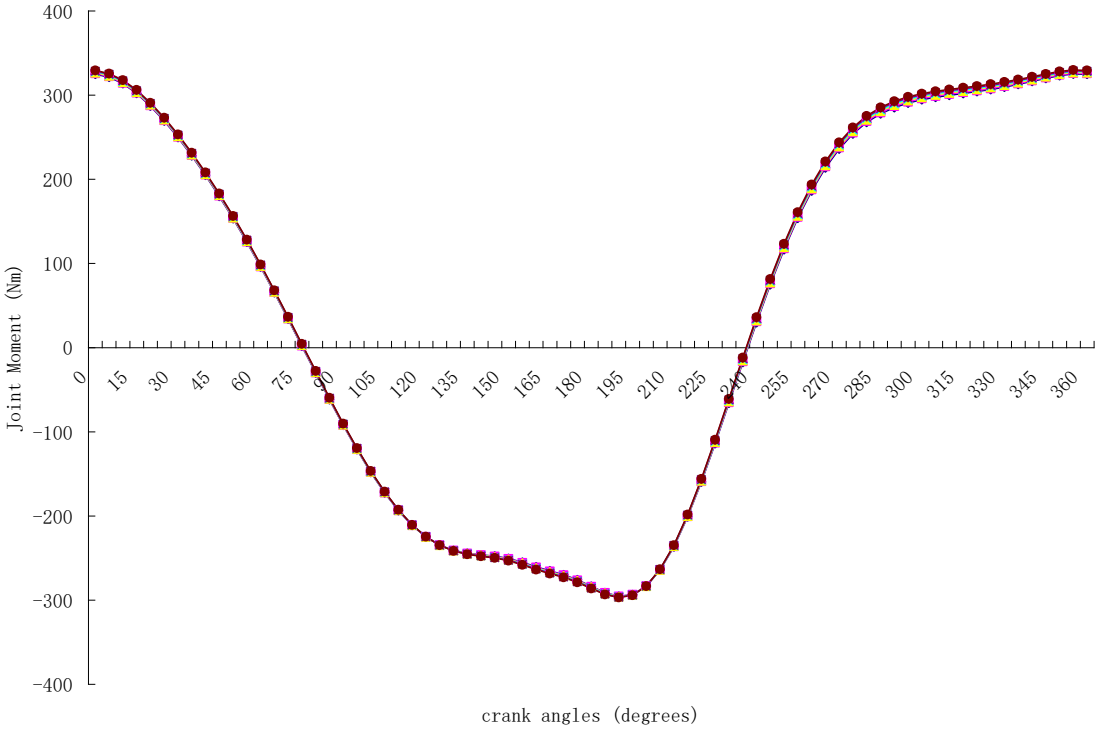

Figure 4.15a: Knee Joint Moments vs crank angles at 130 rpm

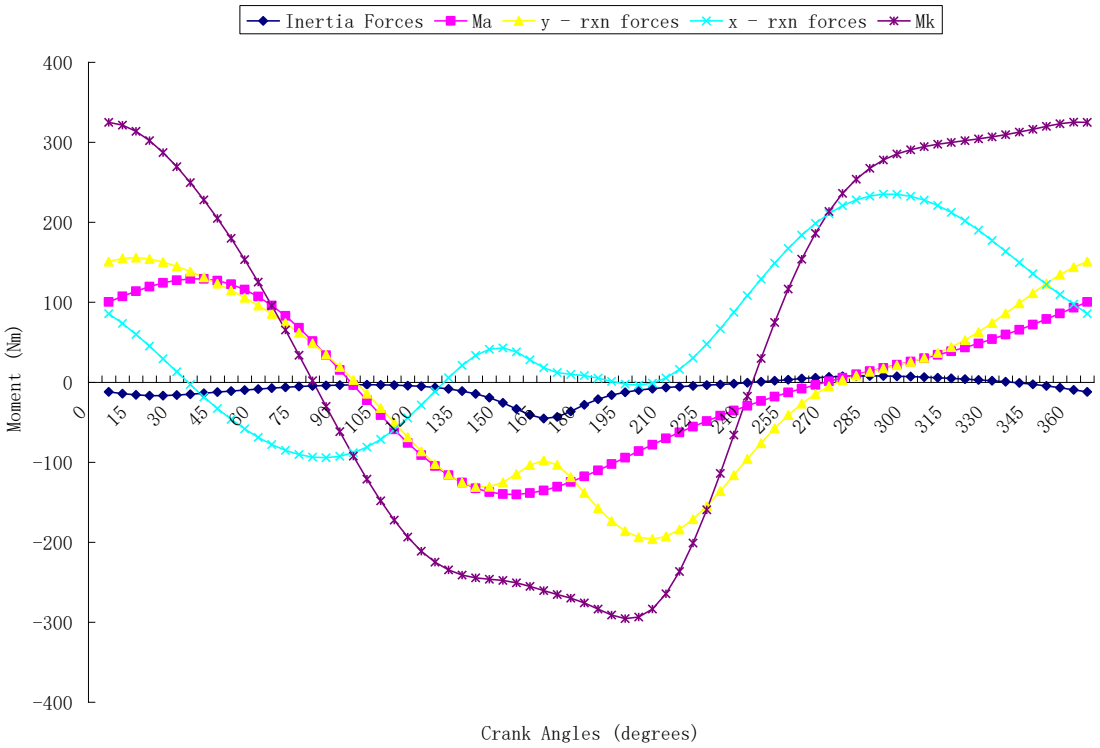

Figure 4.15b: Components of knee joint moments vs crank angles at 130 rpm

Figures 4.16 – 4.20 are the variations of average knee joint moment and horizontal acceleration. These plots were obtained in the same manner as average ankle joint

moment. The knee joint moments increase linearly as the horizontal acceleration increase thereby encouraging lower acceleration during cycling.

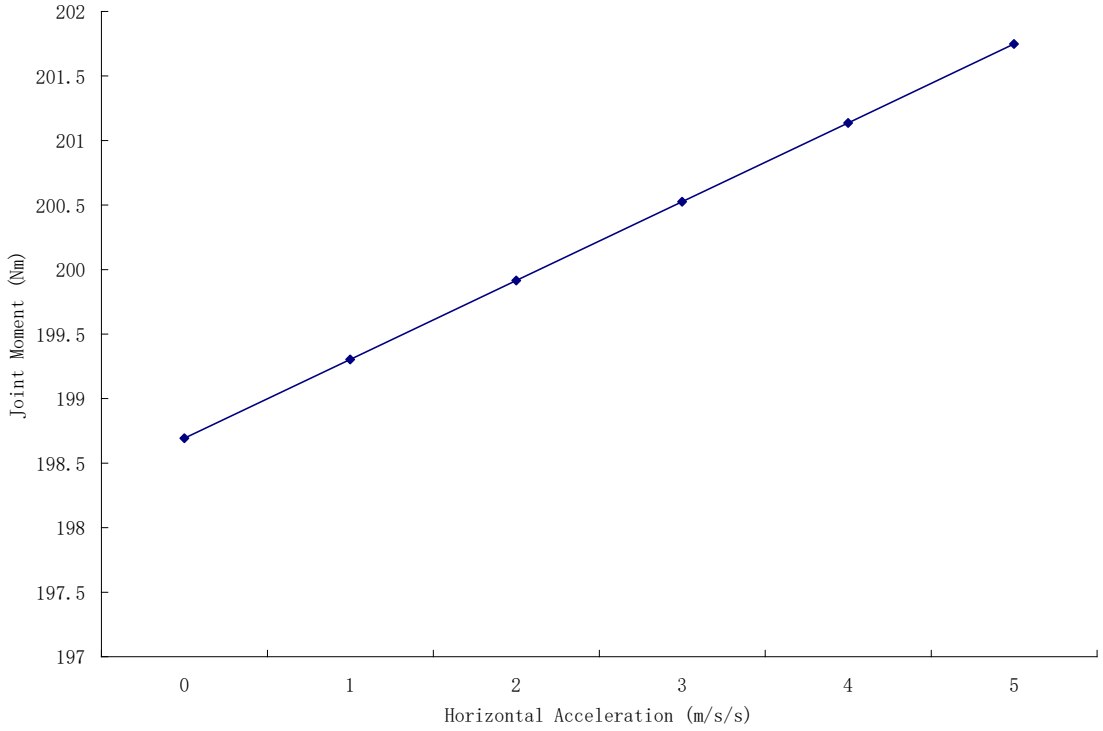

Figure 4.16: Average knee moment vs horizontal accelerations at 10 rpm

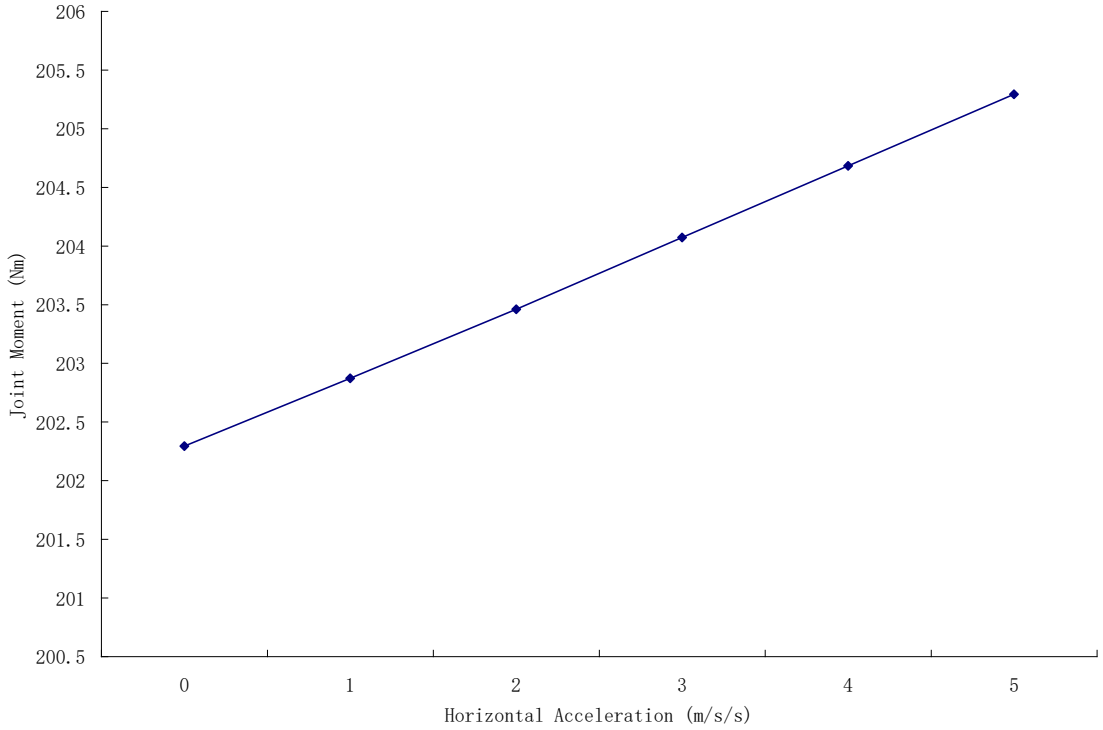

Figure 4.17: Average knee joint moments vs horizontal accelerations at 50 rpm

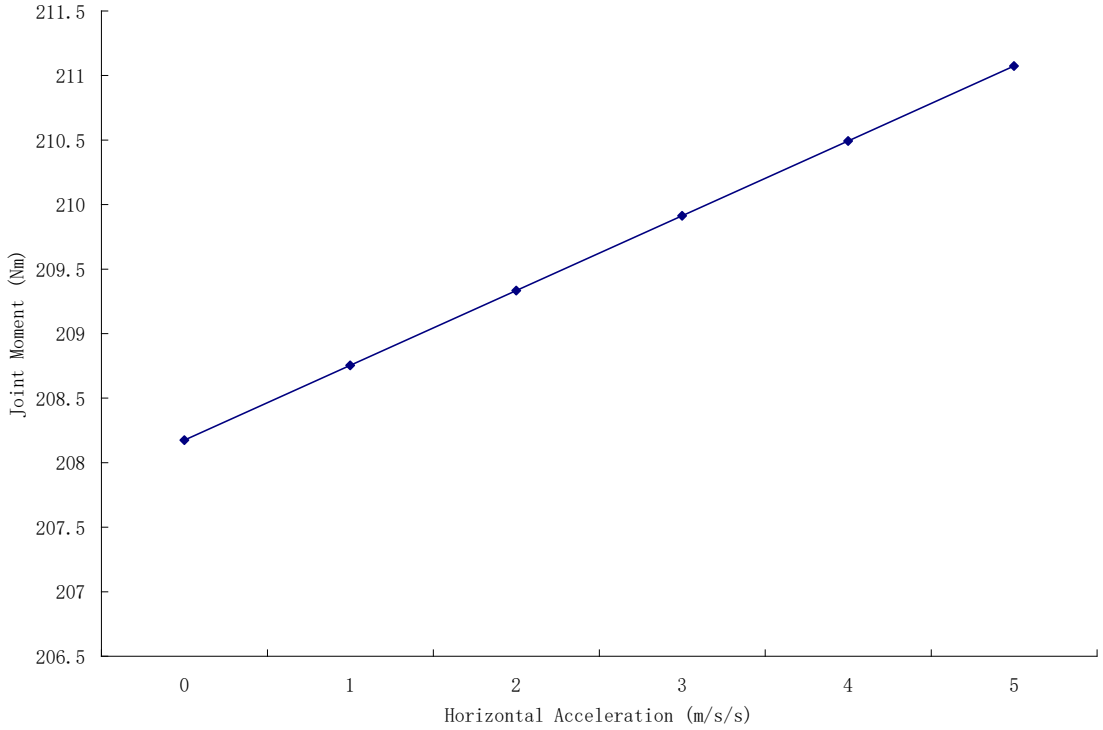

Figure 4.18: Average knee joint moments vs horizontal accelerations at 80 rpm

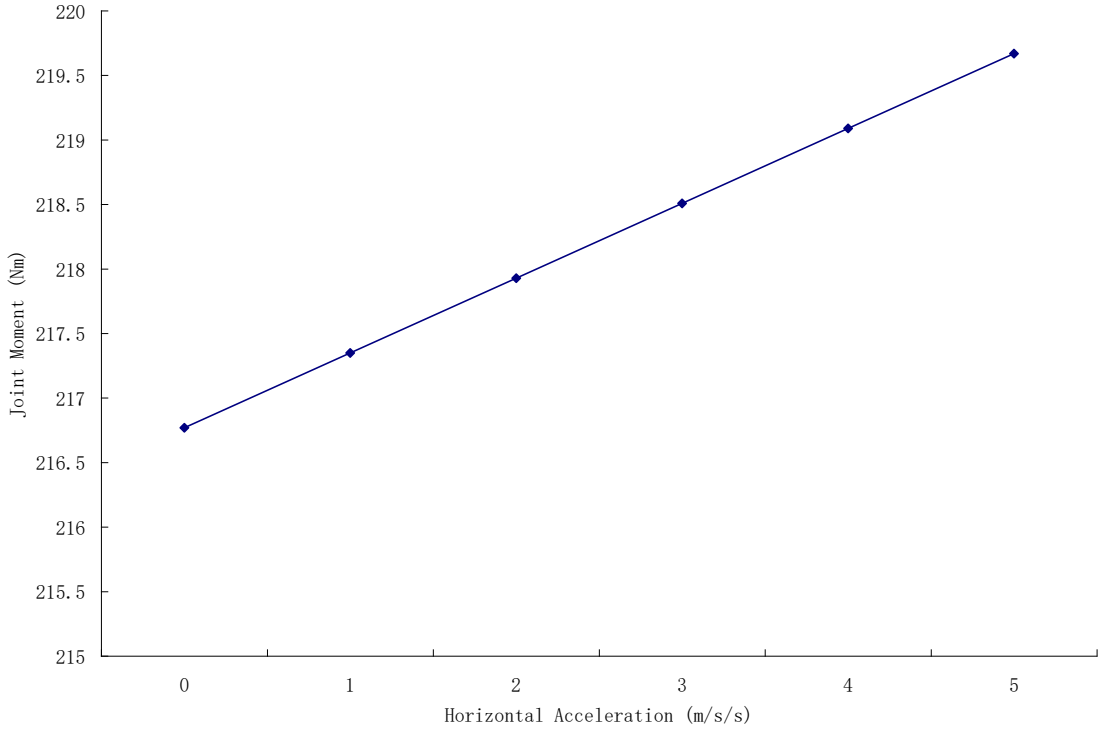

Figure 4.19: Average knee joint moments vs horizontal accelerations at 110 rpm

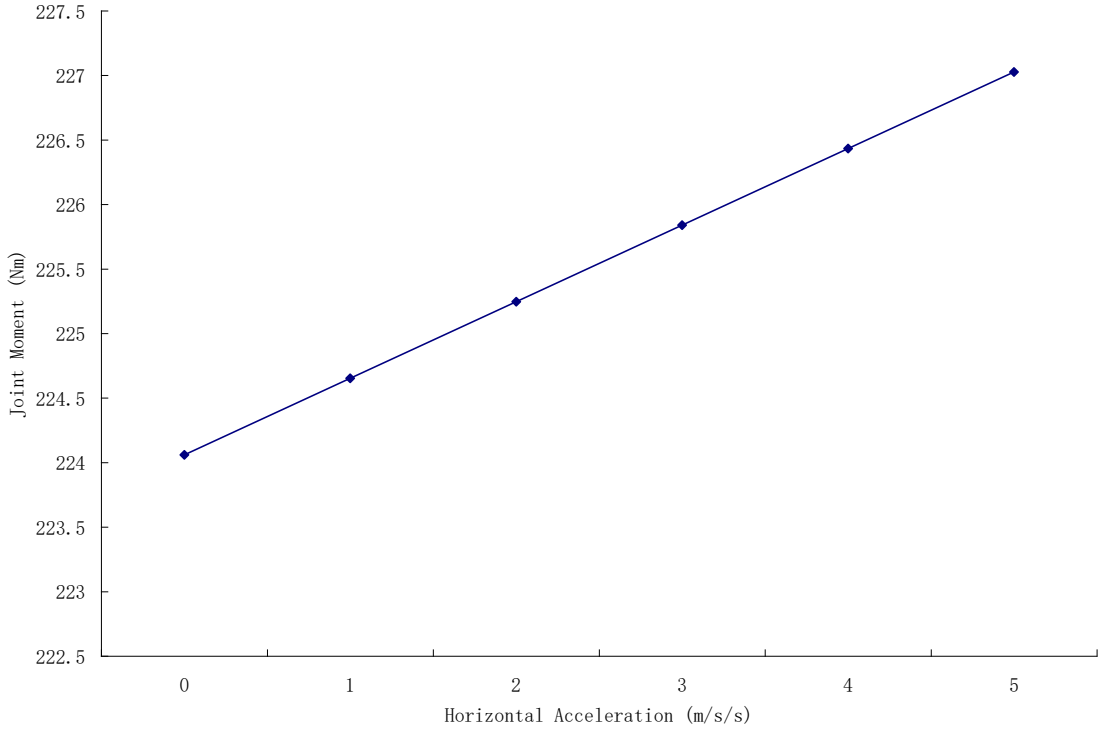

Figure 4.20: Average knee joint moments vs horizontal accelerations at 130 rpm

4.3 Hip Joint Moments

Figures 4.21a – 4.25a are the variation of ankle joint moments with crank angles over a complete revolution at various crank speeds of 10, 50, 80, 110 and 130 rpm respectively while Figures 4.21b – 4.25b are the plots of variations components of ankle joint moments and the crank angles at 10, 50, 80, 110 and 130 rpm respectively. There are also four components that are responsible for the hip joint moment and its pattern, namely the hip torque, the knee joint moment, the horizontal and the vertical moments. The moment generated by the horizontal force start from 0 Nm at 0^0 decreasing to a minimum at 30^0 and increases to zero at 60^0 and crosses the x-axis at this point. It continues to increase until it gets to its maximum at 130^0 then decrease back to minimum at 270^0 then increase to 330^0 and then rises slightly and decrease back to zero at 360^0 while the vertical component starts at almost the same point with the knee joint

moment at 0^0 decreasing to the minimum at 150^0 then starts to increase and decrease again at 225^0 and increase to a maximum crossing x-axis at 285^0 increasing to maximum at 360^0. The torque component is almost constant remaining horizontal straight line along the x-axis except a crest between 15^0 and 180^0 fluctuating around x-axis from crank speed of 80 rpm and above. The horizontal moment decreases in magnitude as the crank speed increases but maintains the same shape while the vertical component does not really change in value above the x-axis but reducing in value as the crank speed is increasing. The sum of these moments gives the hip joint moment its shape as well. The knee joint moment of the five crank speed are of the same shape except for a kink that starts to manifest from 80rpm and became very prominent at 130 rpm which is due to the sharp drop in vertical moment explained earlier. The highest hip joint moments are at 0^0 and 345^0, with the minimum at 200^0.

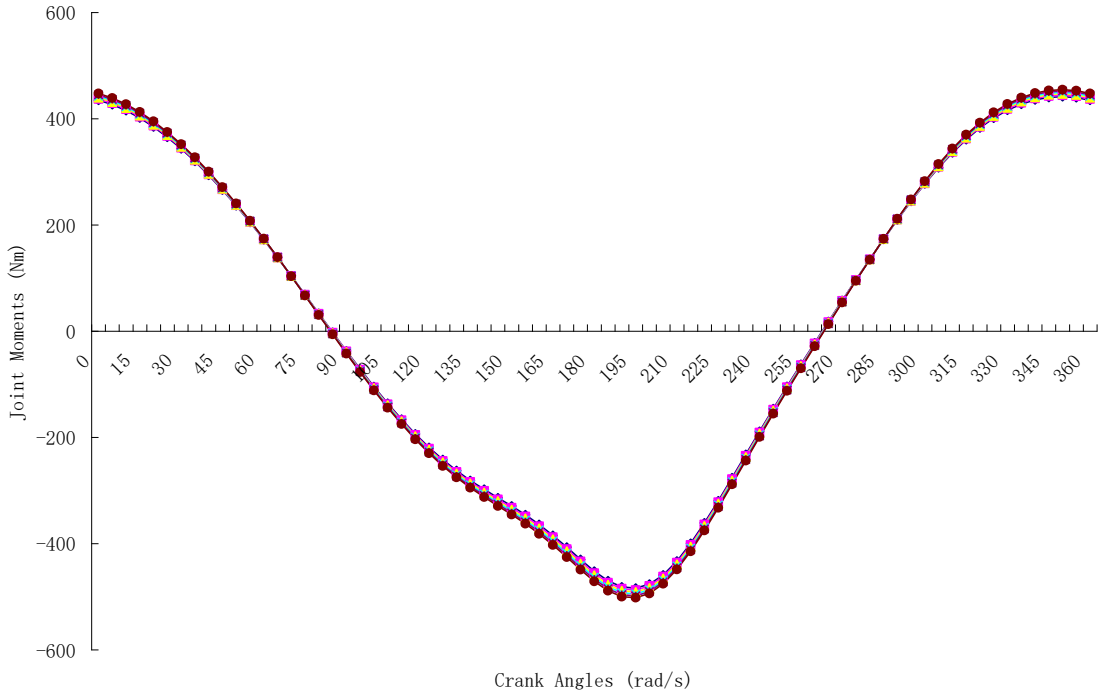

Figure 4.21 (a): Hip joint moments vs crank angles at 10 rpm

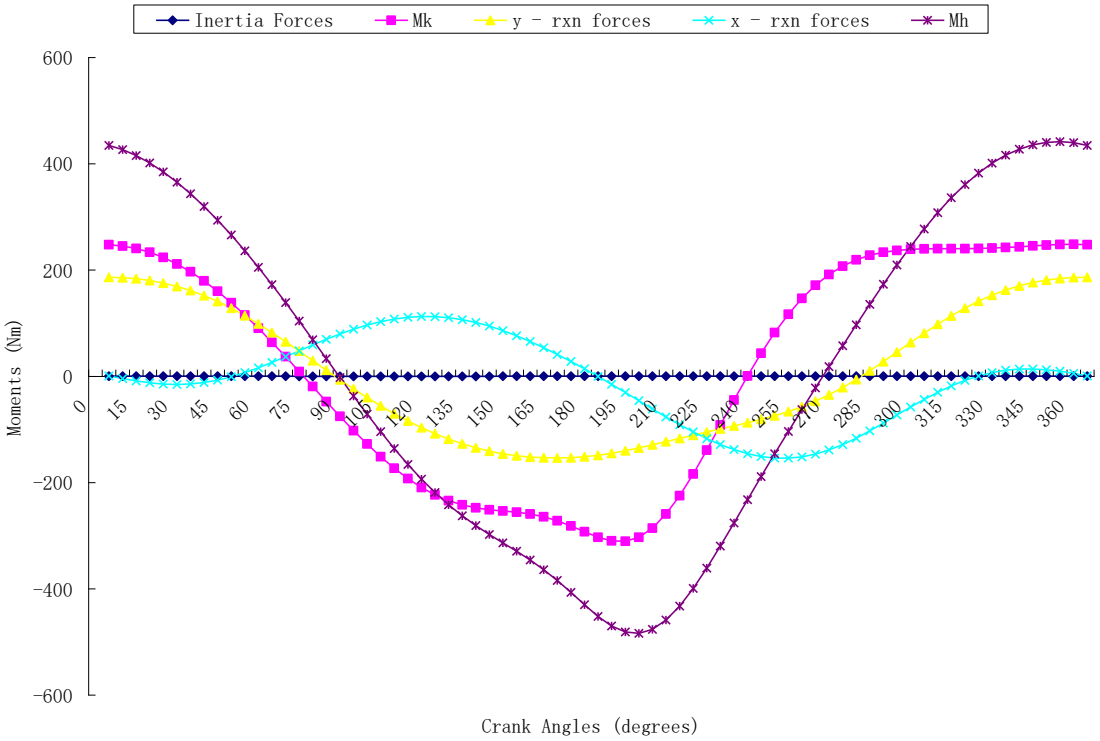

Figure 4.21 (b): Components of hip joint moments vs crank angles at 10 rpm

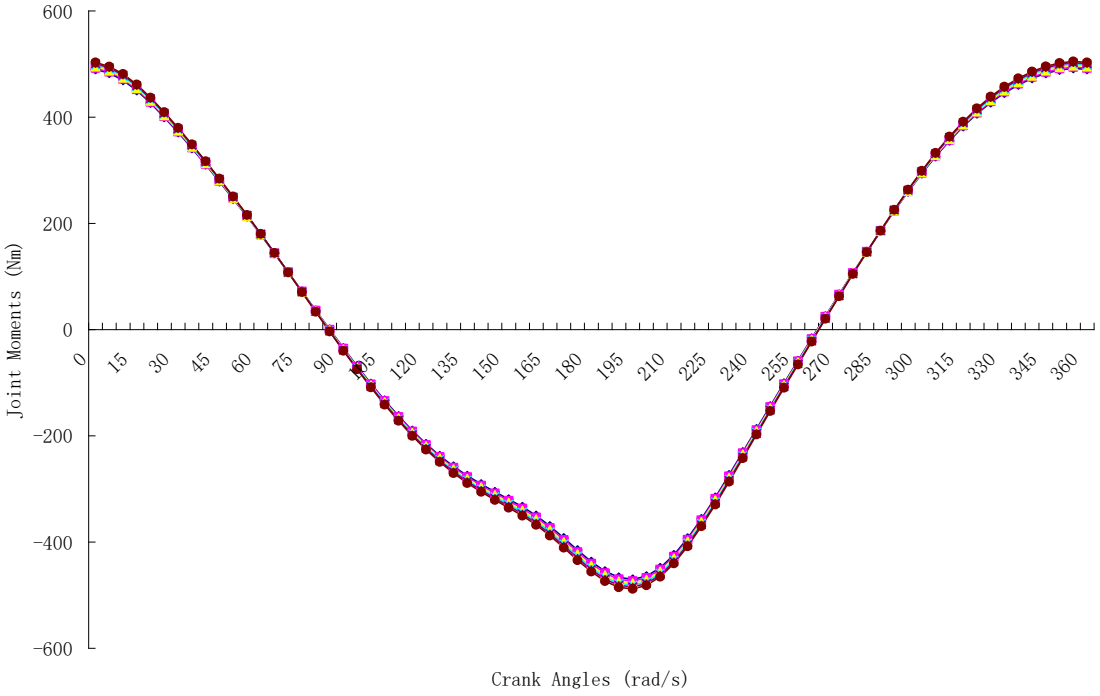

Figure 4.22 (a): Hip joint moments vs crank angles at 50 rpm

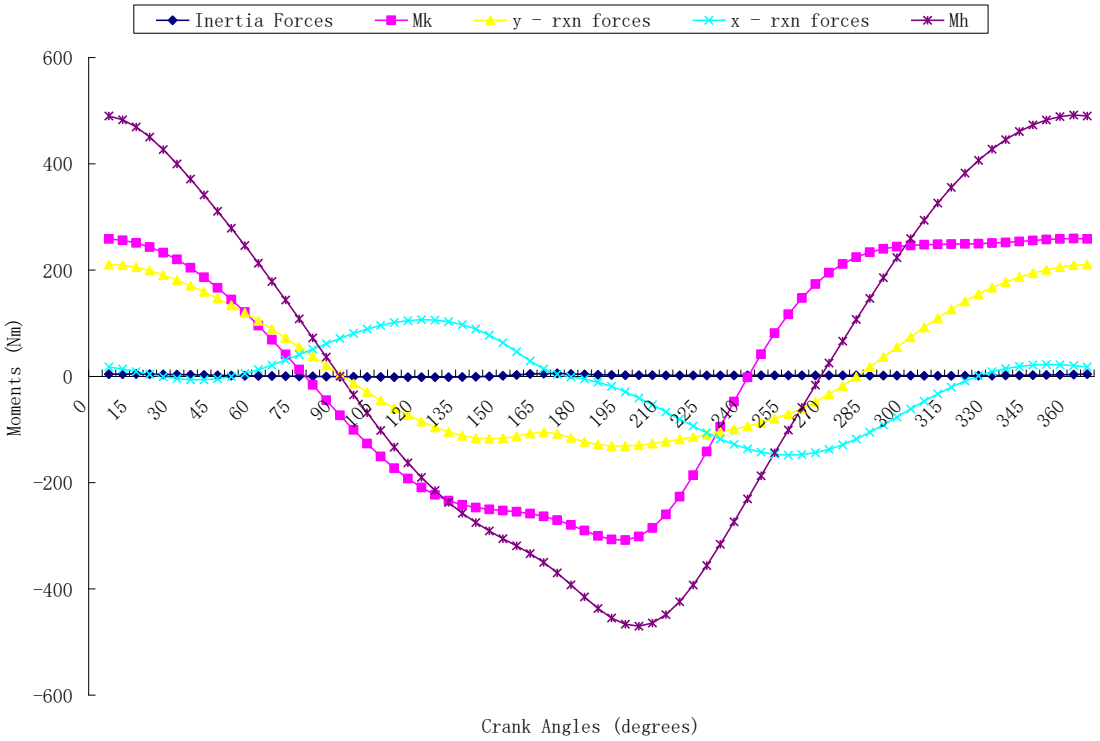

Figure 4.22 (b): Components of hip joint moments vs crank angles at 50 rpm

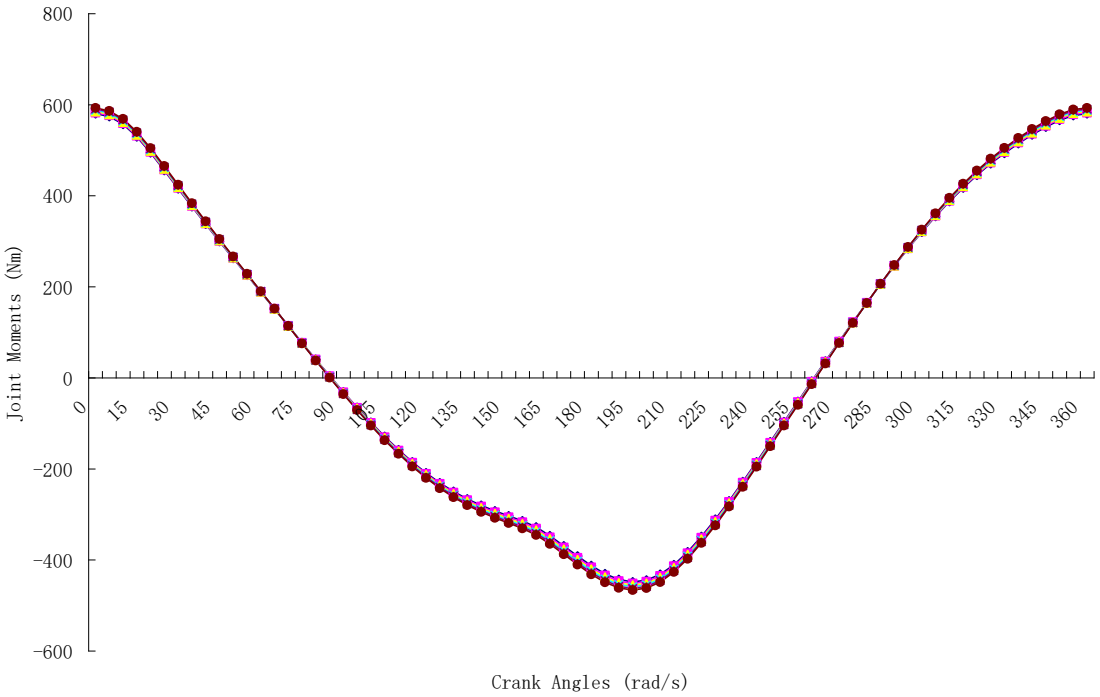

Figure 4.23 (a): Hip joint moments vs crank angles at 80 rpm

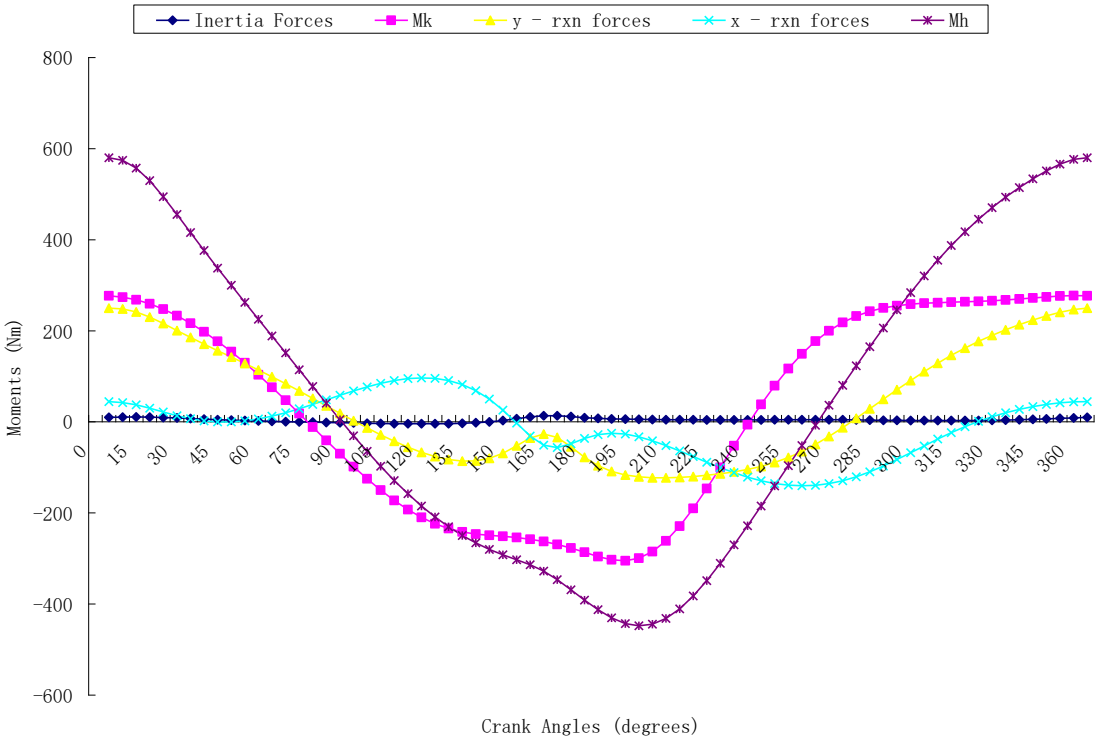

Figure 4.23(b): Components of hip joint moments vs crank angles at 80 rpm

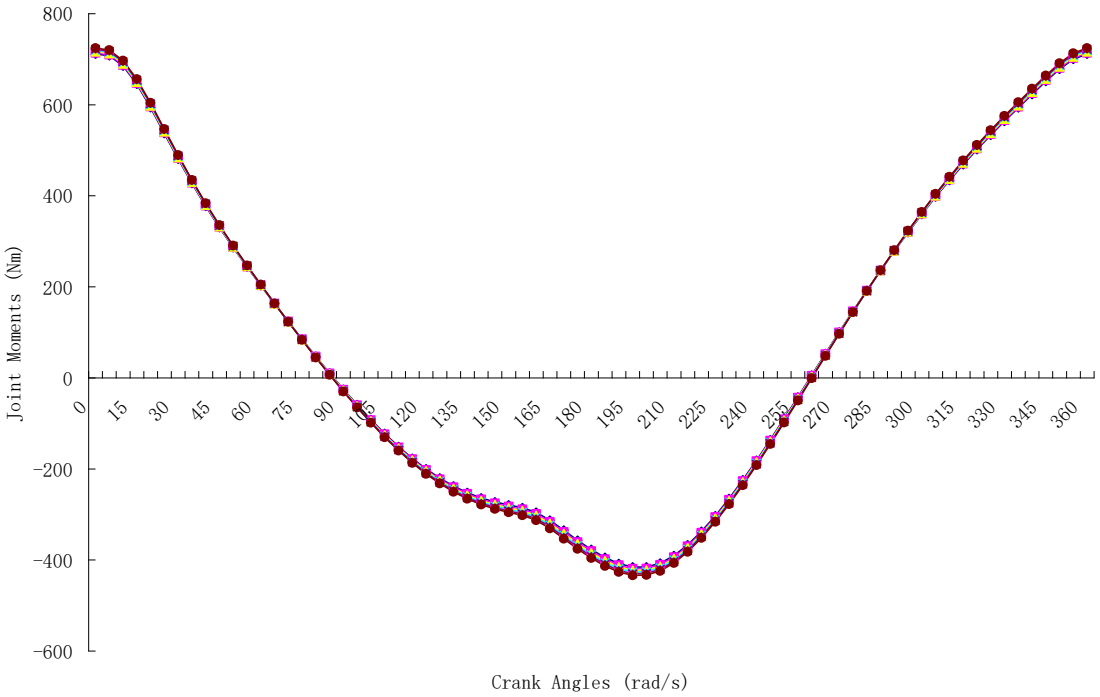

Figure 4.24 (a): Hip joint moments vs crank angles at 110 rpm

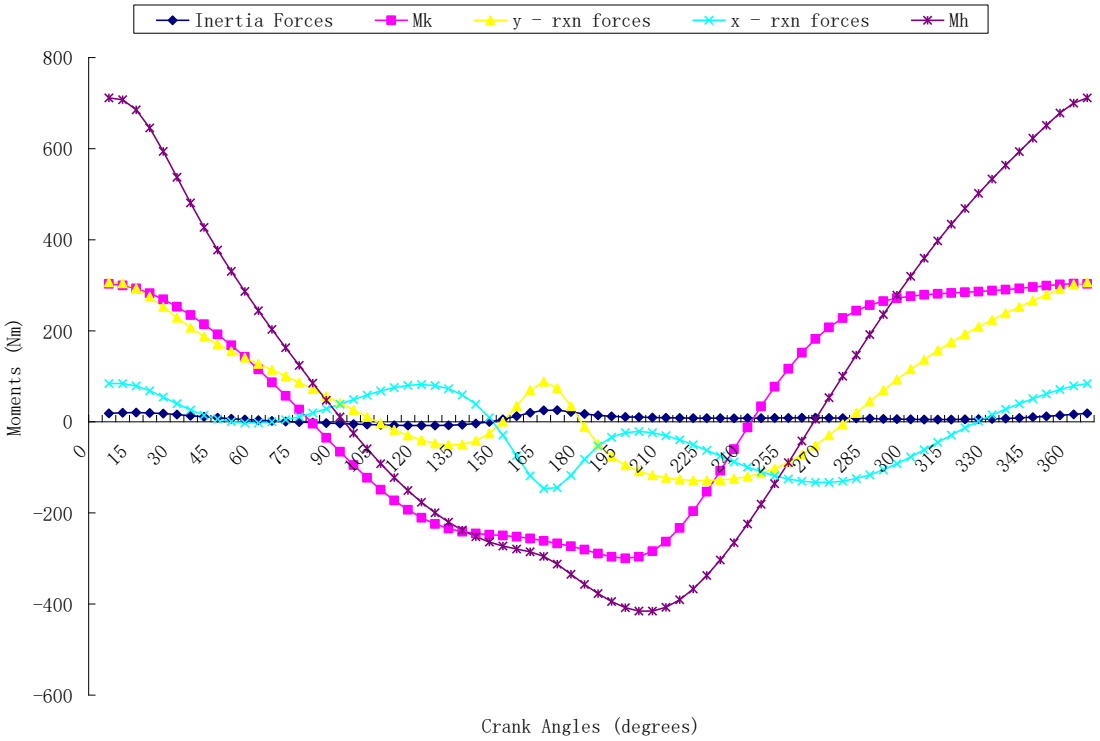

Figure 4.24 (b): Components of hip joint moments vs crank angles at 110 rpm

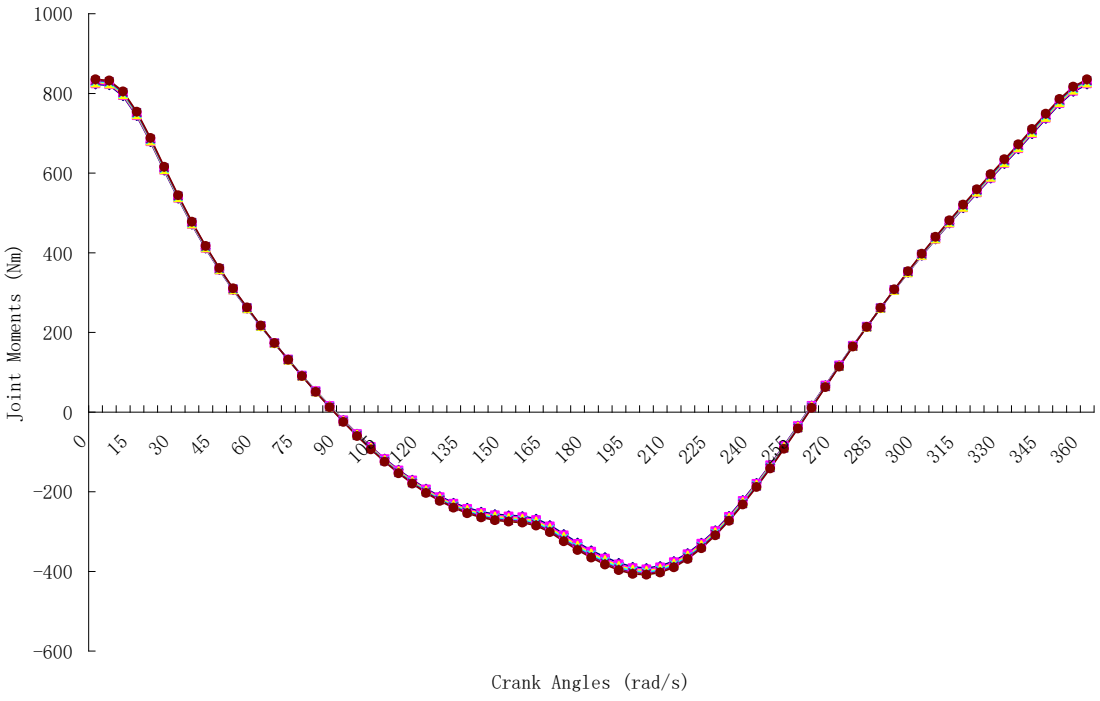

Figure 4.25 (a): Hip joint moments vs crank angles at 130 rpm

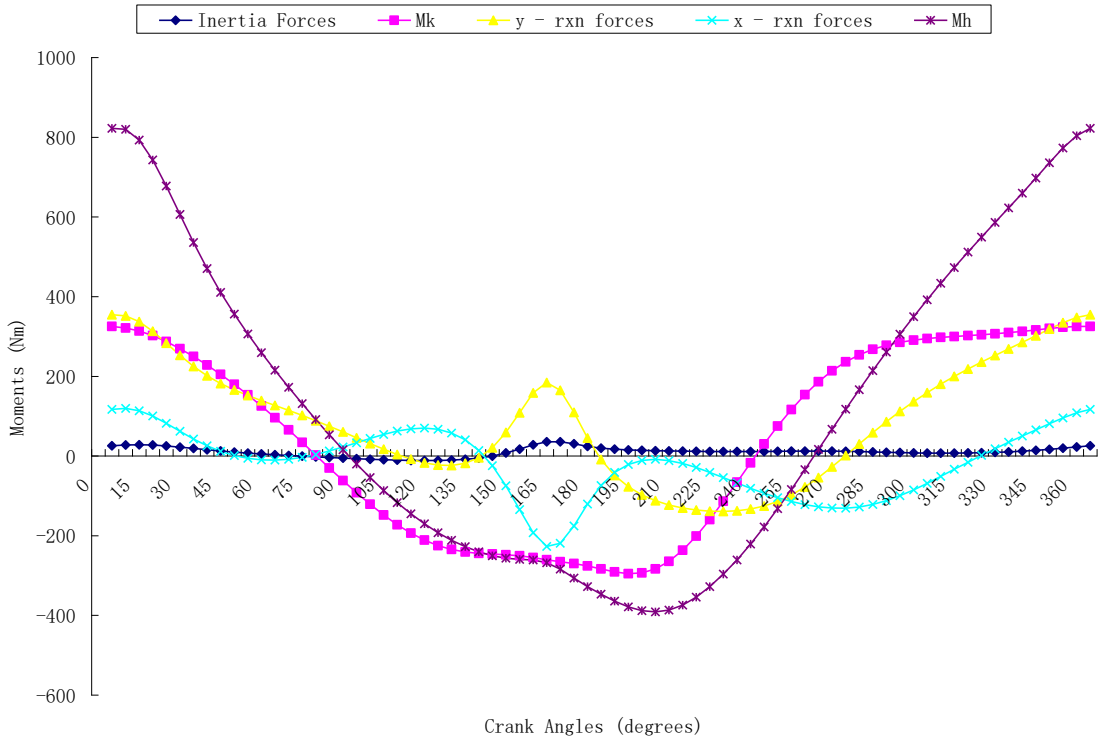

Figure 4.25 (b): Components of hip joint moments vs crank angles at 130 rpm

Figures 4.26 – 4.30 are the variation of average hip joint moment and horizontal acceleration. These plots were obtained in the same manner as average ankle joint moment. The joint moments increase as the horizontal acceleration increase thereby encouraging lower acceleration during cycling.

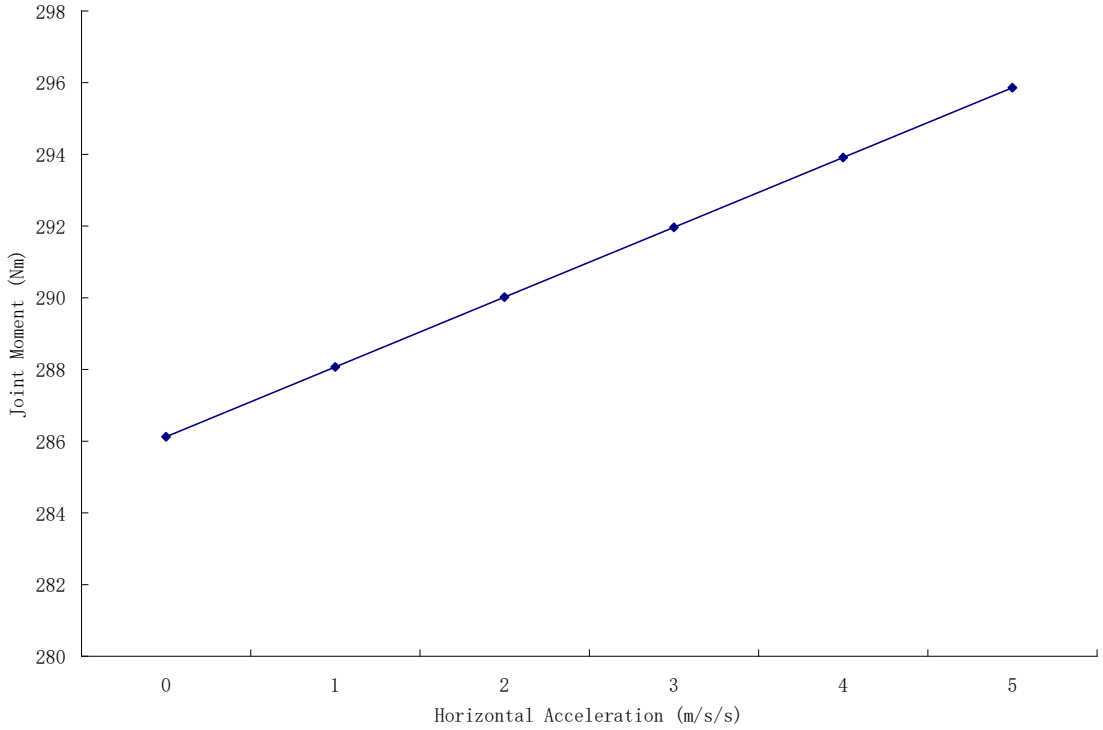

Figure 4.26: Average hip joint moments vs horizontal acceleration at 10 rpm

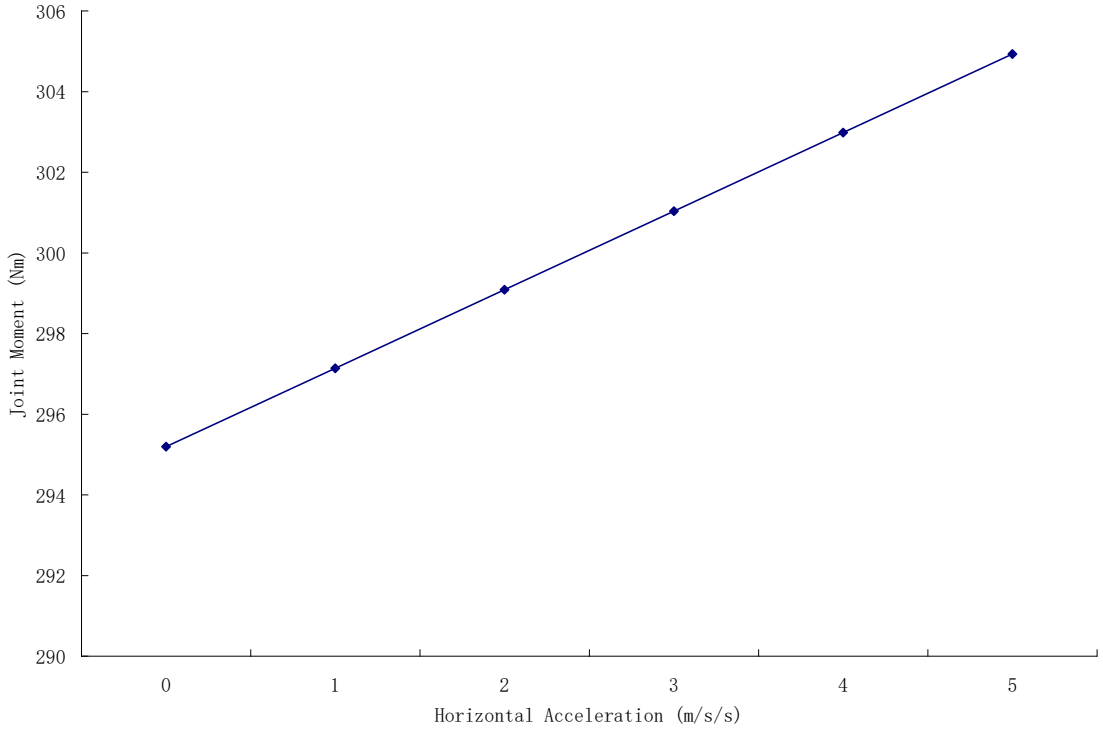

Figure 4.27: Average hip joint moment vs horizontal acceleration at 50 rpm

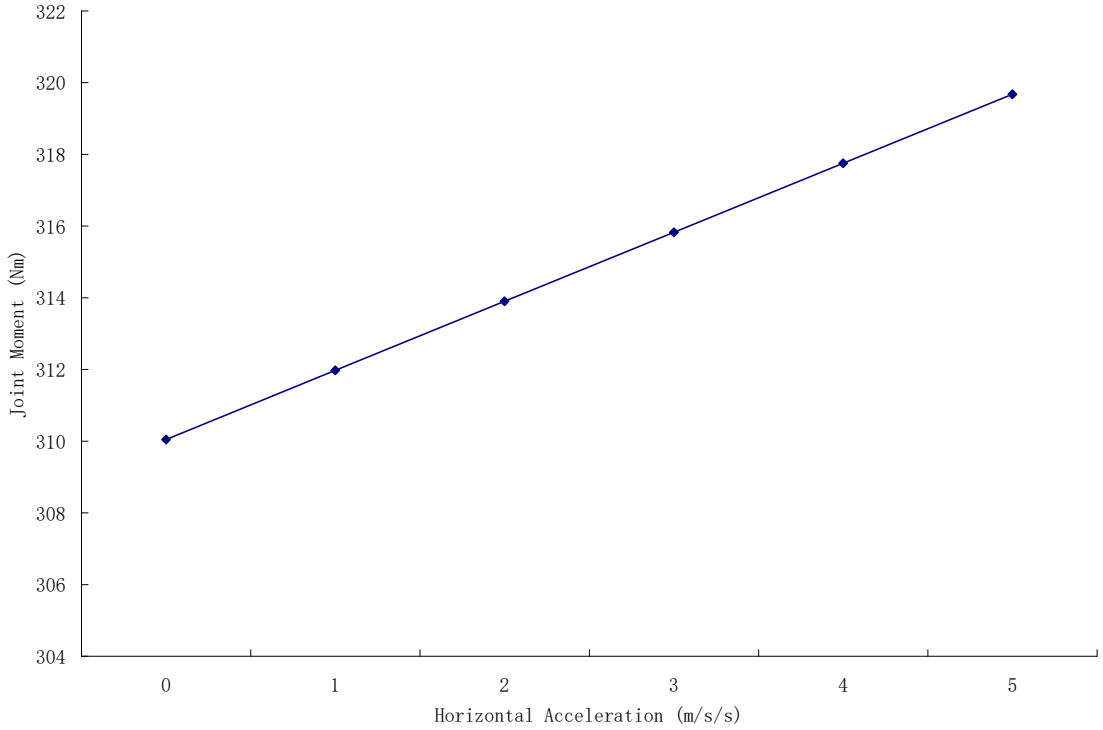

Figure 4.28: Average hip joint moment vs horizontal acceleration at 80 rpm

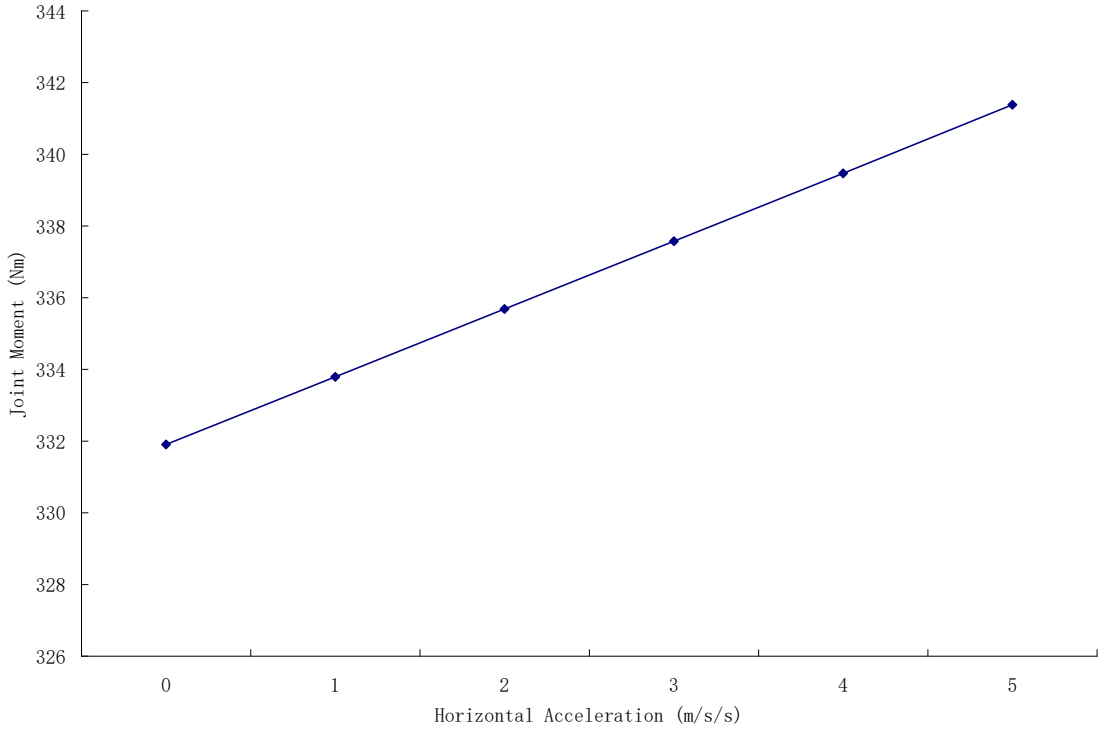

Figure 4.29: Average hip joint moment vs horizontal acceleration at 110 rpm

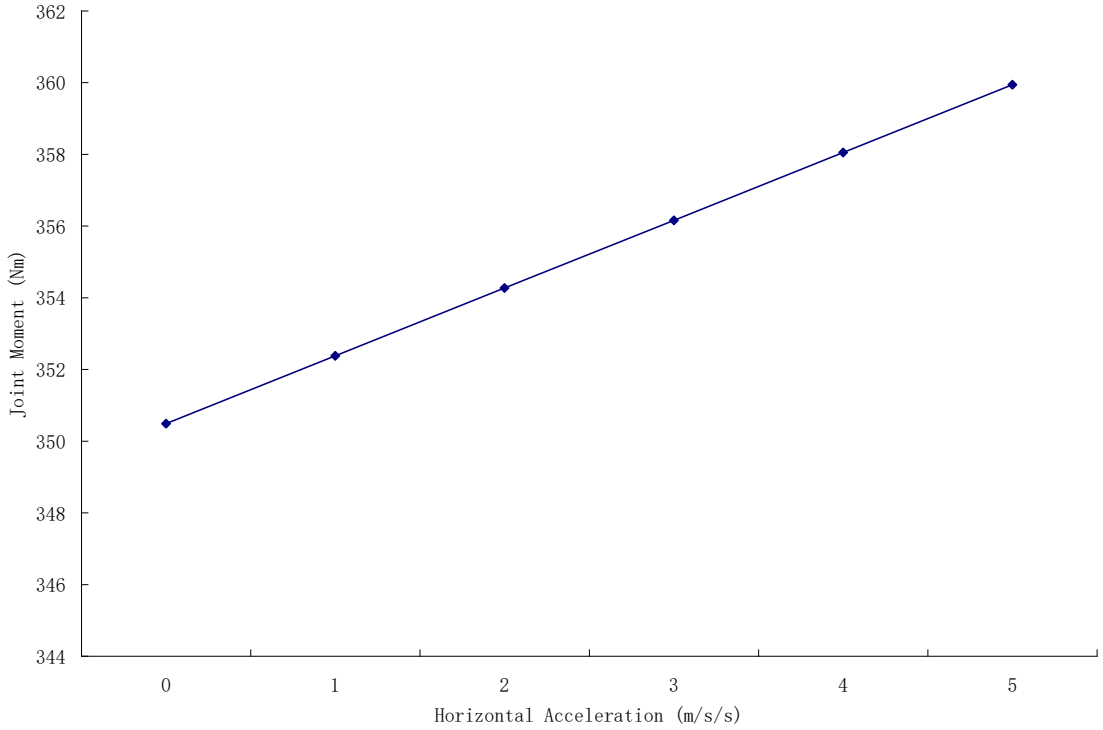

Figure 4.30: Average hip joint moments vs horizontal acceleration at 130 rpm

4.4 Average Joint Moments

Figures 4.31 – 4.35 are the variation of average ankle, knee and hip joints moments and horizontal acceleration for crank speed of 10, 50, 80, 110 and 130 rpm. These plots were obtained in the same manner as average ankle joint moment (a combination of all the average joint moments). This is done to have a graphical picture of the three joint moments on the same axes at different crank speed. The highest of the three is the hip joint moment followed by knee. The thigh segment has the highest mass and therefore highest inertia.

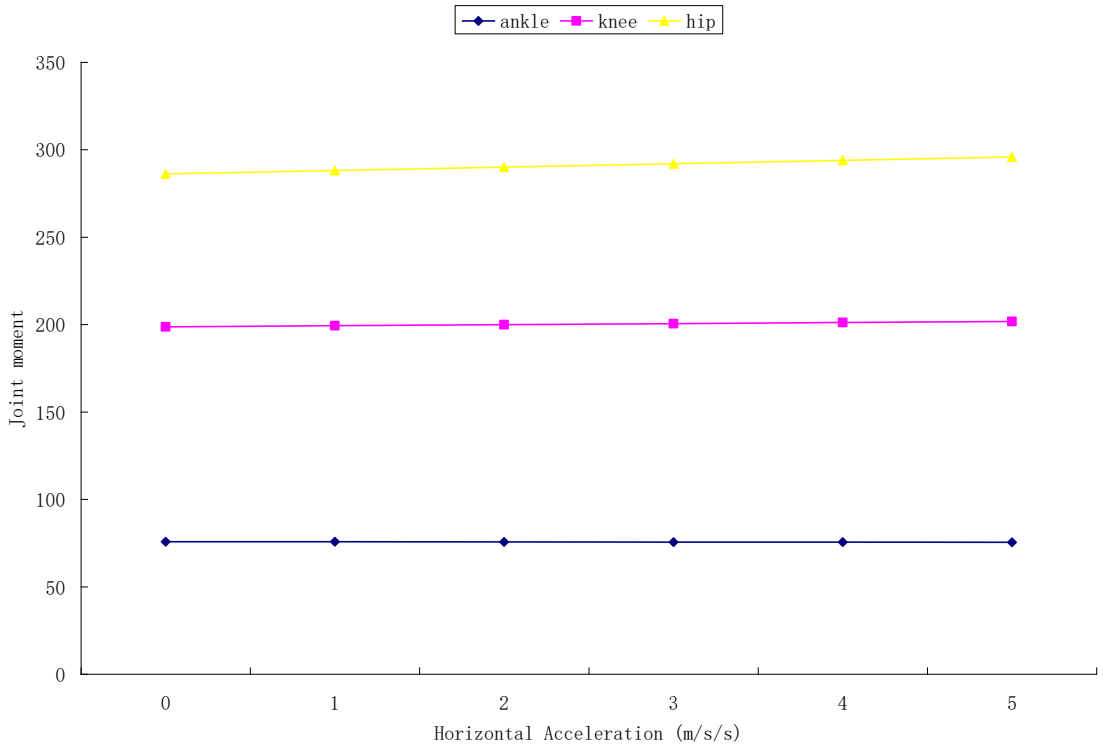

Figure 4.31: Average joint moments vs horizontal acceleration 10 rpm

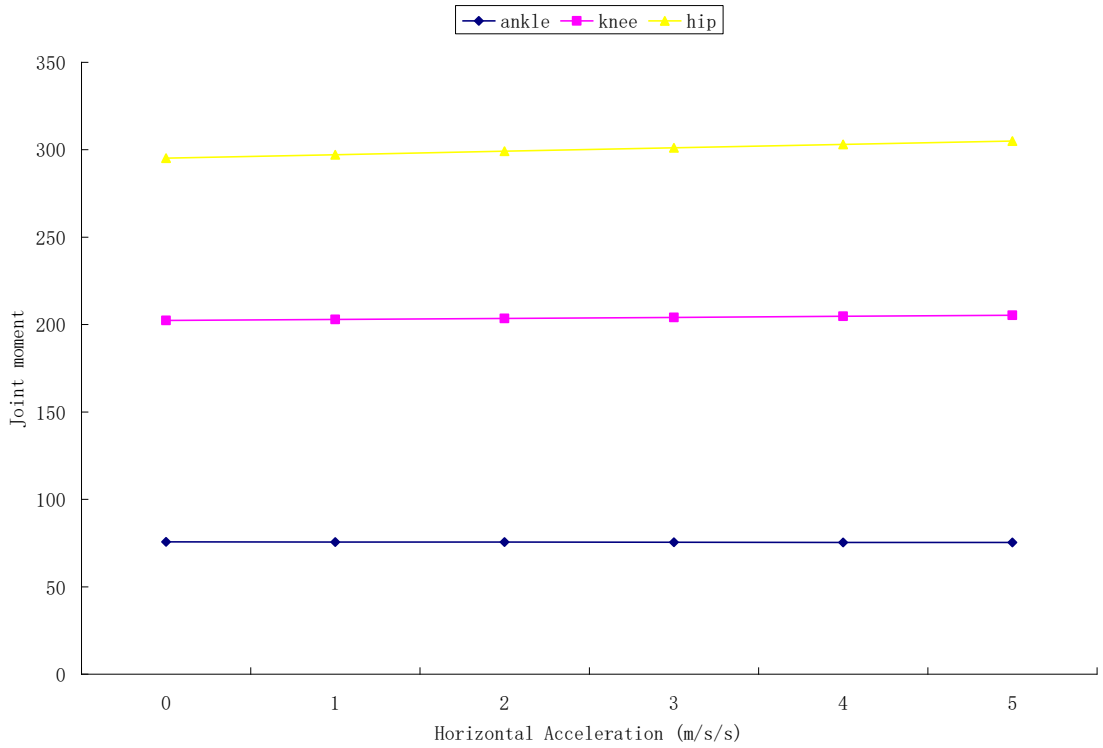

Figure 4.32: Average joint moments vs horizontal acceleration at 50 rpm

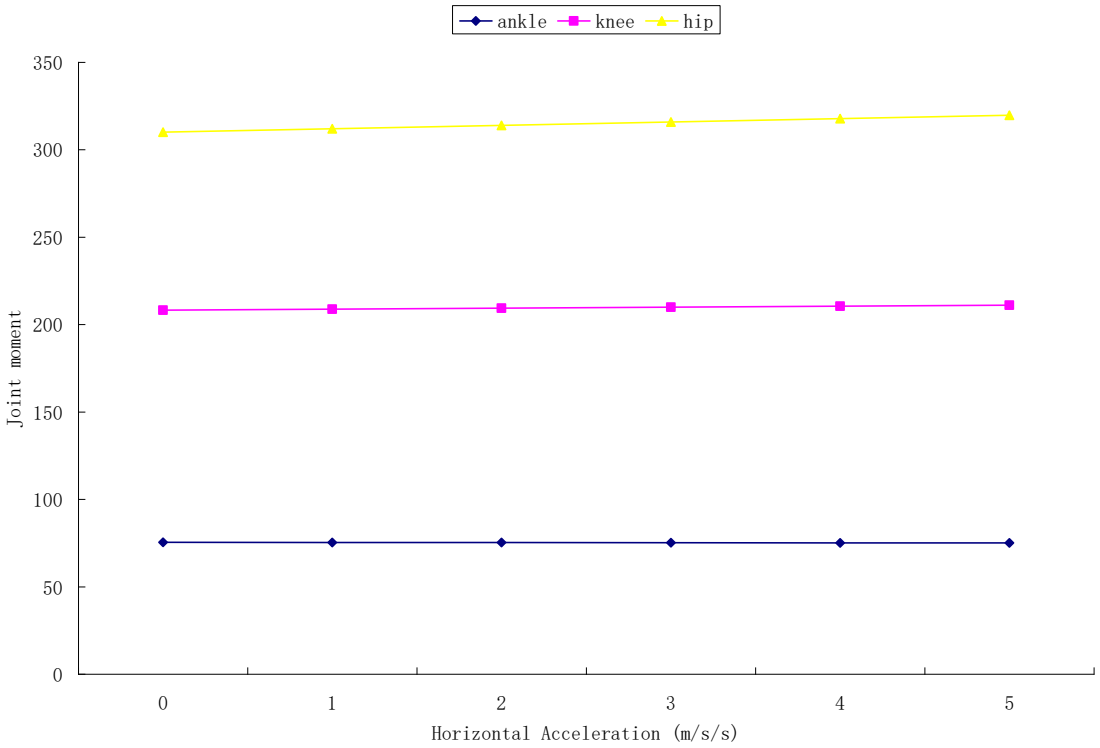

Figure 4.33: Average joint moments vs horizontal acceleration at 80 rpm

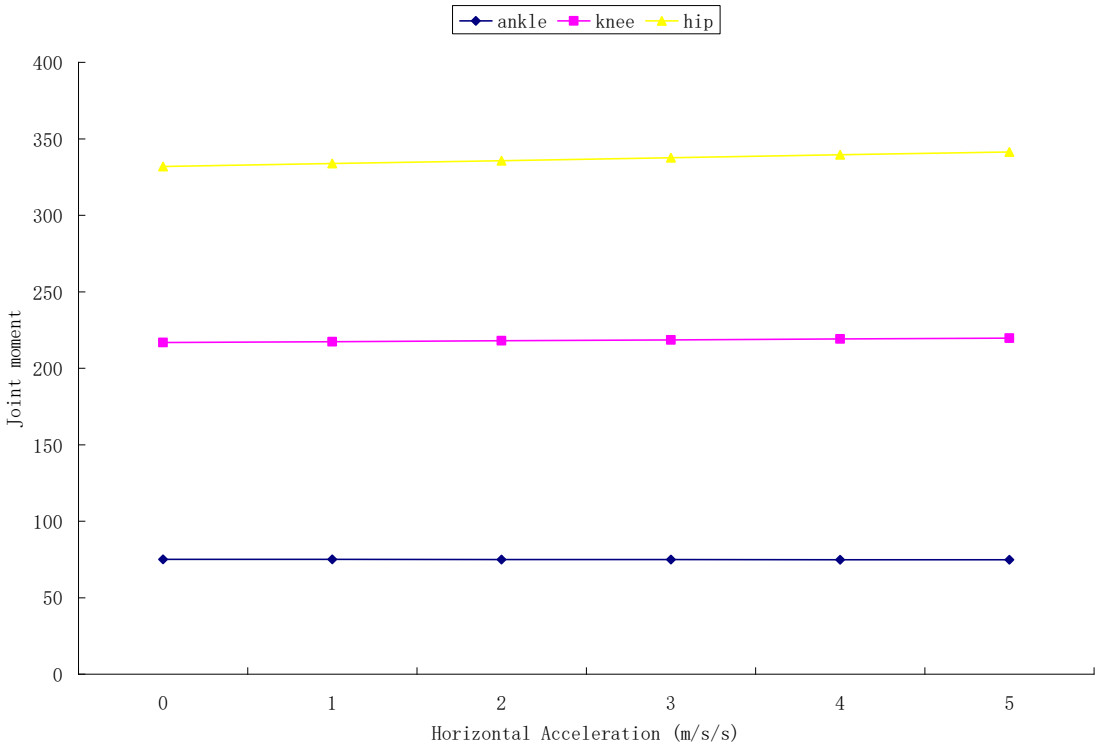

Figure 4.34: Average joint moments vs horizontal acceleration at 110 rpm

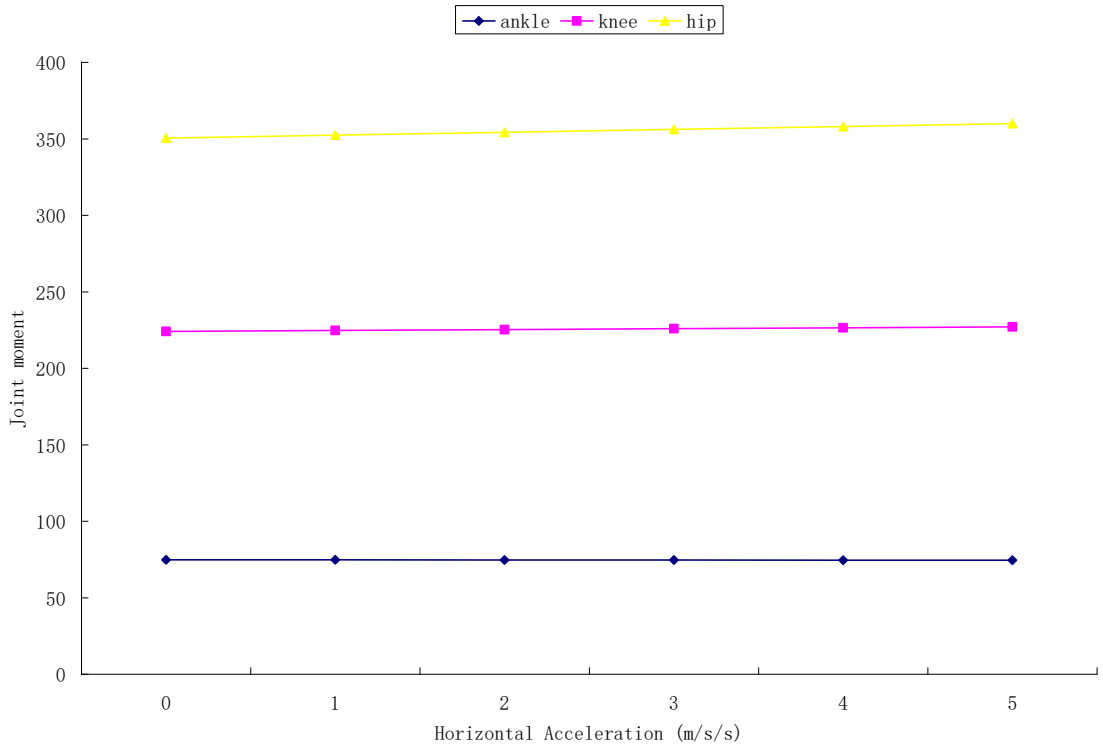

Figure 4.35: Average joint moments vs horizontal acceleration at 130 rpm

4.5 Determination of Optimum Crank Speed

Figures 4.36 (a) and (b) are the plots of joint moments and crank speed from 5 to 130 rpm. In Figures 4.36 (a) and (b), it is observed that the knee and hip joint moments are lower than the ankle joint and they are increasing from the minimum to cross the ankle joint moment, first knee joint moment line at 50 rpm while the hip crossed at 64 rpm. It can be inferred from the graph that cycling above 64 rpm will affect the knee as well as the hip joint. The optimum crank speed is therefore 64 rpm. This will reduce the risk of damage to the lower limb segments.

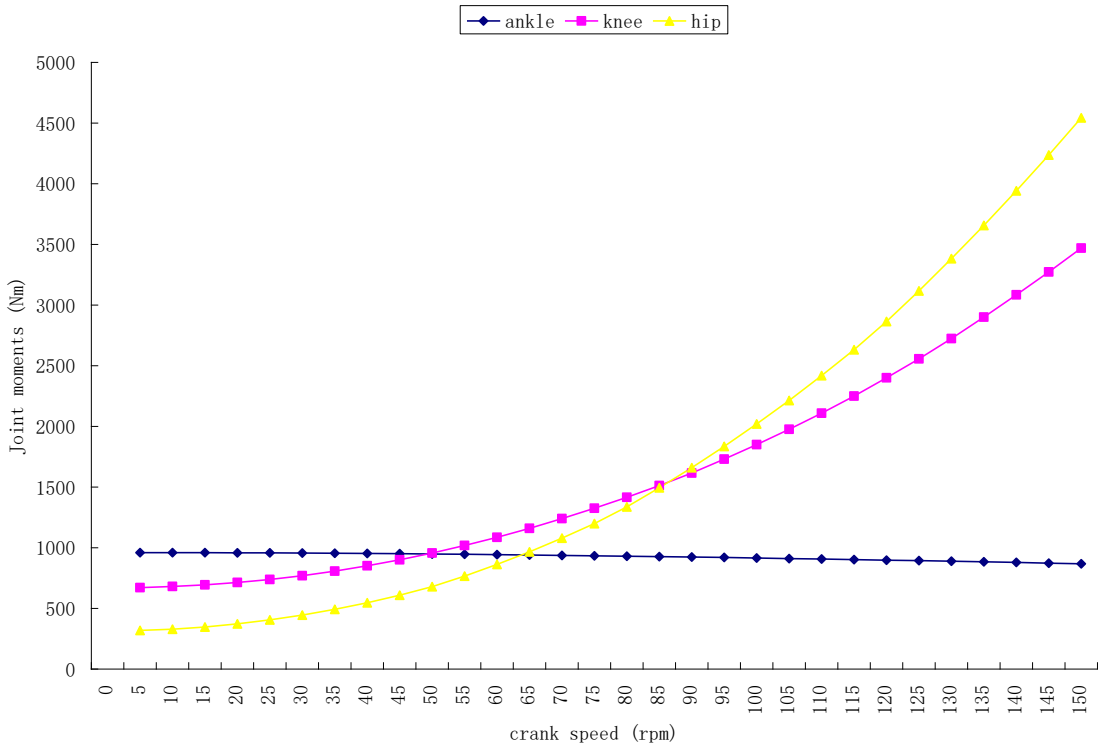

Figure 4.36 (a): Joint Moments vs Crank Speed

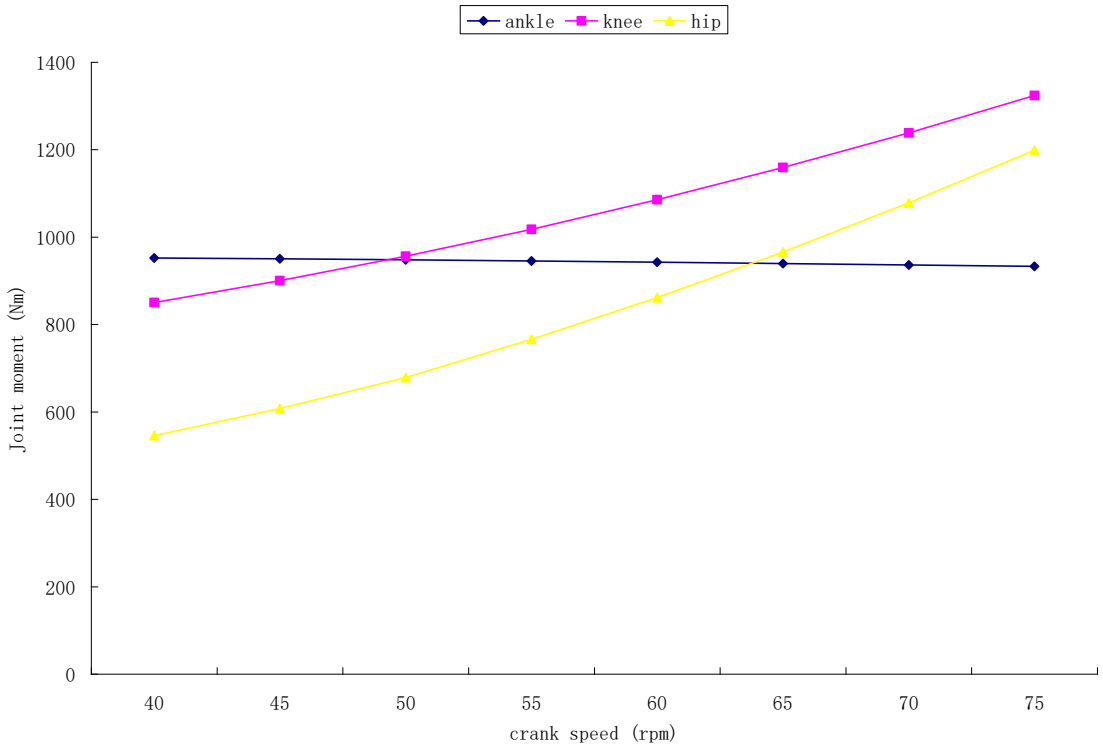

Figure 4.36 (b): Joint Moments vs Crank Speed

Figures 37a – 39a are the variation of the ankle, knee and hip joints and crank angles respectively while Figures 37b – 39b are the components of these joint moments. The shapes of the joint moments bear resemblance to what were discussed earlier.

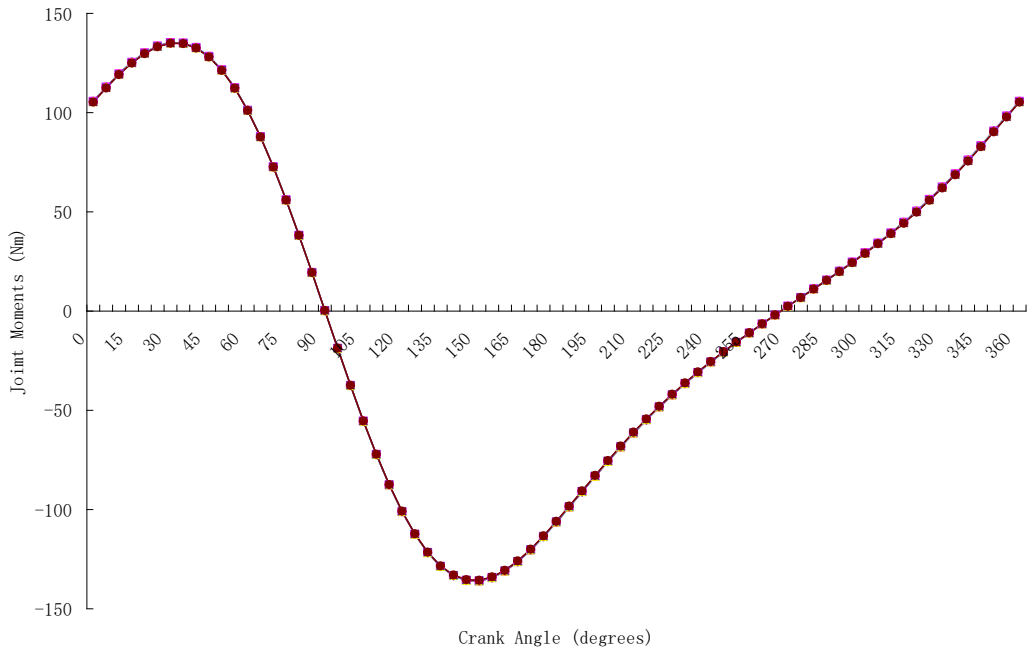

Figure 4.37 (a): Ankle joint moments vs crank angles at 64 rpm

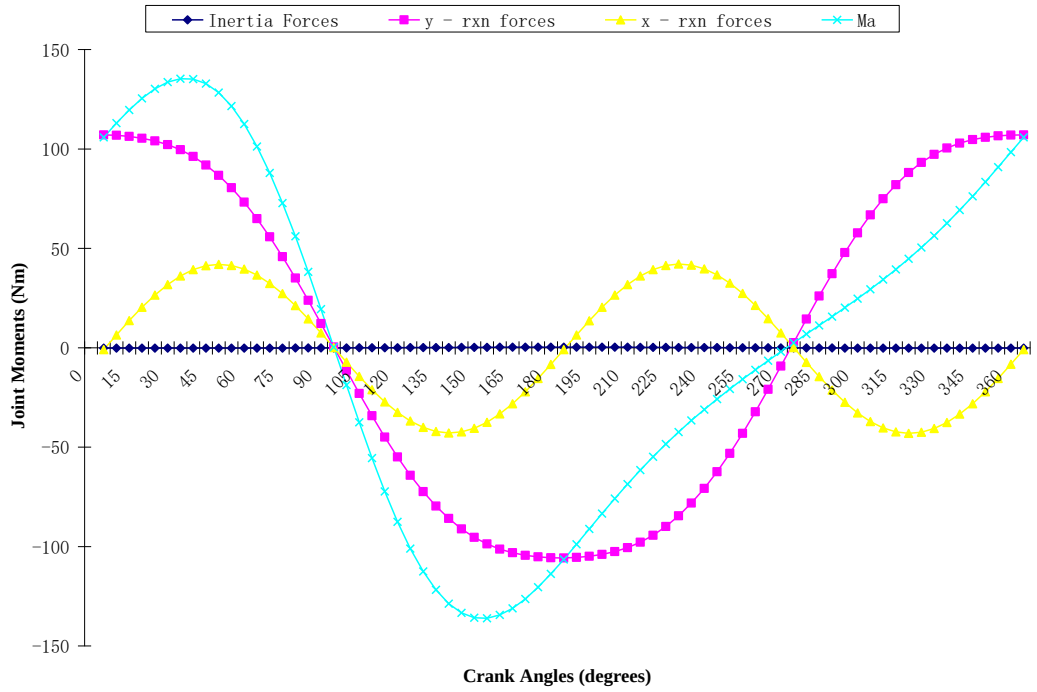

Figure 4.37 (b): Components of ankle joint moments vs crank angles at 64 rpm

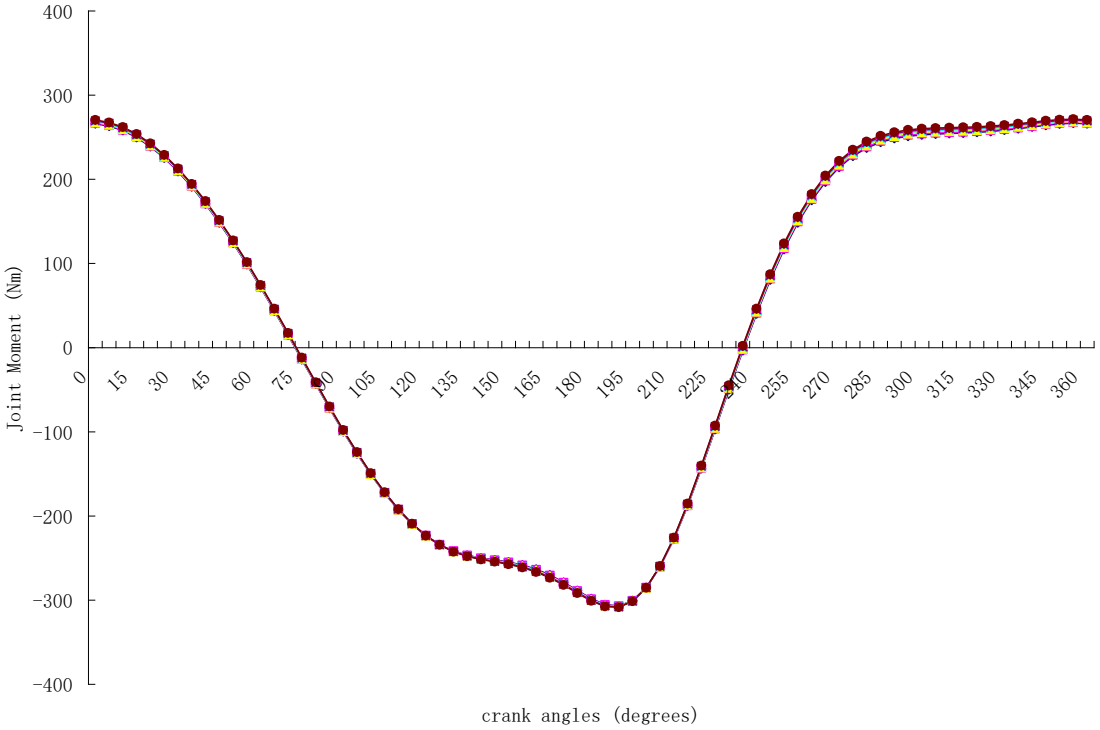

Figure 4.38 (a): Knee joint moments vs crank angles at 64 rpm

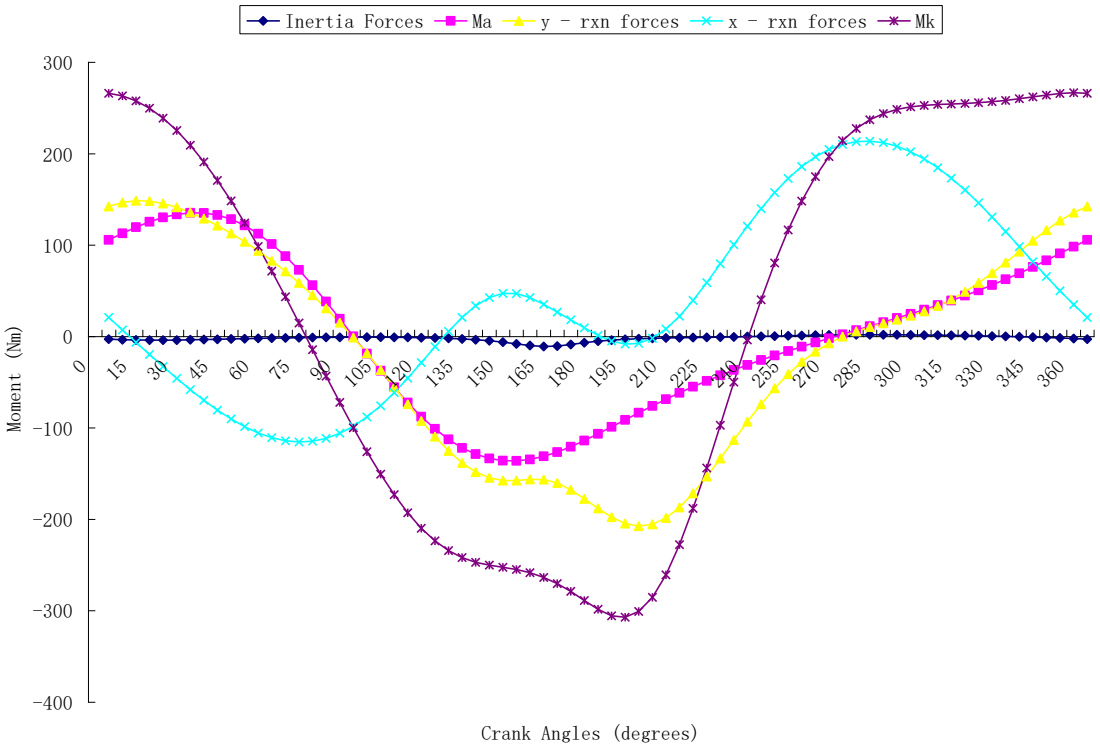

Figure 4.38 (b): Components of knee joint moments vs crank angles at 64 rpm

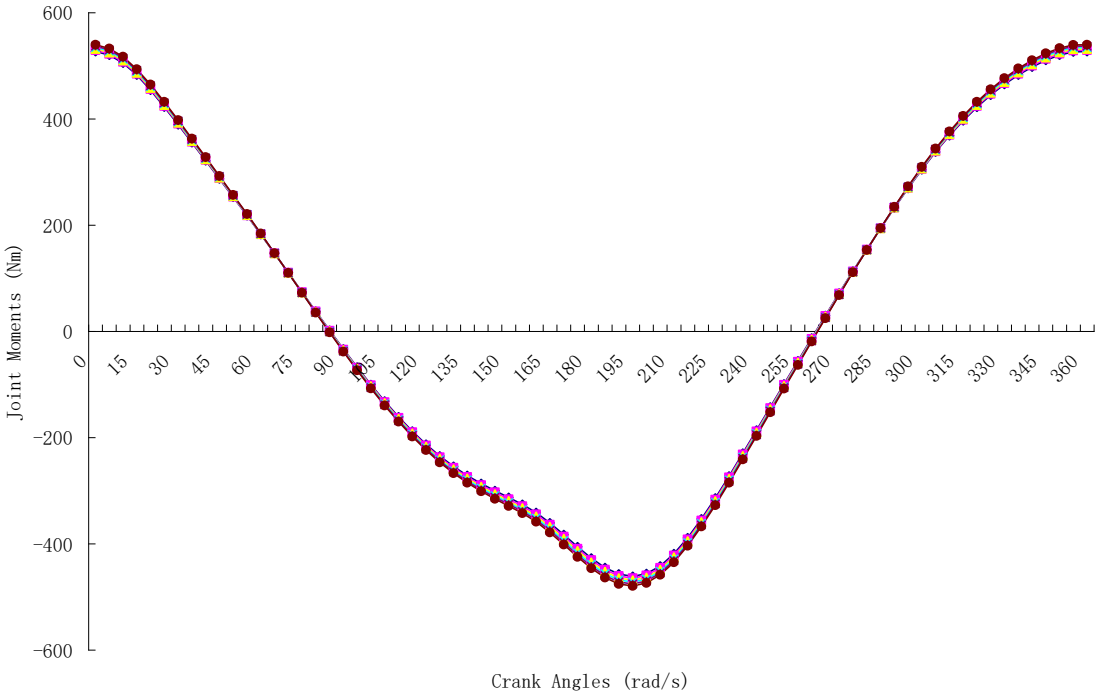

Figure 4.39 (a): Hip joint moments vs crank angles at 64 rpm

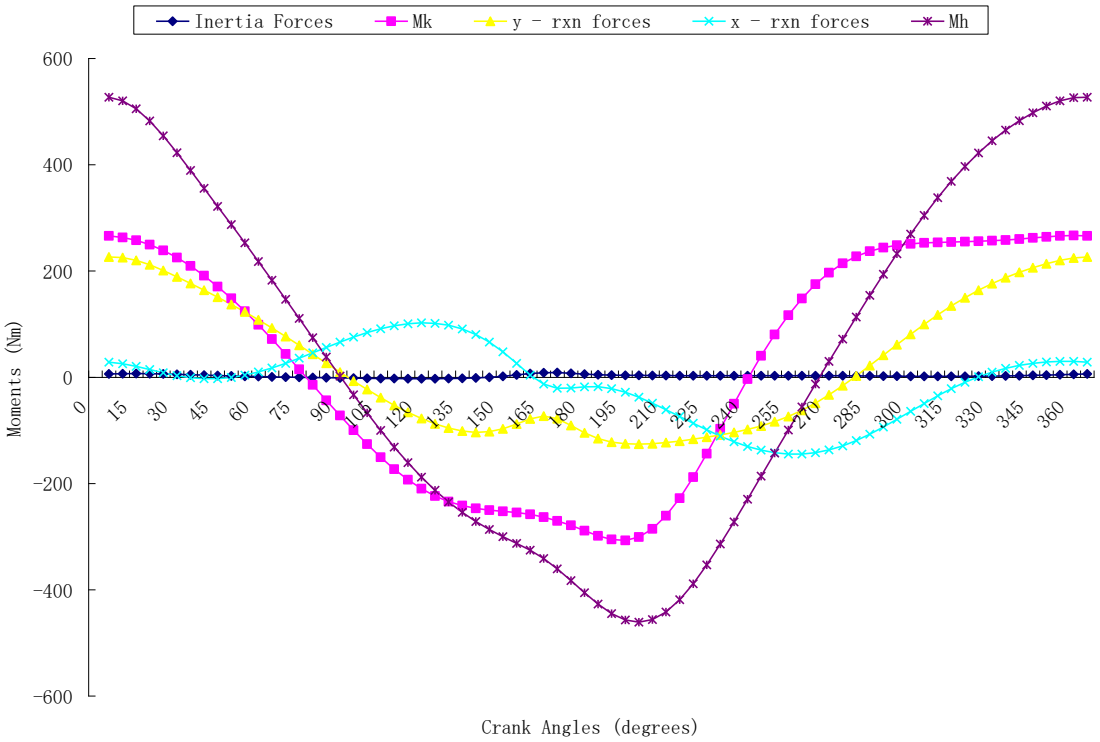

Figure 4.39 (b): Components of hip joint moments vs crank angles at 64 rpm

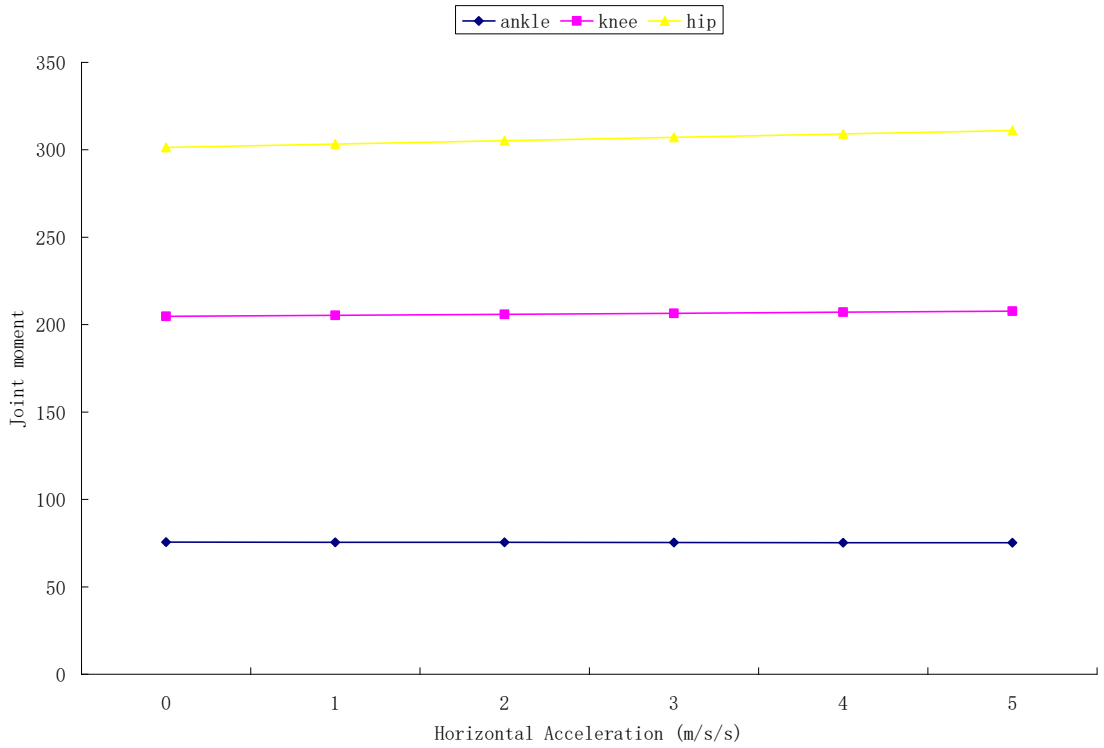

Figure 4.40: Average absolute joint moments vs horizontal acceleration at 64 rpm

4.6 Ankle Joint Moments at 64 rpm and varying Seat Height

Figures 4.41a – 4.47a are the plots of the variation of ankle joint moments with crank angles over a complete revolution at various seat height of 100, 95, 90, 85, 80, 75, and 72% of the total length of the lower limb respectively while Figures 4.41b – 4.47b are the plots of variations components of ankle joint moments and the seat height of 100, 95, 90, 85, 80, 75, and 72% of the total length of the lower limb respectively. The moments generated by the horizontal forces as shown in Figures 4.41b – 4.47b are sinusoidal in shape but completing two cycles in one revolution while the vertical forces generated a cosine shaped moment that completed one cycle in one revolution. The sum of these two forces gave the ankle moment its shape since the moment generated by the torque is virtually zero aligning with the x-axis. The ankle joint moments of the five considered crank speed are almost constant showing no significant difference in shape

and value. The ankle joint moment started to increase from 0^0 until it picked at 30^0 and started to decrease to a minimum value at about 150^0, then started to rise again until it got to 360^0.

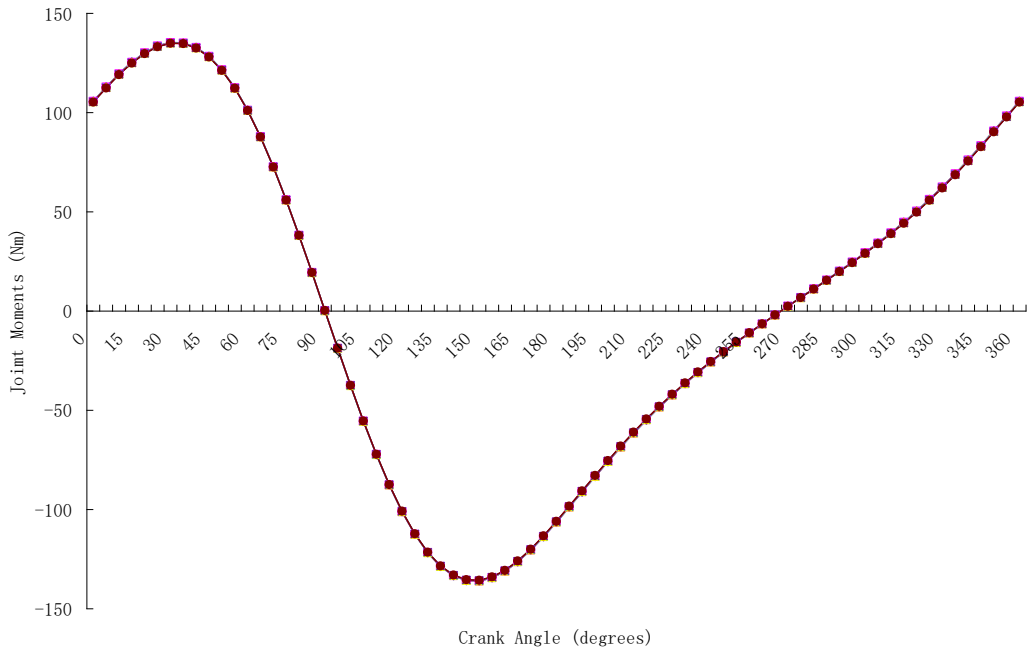

Figure 4.41 (a): Ankle Joint Moments at Seat Height of 100% vs crank angles

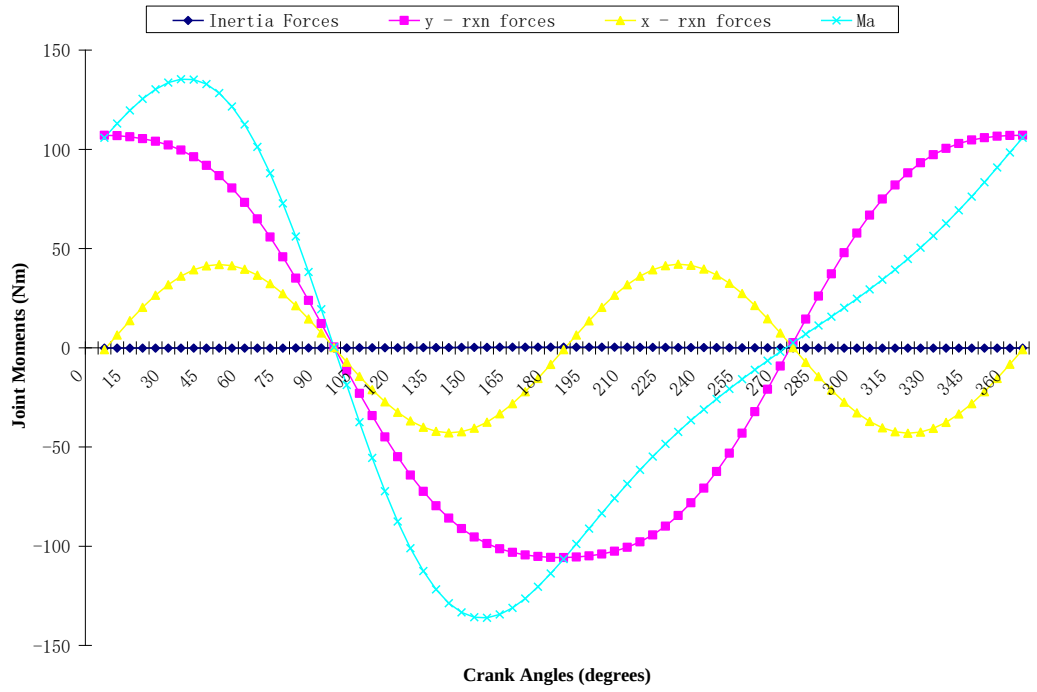

Figure 4.41 (b): Components of Ankle Joint Moments at Seat Height of 100% vs crank angles

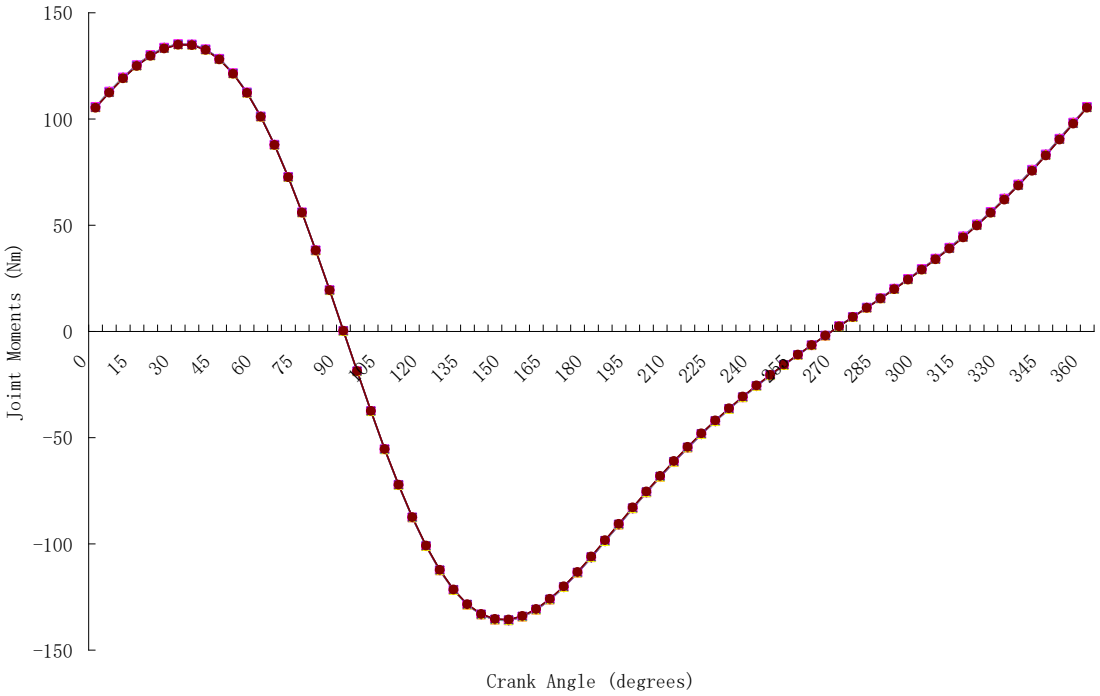

Figure 4.42 (a): Ankle Joint Moments at Seat Height of 95% vs crank angles

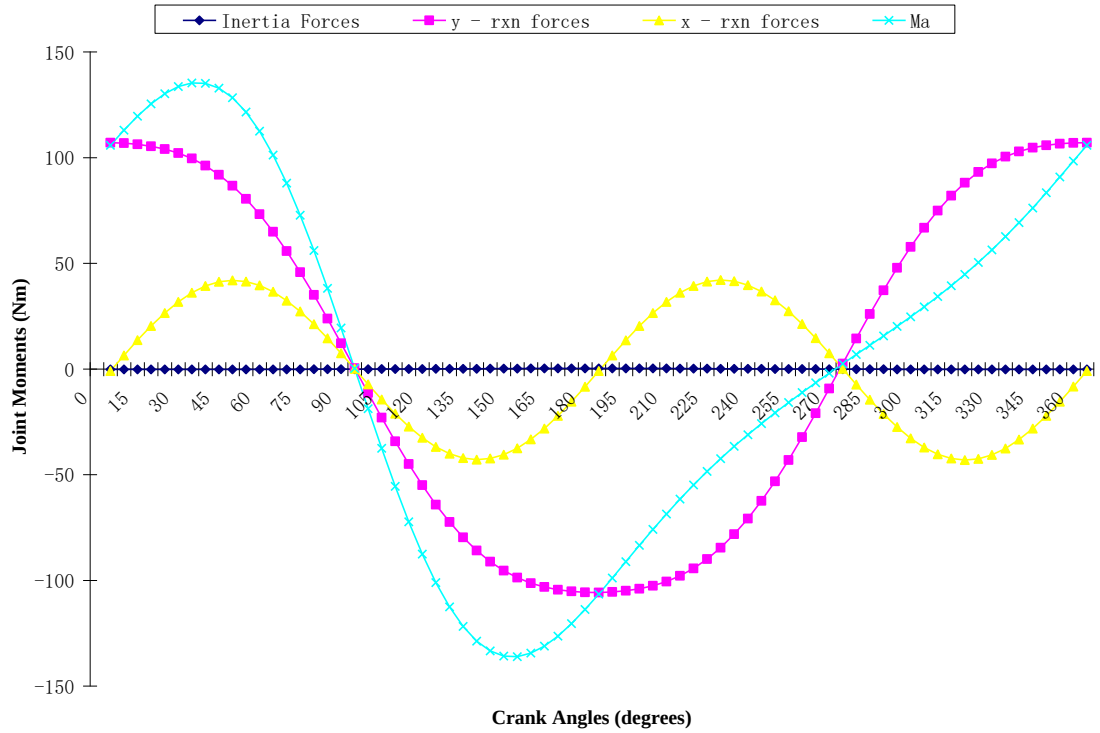

Figure 4.42 (b): Components of Ankle Joint Moments at Seat Height of 95% vs crank angles

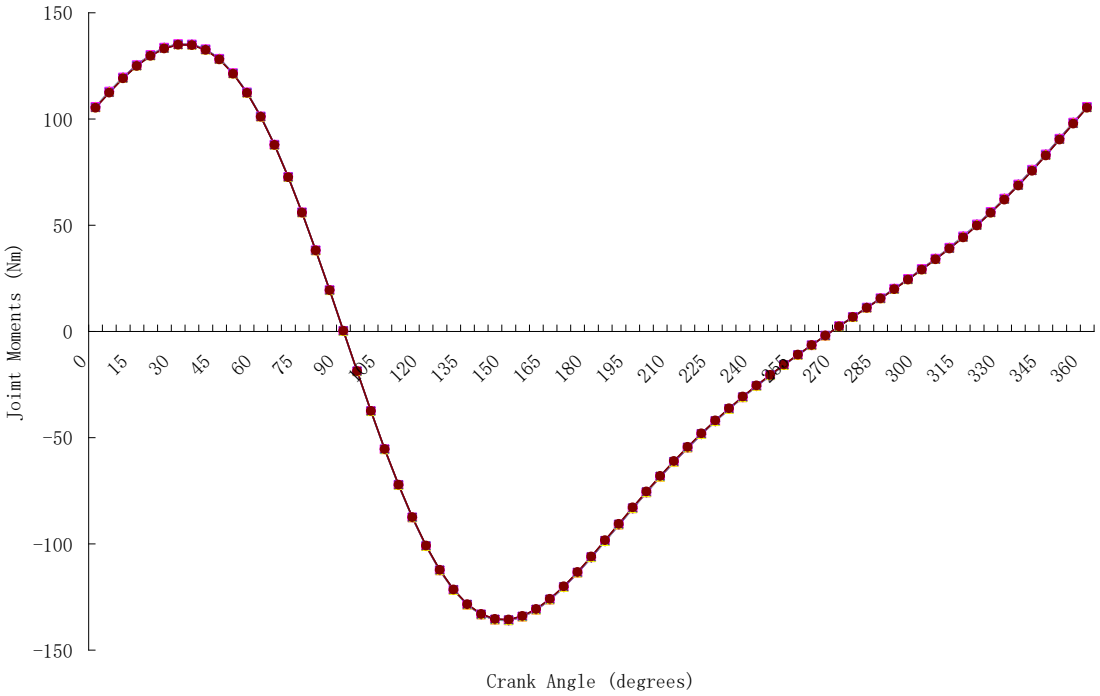

Figure 4.43 (a): Ankle Joint Moments at Seat Height of 90% vs crank angles

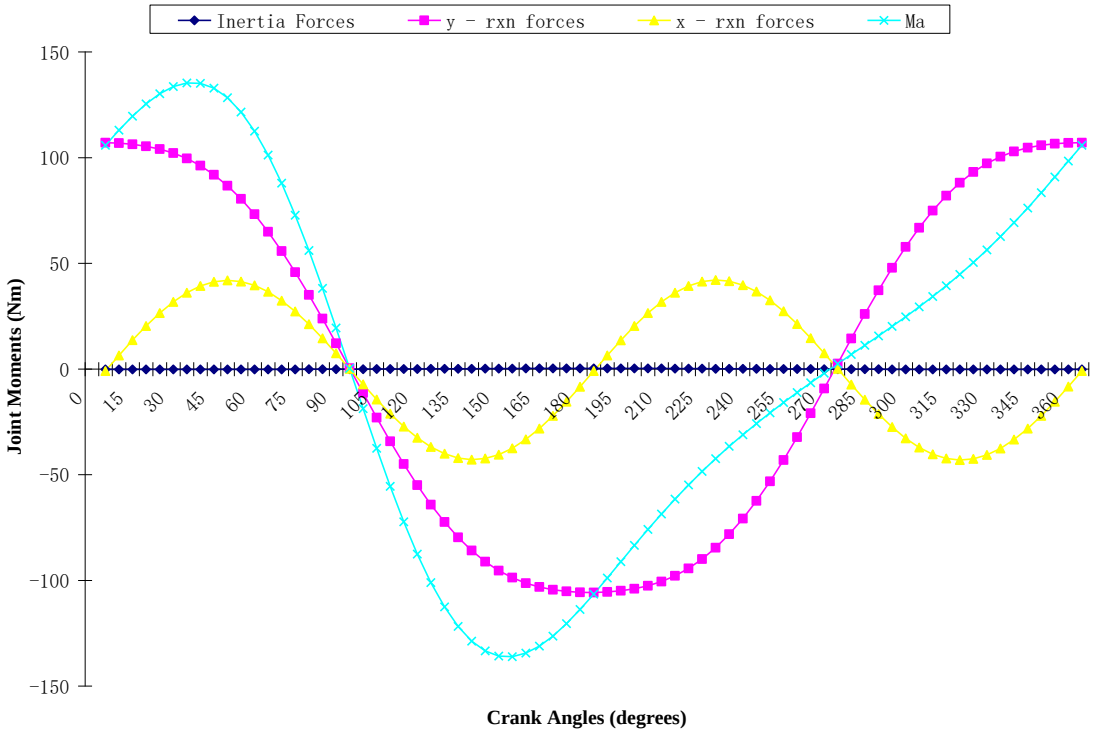

Figure 4.43 (b): Components of Ankle Joint Moments at

Seat Height of 90% vs crank angles

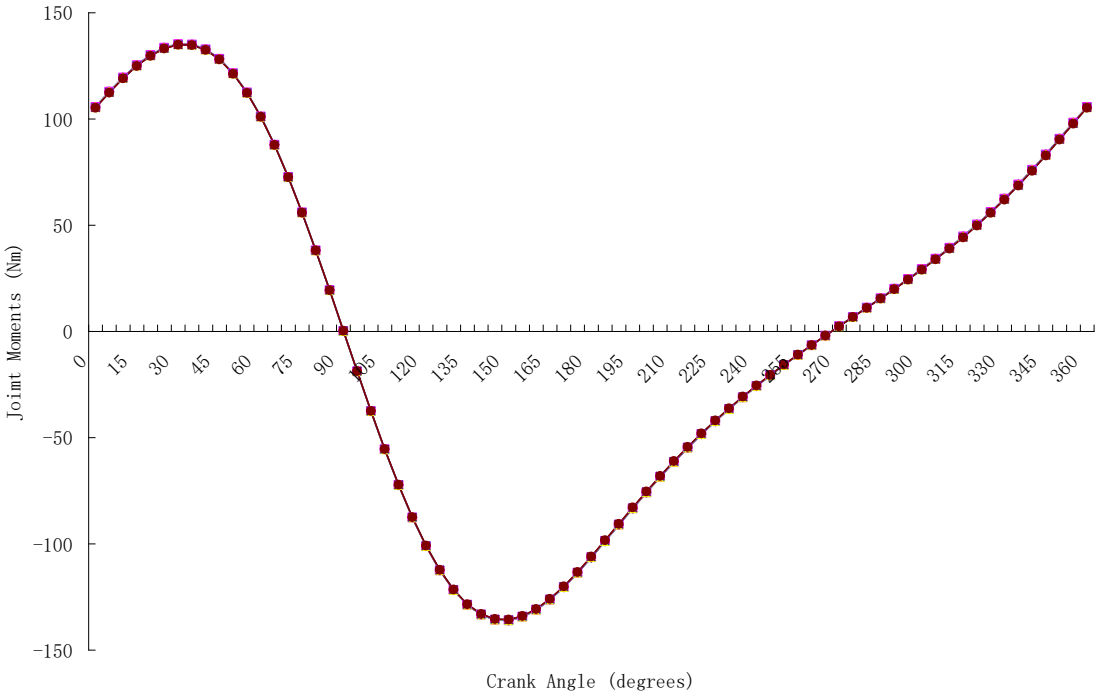

Figure 4.44 (a): Ankle Joint Moments at Seat Height of 85% vs crank angles

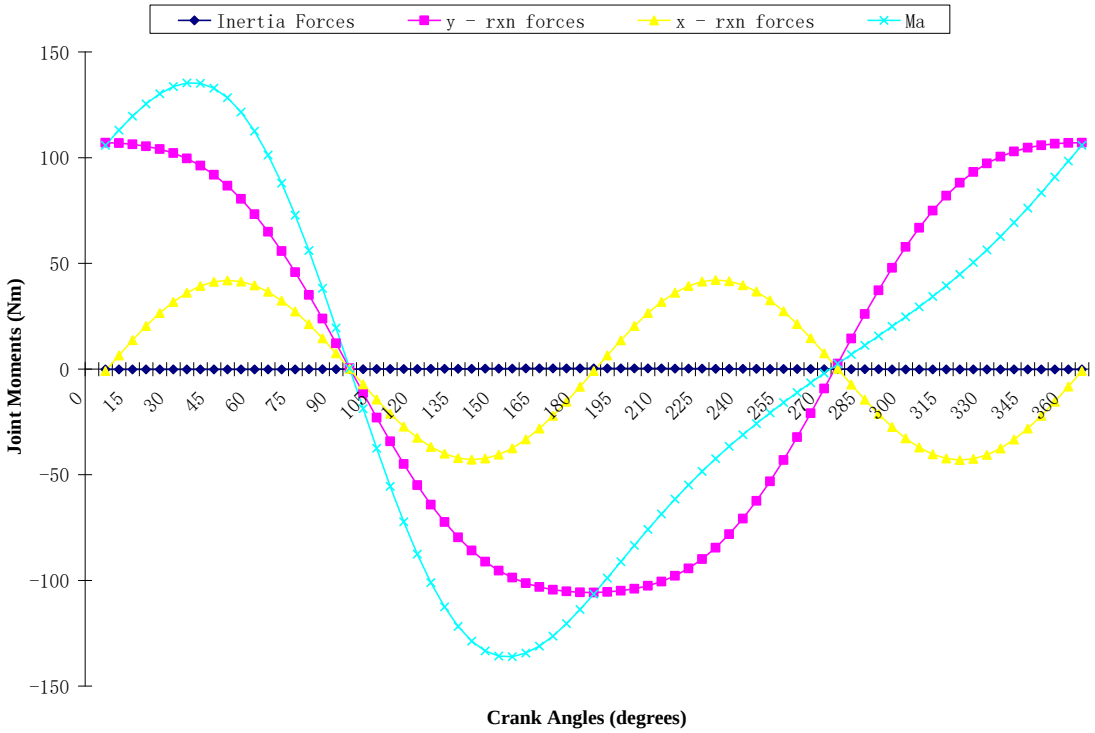

Figure 4.44 (b): Components of Ankle Joint Moments at

Seat Height of 85% vs crank angles

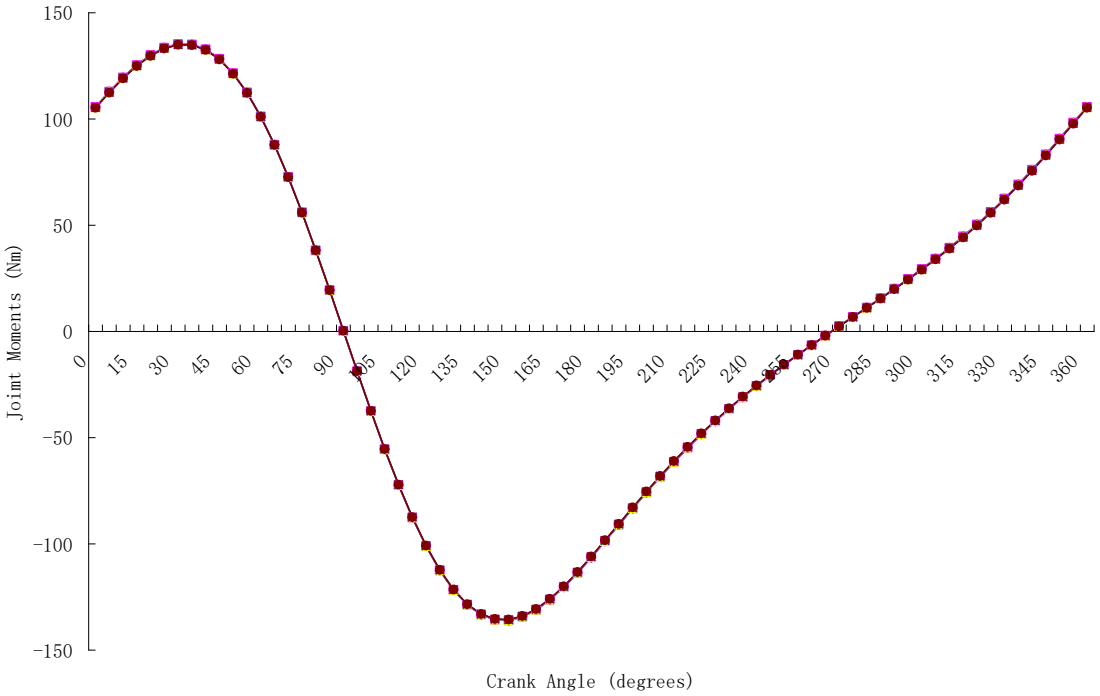

Figure 4.45 (a): Ankle Joint Moments at Seat Height of 80% vs crank angles

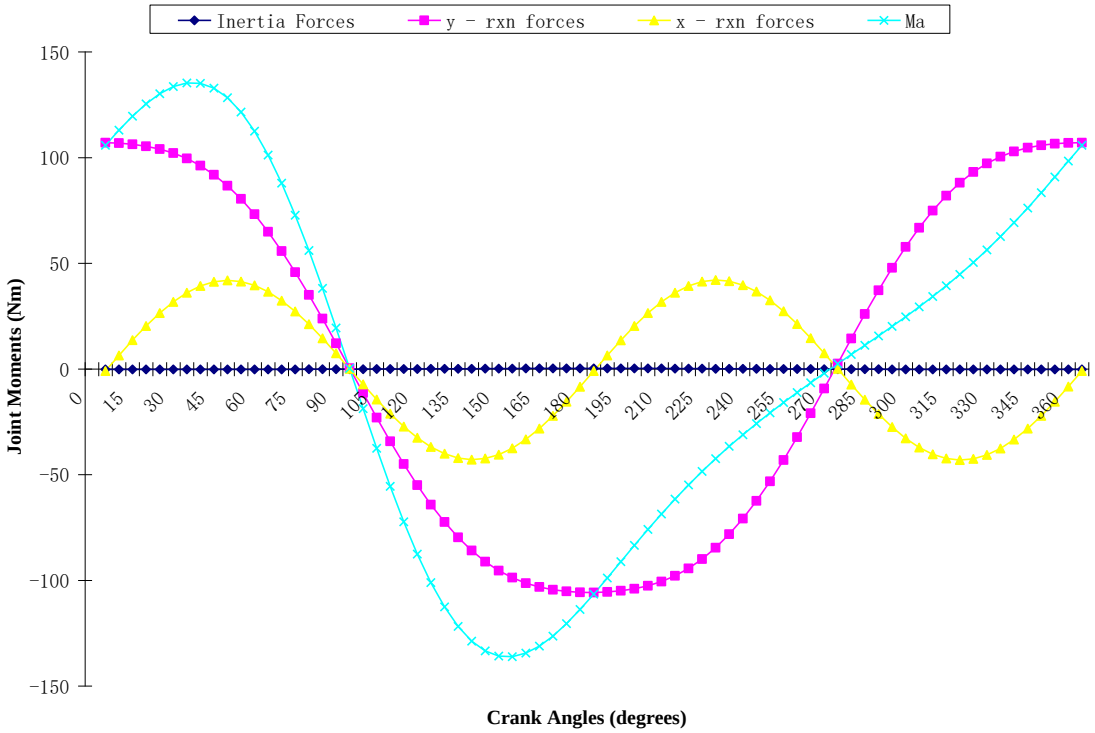

Figure 4.45 (b): Components of Ankle Joint Moments at

Seat Height of 80% vs crank angles

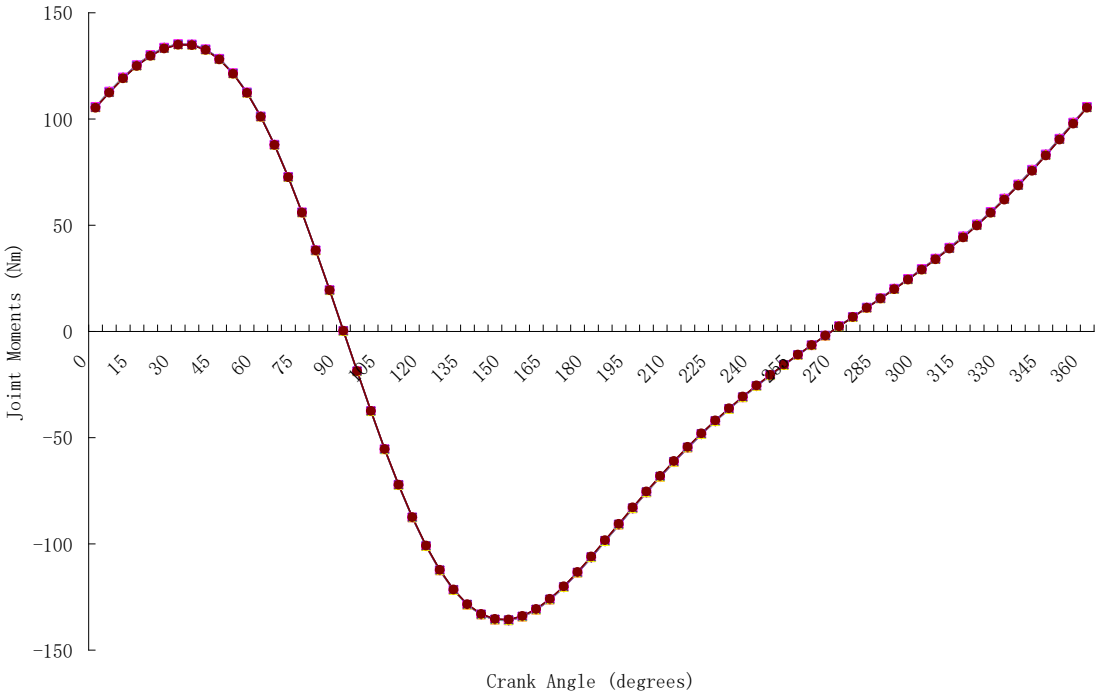

Figure 4.46 (a): Ankle Joint Moments at Seat Height of 75% vs crank angles

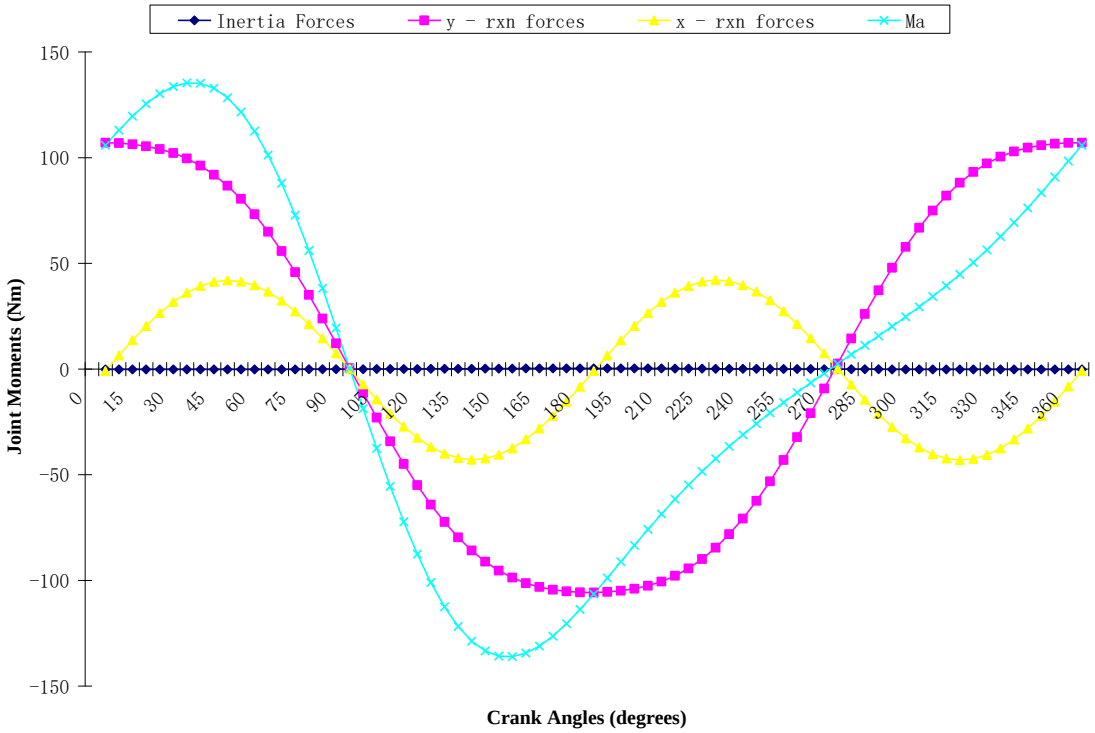

Figure 4.46 (b): Components of Ankle Joint Moments at

Seat Height of 75% vs crank angles

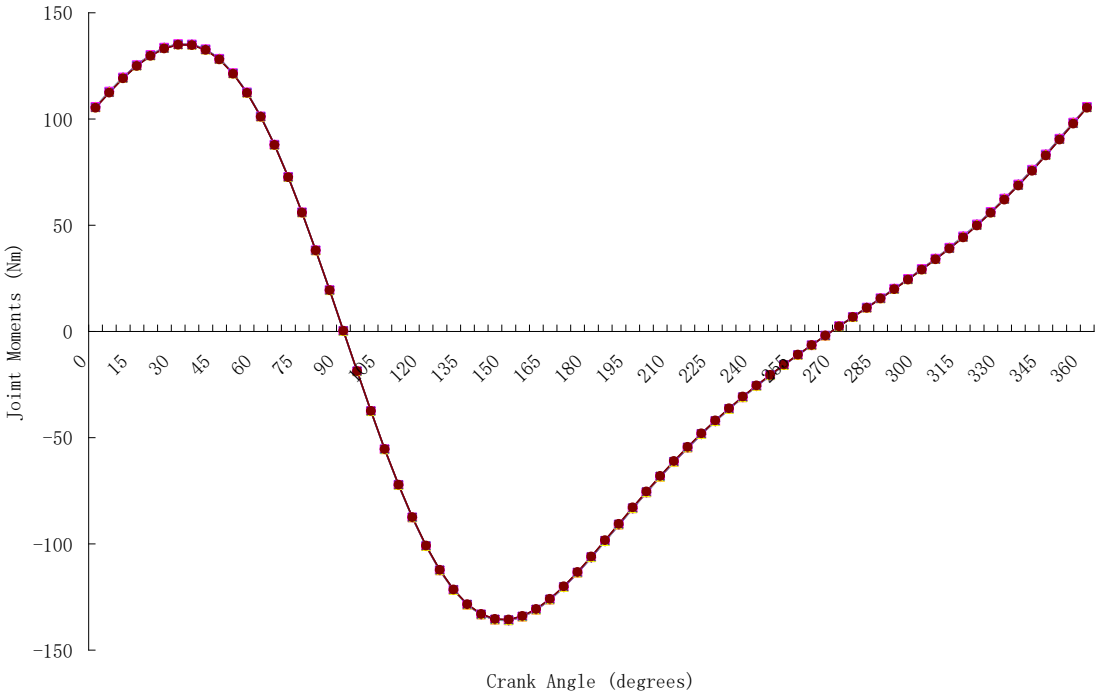

Figure 4.47 (a): Ankle Joint Moments at Seat Height of 72% vs crank angles

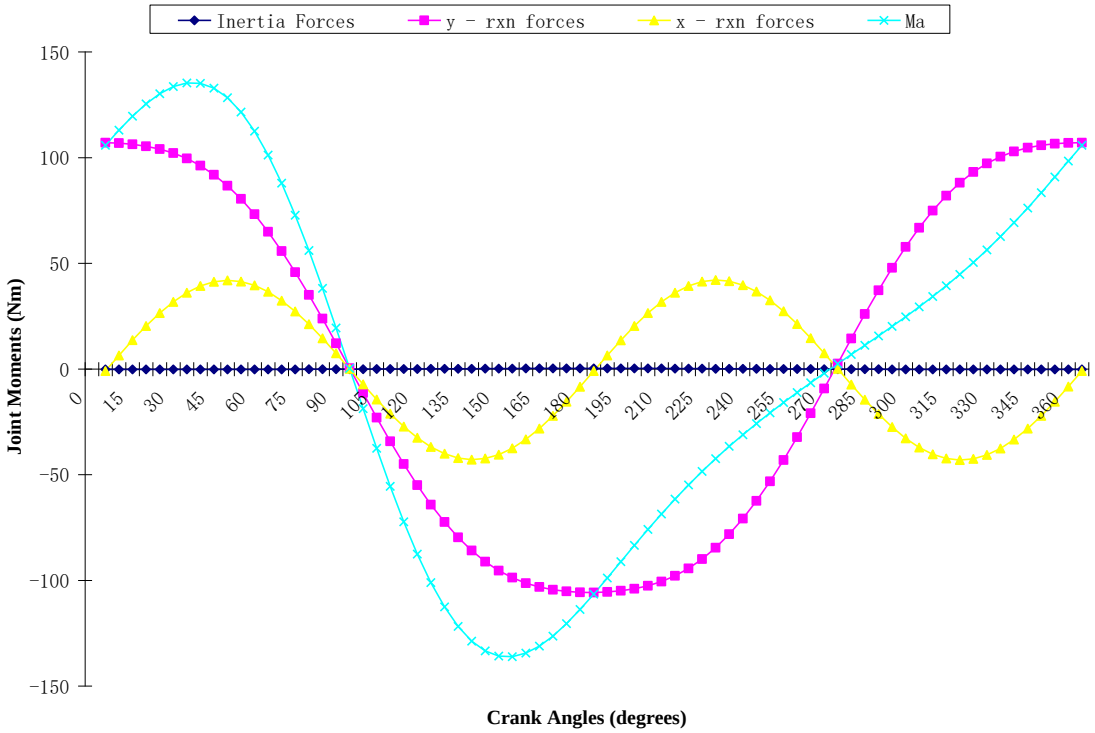

Figure 4.47 (b): Components of Ankle Joint Moments at

Seat Height of 72% vs crank angles

Figure 4.48 is plot of variation of average ankle joint moment with acceleration with varying seat height. It is observed that for all the seat heights considered, the average ankle joint moments significantly remained the same for the acceleration considered but joint moment reduces as the acceleration reduces but not significantly i.e. less than 0.1% of the average ankle joint moment at *0 m/s*^{2}. This reduction can therefore be considered negligible. It is also observed that the seat height can not be lowered than 72% of the total length of the lower limb segment.

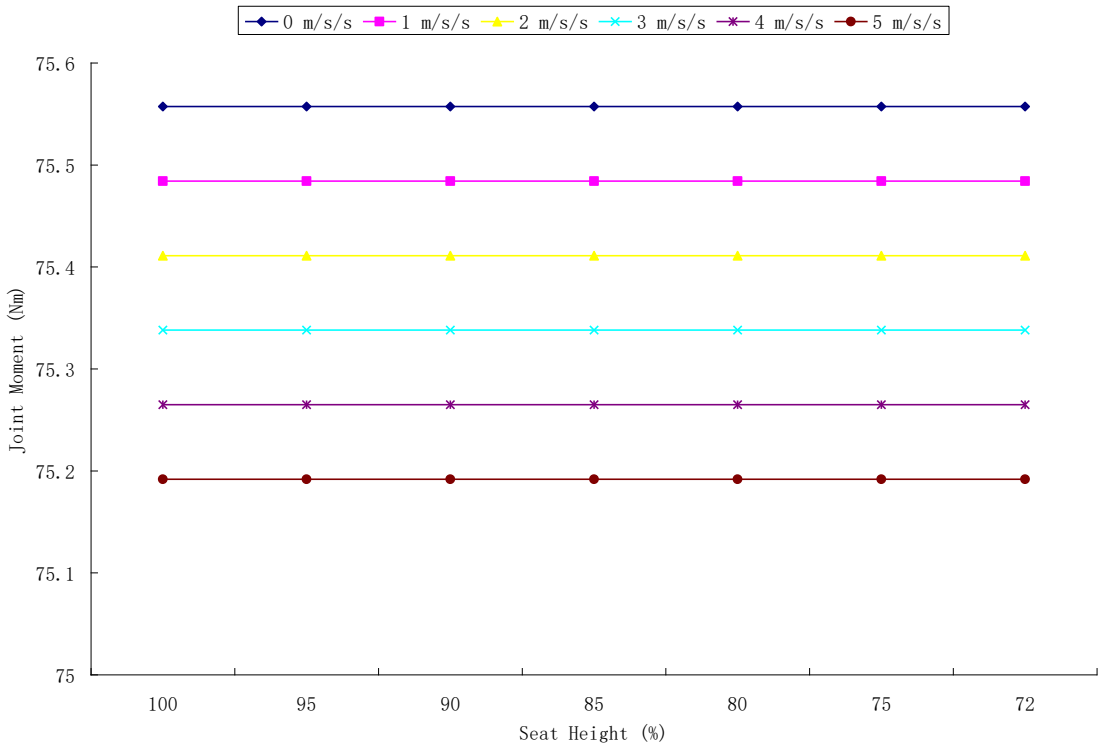

Figure 4.48: Average ankle joint moments at 64 rpm vs seat height

4.7 The Knee Joint Moments at 64 rpm with Varying Saddle Height

Figures 4.49a – 4.55a are the plots of the variation of the knee joint moments and crank angles with varying saddle heights. The saddle height is expressed as a percentage of the total length of lower limb segments. The Figures 4.49b – 4.55b are the plots of variation of the components of knee joint moment and crank angles. The shape of the

knee joint moment were formed by the sum of the four components of the knee joint moment namely the torque, the ankle joint moment, the horizontal and the vertical moments. The shapes formed the knee joint moment for all the saddle height considered are almost the same except at the regions of 150^0 – 195^0 and 270^0 – 360^0. The torque created by the inertia of the shank is almost constant which is demonstrated by the plot overlapping the x axis. It is noted that the horizontal moment has a lot of influence on the final shape of the knee joint moment. The graph started a little above 0 Nm at 0^0, crossed the x-axis at 10^0 decreasing to a minimum at 75^0 and start to increase to zero crossing the x-axis again at 135^0, rising and reducing quickly to the zero at 195^0 then starts to increase to a maximum at 285^0 and decreasing gradually to almost zero at 360^0. The quick rise and fall of 135^0 – 195^0 is among what is responsible for the "wobbling" of the knee joint moment at this region. The other responsibility is vertical moment that exhibits false rise and fall around 150^0 – 210^0. The vertical moment starts at the maximum at 0^0, gradually decreasing to zero, crossing the x-axis at 105^0 decreasing further below zero to a false minimum at 150^0, rising to start falling again at 1800 to a minimum at 225^0, thereafter, it starts increase to maximum at 360^0. The fourth plot that is also contributing to the shape of the knee joint moment is the ankle joint moment which has already been discussed earlier in the previous section. The sum of these four components make the knee joint moment what it is! The knee joint moment start from the maximum from 0^0 and decreasing gradually to cross x-axis to a minimum at about 150^0 rising to maximum above zero 270^0. As the saddle height is being reduced from 100%, the "abnormality" at the region 135^0 – 195^0 is being transferred gradually to the region 285^0 – 360^0. In the power stroke, this abnormality is the region of deceleration,

the activity is being transferred to the back stroke as the saddle height is being reduced and the knee joint moment is being reduced. Lower saddle height is better for the lower limb segments.

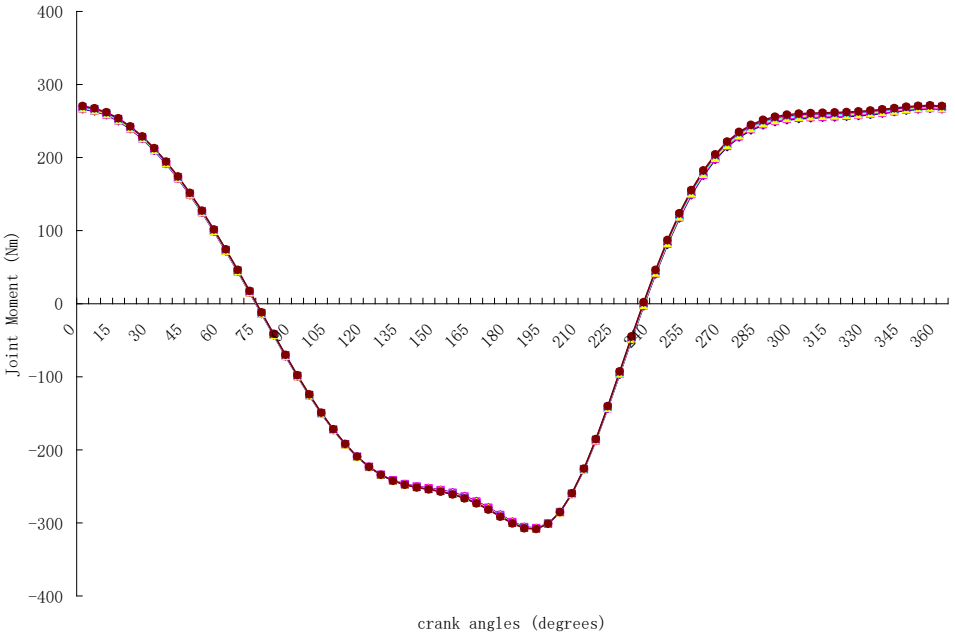

Figure 4.49 (a): Knee Joint Moments at Seat Height of 100% vs crank speed

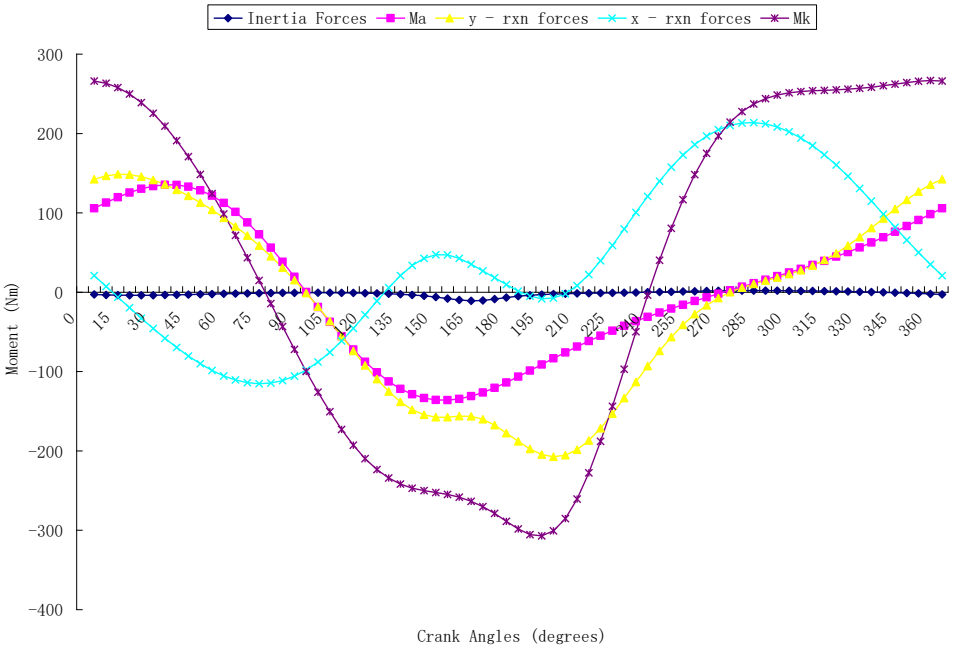

Figure 4.49 (b): Components of knee joint moments at seat height of 100% vs crank speed

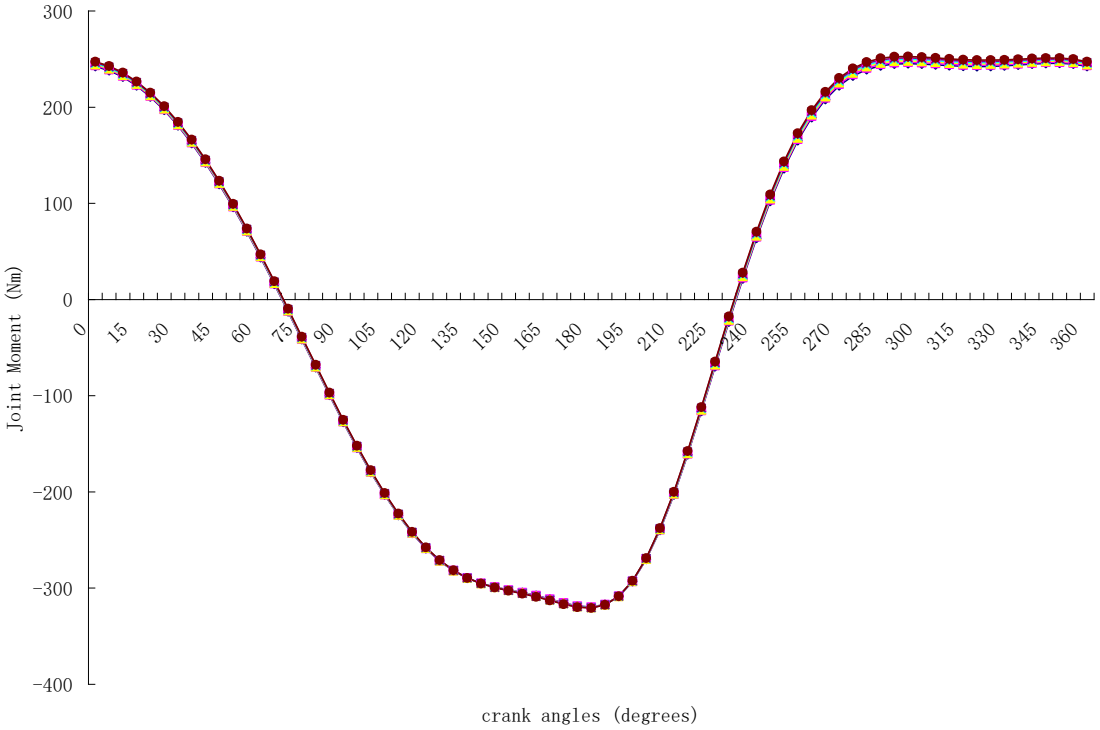

Figure 4.50 (a): Knee Joint Moments at and Seat Height of 95% vs crank speed

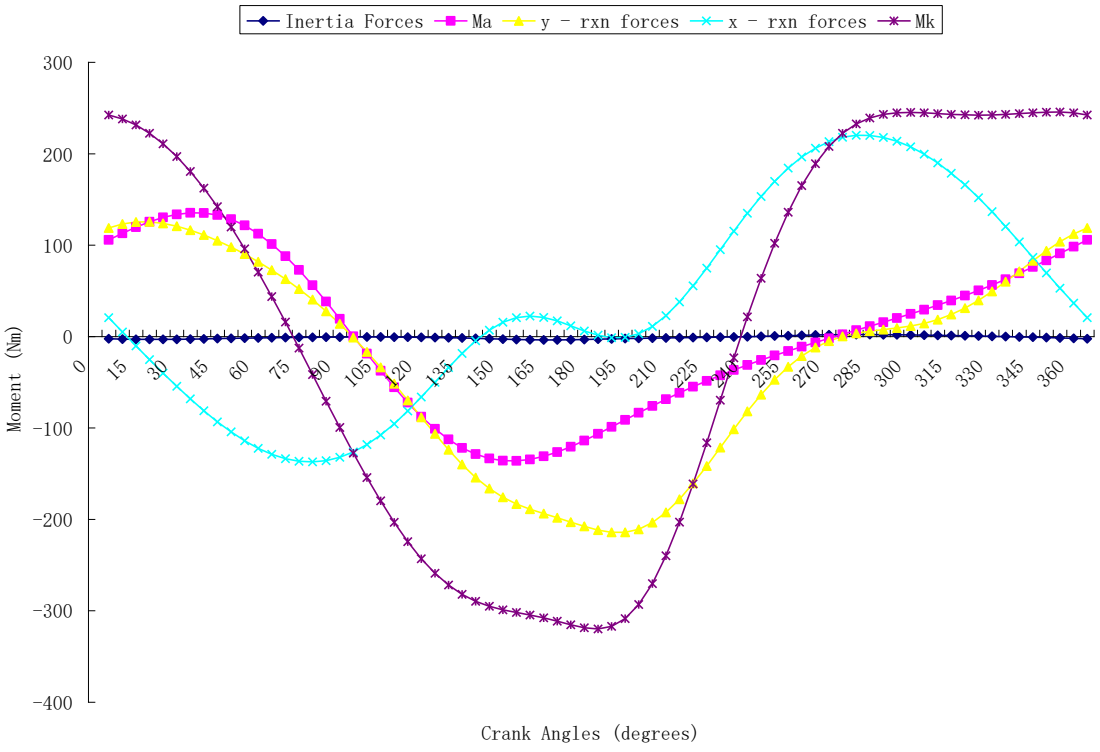

Figure 4.50 (b): Components of Knee Joint Moments at Seat Height of 95% vs crank speed

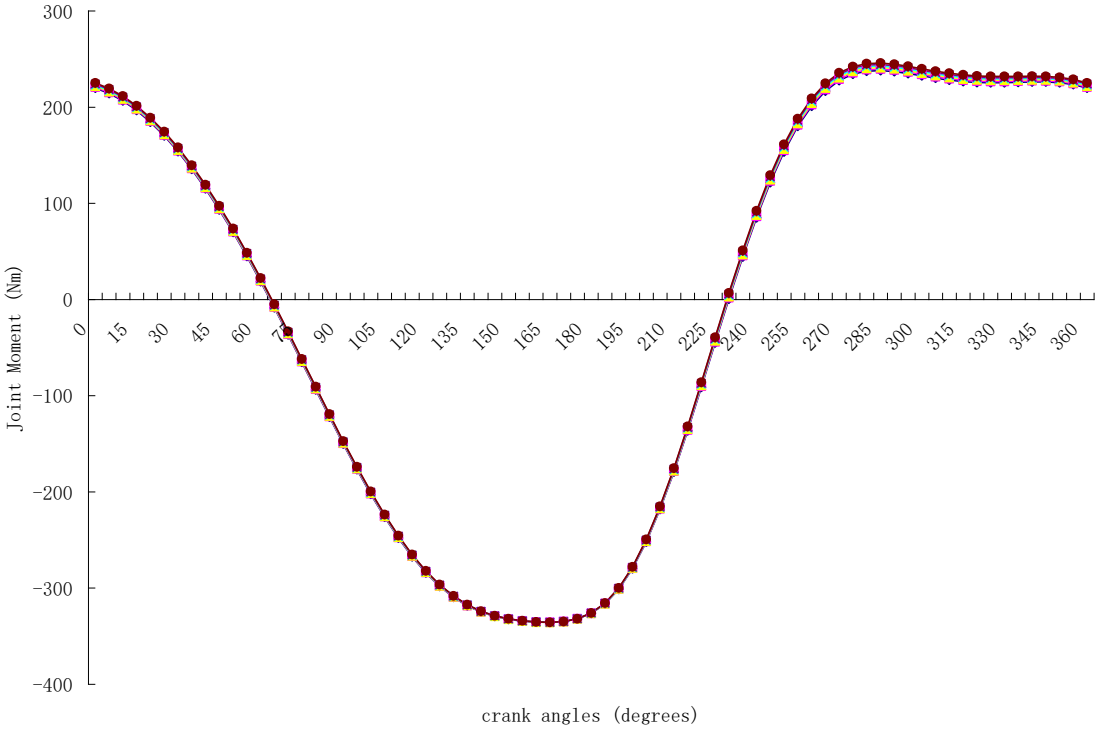

Figure 4.51 (a): Knee Joint Moments Seat Height of 90% vs crank speed

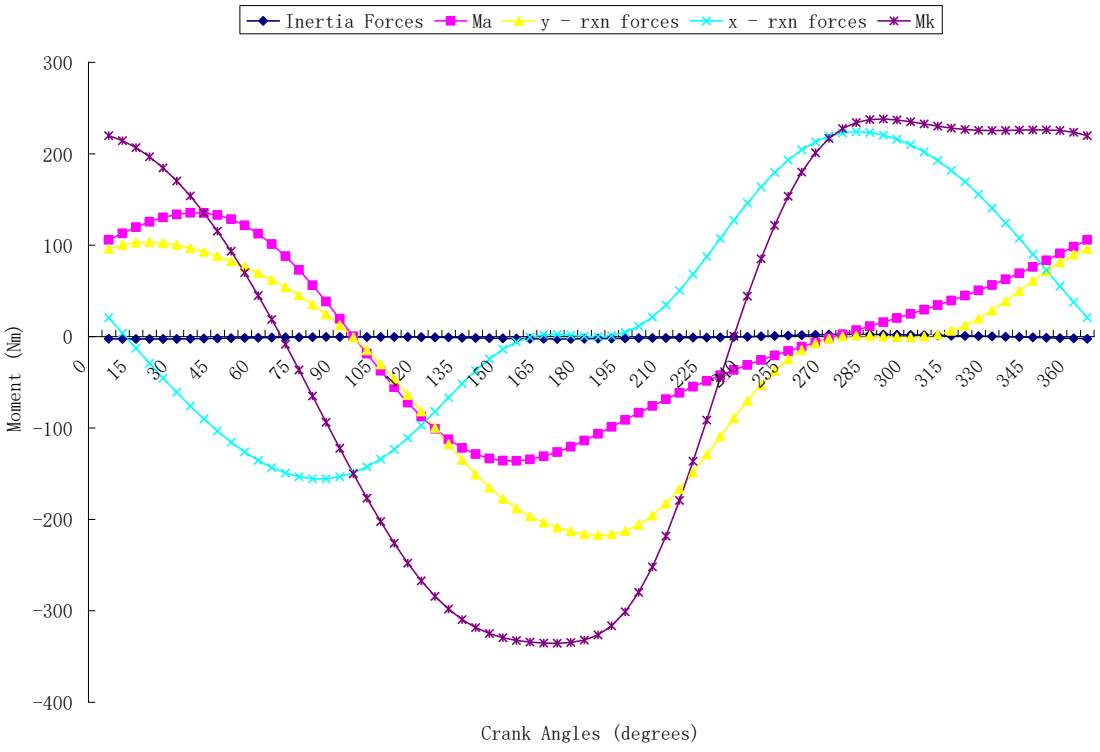

Figure 4.51 (b): Components of Knee Joint Moments at Seat Height of 90% vs crank speed

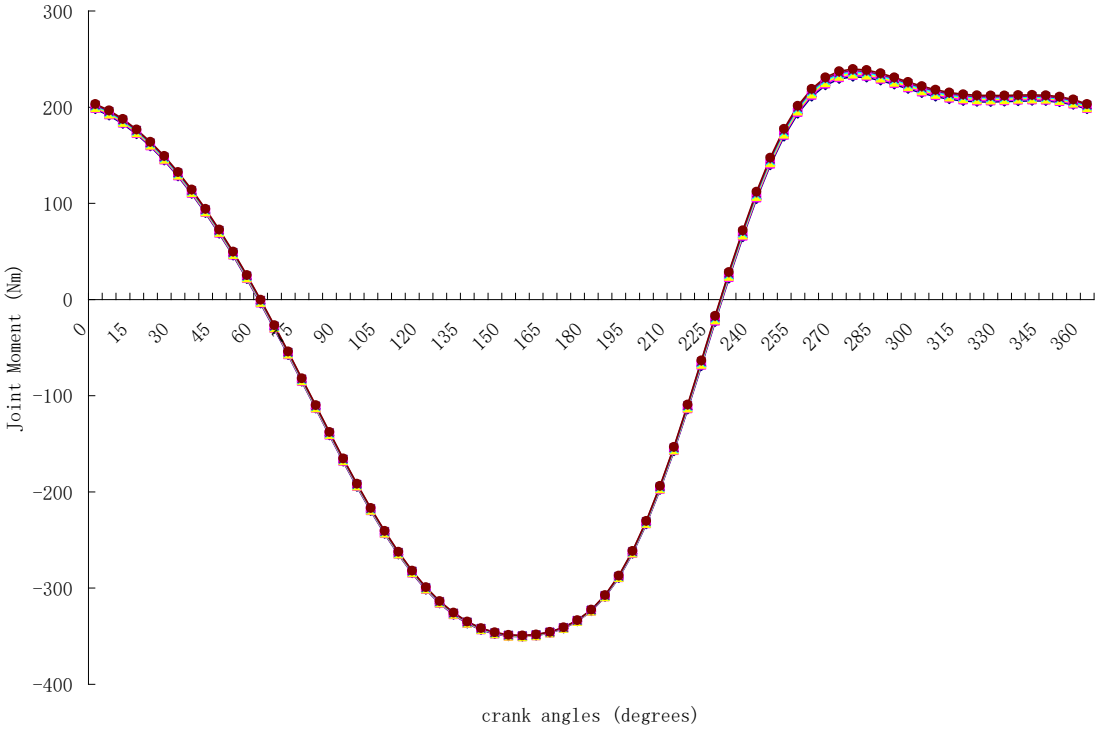

Figure 4.52 (a): Knee Joint Moments at Seat Height of 85% vs crank speed

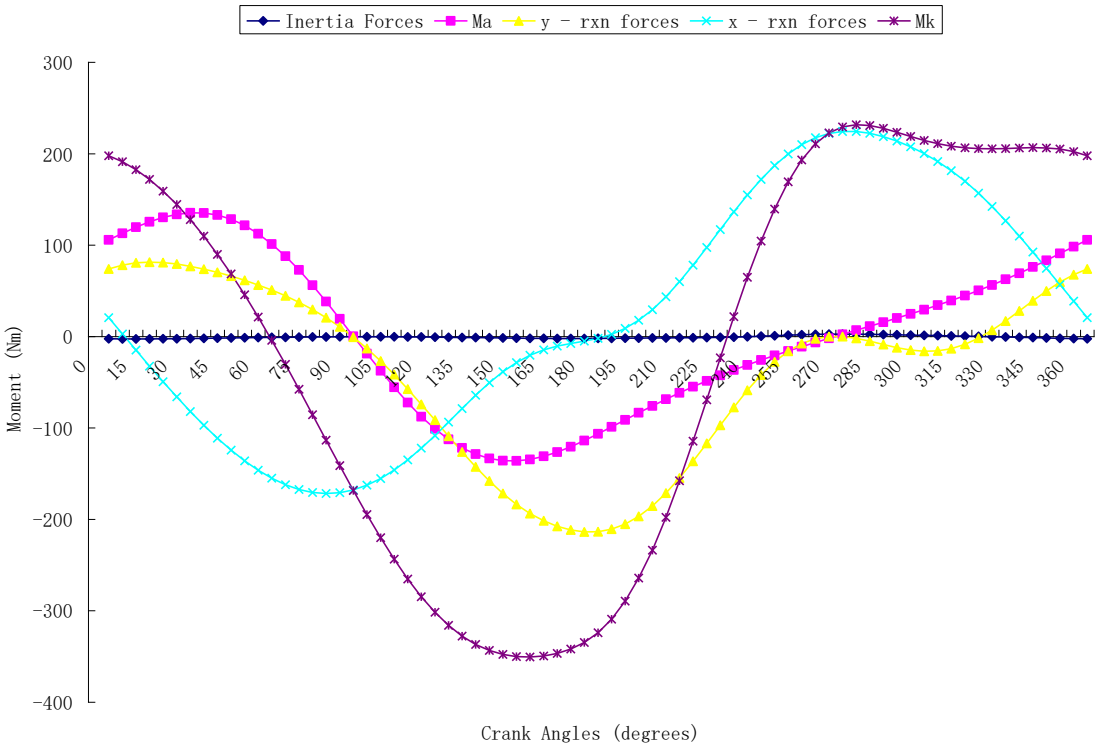

Figure 4.52 (b): Components of Knee Joint Moments at Seat Height of 85% vs crank speed

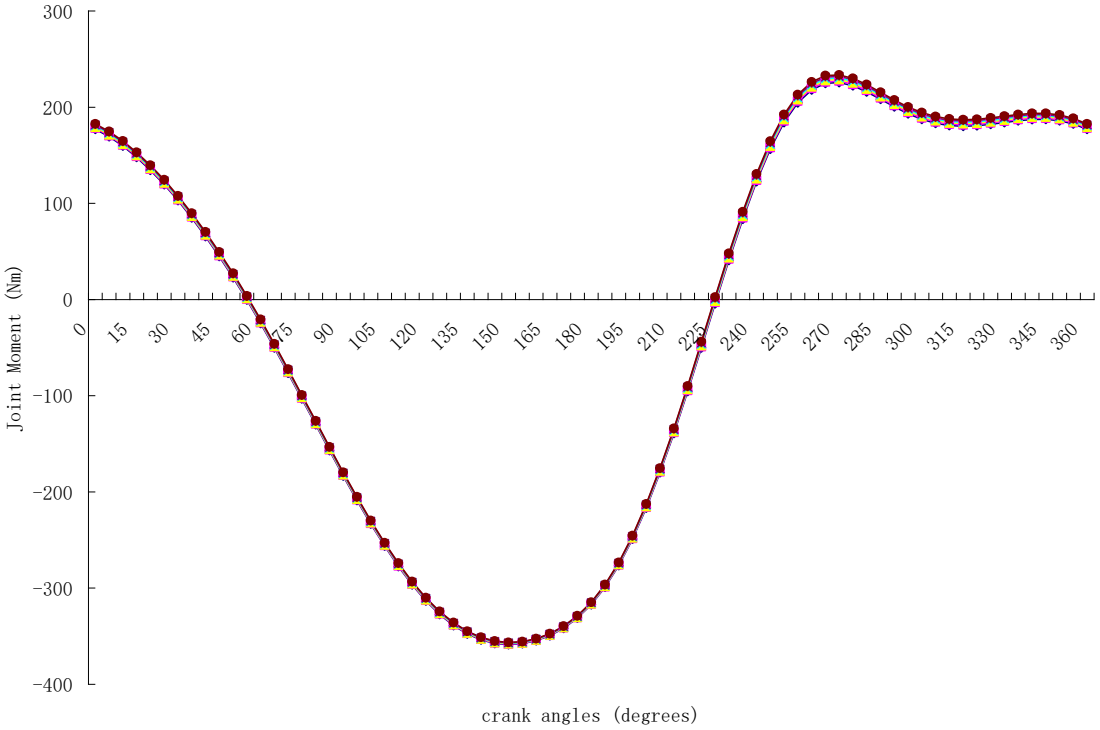

Figure 4.53 (a): Knee Joint Moments at Seat Height of 80% vs crank speed

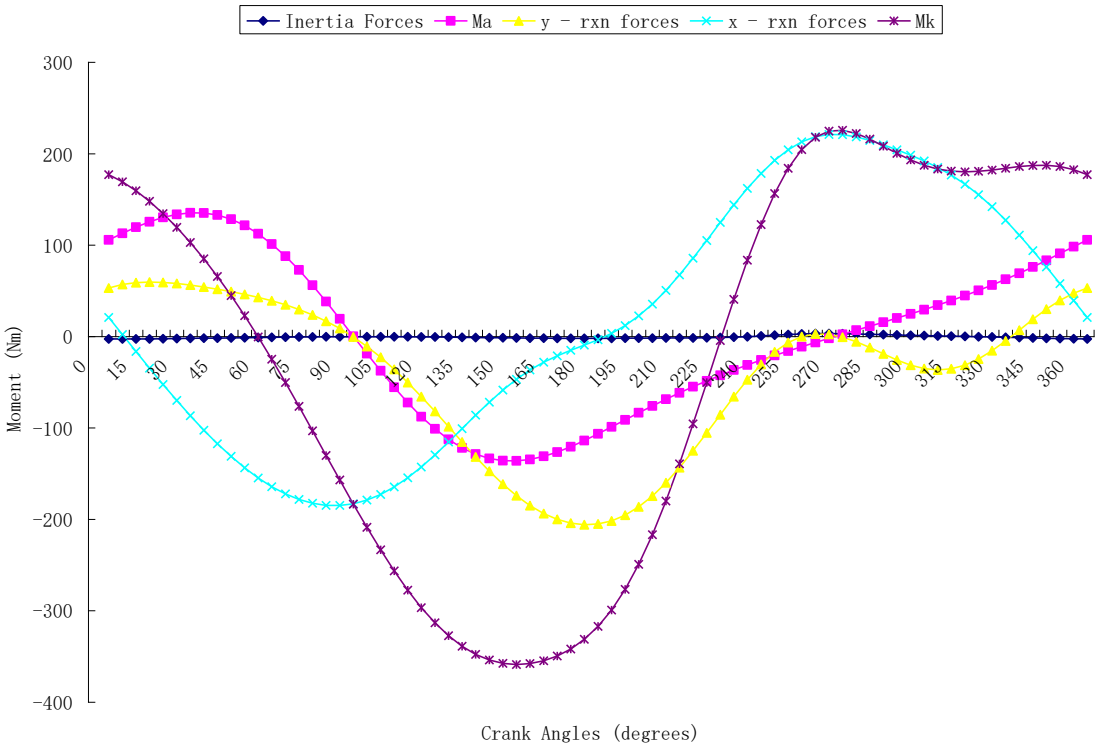

Figure 4.53 (b): Components of Knee Joint Moments at

Seat Height of 80% vs crank speed

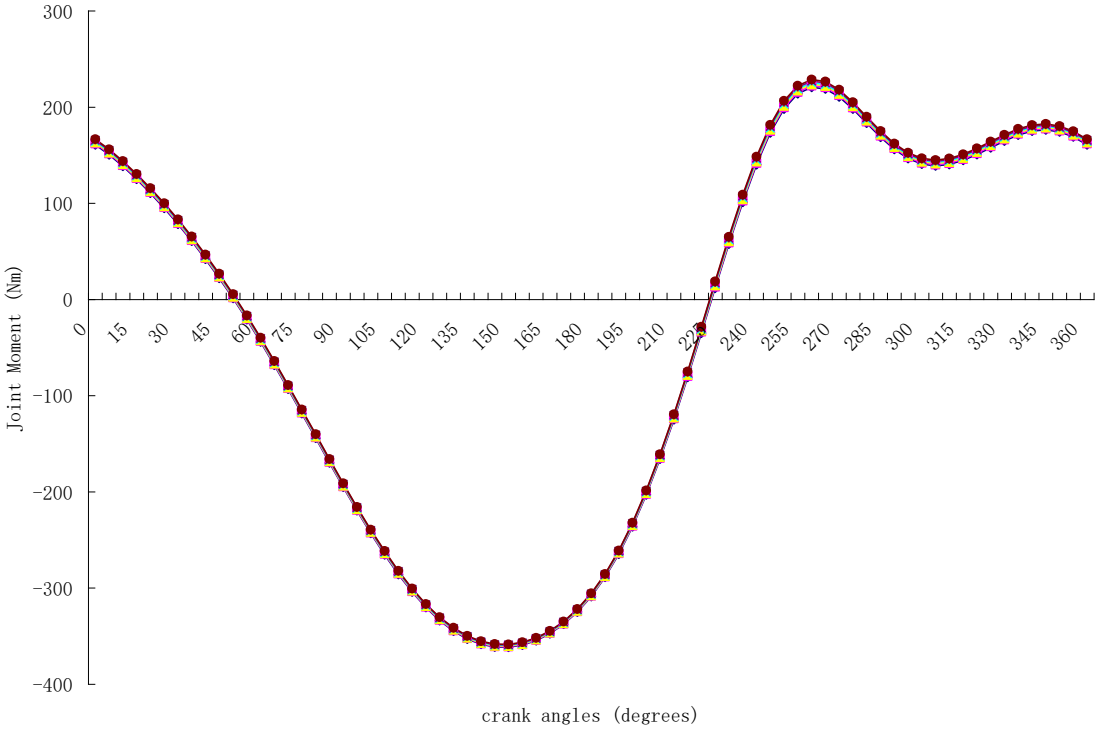

Figure 4.54 (a): Knee Joint Moments at Seat Height of 75% vs crank speed

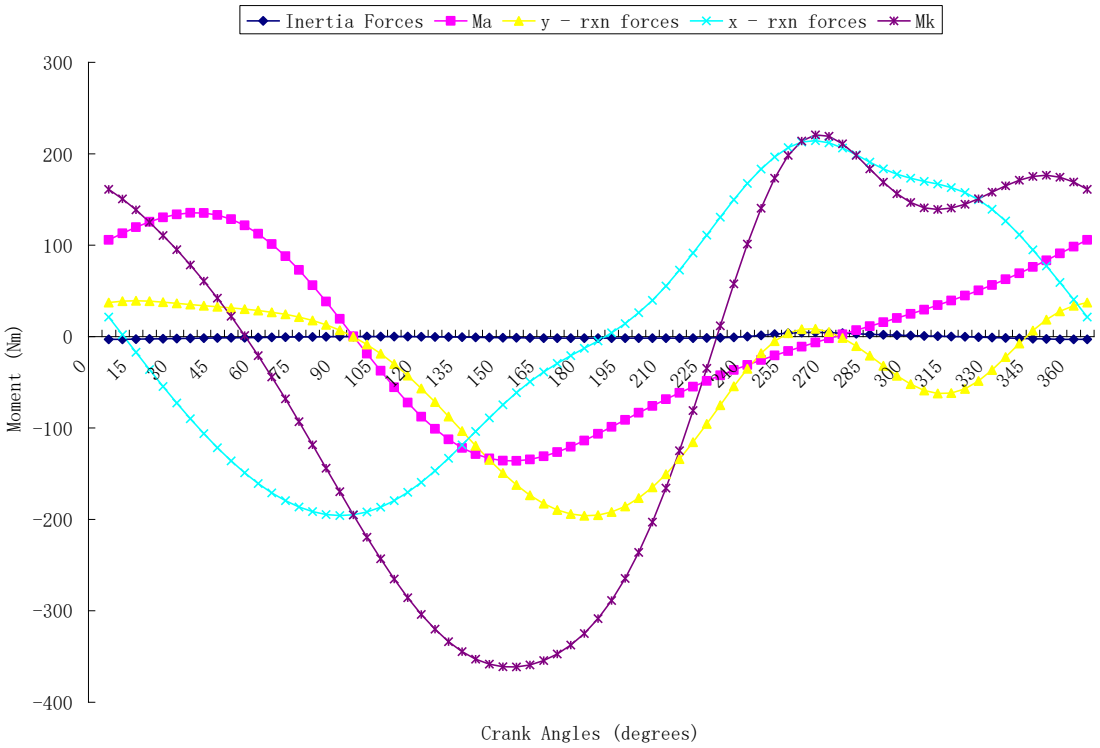

Figure 4.54 (b): Components of Knee Joint Moments at

Seat Height of 75% vs crank speed

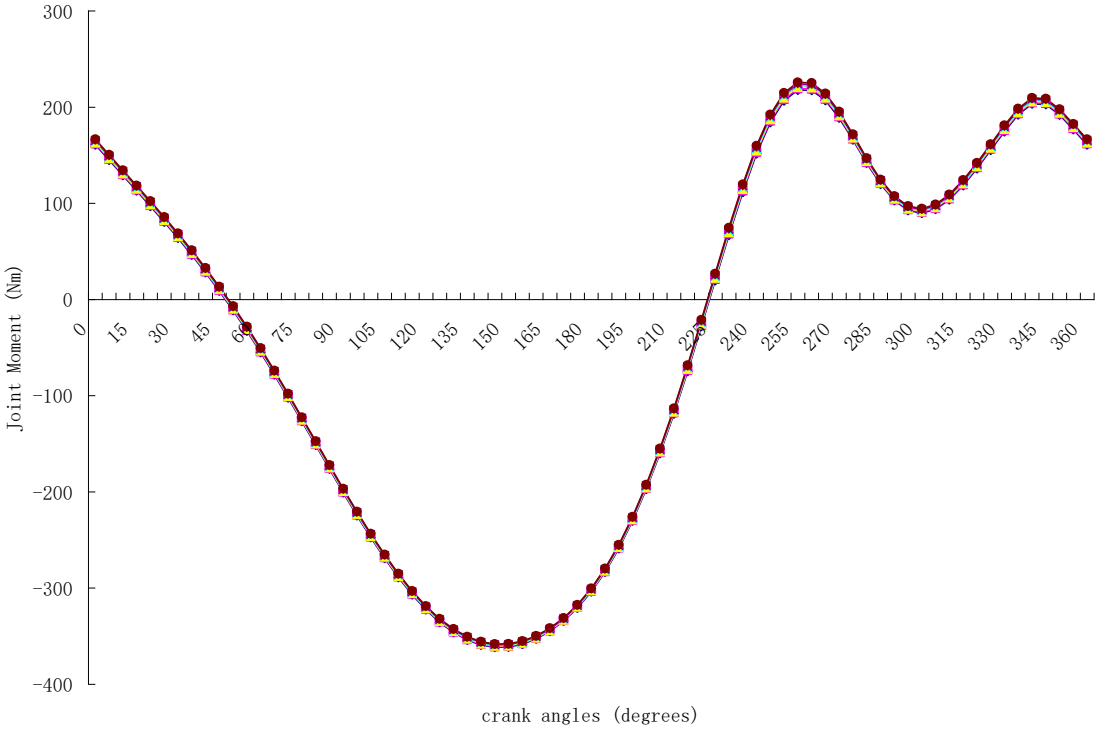

Figure 4.55 (a): Knee Joint Moments at Seat Height of 72% vs crank speed

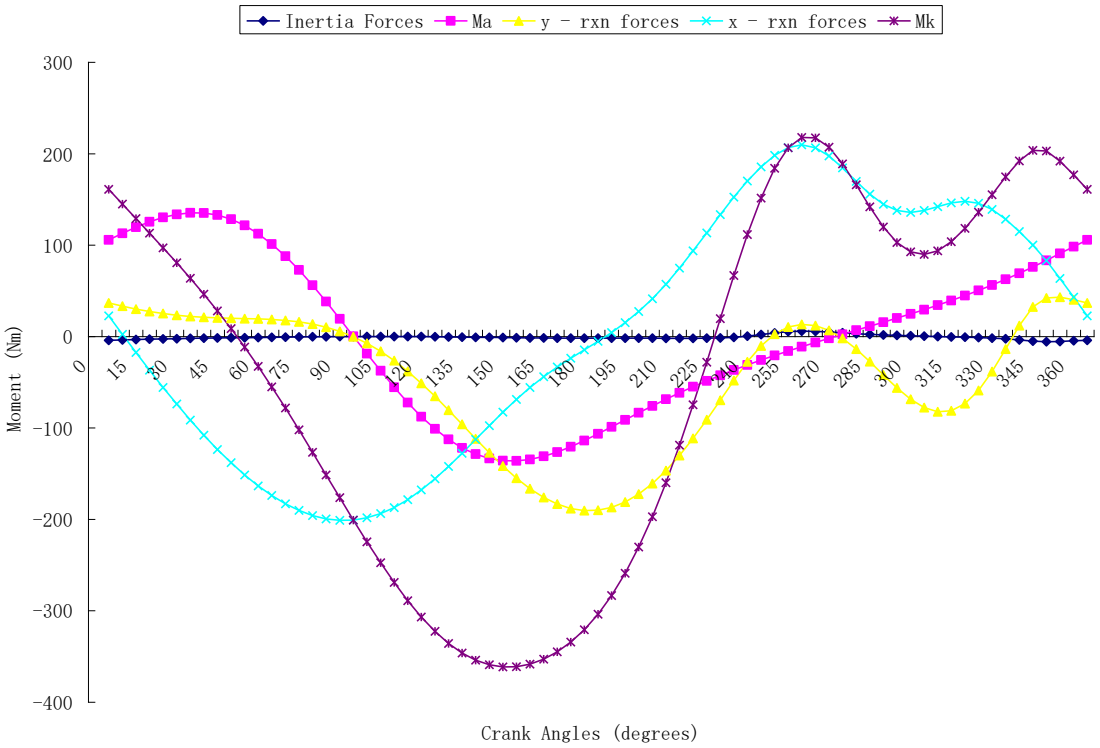

Figure 4.55 (b): Components of Knee Joint Moments at

Seat Height of 72% vs crank speed

Figure 4.56 are the plots of the plot of average knee joint moments and saddle height at different accelerations. The plot started to increase from 100% to 95% then starts to drop continually forming a convex parabolic shape till it got 75% saddle height, then changed direction to concave to get to 72%. This means that for recreation and fitness, where power generated is of less importance, it is better to maintain the minimum theoretically possible saddle height in this case, 72% but for competition, the competitor should freely chose any saddle height above the minimum. It should be noted that in this case a saddle height of 95% of the total length of the lower limb segment will produce maximum knee joint power output. Although, the joint moment i.e. power increases with increase in acceleration but this is not significant.

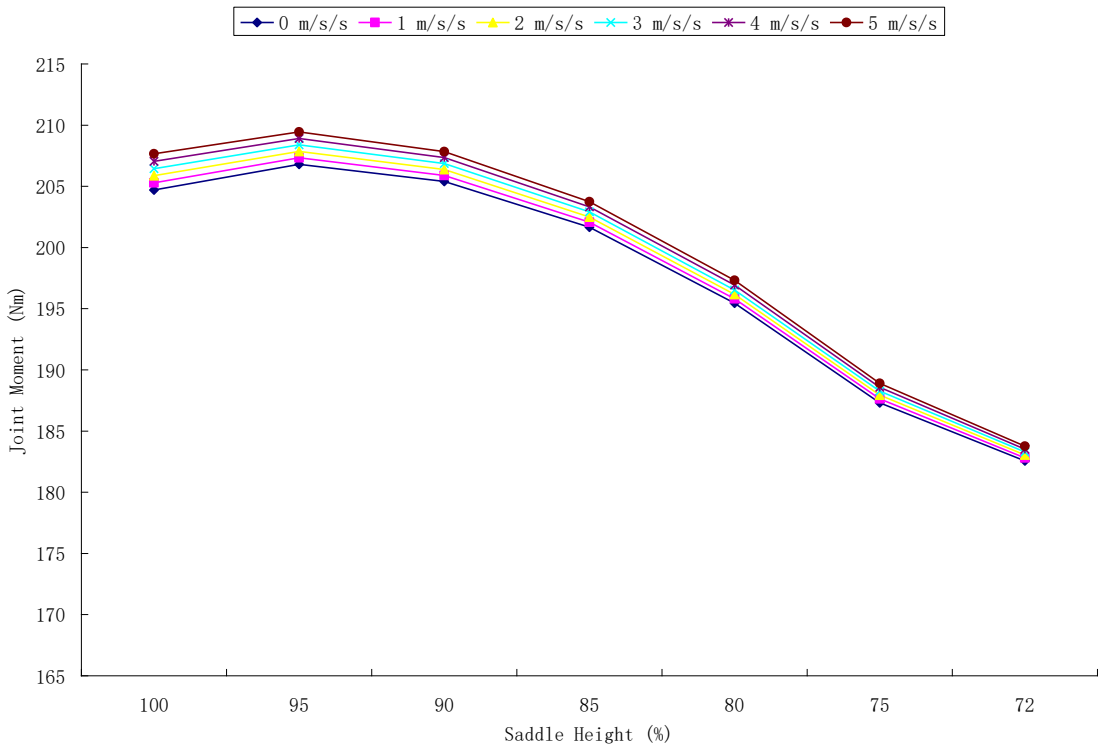

Figure 4.56: Average knee joint moments at 64 rpm vs seat height

4.8 The Hip Joint Moments at 64 rpm with Varying Seat Height

Figures 4.57a – 4.63a are the plots of hip joint moments and crank angle with varying saddle heights, while Figures 4.57b – 4.63b are the plots of variation of the components of the hip joint moments and crank angle with varying seat heights. The seat height is expressed as a percentage of the total length of lower limb segments. The hip joint moment has its peak at 0^0 and trough at 195^0. The hip joint moment decreases gradually crossing x-axis at 90^0 and getting the minimum at 195^0 then rising gradually to maximum at 360^0, but as the saddle height is being reduced there is a sharp drop at 345^0. Like other joint moments, the shape of the hip joint moment is dictated by its components namely, the knee joint moment, the torque at the hip, the horizontal and vertical moments. In this case, the torque does not show any significant effect on the hip joint as seen in Figures 4.57b – 4.63b. The most significant is the knee joint moment followed by the vertical joint moment. The vertical joint moment starts at the peak at 0^0 and starts to fall, crossing the x-axis at 105^0 then with small amplitude of cosine waveform below the x-axis, it crosses back the x-axis at 285^0 rising till 360^0. The horizontal moment starts close to zero and drags along the x-axis line with a hunch between 60^0 and 175^0 crossing x-axis at 175^0 maintaining almost a parallel line with the x-axis till 2100, getting to a minimum at 270^0 then beginning to rise again. As the saddle height is being lowered, the horizontal moment is changing to form a cosine waveform around the x-axis. There is a phenomenon that is exhibited at from 345^0, where there is a sharp drop in value; this is as a result of deceleration by the power leg at this saddle height. This combined with the phenomenon in the knee joint moment;

there is a sharp drop in hip joint moment at 345^0. This sudden change in direction of the graph could portray bad sign at this saddle height.

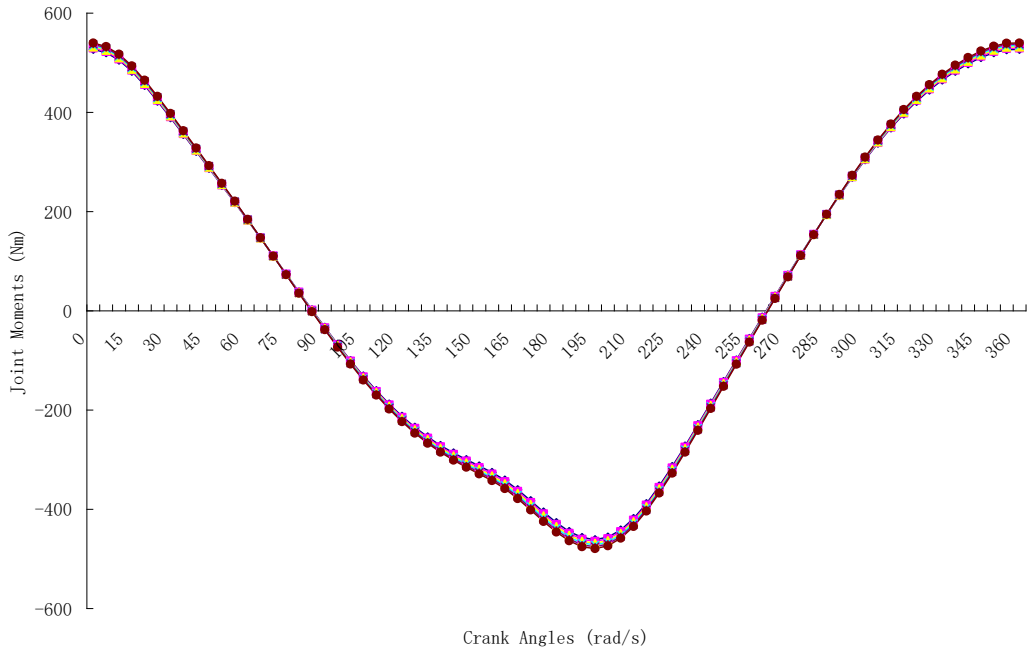

Figure 4.57 (a): Hip Joint Moments at Seat Height of 100% vs crank speed

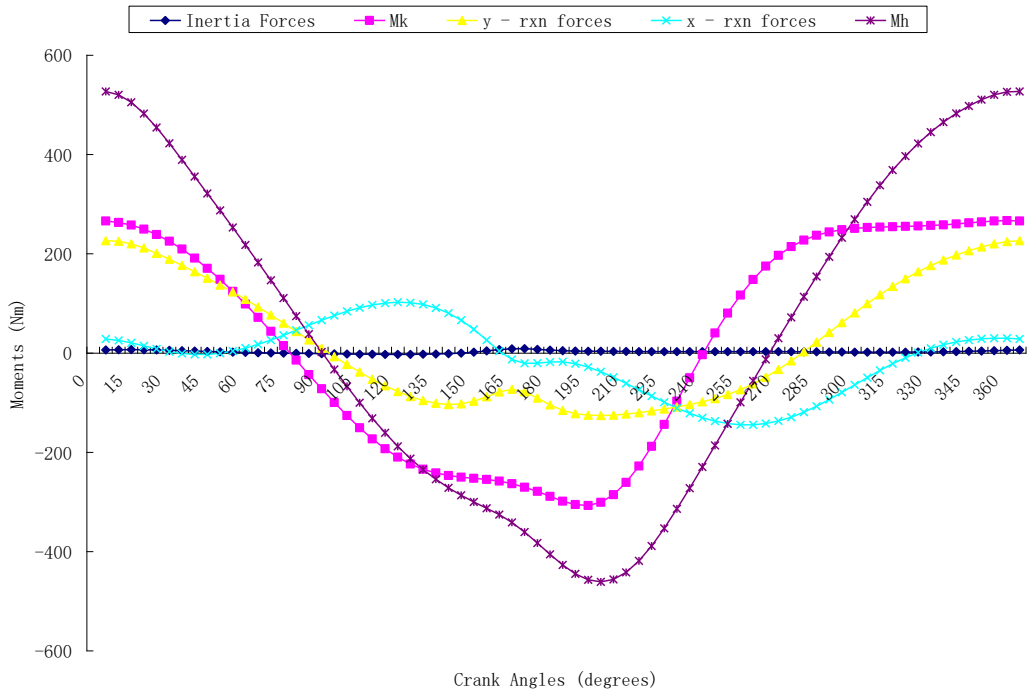

Figure 4.57 (b): Components of Hip Joint Moments at

Seat Height of 100% vs crank speed

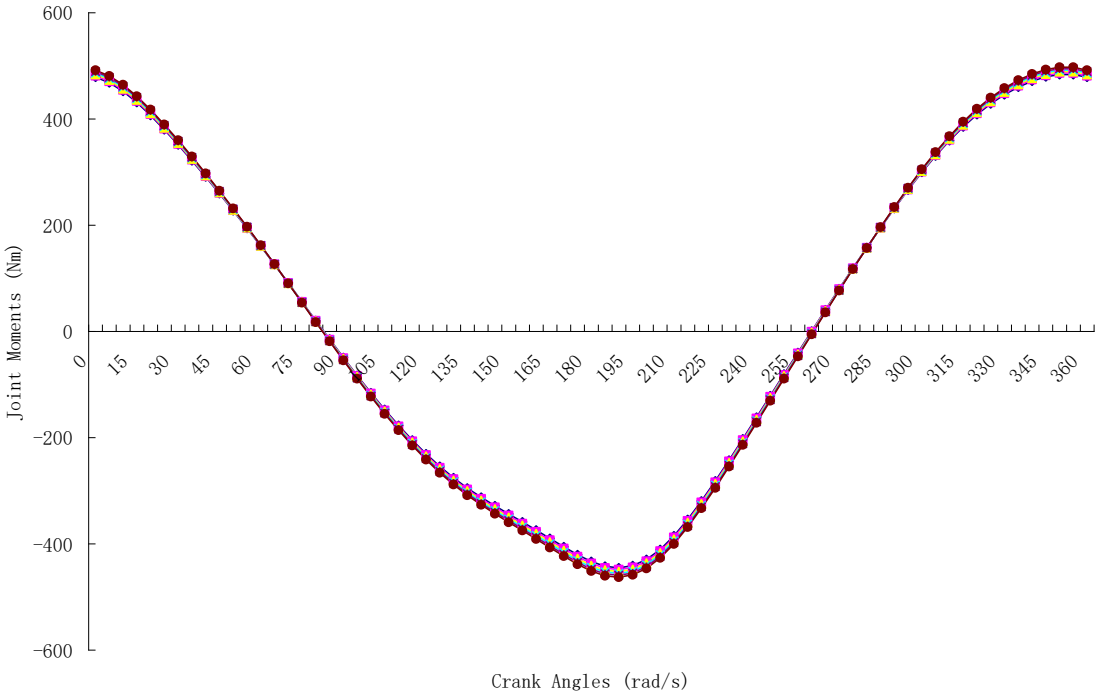

Figure 4.58 (a): Hip Joint Moments at Seat Height of 95% vs crank speed

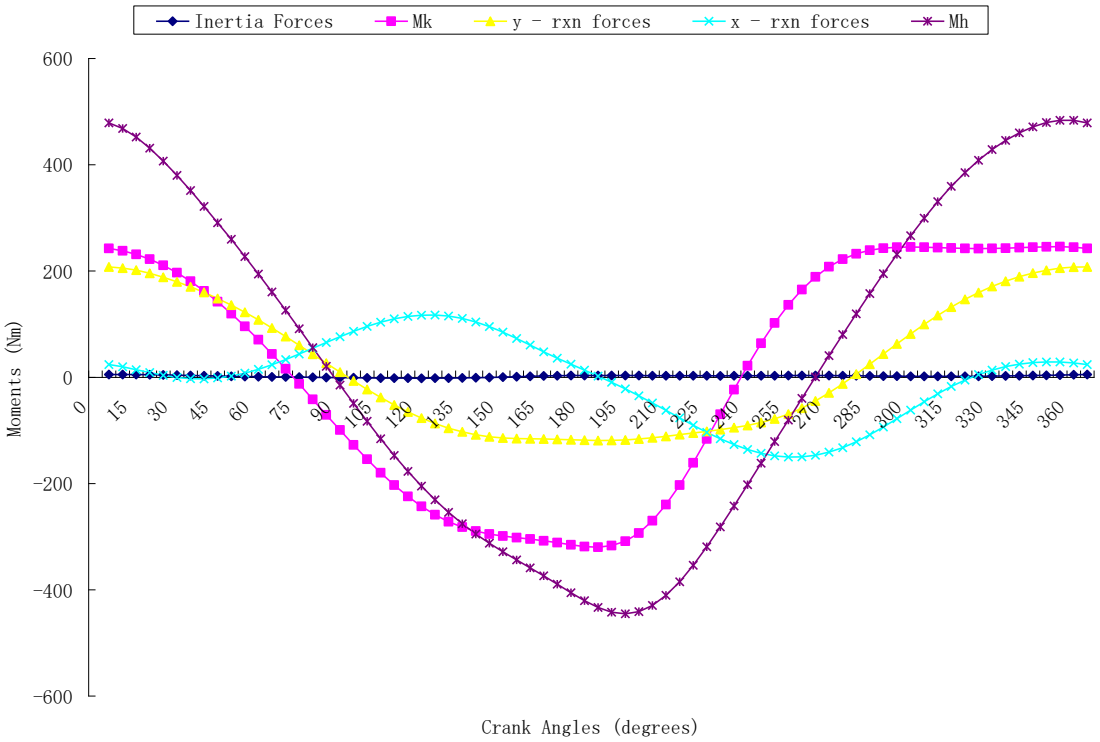

Figure 4.58 (b): Components of Hip Joint Moments at

Seat Height 95% vs crank speed

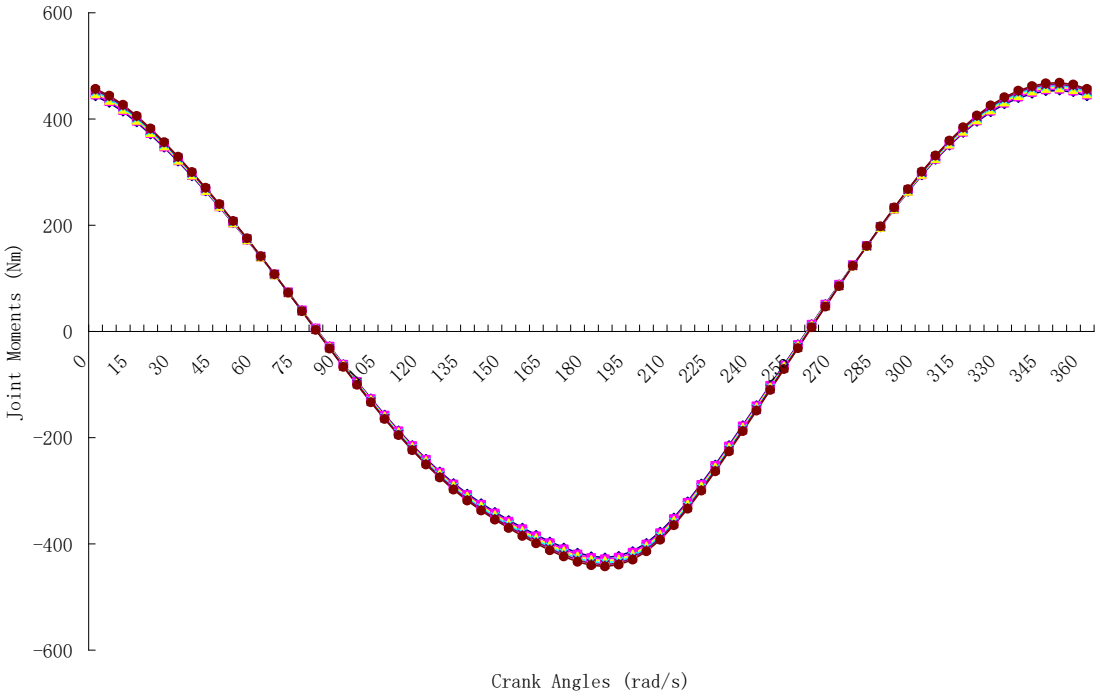

Figure 4.59 (a): Hip Joint Moments at Seat Height of 90% vs crank speed

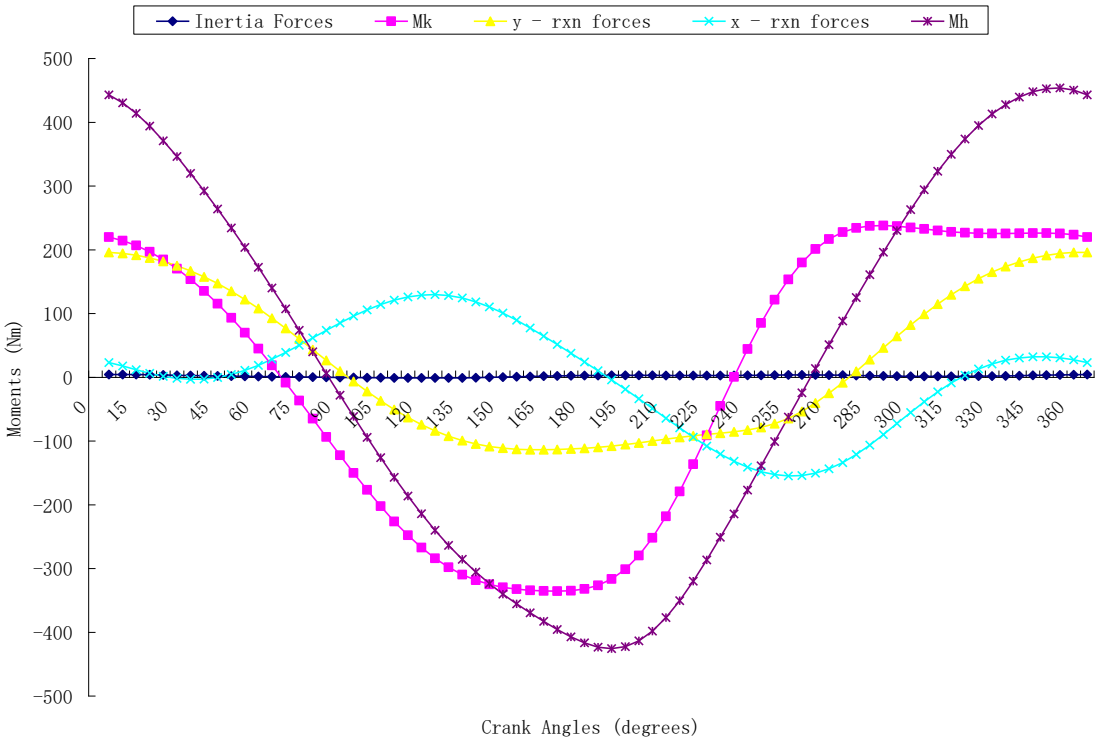

Figure 4.59 (b): Components of Hip Joint Moments at

Seat Height of 90% vs crank speed

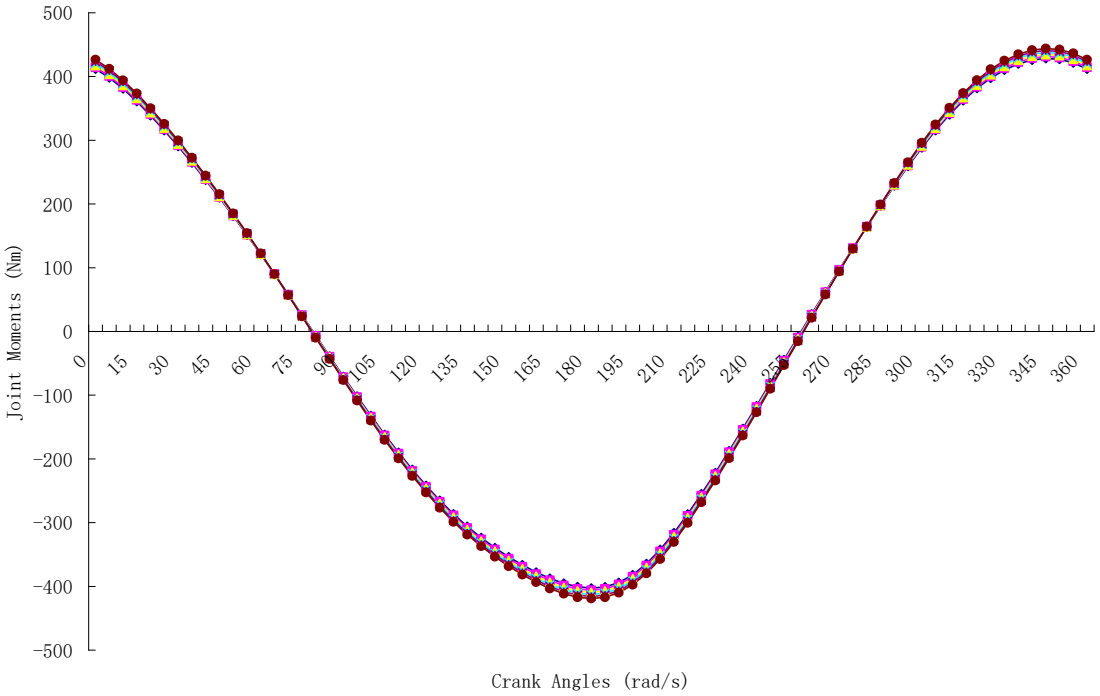

Figure 4.60 (a): Hip Joint Moments at Seat Height of 85% vs crank speed

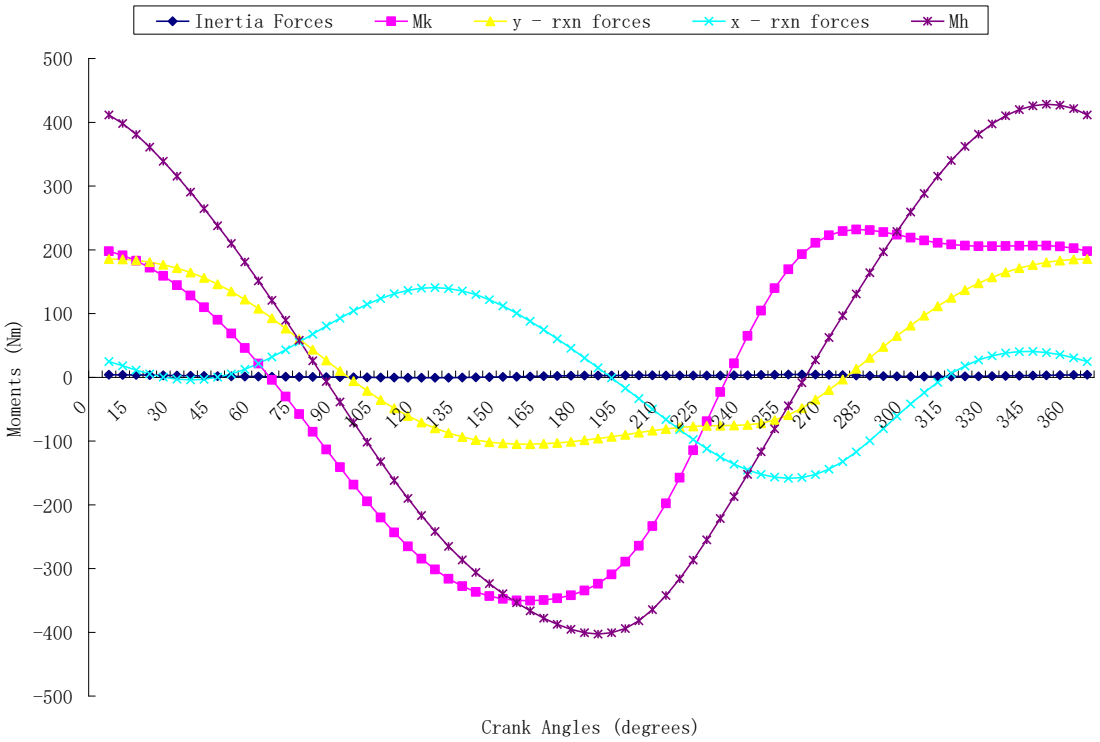

Figure 4.60 (b): Components of Hip Joint Moments at

Seat Height of 85% vs crank speed

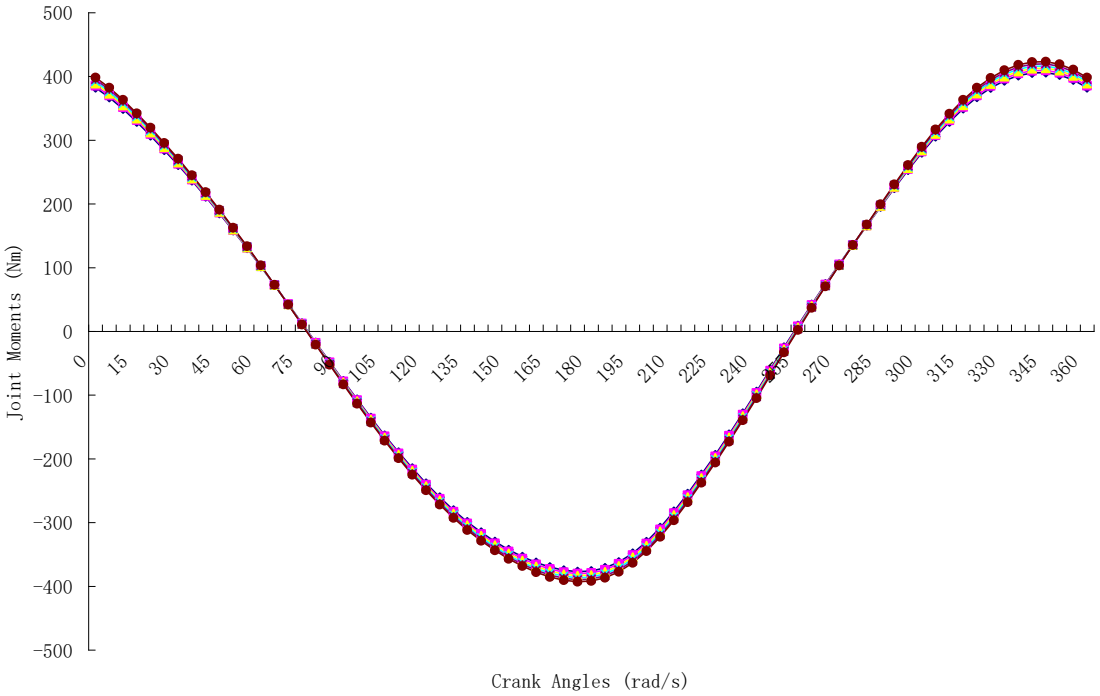

Figure 4.61 (a): Hip Joint Moments at Seat Height of 80% vs crank speed

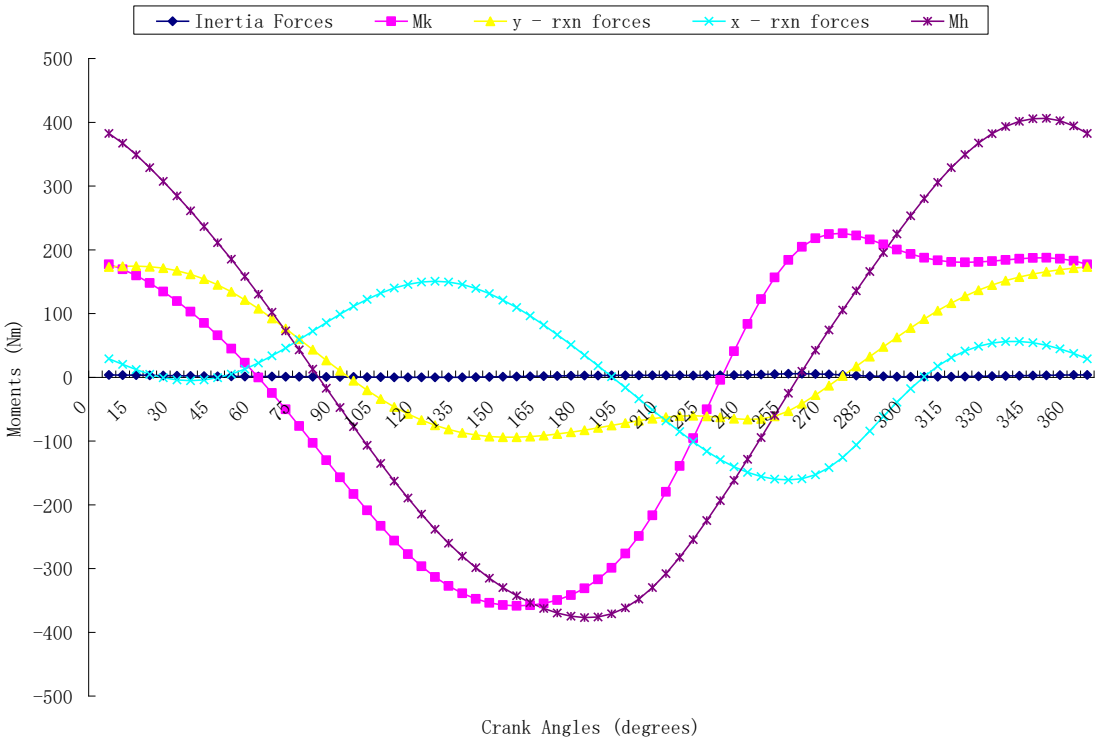

Figure 4.61 (b): Components of Hip Joint Moments at

Seat Height of 80% vs crank speed

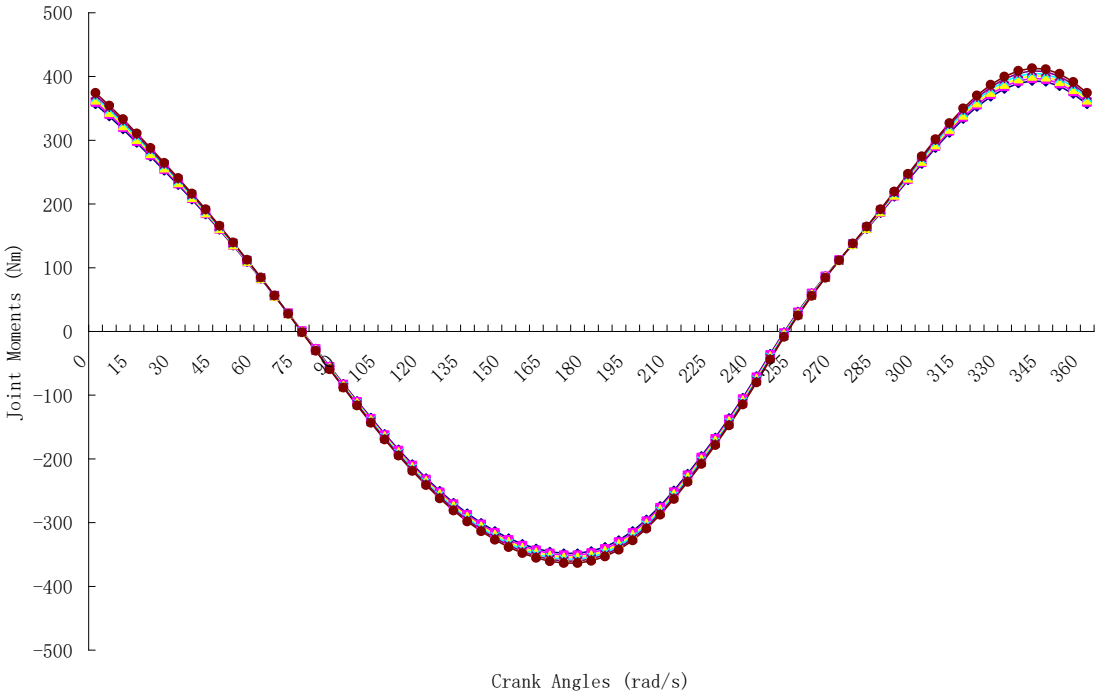

Figure 4.62 (a): Hip Joint Moments at Seat Height of 75% vs crank speed

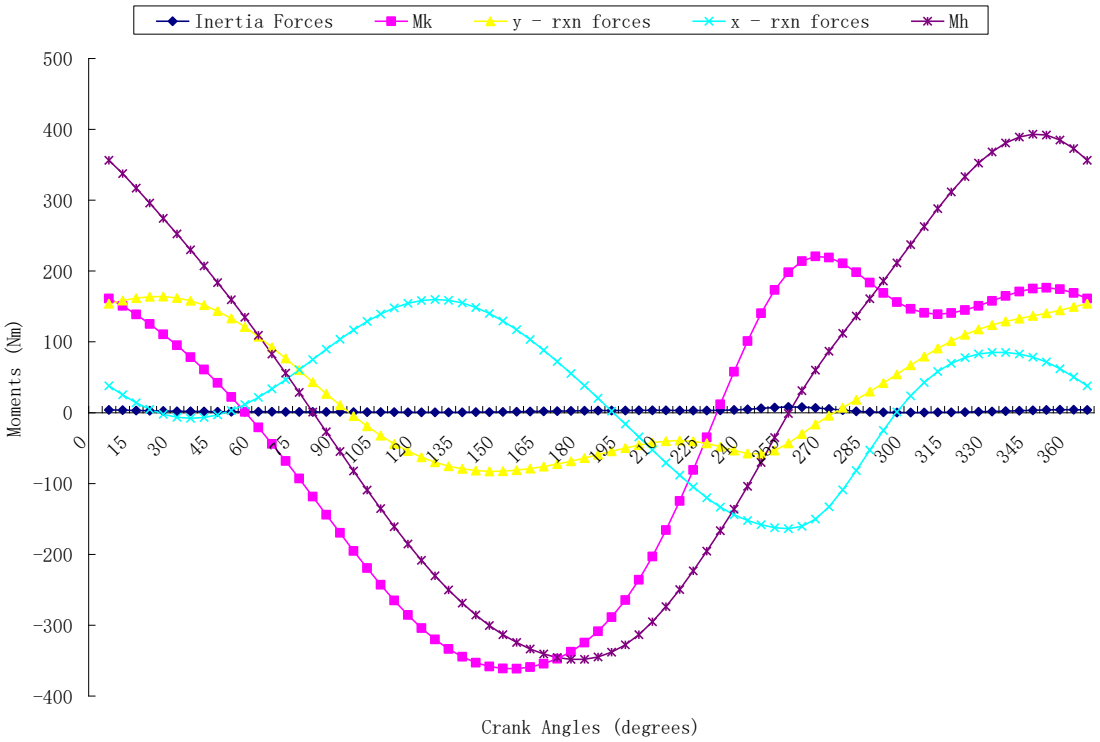

Figure 4.62 (b): Components of Hip Joint Moments at

Seat Height of 75% vs crank speed

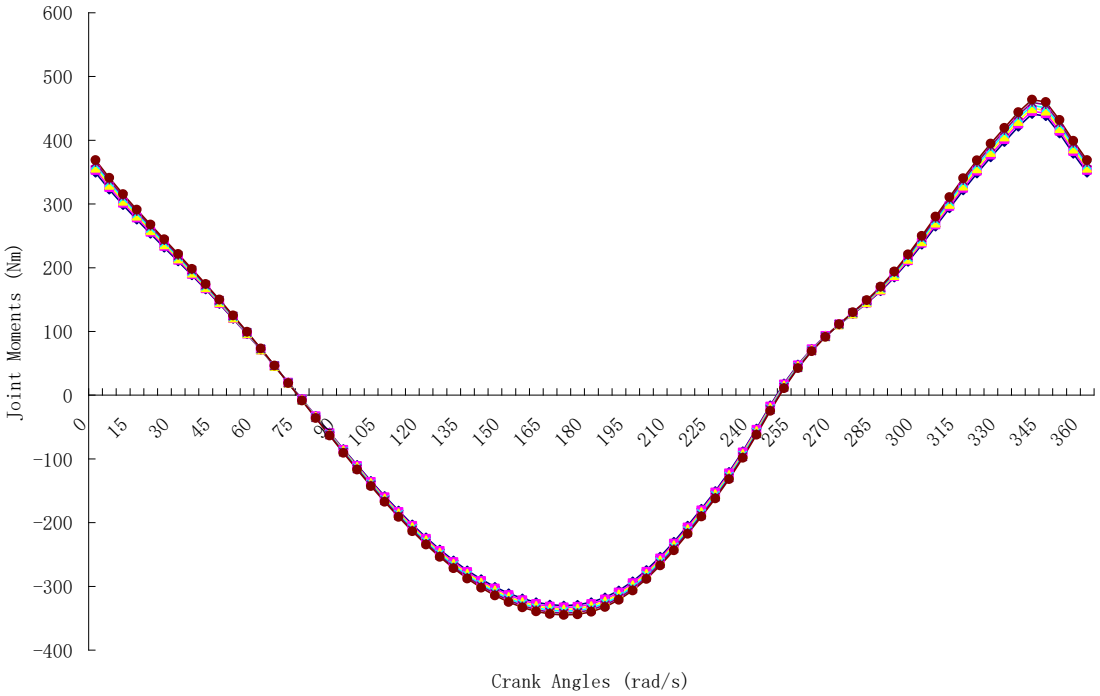

Figure 4.63 (a): Hip Joint Moments at Seat Height of 72% vs crank speed

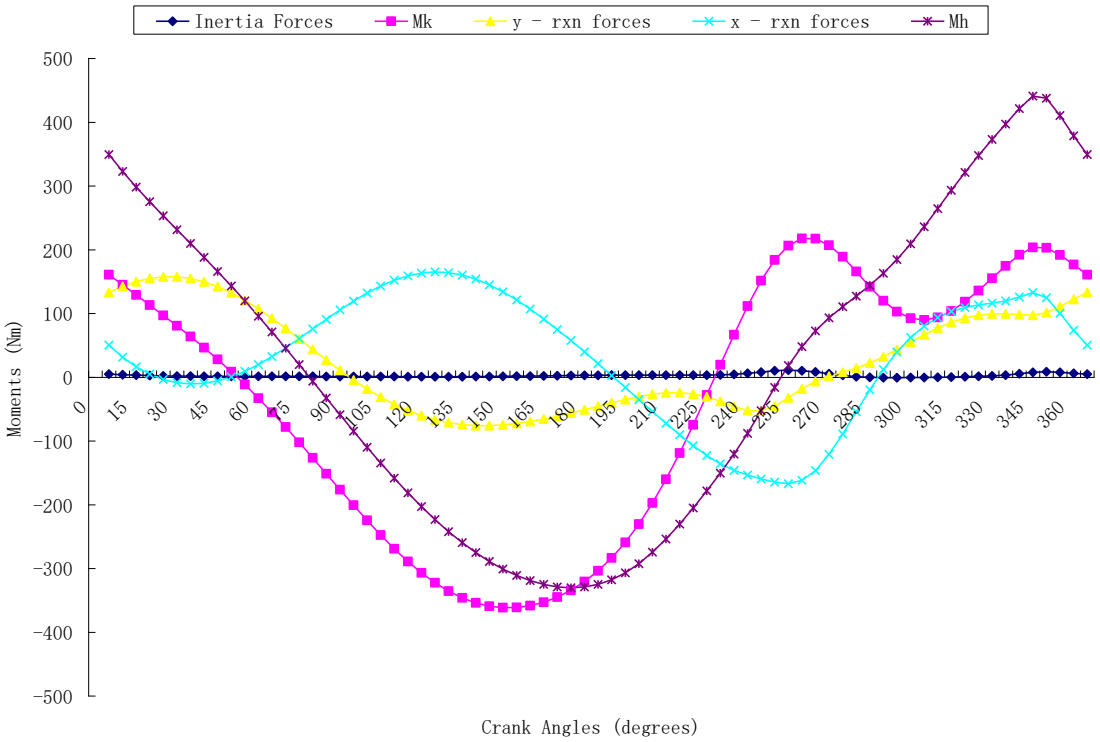

Figure 4.63 (b): Components of Ankle Joint Moments at

Seat Height of 72% vs crank speed

Figure 4.64 is the plot of variation of average hip joint moments with acceleration at varying saddle height. As the seat height is being lowered, there is reduction in average hip joint moments, but as the horizontal acceleration is being increased, the hip joint moments increase. As explained earlier, it is better to maintain minimum saddle height for recreation and transportation especially if power production is not of paramount importance as in competitive cycling. For competitive cycling, the 72% saddle height should be avoided because of lower power production and also for avoiding knee and hip injuries. As the seat height is being lowered, the limb is folded the more and at the 0^0 the folding is the greatest, this results in higher horizontal moments.

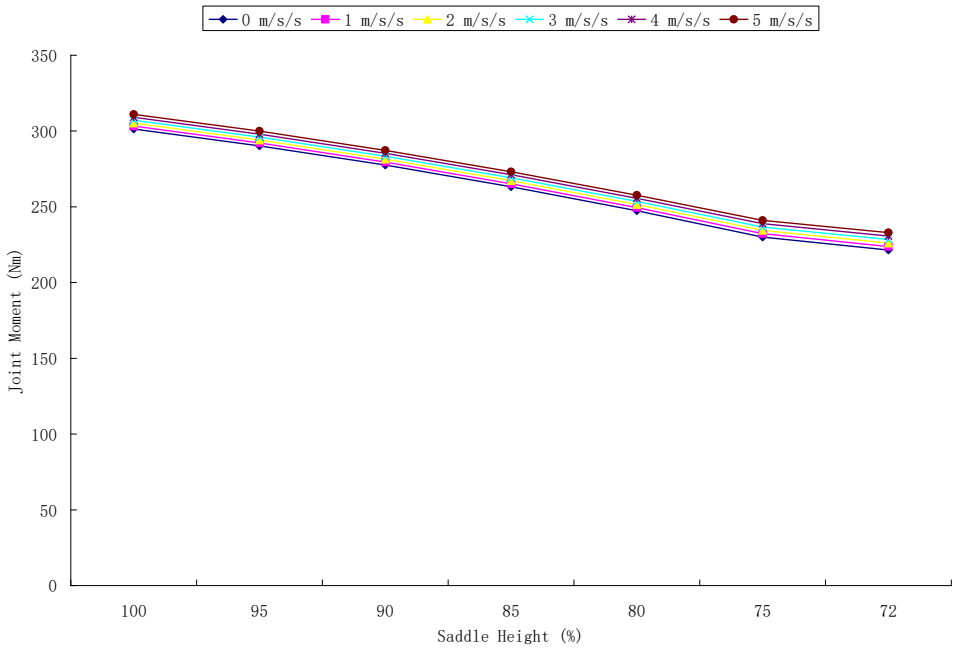

Figure 4.64: Total Hip Joint Moments at 64 rpm vs seat height

4.9 Effect of Friction

The effect of coefficient of friction is shown in Figure 4.65. It is observed that pedal force has a linear relationship with coefficient of friction. As coefficient of friction

increases, the pedal force required increases; this explains the higher pedal force to ride on rough terrains.

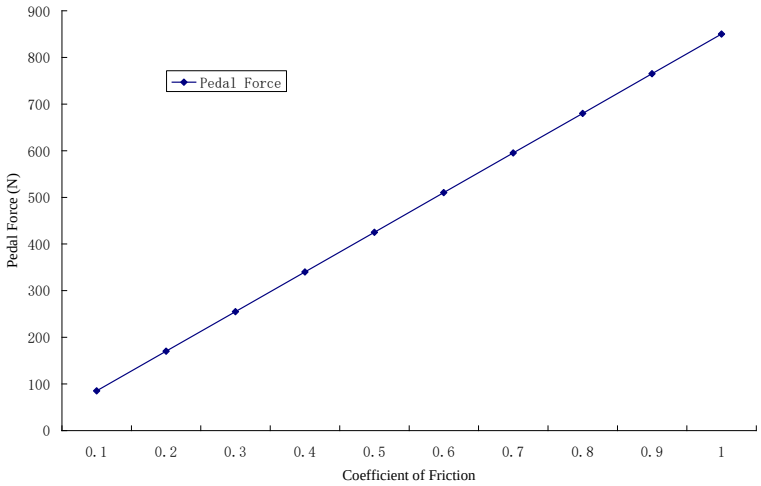

Figure 4.65: The effect of friction

4.10 Model Validation

This current work is validated (i) with experiment and (ii) with the works of Hull and Jorge (1985), and Redfield and Hull (1986).

1. Ten subjects were used for the experiment; eight were none athletic while two of them were. Their weight and height were measured prior to performing the experiment. Saddle height of 90, 75, and 40 % of the total length of the lower limb segment were used. Their experiences were documented after the cycling sessions which were tabulated in Table 3.1 – 3.6. The experience of the subjects tallied with what was obtained from the analysis. It was observed that the most likely saddle height that will give injury is 40% saddle height followed by 90%. The most favourable saddle height is 75% of the total length of the lower limb segments.

2a. Figures 4.66 – 4.68 are the plots of the ankle, knee and hip joints moments against crank angle for three accelerations of 0 (Hull and Jorge, 1985), 3, and 5 m/s^2. Since Hull

and Jorge (1985) assumed constant angular velocity of the crank arm in their work, consequently, the angular and horizontal accelerations must be zero. The three acceleration plots follow the same shape for each joint showing the agreement of this result with the Hull and Jorge (1985).

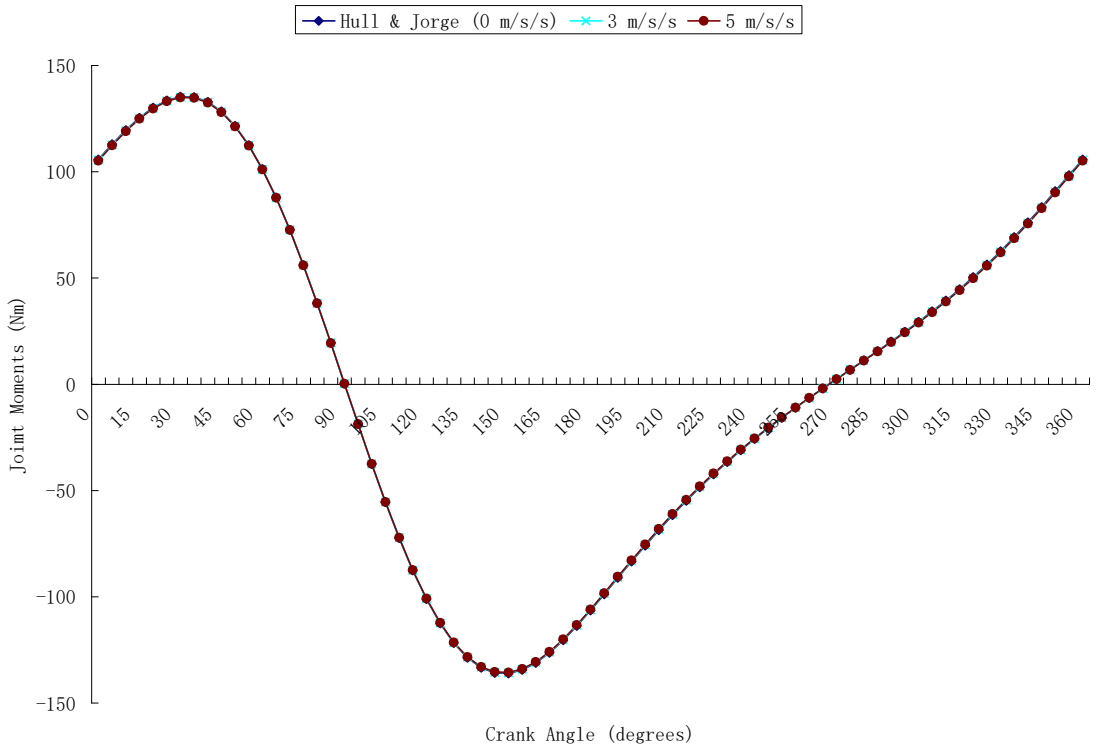

Figure 4.66: Ankle Joint Moments vs crank speed at 10 rpm

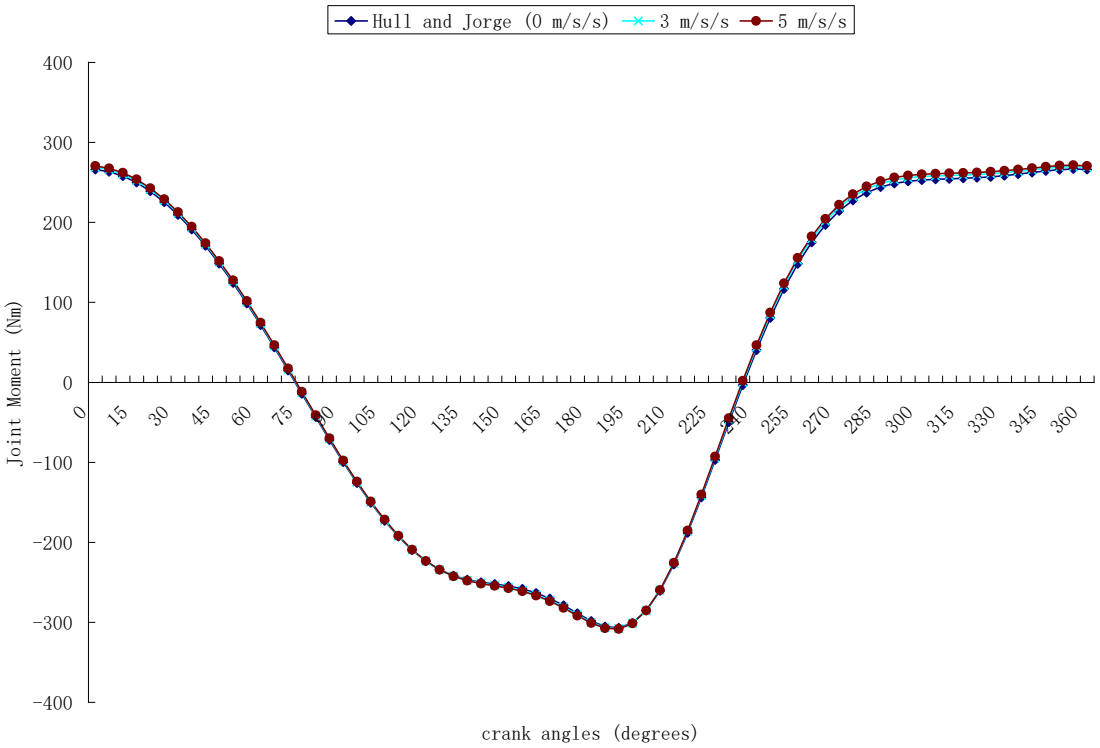

Figure 4.67: Knee Joint Moments vs crank speed at 64 rpm

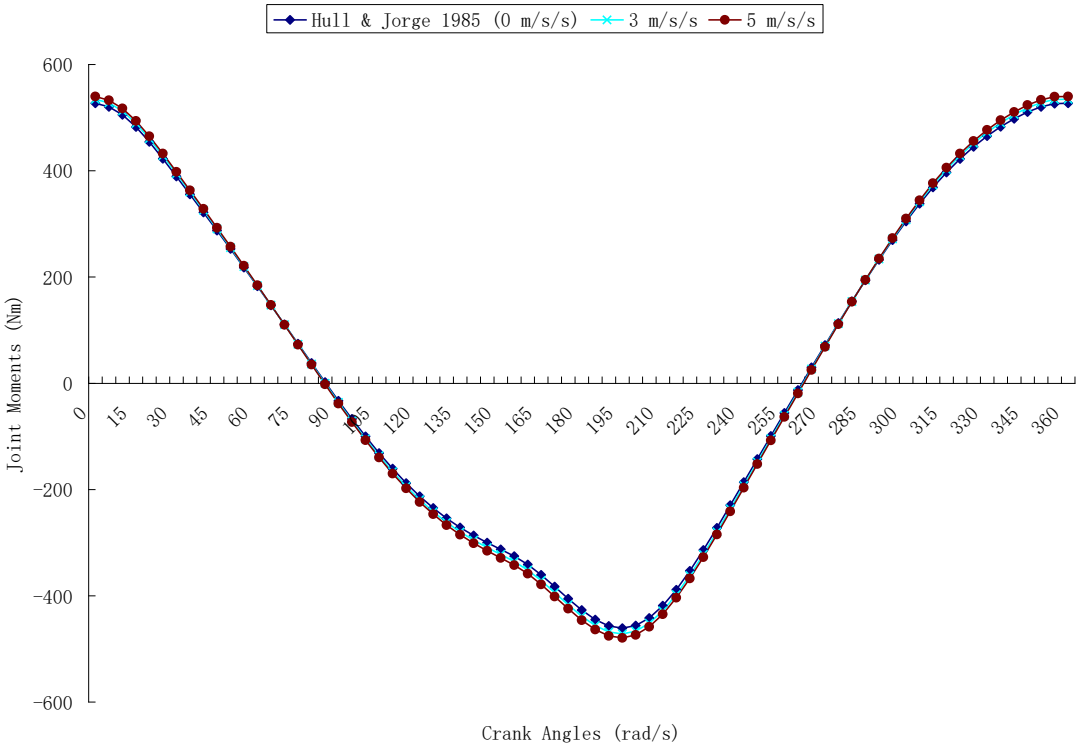

Figure 4.68: Hip Joint Moments vs crank speed at 64 rpm

2b. Figures 4.69a – 4.71a are the plots of ankle, knee and hip joint moments against crank angle respectively for three crank speed of 10, 80 and 130 rpm while Figures

4.69b – 4.71b are the plots of ankle, knee and hip joints moments by Redfield and Hull (1986). Each plots compares together bear resemblance but for the magnification in magnitude of the vertical axis of the work of Redfield and Hull (1986) which was clearly stated in the publication by the authors.

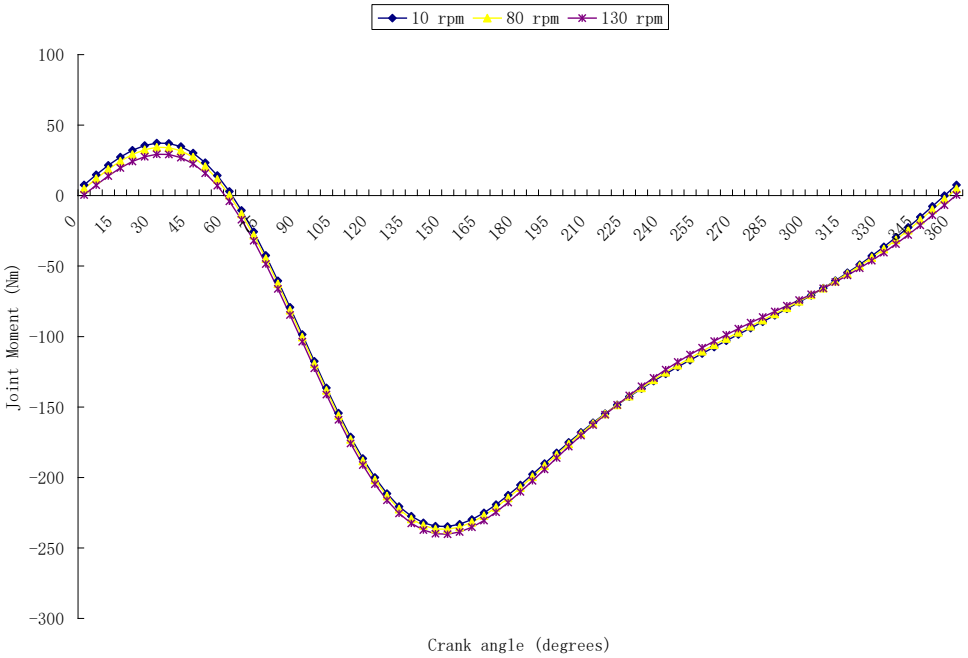

Figure 4.69 (a): Ankle joint moments at seat height of 100% vs crank speed

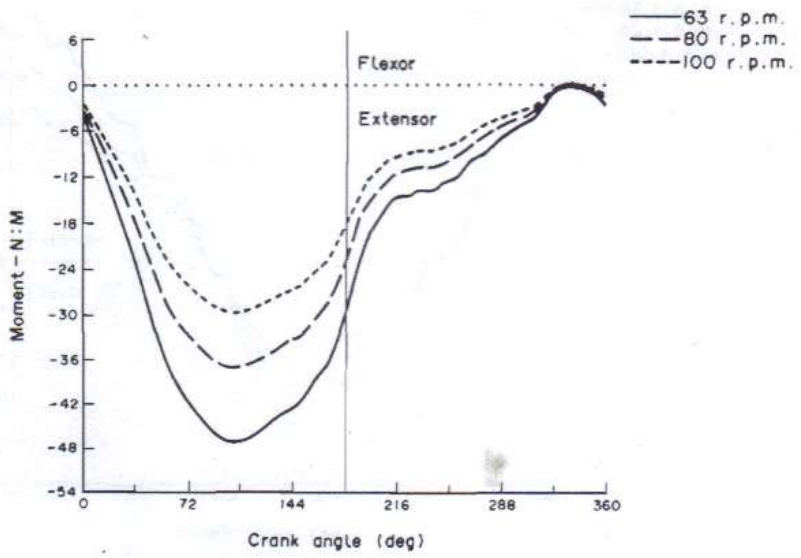

Figure 4.69 (b): Ankle joint moments at seat height of 100% vs crank speed (Redfield and Hull, 1986)

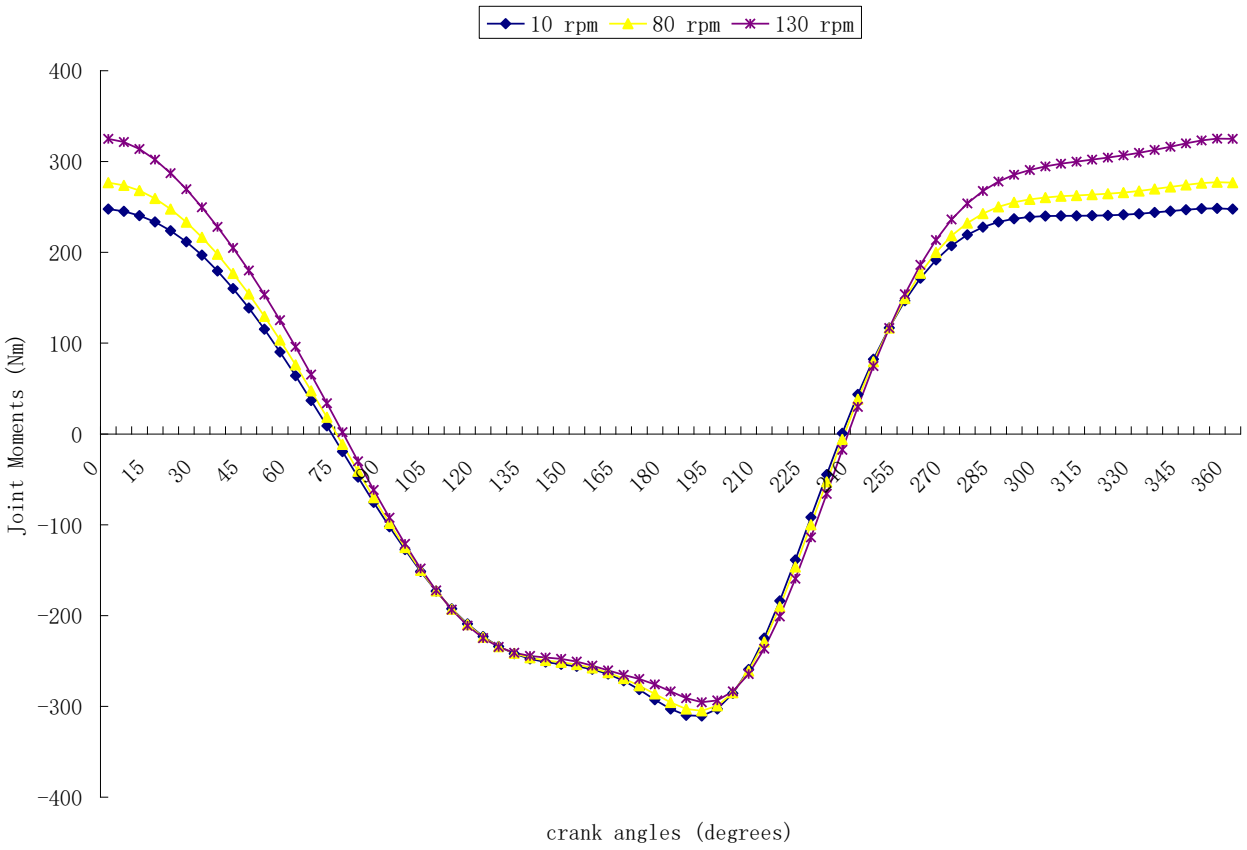

Figure 4.70 (a): Knee joint moments at seat height of 100% vs crank speed

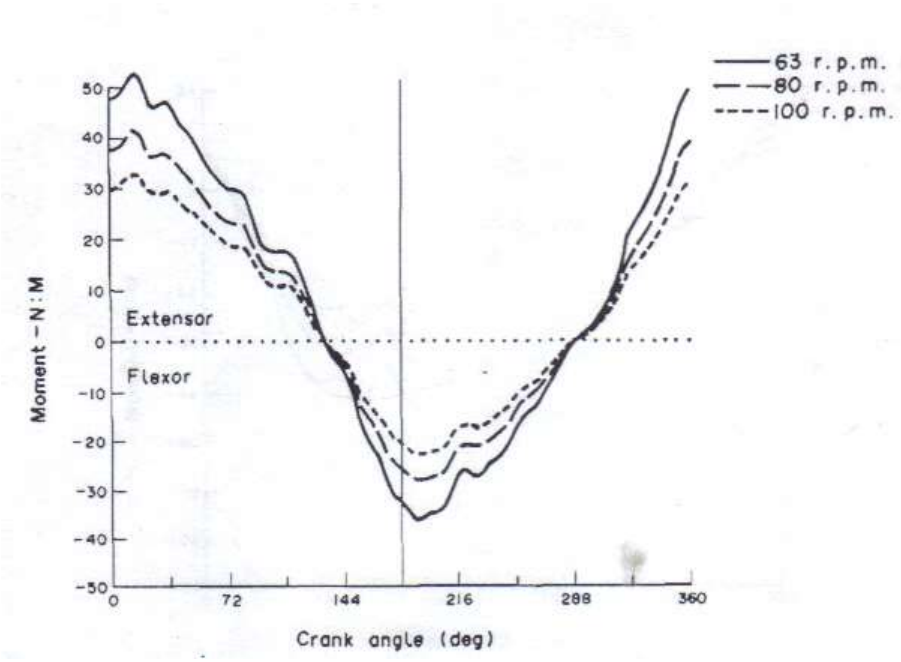

Figure 4.70 (b): Knee joint moments at seat height of 100% vs crank speed

(Redfield and Hull, 1986)

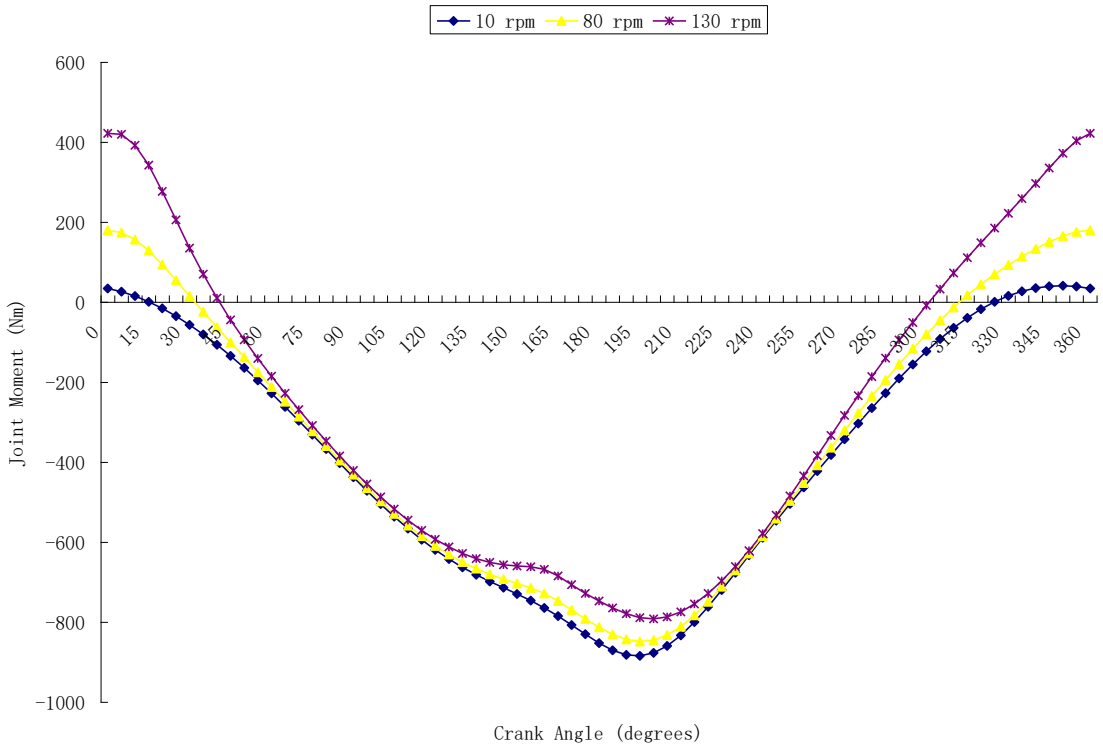

Figure 4.71 (a): Hip joint moments at seat height of 100% vs crank speed

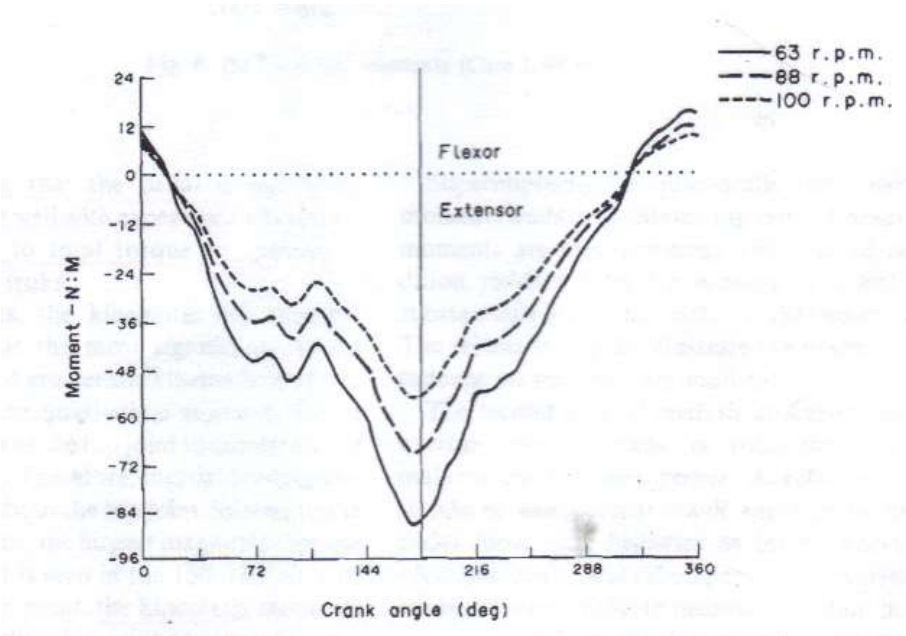

Figure 4.71 (b): Hip joint moments at seat height of 100% vs crank speed (Redfield and Hull, 1986)

CHAPTER 5

SUMMARY OF FINDINGS, CONCLUSION AND CONTRIBUTIONS TO KNOWLEDGE

5.1 Summary of Findings

The biomechanical analysis of the lower limb segments during variable speed cycling has been presented. The summary of findings is hereby presented:

Table 5.1: Summary of Findings

Objectives	**Summary of Findings**
To develop the model that can be used effectively for the biomechanical analysis of the lower limb segments during variable speed cycling.	The model for joint moment, saddle height and horizontal acceleration for the biomechanical analysis of lower limb segments during variable speed cycling has been developed.
To evaluate the effects of crank speed, saddle height and horizontal acceleration on the lower limb segments during variable speed cycling.	i) It was established that the hip and knee joint moments increased in magnitude significantly (up to 700 % increase) as the crank speed increased from 5 to 130 rpm, but there is no corresponding significant increase (about 100% increase) in ankle ii) It was established that, with a constant saddle height, the horizontal acceleration of the bicycle does have significant effect (up to 150% increase

	in joint moment) on the hip joint during variable speed cycling. iii) It was also established that lowering the saddle height below 50% of the total length of the lower limb segments will cause severe injuries to the lower limb segments especially the knee region during variable speed cycling.
To determine the optimum crank speed, saddle height and horizontal acceleration during variable speed cycling.	i) It was established that the optimum crank speed for transportation, fitness and recreation is 64 rpm. For rehabilitation therapy, the appropriate speed is 50 rpm. ii) For competition, it was established that the optimum saddle height is 90 – 100% of the total length of the lower limb segments in order to minimize the knee related injuries and for fitness or recreation, it is 72% of the total length of the lower limb segments. iii) It was established that as the acceleration is increasing the joint moment is increasing thereby increasing the power generated, for balance the optimum horizontal acceleration should be $2m/s^2$.

5.2 Conclusion

The biomechanical analysis of lower limb segments variable speed cycling has been presented. The research provides a basis for injury-free and healthy cycling at variable speed. The power, moments and forces generated during cycling are greater during the power stroke than the back stroke. This is what happened in reality.

To avoid knee injury by cyclists, an optimum saddle height relative to the total length of the lower limb segments for recreation, rehabilitation and competition has been established.

5.3 Contributions to Knowledge

Contributions of this research to knowledge in the field of biomechanics include:

i. The model that can be effectively be used for the biomechanical analysis of the lower limb segments during variable speed cycling has been developed.

ii. This research established that for fitness, recreation and transportation, it is safe to pedal below 64 rpm while for rehabilitation and therapy, it is save to pedal around 50 rpm so as to avoid fatigue that can lead to overuse injuries at the knee joint.

iii. This work established that saddle height below 50% of the total length of the lower limb segments leads to fatigue of the lower limb segments. Therefore, for competition, the saddle height should be 90 – 100% of the total length of the lower limb segments while for

fitness, recreation, transportation and therapy, the saddle height should be between 72 - 75% of the total length of lower limb segments.

iv. Horizontal acceleration has significant effect on the knee and hip joint moments. The optimum horizontal acceleration is discovered to be 2 m/s^2.

REFERENCES

Attia, H. A. (2005). "Point-Joint coordinate formulation for the dynamic analysis of generalized planar linkages". *ANZIAM Journal*. **46:** 575 – 589.

Baum, B. S. and Li, L. (2003). "Lower extremity muscle activities during cycling are influenced by load and frequency." *Journal of Electromyography and Kinesiology*. **13:** 181 – 190.

Bei, Y. and Fregly, B. J. (2004). "Multi-body dynamic simulation of knee contact mechanics." *Medical Engineering and Physics*. **26:** 777 – 789.

Bertucci, W., Grappe, F., Girard, A., Betik, A., and Rouillon, J. D. (2005). "Effects on the crank torque profile when changing pedaling cadence in level linear and uphill road cycling." *Journal of Biomechanics.* **38:** 1003 – 1010.

Bini, R. R., Tamborindeguy, A. C., and Mota, C. B (2010) "Effects of saddle height, pedaling cadence and workload on joint kinetics and kinematics during cycling". *Journal of Sport Rehabilitation.* **19:** 301 – 314.

Bini, R., Hume, P. A., and Croft, J. L. (2011) "Effects of bicycle saddle height on knee injury risk and cycling performance." *Journal of Sports Medicine.* **41(6):** 463 – 476.

Bini, R. R., Hume, P. A., and Kilding, A. E. (2012) "Saddle height effects on pedal forces, joint mechanical work and kinematics of cyclists and triathletes." *European Journal of Sport Science*. **12:** 1 – 9.

Boyd, T., Hull, M. L. and Wotten, D. (1996). "An improved accuracy six-load component pedal dynamometer for cycling" *Journal of Biomechanics.* **29(8):** 1105 – 1110.

Boyd, T. F., Neptune, R. R. and M. L. Hull (1997). “Pedal and knee loads using a multi-degree-of-freedom pedal platform in cycling” *Journal of Biomechanics.* **30(5):** 505 – 511.

Brown, N. A. T. and Jensen, J. L. (2003). "The development of contact force construction in the dynamic-contact task of cycling". *Journal of Biomechanics.* **36:** 1-8.

Busko, K (2004). “The influence of pedaling frequency on mechanical efficiency in exercises with the same intensity”. *Biology of Sport.* **21:** 51 – 66.

Cerone, V., Andreo, D., Larsson, M. and Regruto, D. (2010) “Stabilization of a riderless bicycle: A linear-parameter-varying approach.” IEEE Control Systems. **9:** 23 – 32.

Chang, Z. (2007). “Nonlinear dynamics and analysis of a four bar linkage with clearance.” In the Proceedings of IFToMM World Congress. June 18 – 21.

Chavdarov, I. (2005). “Kinematics and forces of a five-link mechanism by the four spaces Jacoby Matrix.” *Problems of Engineering Cybernetics and Robotics*. **55:** 53 – 63.

Crouch, I. (2004). “Optimal gear selection on an automatic bicycle.” *Human Power*. **55:** 7 - 10

Drillis, R. and Contini, R. (1966). “Body segments parameters”. Technical Report 1166.03 New York University, School of Engineering and Science, New York, USA.

Fregly, B. J. (1993). “The significance of crank load dynamics to steady state pedaling biomechanics: an experimental and computer modeling study.” Ph. D. dissertation, Stanford University, Stanford, CA. USA.

Fregly, B. J. (2009). “Design of optimal treatments for neuromusculoskeletal disorder using patient-specific multibody dynamic models.” *International Journal of Computational Vision and Biomechanics.* **2 (2):** 145 – 155.

Fregly, B. J., Lin, Y.-C., Walter, J. P., Pandy, M. G., Banks, S. A. and D’Lima, D. D. (2009). “Muscle and contact contribution to inverse dynamic knee loads during gait”. Proceeding of the ASME Summer Bioengineering Conference. June 17 – 21, Resort at Square Creek, Lake Tahoe, CA. USA. 1 – 2.

Fregly, B. J., Zajac, F. E. and Dairaghi, C. A. (1996). “Crank inertia load has little effect on steady-state pedaling coordination” *Journal of Biomechanics.* **29(12):** 1559 – 1567.

Haapala, S. A., Faghri, P. and Adams, D. J. (2008). "LLS joint power output during progressive resistance FES-LCE cycling in SCI subjects: developing an index of fatigue". *Journal of Neuro-Engineering and Rehabilitation.* **5:**14.

Hansen E. A., Jorgensen, L. V., Jensen, K., Fregly, B. J. and Sjogaard, G. (2002). “Crank inertia load affects freely chosen pedal rate during cycling”. *Journal of Biomechanics*. **35:** 277 – 285.

Hasson, C. J., Van Emmerik, R. E. A. and Caldwell, G. E. (2006). “Changes in pedal and joint kinetics after learning to direct pedal forces”. *30th Conference of American Society of Biomechanics.* Virginia, Blacksbury. VA.

Hill, A. Vivian. (1938). "The heat of shortening and the dynamic constants of muscle". *Proceeding of Royal Society* **126:** 136 - 195.

Hue O., Chamari, K., Damiani, M., Blonc S., and Hertogh, C. (2007). “The use of an eccentric chainring during an outdoor 1 km all-out cycling test”. *Journal of*

Science and Medicine in Sport. **10:** 180 – 186.

Hull, M. L. and Davies, R. R. (1981). "Measurement of pedal loading in bicycle: I. Instrumentation". *Journal of Biomechanics* **14 (12):** 843 - 856.

Hull, M. L. and Jorge, M. (1985). "A method for biomechanical analysis of bicycle pedaling". *Journal of Biomechanics* **18 (9):** 631 - 644.

Johnston, T. E. (2007) "Biomechanical consideration for cycling interventions in rehabilitation." *Physical Therapy* **87:** 1243 – 1252.

Jansen, A. (2011). "Human Power Empirically Explored". Ph. D. dissertation, Delft University of Technology, Delft, Netherlands.

Kautz, S. A. and Neptune, R. R. (2002). "Biomechanical determinants of pedaling energetics: Internal and external work are not independent". *Exercise and Sport Sciences Reviews*. **30 (4):** 159 – 165.

Lieh, J. (2006). "Determination of cycling speed using a closed-form solution from nonlinear dynamic equations". *Human Power e-Journal.* 1 - 9.

Lin, Y.-C., Haftka, R. T., Queipo, N. V. and Fregly, B. J. (2010). "Surrogate articular contact models for computationally efficient multibody dynamic simulations". *Medical Engineering and Physics*. **32:** 584 – 594.

Marsh, A. P., Martin, P. E. and Sanderson, D. J. (2000) "Is a joint moment-based cost function associated with preferred cycling cadence?" *Journal of Biomechanics*. **33:** 173 – 180.

Martin, J. C., and Spirduso, W. W. (2001) "Determinants of maximal cycling power: crank length, pedaling rate and pedaling speed." *Eur. J. Appl Physiol.* **84:** 419 – 418.

McCane, B., Abbott, J. H, and King, T. (2005). "On calcaluting the finite centre of rotation for rigid planar motion." *Medical Engineering and Physics.* **27:** 75 – 79.

Nott, C. R., Zajac, F. E., Neptune, R. R. and Kautz, S. A. (2010). "All joint moments significantly contribute to trunk angular acceleration". *Journal of Biomechanics*. **43:** 2648 – 2652.

Omi, Shigeru, (2007). UN calls for pedal power to reduce environmental damage. Common Dreams.org News Centre. Online resources: http://www.commondreams.org/archive/2007/07/02/2247 [Accessed on Sept. 12, 2008]

Rankin, J. W. and Neptune, R. R. (2010). "The influence of seat configuration on maximal average crank power during pedaling: a simulation study". *Journal of Applied Biomechanics*. **26:** 493 – 500.

Redfield, R. and Hull, M. L. (1986). "On the relation between joint moment and pedaling rates at constant power in bicycling". Journal of Biomechanics. **19(4):** 317 – 329.

Sergeant, A. J., Hoinville, E, and Young, A. (1981). "Maximum leg force and power output during Short-term Dynamic Exercise". *Journal of Applied Physiology,* **51(5):** 1175-1182.

Slob, P. (2000). "The human power chart: Sustained comfortable cranking." Ph. D. Dissertation, Delft University of Technology, Delft, Netherlands.

Stobbe, Michael (2010). Dieting for Dollars? More US employees trying it. Yahoo News. Online Resources:

http://news.yahoo.com/s/ap/20100602/ap_on_he_me/us_med_dieting_for_dollars

[Accessed on: June 03, 2010] Street, Roger. (1998).

Too, D. and Williams, C. (2001). "Determination of crank-arm length to maximize power production in recumbent cycle ergonometry". *Human Power.* **51:** 3 – 6.

Trumbower, R. D. and Faghri, P. D. (2005). "Relationship between isometric pedal force generation and stimulation intensity of individual LLS muscles involved in FES-induced LLS cycling". *International Functional Electrical Stimulation,* **10 (8)**: 238-240

Vercruyssen, F. and Brisswalter, J. (2010). "Which factors determine the freely chosen cadence during submaximal cycling?" *Journal of Science and Medicine in Sports.* **13:** 225 – 231.

Wilber, C. A., Holland, G. J., Madison, R. E. and Loy, S. F. (1995). "An epidemiological analysis of overuse injuries among recreational cyclists". *International Journal of Sports Medicine.* **16(3):** 201 – 6.

Wilson, D. G. (2004). "Bicycling Science" The MIT Press. Cambridge, Massachusetts, USA.

Yoshihuku, Y and Herzog, W. (1990). "Maximal muscle power output in cycling: a modeling approach". *Journal of Sport Science.* **14 (2):** 139 - 157.

APPENDIX

A.1 Partitioning of the Total Joint Moments

Having obtained the angular acceleration of the leg segments, the normal and the tangential pedal forces and the centre of mass accelerations, the joint moments of the leg segments were computed in equations 3.103, 3.107 and 3.111

Recall the joint moment equations for the ankle, knee and hip

Ankle $$M_a = -I_{FCG}\ddot{q}_2 + \frac{l_f}{2}\left(F_{ay}\sin q_2 - F_{ax}\cos q_2 - F_R\cos(q_1+q_2)\right) \quad \text{(A.1)}$$

Knee $$M_k = -I_{SCG}\ddot{\theta}_1 + \frac{l_s}{2}\left(\left(F_{ky}+F_{ay}\right)\sin\theta_1 - \left(F_{kx}+F_{ax}\right)\cos\theta_1\right) + M_a \quad \text{(A.2)}$$

Hip $$M_h = -I_{TCG}\ddot{\theta}_2 + \frac{l_t}{2}\left(\left(F_{hy}+F_{hy}\right)\sin\theta_1 - \left(F_{hx}+F_{kx}\right)\cos\theta_1\right) + M_k \quad \text{(A.3)}$$

These moments can be partitioned into the moments due to motion only (kinematics moments) and the moments due to pedal force only (static moments) according to Hull and Jorge, 1985.

$$M_i = M_i^{static} + M_i^{kinematic} \qquad i = a,\ k,\ h. \quad \text{(A.4)}$$

where a, k, and h, are ankle, knee and hip respectively.

A.1.1 Kinematics Moments

Kinematics moments are moments due to motion only and it can be obtained by setting the pedal forces in equations 3.103, 3.107 and 3.111 to zero.

Kinematics moments of the foot bone is obtained taking moments about point *a* in Figure A.1,

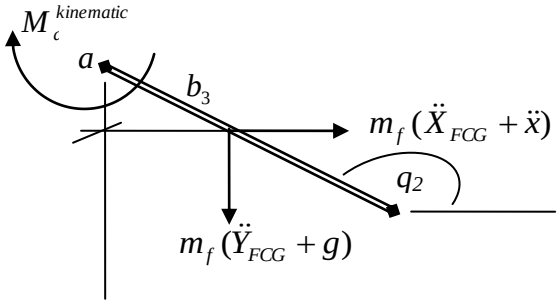

Figure A.1: Free-body diagram of the Kinematics moments for the foot bone

$$-M_a^{kinematic}-I_{FCG}\ddot{q}_2-m_f b_3\left(\left(\ddot{Y}_{FCG}+g\right)\sin q_2+\left(\ddot{X}_{FCG}+\ddot{x}\right)\cos q_2\right)=0 \qquad \text{(A.5)}$$

$$M_a^{kinematic}=-I_{FCG}\ddot{q}_2-m_f b_3\left(\left(\ddot{Y}_{FCG}+g\right)\sin q_2+\left(\ddot{X}_{FCG}+\ddot{x}\right)\cos q_2\right) \qquad \text{(A.6)}$$

Kinematics moment for the shank bone, Figure A.2,

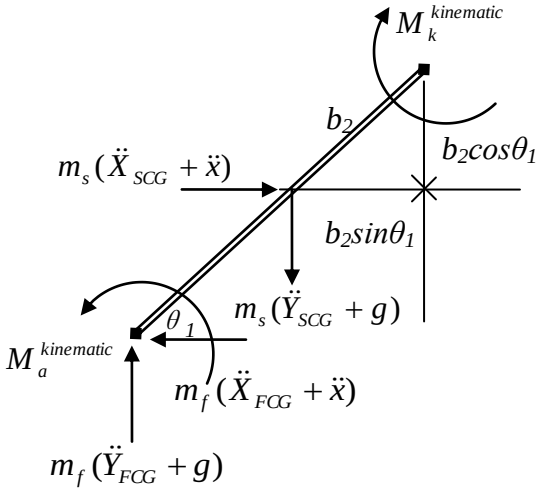

Figure A.2: Free-body diagram of shank bone for kinematics moment analysis

$$\left\{\begin{matrix} M_a^{kinematic}-I_{SCG}\ddot{\theta}_1-M_k^{kinematic}-m_f(\ddot{Y}_{FCG}+g)l_s\sin\theta_1- \\ m_f(\ddot{X}_{FCG}+\ddot{x})l_s\cos\theta_1-m_s(\ddot{Y}_{SCG}+g)d_2\sin\theta_1-m_s(\ddot{X}_{SCG}+\ddot{x})d_2\cos\theta_1 \end{matrix}\right\}=0 \qquad \text{(A.7)}$$

$$M_k^{kinematic}=\left\{\begin{matrix} M_a^{kinematic}-I_{SCG}\ddot{\theta}_1-m_f(\ddot{Y}_{FCG}+g)l_s\sin\theta_1-m_f(\ddot{X}_{FCG}+\ddot{x})l_s\cos\theta_1- \\ m_s(\ddot{Y}_{SCG}+g)d_2\sin\theta_1-m_s(\ddot{X}_{SCG}+\ddot{x})d_2\cos\theta_1 \end{matrix}\right\} \qquad \text{(A.8)}$$

Kinematics moment for the thigh bone, Figure A.3,

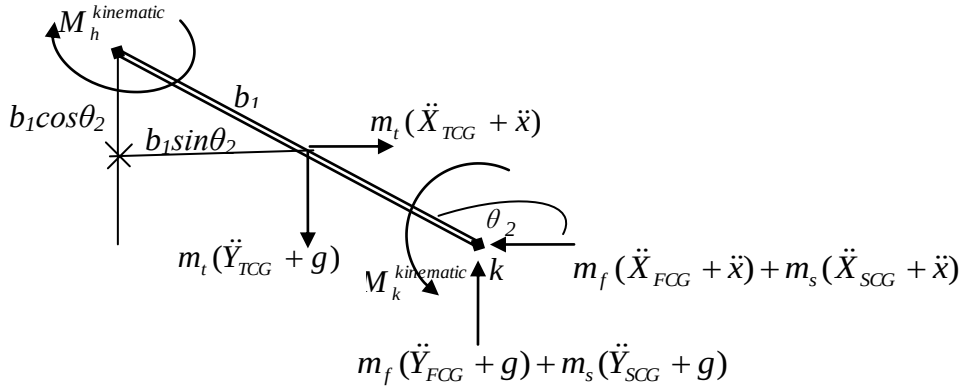

Figure A.3: Free-body diagram of the thigh bone for kinematics moment analysis

Taking moments about point *h*, in Figure A.3, we have

$$\left\{\begin{array}{l} -M_h^{kinematic} - I_{TCG}\ddot{\theta}_2 + M_k^{kinematic} - \left[m_s\left(\ddot{Y}_{SCG} + g\right) + m_f\left(\ddot{Y}_{FCG} + g\right)\right] l_t \sin\theta_2 - \\ \left(m_s(\ddot{X}_{SCG} + \ddot{x}) + m_f(\ddot{X}_{FCG} + \ddot{x})\right) l_t \cos\theta_2 - m_t(\ddot{X}_{TCG} + \ddot{x}) d_1 \cos\theta_2 - m_t\left(\ddot{Y}_{TCG} + g\right) d_1 \sin\theta_2 \end{array}\right\} = 0$$

(A.9)

$$M_h^{kinematic} = \left\{\begin{array}{l} -I_{TCG}\ddot{\theta}_2 + M_k^{kinematic} - \left[m_s\left(\ddot{Y}_{SCG} + g\right) + m_f\left(\ddot{Y}_{FCG} + g\right)\right] l_t \sin\theta_2 - \\ \left(m_s(\ddot{X}_{SCG} + \ddot{x}) + m_f(\ddot{X}_{FCG} + \ddot{x})\right) l_t \cos\theta_2 - m_t(\ddot{X}_{TCG} + \ddot{x}) d_1 \cos\theta_2 - m_t\left(\ddot{Y}_{TCG} + g\right) d_1 \sin\theta_2 \end{array}\right\}$$

(A.10)

A.1.2 Static Moments

Static moments are due to pedal forces only without motion.

Static moment for the foot bone is given below in Figure A.4,

$$M_a^{static} = F_R \sin q_1 \sin q_2 + M_{BR}(\ddot{x} + \mu g)\cos q_2 \qquad \text{(A.11)}$$

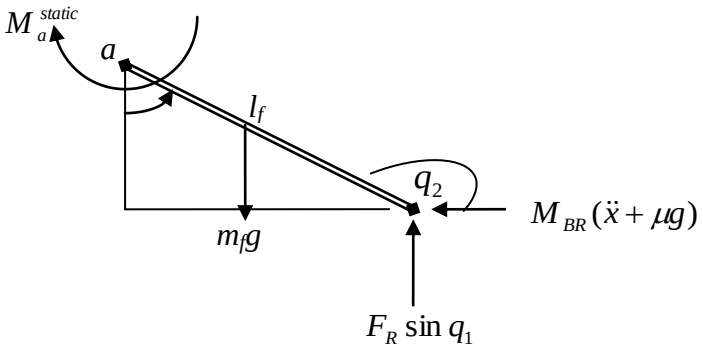

Figure A.4: Free-body diagram of foot bone for static moment analysis

Static Moment of the shank bone can be determined from Figure A.5, below

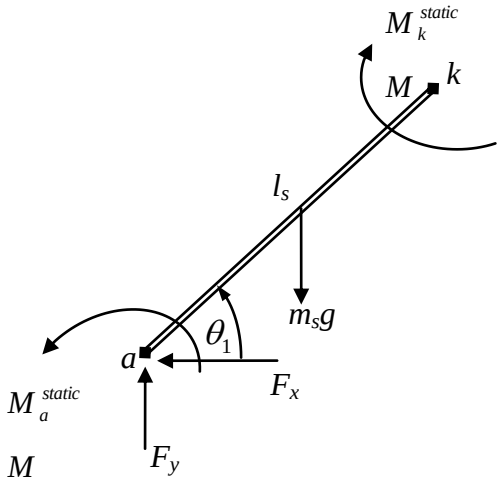

Figure A.5: Free-body diagram of shank bone for static moment analysis

Taking moment about point k in Figure A.5, we have

$$M_a^{static} - M_k^{static} + F_y l_s \sin\theta_1 - F_x l_s \cos\theta_1 = 0 \qquad \text{(A.12)}$$

$$M_k^{static} = M_a^{static} + F_y l_s \sin\theta_1 - F_x l_s \cos\theta_1 \qquad \text{(A.13a)}$$

$$M_k^{static} = F_R \sin q_1 \sin q_2 + M_{BR}(\ddot{x}+\mu g)\cos q_2 + F_y l_s \sin\theta_1 - F_x l_s \cos\theta_1 \qquad \text{(A.13b)}$$

Static Moment for the thigh bone can be determined from Figure A.6, below

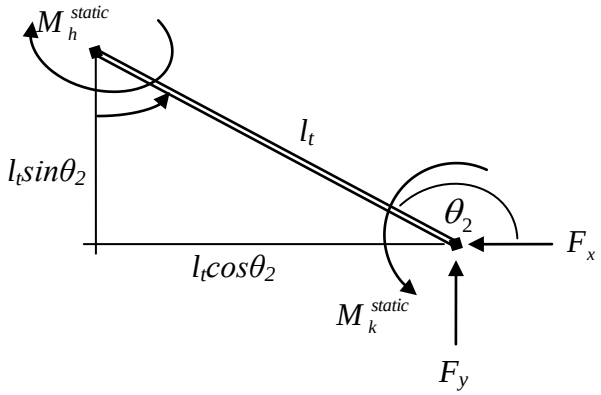

Figure A.6: Free-body diagram of shank bone for static moment analysis

Taking moment about point *h* in Figure A.6, we have

$$M_k^{static} - M_h^{static} + F_y l_t \sin\theta_2 + F_x l_t \cos\theta_2 = 0 \qquad \text{(A.14)}$$

$$M_h^{static} = M_k^{static} + F_y l_t \sin\theta_2 + F_x l_t \cos\theta_2 \qquad \text{(A.15a)}$$

$$M_h^{static} = F_R \sin q_1 \sin q_2 + M_{BR}(\ddot{x} + \mu g)\cos q_2 + F_y l_s \sin\theta_1 - F_x l_s \cos\theta_1 + F_y l_t \sin\theta_2 + F_x l_t \cos\theta_2$$

(A.15b)